# DYNAMIC ANALYSIS OF A MONOSTABLE FLUID AMPLIFIER

By


HYO WHAN CHANG

Bachelor of Science in Engineering
Seoul National University
Seoul, Korea
1968

Master of Science
State University of New York at Buffalo
Buffalo, New York
1972


Submitted to the Faculty of the Graduate College
of the Oklahoma State University
in partial fulfillment of the requirements
for the Degree of
DOCTOR OF PHILOSOPHY
July, 1978

DYNAMIC ANALYSIS OF A MONOSTABLE FLUID AMPLIFIER

Thesis Approved:

Karl N. Reid
Thesis Adviser

W. G. Tiederman

Jerald D. Parker

Robert J. Mulholland

Norman N. Durham
Dean of the Graduate College

ACKNOWLEDGMENTS

I wish to express my sincere appreciation and thanks to my thesis adviser, Dr. Karl N. Reid, for his invaluable guidance and encouragement throughout my doctoral program. Discussions with him have been most valuable not only in the preparation of this thesis, but also in my professional development and growth.

I wish to thank Dr. William G. Tiederman, Dr. Jerald D. Parker, and Dr. Robert J. Mulholland for serving on my thesis committee. Their valuable advice and criticisms are greatly appreciated.

I wish to thank my colleagues and friends: especially Dr. Syed Hamid for his encouragement and help; Vijay Maddali, Dave Smith, Steve Mhoon, and John Perrault for their companionship.

I also wish to thank Ms. Charlene Fries for her expert typing of this thesis.

Lastly, my wife, Young Mi, deserves special thanks for her patience and sacrifices.

TABLE OF CONTENTS

## LIST OF TABLES

LIST OF FIGURES

Figure Page

## NOMENCLATURE

| | |
|---|---|
| $a_c$ | flow passage width (see Figure 13), in. |
| $a_v$ | flow passage width (see Figure 16), in. |
| $a_w$ | flow passage width (see Figure 19), in. |
| $A_c$ | normalized flow passage width $a_c$ $(a_c/b_s)$ |
| $A_v$ | normalized flow passage width $a_v$ $(a_v/b_s)$ |
| $A_w$ | normalized flow passage width $a_w$ $(a_w/b_s)$ |
| AR | supply nozzle aspect ratio (height to width) |
| $b_b$ | bias vent width, in. |
| $b_c$ | control nozzle width, in. |
| $b_s$ | supply nozzle width, in. |
| $b_{v1}$ | NOR output vent width, in. |
| $b_{v2}$ | OR output vent width, in. |
| $B_b$ | normalized bias vent width $(b_b/b_s)$ |
| $B_c$ | normalized control nozzle $(b_c/b_s)$ |
| $B_{v1}$ | normalized NOR output vent width $(b_{v1}/b_s)$ |
| $B_{v2}$ | normalized OR output vent width $(b_{v2}/b_s)$ |
| $B_b$ | normalized bias vent width $(b_b/b_s)$ |
| $B_c$ | normalized control nozzle width $(b_c/b_s)$ |
| $B_{v1}$ | normalized NOR output vent width $(b_{v1}/b_s)$ |
| $B_{v2}$ | normalized OR output vent width $(b_{v2}/b_s)$ |
| c | 67/90 |
| $C_{dc}$ | control nozzle discharge coefficient |
| $C_{ds}$ | supply nozzle discharge coefficient |

| | |
|---|---|
| $d_s$ | splitter distance downstream of the supply nozzle exit, in. |
| $d_1$ | attachment wall offset, in. |
| $d_2$ | opposite wall offset, in. |
| $d_3$ | splitter offset, in. |
| $D_s$ | normalized splitter distance $(d_s/b_s)$ |
| $D_1$ | normalized attachment wall offset $(d_1/b_s)$ |
| $D_2$ | normalized opposite wall offset $(d_2/b_s)$ |
| $D_3$ | normalized splitter offset $(d_3/b_s)$ |
| $e_1$ | distance (see Figure 11), in. |
| $e_2$ | distance (see Figure 24), in. |
| $E_1$ | normalized distance $e_1$ $(e_1/b_s)$ |
| $E_2$ | normalized distance $e_2$ $(e_2/b_s)$ |
| $g$ | distance (see Figure 14), in. |
| $G$ | normalized distance $g$ $(g/b_s)$ |
| $I_c$ | control channel inertance (per unit depth), lbf $sec^2/in.^4$ |
| $I_{o1}$ | NOR output channel inertance (per unit depth), lbf $sec^2/in.^4$ |
| $I_{o2}$ | OR output channel inertance (per unit depth), lbf $sec^2/in.^4$ |
| $I'_c$ | dimensionless control channel inertance parameter |
| $I'_{o1}$ | dimensionless NOR output channel inertance parameter |
| $I'_{o2}$ | dimensionless OR output channel inertance parameter |
| $J$ | supply jet momentum flux (per unit depth), lbf/in. |
| $J_b$ | momentum flux (per unit depth) of the induced flow from the bias vent, lbf/in. |
| $J_d$ | momentum flux (per unit depth) proceeding downstream along the wall (see Figure 18), lbf/in. |
| $J_m$ | momentum flux (per unit depth) of the combined (supply and control) jet, lbf/in. |
| $J_s$ | momentum flux (per unit depth) separated by the splitter, lbf/in. |

| | |
|---|---|
| $k$ | scale factor in the entrainment streamline path equation |
| $K$ | normalized scale factor ($k/b_s$) |
| $K_L$ | minor loss coefficient |
| $\ell_c$ | control channel length, in. |
| $\ell_{o1}$ | NOR output channel length, in. |
| $\ell_{o2}$ | OR output channel length, in. |
| $L_c$ | normalized control channel length ($\ell_c/b_s$) |
| $L_{o1}$ | normalized NOR output channel length ($\ell_{o1}/b_s$) |
| $L_{o2}$ | normalized OR output channel length ($\ell_{o2}/b_s$) |
| $Re_c$ | control jet Reynolds number based on the control nozzle width |
| $Re_c'$ | modified control jet Reynolds number defined in Equation (B.2) |
| $Re_s$ | supply jet Reynolds number based on the supply nozzle width |
| $p_b$ | bias vent exit pressure, psig |
| $p_c$ | pressure at section $Z_1$ (see Figure 12), psig |
| $p_{cb}$ | pressure at section $Z_2$ (see Figure 13), psig |
| $p_{d1}$ | dynamic pressure at the inlet of the NOR output channel, psig |
| $p_{d2}$ | dynamic pressure at the inlet of the OR output channel, psig |
| $p_{o1}$ | total pressure at the exit of NOR output channel, psig |
| $p_{o2}$ | total pressure at the exit of OR output channel, psig |
| $p_r$ | static return pressure (see Figure 4), psig |
| $p_s$ | static switching pressure (see Figure 4), psig |
| $p_{tc}$ | total pressure at the inlet of the control channel, psig |
| $p_1$ | separation bubble pressure, psig |
| $p_2$ | average pressure in the unattached side of the jet, psig |
| $p_{2a}$ | average pressure in region 1 (see Figure 19), psig |
| $p_{2b}$ | average pressure in region 2 (see Figure 19), psig |
| $\Delta p$ | pressure difference across the jet ($p_2 - p_1$), psig |

| | |
|---|---|
| $P_b$ | normalized pressure $p_b$ $(p_b/\frac{1}{2}\rho U_s^2)$ |
| $P_c$ | normalized pressure $p_c$ $(p_c/\frac{1}{2}\rho U_s^2)$ |
| $P_{cb}$ | normalized pressure $p_{cb}$ $(p_{cb}/\frac{1}{2}\rho U_s^2)$ |
| $P_{d1}$ | normalized pressure $p_{d1}$ $(p_{d1}/\frac{1}{2}\rho U_s^2)$ |
| $P_{d2}$ | normalized pressure $p_{d2}$ $(p_{d2}/\frac{1}{2}\rho U_s^2)$ |
| $P_{o1}$ | normalized pressure $p_{o1}$ $(p_{o1}/\frac{1}{2}\rho U_s^2)$ |
| $P_{o2}$ | normalized pressure $p_{o2}$ $(p_{o2}/\frac{1}{2}\rho U_s^2)$ |
| $P_{tc}$ | normalized pressure $p_{tc}$ $(p_{tc}/\frac{1}{2}\rho U_s^2)$ |
| $P_1$ | normalized pressure $p_1$ $(p_1/\frac{1}{2}\rho U_s^2)$ |
| $P_2$ | normalized pressure $p_2$ $(p_2/\frac{1}{2}\rho U_s^2)$ |
| $P_{2a}$ | normalized pressure $p_{2a}$ $(p_{2a}/\frac{1}{2}\rho U_s^2)$ |
| $P_{2b}$ | normalized pressure $p_{2b}$ $(p_{2b}/\frac{1}{2}\rho U_s^2)$ |
| $q_b$ | volumetric flow rate (per unit depth) through the bias vent, in.$^2$/sec |
| $q_c$ | volumetric flow rate (per unit depth) of control jet, in.$^2$/sec |
| $q_{e1}$ | volumetric flow rate (per unit depth) entrained by the convex side of the jet, in.$^2$/sec |
| $q_{e2}$ | volumetric flow rate (per unit depth) entrained by the convex side of the jet ($q_{e2} = q_{e3} + q_{e4}$), in.$^2$/sec |
| $q_{e3}$ | volumetric flow rate (per unit depth) entrained from region 1 by the convex side of the jet (see Figure 10), in.$^2$/sec |
| $q_{e4}$ | volumetric flow rate (per unit depth) entrained from region 2 by the convex side of the jet (see Figure 19), in.$^2$/sec |
| $q_{o1}$ | volumetric flow rate (per unit depth) through the NOR output channel, in.$^2$/sec |
| $q_{o2}$ | volumetric flow rate (per unit depth) through the OR output channel, in.$^2$/sec |
| $q_{out}$ | volumetric flow rate (per unit depth) leaving the separation bubble (see Figure 10), in.$^2$/sec |
| $q_s$ | volumetric flow rate (per unit depth) of supply jet, in.$^2$/sec |

$q_{v1}$ volumetric flow rate (per unit depth) through the NOR output vent, in.$^2$/sec

$q_{v2}$ volumetric flow rate (per unit depth) through the OR output vent, in.$^2$/sec

$q_w$ volumetric flow rate (per unit depth) through the flow passage width $a_w$ (see Figure 19), in.$^2$/sec

$Q_b$ normalized volumetric flow rate $q_b$ $(q_b/q_s)$

$Q_c$ normalized volumetric flow rate $q_c$ $(q_c/q_s)$

$Q_{e1}$ normalized volumetric flow rate $q_{e1}$ $(q_{e1}/q_s)$

$Q_{e2}$ normalized volumetric flow rate $q_{e2}$ $(q_{e2}/q_s)$

$Q_{e3}$ normalized volumetric flow rate $q_{e3}$ $(q_{e3}/q_s)$

$Q_{e4}$ normalized volumetric flow rate $q_{e4}$ $(q_{e4}/q_s)$

$Q_{o1}$ normalized volumetric flow rate $q_{o1}$ $(q_{o1}/q_s)$

$Q_{o2}$ normalized volumetric flow rate $q_{o2}$ $(q_{o2}/q_s)$

$Q_{v1}$ normalized volumetric flow rate $q_{v1}$ $(q_{v1}/q_s)$

$Q_{v2}$ normalized volumetric flow rate $q_{v2}$ $(q_{v2}/q_s)$

$Q_w$ normalized volumetric flow rate $q_w$ $(q_w/q_s)$

$r$ geometric variable defined by Equation (3.2), in.

$r_c$ average radius of curvature of the jet centerline, in.

$r_e$ distance (see Figure 11), in.

$r_{es}$ radius of the circular arc which is tangent to the entrainment streamline at point $A_1$ (see Figure 14), in.

$R$ normalized geometric variable $r$ $(r/b_s)$

$R_c$ normalized average radius of curvature of the jet centerline curvature $(r_c/b_s)$

$R_e$ normalized distance $r_e$ $(r_e/b_s)$

$R_{es}$ normalized radius $r_{es}$ $(r_{es}/b_s)$

$s$ distance along the jet centerline, in.

$s_e$ distance along the entrainment streamline $\widehat{A_1E}$ (see Figure 10), in.

| | |
|---|---|
| $s_f$ | distance along the jet centerline, $\widehat{C_IF}$ (see Figure 10), in. |
| $s_o$ | distance from the "hypothetical nozzle" exit to the "virtual origin" of the jet, in. |
| $s_p$ | distance along the entrainment streamline, $\widehat{A_1P}$ (see Figure 14), in. |
| $s_s$ | distance along the jet centerline from the hypothetical nozzle exit to the splitter point (see Figure 12), in. |
| $s_v$ | distance along the jet centerline from the hypothetical nozzle exit to the output vent flow passage (see Figure 16a) |
| $s_w$ | distance along the jet centerline from the hypothetical nozzle exit to the flow passage $\overline{W_1W_2}$ (see Figure 19), in. |
| $S_e$ | normalized distance $s_e$ $(s_e/b_s)$ |
| $S_o$ | normalized distance $s_o$ $(s_o/b_s)$ |
| $S_p$ | normalized distance $s_p$ $(s_p/b_s)$ |
| $S_s$ | normalized distance $s_s$ $(s_s/b_s)$ |
| $S_v$ | normalized distance $s_v$ $(s_v/b_s)$ |
| $S_w$ | normalized distance $s_w$ $(s_w/b_s)$ |
| $t$ | time, sec |
| $t_d$ | decay time of control input pressure signal to wall-attachment fluid amplifier (see Figure 7), sec |
| $t'_d$ | decay time of input pressure signal to the transmission line (see Figure 7), sec |
| $t_\ell$ | pure sonic delay in the transmission (see Figures 6 and 7), sec |
| $t_r$ | return time, sec |
| $t_{ri}$ | rise time of control input pressure signal to wall-attachment fluid amplifier (see Figure 6), sec |
| $t'_{ri}$ | rise time of input pressure signal to the transmission line (see Figure 6), sec |
| $t_s$ | switching time, sec |
| $t_t$ | transport time $(b_s/U_s)$, sec |

| | |
|---|---|
| $T_r$ | variable defined by Equation (3.6b) |
| $T_s$ | variable defined by Equation (3.45) |
| $u$ | velocity component parallel to jet centerline at any point in the jet, in./sec |
| $\overline{u'^2}$ | mean square value of turbulent velocity fluctuations parallel to jet centerline, in.$^2$/sec$^2$ |
| $u_c$ | jet centerline axial velocity |
| $U_{o1}$ | mean velocity at the NOR output channel exit plane $(q_{o1}/W_{o1})$, in./sec |
| $U_s$ | continuity averaged velocity at the supply nozzle exit plane, in./sec |
| $v$ | separation bubble volume (per unit depth), in.$^2$ |
| $v_1$ | volume per unit depth (see Figure 20), in.$^2$ |
| $v_2$ | volume per unit depth (see Figure 20), in.$^2$ |
| $v_3$ | volume per unit depth (see Figure 20), in.$^2$ |
| $V$ | normalized separation bubble volume $(v/b_s^2)$ |
| $w_{o1}$ | NOR output channel width, in. |
| $w_{o2}$ | OR output channel width, in. |
| $W_{o1}$ | normalized width $w_{o1}$ $(w_{o1}/b_s)$ |
| $W_{o2}$ | normalized width $w_{o1}$ $(w_{o2}/b_s)$ |
| $x_e$ | distance (see Figure 11), in. |
| $x_r$ | reattachment distance (see Figure 10), in. |
| $x_{v1}$ | attachment wall length (see Figure 27), in. |
| $x_{v2}$ | opposite wall length (see Figure 27), in. |
| $x_1$ | distance (see Figure 11), in. |
| $x_2$ | distance (see Figure 11), in. |
| $X_e$ | normalized distance $x_e$ $(x_e/b_s)$ |
| $X_r$ | normalized distance $x_r$ $(x_r/b_s)$ |

| | |
|---|---|
| $X_{v1}$ | normalized distance $x_{v1}$ ($x_{v1}/b_s$) |
| $X_{v2}$ | normalized distance $x_{v2}$ ($x_{v2}/b_s$) |
| $X_1$ | normalized distance $x_1$ ($x_1/b_s$) |
| $X_2$ | normalized distance $x_2$ ($x_2/b_s$) |
| $y$ | distance normal to the jet centerline (see Figure 10), in. |
| $y_e$ | distance (see Figure 10), in. |
| $y_p$ | distance (see Figure 14), in. |
| $y_r$ | distance (see Figure 10), in. |
| $y_s$ | distance (see Figure 14), in. |
| $Y_e$ | normalized distance $y_e$ ($y_e/b_s$) |
| $Y_I$ | normalized distance defined by Equation (3.63) |
| $Y_p$ | normalized distance $y_p$ ($y_p/b_s$) |
| $Y_r$ | normalized distance $y_r$ ($y_r/b_s$) |
| $Y_s$ | normalized distance $y_s$ ($y_s/b_s$) |

Greek Symbols

| | |
|---|---|
| $\alpha_1$ | attachment wall angle, radian |
| $\alpha_2$ | opposite wall angle, radian |
| $\beta$ | jet deflection angle, radian |
| $\gamma$ | jet reattachment angle, radian |
| $\delta_v$ | jet half-width at $s = s_v$ (see Figure 16a), in. |
| $\delta_w$ | jet half-width at $s = s_w$ (see Figure 19), in. |
| $\Delta_v$ | normalized width $\Delta_v$ ($\Delta_v/b_s$) |
| $\Delta_w$ | normalized width $\Delta_w$ ($\Delta_w/b_s$) |
| $\zeta$ | angle between the entrainment streamline and r (see Figure 11), radian |
| $\zeta_e$ | angle $\zeta$ at point E (see Figure 11), radian |

| | |
|---|---|
| $\eta_1$ | angle (see Figure 14), radian |
| $\eta_2$ | angle (see Figure 14), radian |
| $\theta$ | angle (see Figure 11), radian |
| $\theta_e$ | angle (see Figure 11), radian |
| $\theta_p$ | angle (see Figure 14), radian |
| $\lambda$ | parameter defined by Equation (3.46) |
| $\nu$ | fluid kinematic viscosity, in.$^2$/sec |
| $\xi$ | angle (see Figure 16), radian |
| $\rho$ | fluid density, lbf sec$^2$/in.$^4$ |
| $\sigma$ | jet spread parameter |
| $\tau$ | normalized time $(U_s t/b_s)$ |
| $\tau_s$ | normalized switching time $t_s$ $(t_s/t_t)$ |
| $\tau_r$ | normalized return time $t_r$ $(t_r/t_t)$ |

CHAPTER I

# INTRODUCTION

## 1.1 Background

The utilization of fluidic technology in industrial, military, and medical control systems has increased substantially in the last several years [2] [11] [27].[1] The well-known advantages of fluidic devices are insensitivity to hostile environments (e.g., high temperature, radiation and vibration), simplicity, ruggedness, reliability, and low maintenance cost.

Digital fluidic devices or "fluid amplifiers" which utilize the "wall-attachment" phenomenon (called "wall-attachment fluid amplifiers") are used to implement logic circuits for a broad range of applications. As the application of digital fluid amplifiers in circuits requiring fast operating speed has increased, it has become essential to consider the dynamic behavior of the fluid amplifiers and connecting transmission lines in the course of system design. The switching times[2] of digital fluid amplifiers often govern the operating speed of the associated logic system.

The operation of a wall-attachment fluid amplifier is based on the fluid flow phenomenon known as the "Coanda effect" or the "wall-attachment effect." A simple explanation of the Coanda effect is as follows: Consider a two-dimensional, turbulent jet emerging from a nozzle into a region between two adjacent walls (see Figure 1a). Because

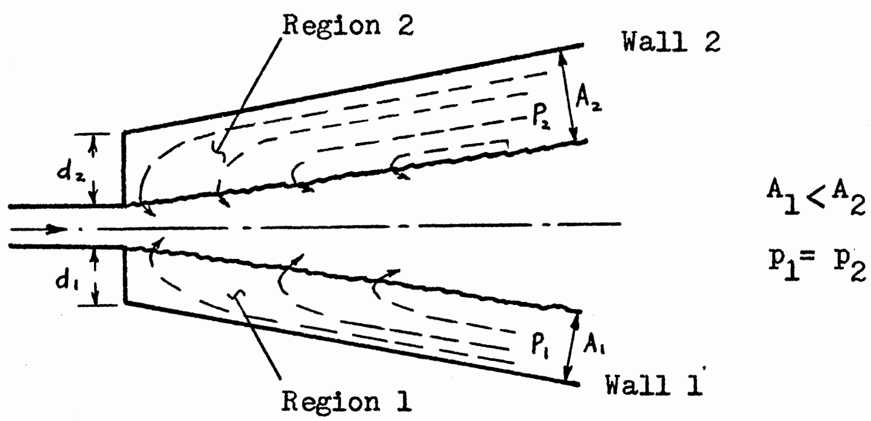


(a) Jet in the Initial (Hypothetical) Central Position

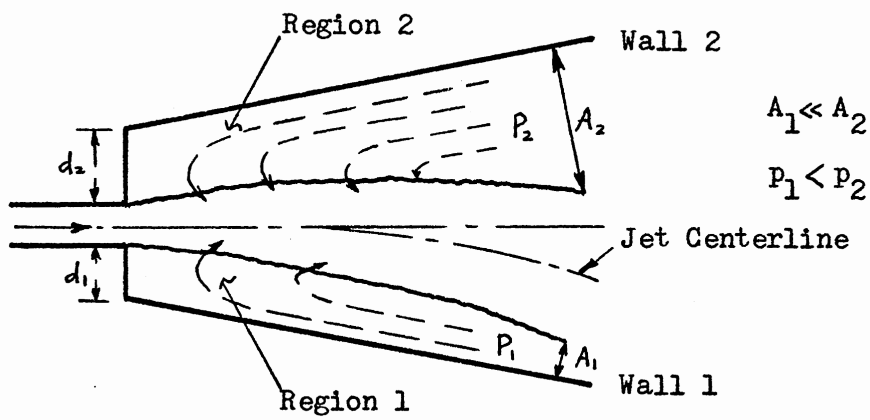


(b) Jet Deflected Toward Wall 1

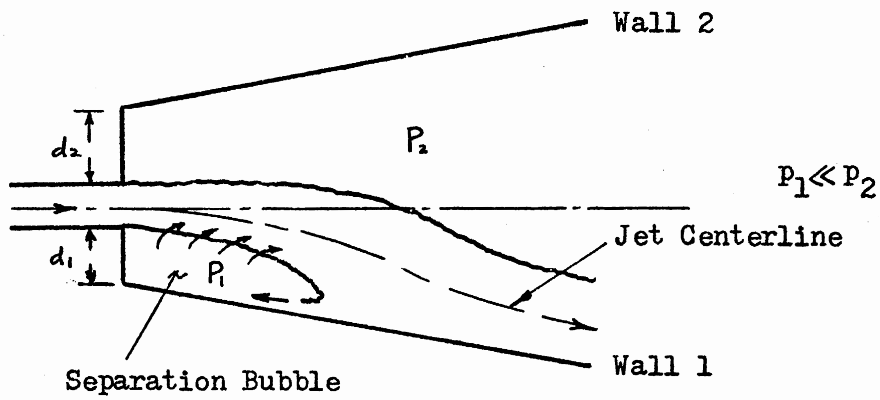


(c) Jet Attached to Wall 1

Figure 1. Illustration of the Coanda Effect

of the turbulent shearing action, the jet entrains fluid from the surrounding regions [31]. If offset $d_1$ of wall 1 is smaller than offset $d_2$ of wall 2, the spacing $A_1$ between wall 1 and the jet edge is smaller than the spacing $A_2$ between wall 2 and the jet edge (see Figure 1(a)). Since the jet entrains the same amount of fluid from region 1 and from region 2 (Figure 1(a)), the average static pressure in region 1 becomes less than that in region 2 to satisfy the jet entrainment. The resulting static pressure difference $(p_2 - p_1)$ causes the jet to deflect toward wall 1 (see Figure 1(b)), which results in an even further increase in the pressure difference. The only "stable" position for the jet is attachment to wall 1; a low pressure cavity or bubble (called the separation bubble) is formed as shown in Figure 1(c). A state of equilibrium is reached when the mass flow rate of fluid returned to the bubble is equal to the mass flow rate of fluid entrained from it.

Simplified representations of wall-attachment fluid amplifiers are shown in Figures 2 and 3. If the geometry of the wall-attachment amplifier is symmetric (Figure 2), the supply jet attaches to either one of the two walls due to the Coanda effect. This kind of wall-attachment amplifier is called a <u>bistable</u> fluid amplifier. A typical static switching characteristic of a bistable amplifier is shown in Figure 4(a). If the jet is initially attached to wall 1, the total pressure at output port 1 ($p_{o1}$) is maximum and the total pressure at output port 2 ($p_{o2}$) is minimum. The jet will switch to wall 2 and pressure $p_{o2}$ will be maximum and pressure $p_{o1}$ minimum if a control signal is applied at control port 1 which is equal to or greater than $p_s$. The jet will remain attached to wall 2 even if the control signal at port 1 is removed. Switching of the jet from wall 2 to wall 1 requires the application of a positive pressure

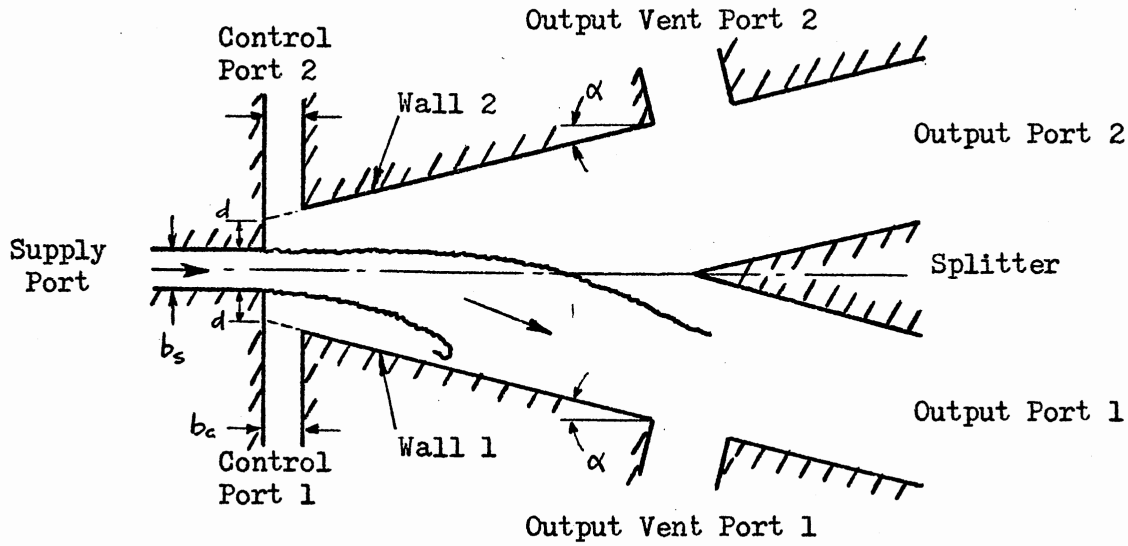


Figure 2. Simplified Representation of a <u>Bistable</u> Fluid Amplifier

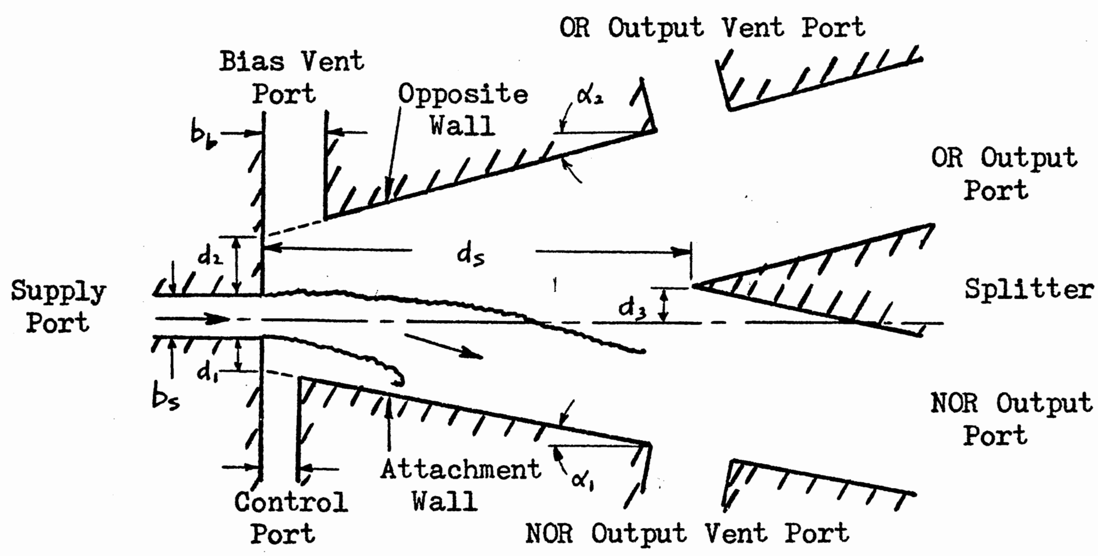


Figure 3. Simplified Representation of a <u>Monostable</u> Fluid Amplifier

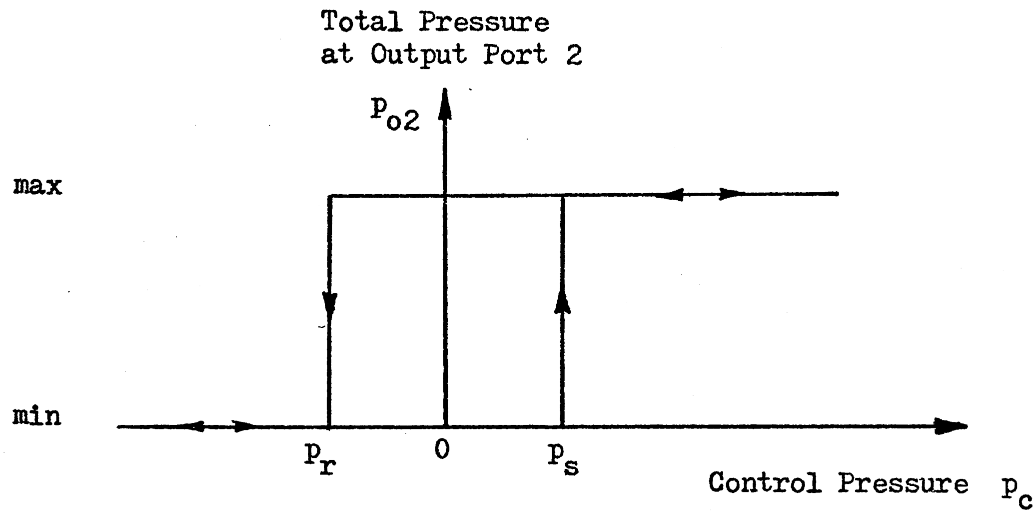


(a) Typical Static Switching Characteristic of a Bistable Fluid Amplifier

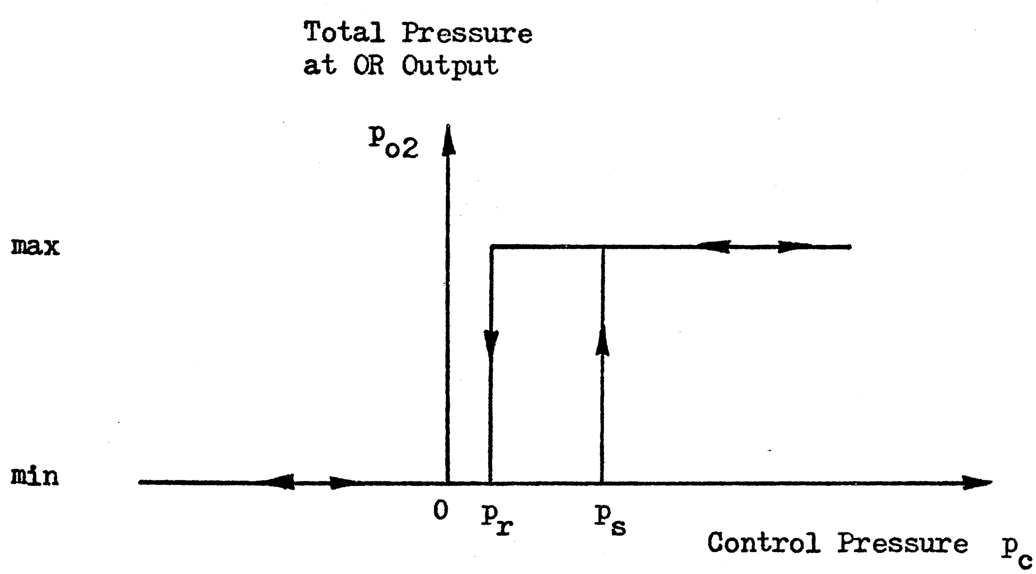


(b) Typical Static Switching Characteristic of a Monostable Fluid Amplifier

Figure 4. Typical Static Switching Characteristics of Wall-Attachment Amplifiers

signal at control port 2 which is equal to or greater than $p_s$ in magnitude, or the application of a negative pressure signal at control port 1 equal to or less than $p_r$.

If the geometry of the wall-attachment amplifier is asymmetric (e.g., $d_1 < d_2$, $b_c < b_b$, $\alpha_1 < \alpha_2$, and $d_3 \neq 0$ in Figure 3), the supply jet tends to attach to the "attachment wall" in the absence of a control signal. This kind of wall-attachment amplifier is called a monostable fluid amplifier. A typical static switching characteristic of a monostable amplifier is shown in Figure 4(b). The jet is initially attached to the "attachment wall" and the total pressure at NOR output port ($p_{o1}$) is maximum, while the total pressure at OR output port ($p_{o2}$) is minimum. The jet will switch to the "opposite wall" and pressure $p_{o2}$ will be maximum and pressure $p_{o1}$ minimum, if a control signal is applied which is equal to or greater than $p_s$. If this control signal is then reduced to a level equal to or less than $p_r$, the jet will switch back to the "attachment wall."

Output vents (see Figures 2 and 3) are provided in wall-attachment amplifiers to avoid false switching due to a partial or complete blockage of an output port.

The monostable amplifier is logically an OR/NOR device. It is a fundamental building block of any logic circuit, since all other logic functions (e.g., AND, NAND, FLIP-FLOP, etc.) can be generated by circuits containing only OR/NOR elements. Nevertheless, no analytical studies and only a few experimental studies have been done on the switching dynamics of monostable fluid amplifiers, while there have been a large number of analytical and experimental studies on the switching dynamics of bistable fluid amplifiers.

It is known that a monostable fluid amplifier can be derived from a bistable amplifier by minor geometric changes in the design. For example, a bistable fluid amplifier can be made monostable by the following geometric change(s) in the design (see Figure 3):

1. by making opposite wall offset $d_2$ greater than attachment wall offset $d_1$, or

2. by making bias vent width $b_b$ greater than control nozzle width $b_c$, or

3. by making opposite wall angle $\alpha_2$ greater than attachment wall angle $\alpha_1$, or

4. by combinations of the above changes.

But, how the above changes affect switching and return times[3] and static characteristics (e.g., static switching and return pressures, pressure and flow gains, etc.) of a monostable fluid amplifier is not well understood. For lack of an analytical model, monostable fluid amplifier designs have been based primarily on trial-and-error procedures, with design guides provided by experiments and very limited theories such as a wall-attachment theory. The need for additional design information was also suggested by Foster and Parker [22].

The switching times of digital fluid amplifiers are known to be dependent on the control input pulse characteristics (i.e., input pulse shape and magnitude). A pulse signal transmitted from the output of a fluidic sensor or amplifier to the control input of a wall-attachment fluid amplifier through a connecting transmission line usually experiences a certain amount of pure time delay, attenuation and dispersion. The change in pulse shape depends on the signal pressure level, the input characteristic of the driven amplifier, and the geometry of the connecting transmission line. Moreover, an input vent port (see Figure 5) provided for control input signal isolation in a wall-attachment amplifier may result in significant input pulse signal attenuation and dispersion.

Figures 6 and 7 show the effects of a connecting transmission line on the switching and return times of the monostable fluid amplifier used in the present study. A solid line in the output velocity trace indicates the measured result; a dashed line indicates the actual magnitude and sign of the velocity where there is a flow reversal. That is, the hot-wire probe used in the measurements is not directional sensitive. A 42 foot long (1/4 inch inside diameter and 3/8 inch outside diameter) flexible plastic tubing served as a connecting transmission line between the control pressure source and the control chamber of the test amplifier for the measurements in Figures 6(b) and 7(b). "Step-like" pressure pulses were generated at the control port of the amplifier (Figures 6(a) and 7(a)) and at the inlet of the transmission line (Figures 6(b) and 7(b) by means of a solenoid valve connected to a constant-pressure source. When the transmission line was connected to the control part of the amplifier, the magnitude of the pressure pulse at the control port was kept the same as that without a transmission line by adjusting the magnitude of the pressure pulse at the inlet of the transmission line.

The transmission line caused the pure time delay $t_\ell$ and long rise time[4] of the control input pressure to the amplifier. Due to the increased rise time in the control input pressure to the amplifier, the switching time[5] of the amplifier with the transmission line was approximately five times longer than that of the amplifier without the transmission line (see Figures 6(a) and 6(b)). The transmission line caused

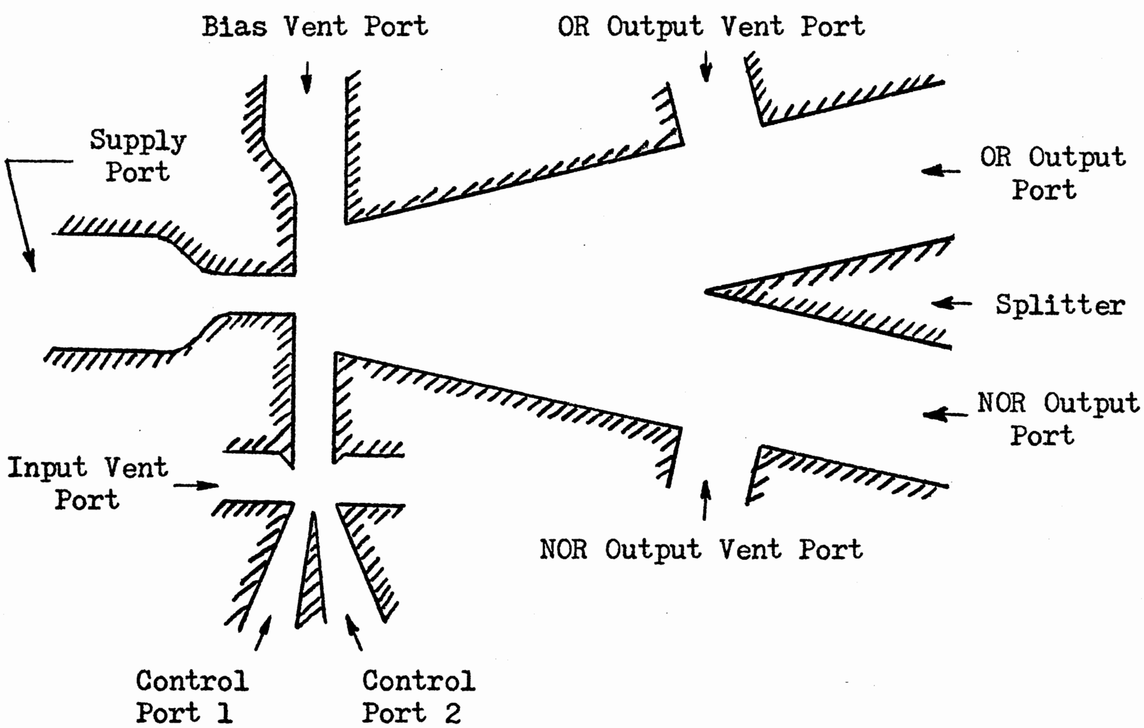


Figure 5. Monostable Fluid Amplifier With an Input Vent Port

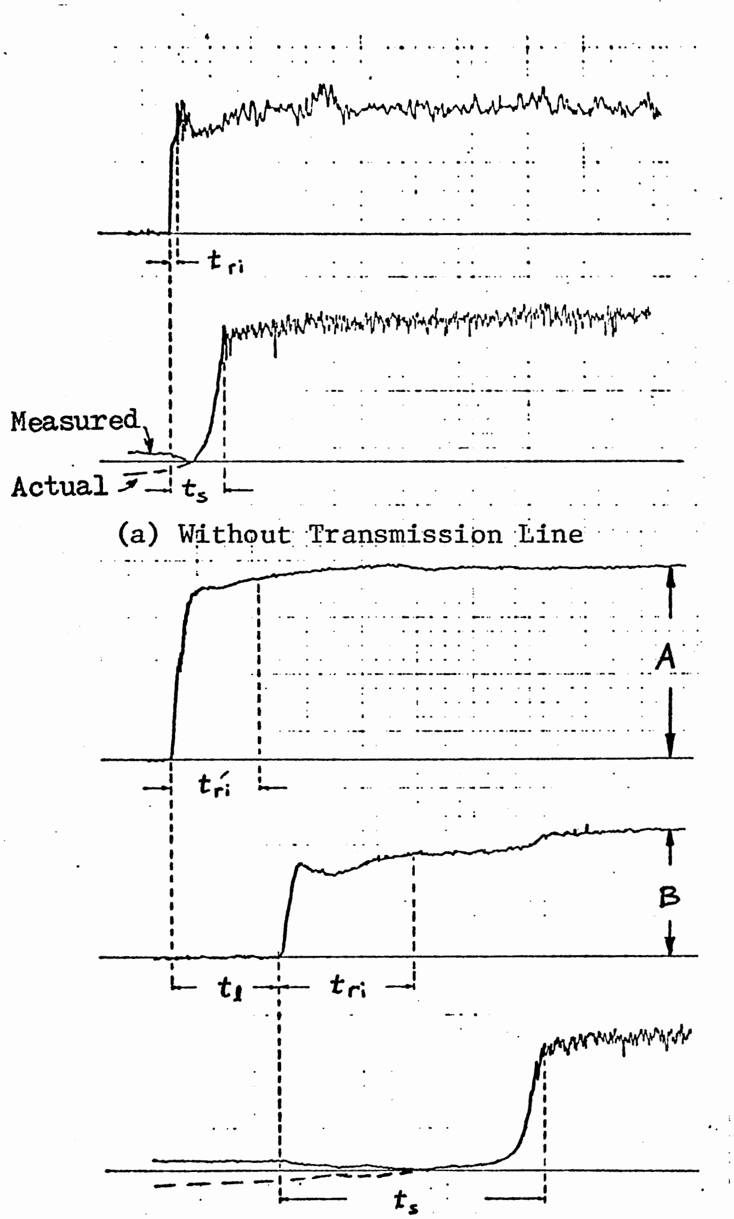


Control input pressure to amplifier

OR output velocity

$t_{ri}$ = 2.5 ms

$t_s$ = 19.3 ms

Input pressure to transmission line

Control input pressure to amplifier (B < A due to attenuation)

OR output velocity

$t'_{ri}$ = 32.8 ms

$t_\ell$ = 38.9 ms

$t_{ri}$ = 49.2 ms

$t_s$ = 94.6 ms

(b) With Transmission Line

Figure 6. Effect of Connecting Transmission Line on the Switching Time of the Monostable Fluid Amplifier for $P_{tc}$ = 0.41

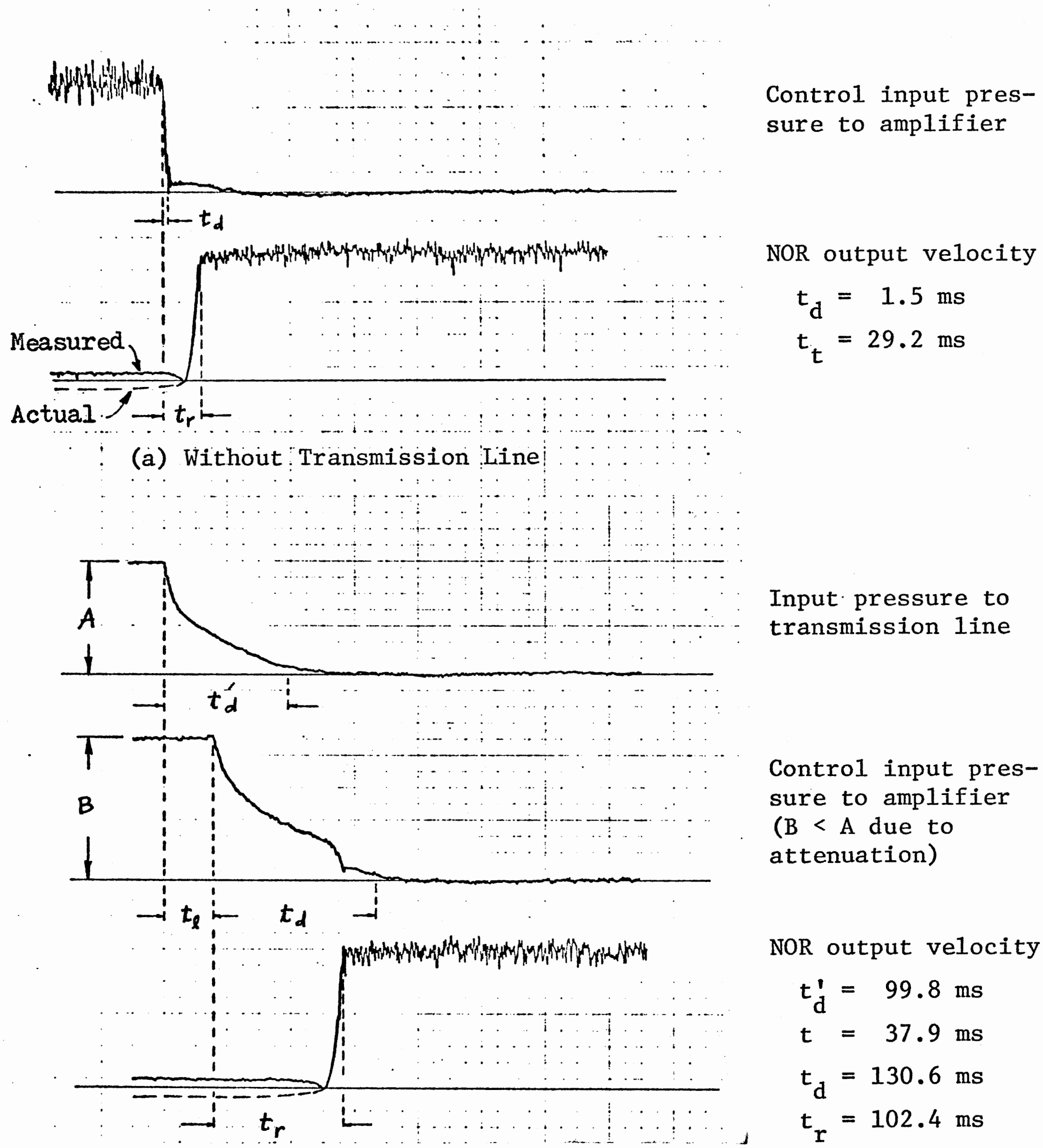


Figure 7. Effect of Connecting Transmission Line on the Return Time of the Monostable Fluid Amplifier for $P_{tc} = 0.41$

a similar effect on the return time of the amplifier (see Figures 7(a) and 7(b)).

These undesirable signal delays due to the pure time delay and the increase in the switching or return time are principal causes of hazards[6] in fluidic circuits. Hazards can result in serious malfunction of the circuit. However, no techniques for the analytical prediction of the effects of the control input pulse characteristics on the switching and return times are available in the open literature.

## 1.2 Objectives of Study

Three principal objectives were established for this study:

1. to develop an analytical dynamic model for a monostable fluid amplifier which can be used to predict the switching time, the return time, and the transient response of the amplifier to any time-varying control input signal,

2. to conduct experiments to validate the analytical model, and

3. to conduct an experimental and analytical investigation of the effects of geometric variations on the switching and return times of a monostable fluid amplifier.

The scope of this study was limited to a <u>monostable</u> fluid amplifier with (1) a single control input, (2) straight walls, and (3) a "sharp" splitter (see Figure 3); operation was limited to the turbulent flow regime. Commercial monostable fluid amplifiers normally have two or more control inputs. However, the multiple inputs are combined external to the basic monostable element and introduced through a single control port; an input vent port is provided for decoupling input signals (see Figure 5).

The geometric variations considered were limited to the following parameters: attachment wall offset, opposite wall offset and angle, splitter distance and offset, and bias vent width (see Figure 3).

## 1.3 Thesis Outline

A summary of the literature reviewed for this study is presented in Chapter II. An analytical steady-state jet reattachment model (with control flow) is developed in the first part of Chapter III. An analytical dynamic model is developed in the second part of Chapter III, based on the steady-state jet reattachment model and additional reasoning related to dynamic processes within a monostable fluid amplifier.

The experimental apparatus and procedure used to measure the switching and return times and the output transient response of a monostable fluid amplifier are discussed in Chapter IV.

Analytical predictions are compared with measurements in Chapter V to validate the analytical models (steady-state jet reattachment model and dynamic model). Also presented in Chapter V are the results of experimental and analytical investigations of the effects of geometric variations on the switching and return times of the monostable fluid amplifier. Chapter VI includes a summary, important conclusions and recommendations for future study.

ENDNOTES

[1]Numbers in brackets designate references in the Bibliography.

[2]Switching time is defined as the time elapsed from the instant the control input signal is applied to the control port (see Figures 2 and 3) until the associated output pressure (or flow rate) reaches 95 percent of its final value.

[3]Switching times in the monostable amplifier consist of the switching time from the NOR to OR output and the switching time from the OR to NOR output (see Figure 3). In this study the former is called "switching time" and the latter "return time." The return time is defined in a manner similar to that of the switching time.

[4]The rise (or decay) time is defined as the time elapsed from the first discernible change in the control input pressure (within 5 percent) until the pressure reaches 5 percent of its final value. The control input pressure was slightly increased after the jet switched to the opposite wall. Therefore, the steady-state value of the control input pressure just before switching was taken as the final value.

[5]The switching (or return) time is defined in this measurement as the time elapsed from the first discernible change in the control input pressure (within 5 percent) until the associated output velocity reaches 95 percent of its final value.

[6]The various types of hazards in fluidic circuits are discussed by Parker and Jones [49].

# CHAPTER II

# LITERATURE SURVEY

Dynamic analysis of a monostable fluid amplifier requires an understanding of both steady-state jet reattachment phenomena and dynamic flow processes inside the wall-attachment device. Previous work on these two topics is surveyed in this chapter.

In brief, a survey of the literature reveals the following:

1. No analytical studies on the dynamic behavior of a monostable fluid amplifier have been reported in the open literature.

2. Although extensive analytical and experimental work has been done on the basic jet reattachment phenomena in wall-attachment devices, no analytical model has been successful in accurately predicting the position of the jet reattachment in the presence of control flow.

3. No comprehensive experimental results have been reported in the open literature concerning the effects of the geometric variations on the switching and return times of a monostable fluid amplifier.

## 2.1 Jet Reattachment Analysis

Studies on jet reattachment have been conducted for cases with and without a control port (see Figures 2 and 9).

### 2.1.1 Jet Reattachment With No Control Port

Early jet reattachment analyses were directed towards defining the position of reattachment of a two-dimensional, incompressible, turbulent jet on an adjacent flat wall without a control port. Bourque and Newman [5] extended Dodd's analysis [13] and for the first time developed a model to predict the position of reattachment of the jet for the following two geometries:

1. A wall parallel to but offset from the nozzle centerline (Figure 8(a)).

2. A wall inclined with respect to the nozzle centerline, but with no offset (Figure 8(b)).

The agreement between predictions and experimental data was satisfactory for the first geometry (Figure 8(a)), but poor for the second geometry (Figure 8(b)).

Sawyer [57] developed a jet reattachment model for the above two geometries (Figure 8) by taking into account different rates of entrainment along the two edges of the curved jet and introducing other refinements at the cost of more complex calculations. His analytical predictions showed good agreement with experimental data in both cases.

Levin and Manion [34] extended the study of Bourque and Newman [5] to the more general case of a flat wall that is both offset and inclined. However, in order to match analytical predictions with experimental data, it was necessary to use different values of Goertler's jet spread parameter $\sigma$ for different geometries [31].

Using a nonconstant curvature for the path of the reattachment streamline (see Figure 9), Bourque [6] developed a model which is capable of predicting the reattachment position for any offset and any inclination angle of the wall. The agreement between analytical predictions and other investigators' experimental data was reasonably good over a large

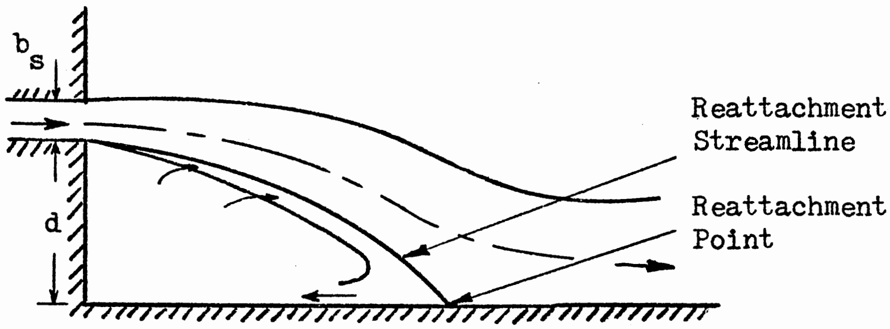


(a) An Offset Parallel Wall

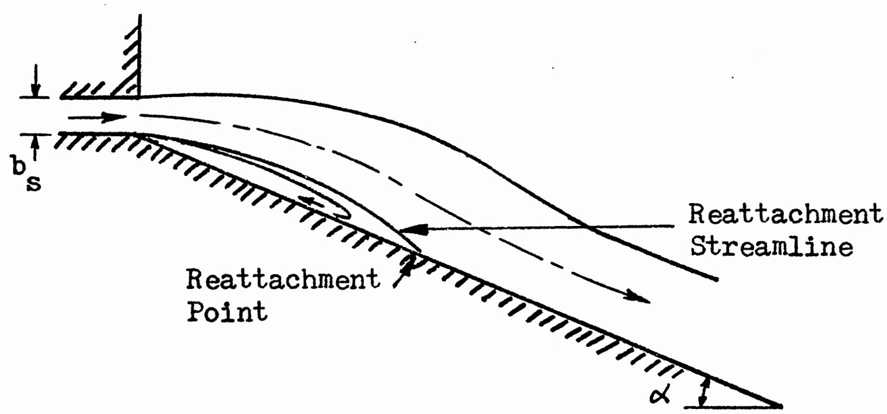


(b) An Inclined Wall With No Offset

Figure 8. Two Geometries Studied by Bourque and Newman [5]

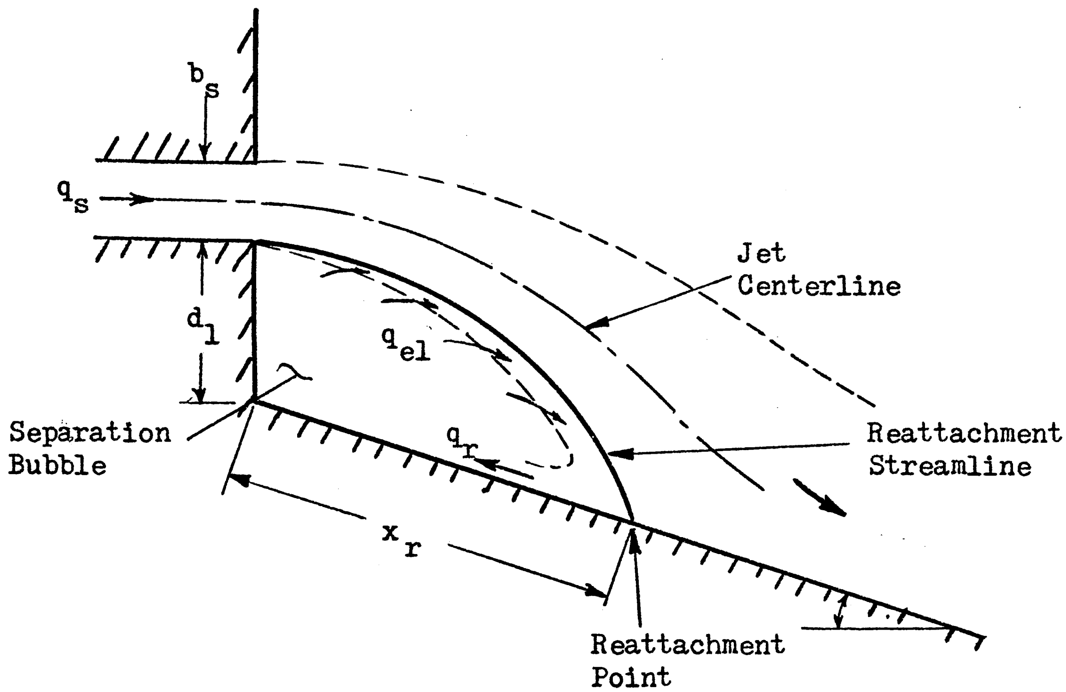


Figure 9. Bourque's Reattachment Model (With No Control Port) [6]

range of wall offsets and angles, using a constant value of the jet spread parameter (i.e., $\sigma = 10.5$).

McRee and Moses [37] studied the effect of supply nozzle aspect ratio (height to width) on the jet reattachment position with an offset parallel wall (Figure 8(a)). Their data indicated that the reattachment distance increased as the aspect ratio is decreased. But, at small values of offset and at Reynolds numbers[1] which are of practical interest in fluid amplifiers, increasing the aspect ratio above two had negligible effect on reattachment distance. In experiments with symmetrically offset parallel walls (for $d/b_s = 4$, $Re_s = 13{,}000$), Perry [51] observed that the reattachment distance is unaffected by the aspect ratio for ratios between 1 and 100. The aspect ratio of the test amplifier used in this study was chosen based on McRee and Moses' study [37].

### 2.1.2 Jet Reattachment With Control Port

Brown [9] adapted the Bourque and Newman model [5] to include the effect of control flow on the jet reattachment to the parallel offset wall. However, Brown considered only the parallel control flow (i.e., the control flow parallel to the supply flow).

Sher [59] first included the effects of the interaction of the supply jet with a perpendicularly-oriented control jet in a jet reattachment model based on the Bourque and Newman model [5]. In order to obtain reasonable agreement with experimental data, however, Sher had to use an unusually low value of the jet spread parameter, i.e., $\sigma = 4$.

J. N. Wilson [68] and M. P. Wilson [69] also included the effect of supply and control jet interaction in a reattachment model based on the

Bourque and Newman model [5]. Neither of their models was in good agreement with experimental data.

Using a modified Goertler's free jet model (including a potential core and nonsymmetric velocity profile), Kimura and Mitsuoka [30] developed a complex model where two different mechanisms of reattachment were taken into account: (1) reattachment in the zone of established flow, and (2) reattachment in the zone of flow establishment. In spite of its complexity, the model was not in good agreement with experimental data. Moreover, it was necessary to use different values of the jet spread parameter $\sigma$ for different geometries. However, their experimental data [30] are believed to be the best in thoroughness among that available in the open literature. Therefore, their experimental data are used in this thesis for the validation of the analytical steady-state jet reattachment model.

Epstein [19] developed a jet reattachment model based on Bourque's model [6]. Since he did not provide actual computed results, his model was solved numerically by the author. The computed results were compared with the experimental data of Kimura and Mitsuoka [30]; the agreement was poor for all possible values of the jet spread parameter (see Figures 30 and 31 in Chapter V). This poor agreement is believed due to his weak assumption that the control and supply jets form a <u>combined jet</u> emerging from a "hypothetical nozzle," the center of which is at the intersection of the centerlines of the supply and control nozzles. By his assumption, for one example, the width of the <u>combined jet</u> is more than two times that of the supply jet at the exit of the "hypothetical nozzle" when the control flow rate is $0.48q_s$. Evidence from flow visualization and velocity field studies [14, 26] indicates that Epstein's assumption is unreasonable. In this thesis, Epstein's "hypothetical nozzle" concept with modification (i.e., the deflected supply jet emerges from the "hypothetical nozzle" without mixing with the control jet) is used in the development of an improved steady-state jet reattachment model. Certain geometric relations used in Epstein's model are also utilized in this thesis (see Chapter III for more details).

Olson and Stoeffler [45] and Brown and Belen [8] have developed semi-empirical models to predict the effect of control flow on the reattachment location. Experimental studies in this area have been done by Foster and Jones [21], Olsen and Chin [43], and Wada and Shimizu [62].

In summary, no analytical model has been successful in accurately predicting the position of the jet reattachment in the presence of control flow. An improved steady-state jet reattachment model is developed in this thesis based on a modification of Bourque's model [6] to include the effect of control flow and the opposite wall.

## 2.2 Switching Analysis

### 2.2.1 Switching Analysis of the Bistable Amplifier

Due to the complexity of the fluid dynamic phenomena involved in the transient switching process, and the many geometric and fluid flow parameters affecting the switching, most of the early work in this area has been experimental.

Warren [32, 64] made qualitative experimental observations concerning the effects of changing parameters on the characteristics of the bistable amplifier, and classified the switching processes into three types as follows: (1) "terminated-wall" (or "end-wall"), (2) "contacting-both-walls" (or "opposite-wall"), and (3) "splitter switching." Comparin et al. [10] first measured the switching time by using a high speed motion picture camera. Keto [29] and Sarpkaya [54] conducted qualitative studies on the transient switching behavior of the bistable amplifier. Savkar et al. [55] studied the effect of varying geometric parameters on the switching times of a large scale test model of a bistable amplifier; but, these data are not of value in the present study, since the geometry of the model was somewhat different than that of the typical bistable amplifier.

Semi-empirical models for the separation time[2] of a jet in a single-wall amplifier were developed by Johnston [28], Muller [41, 42], Olson and Stoeffler [44], and J. N. Wilson [68].

Lush [35, 36] first developed a theoretical model to predict switching times for "end-wall type switching" in a bistable amplifier, which is based on the work done by Sawyer [56, 57] and Bourque and Newman [5]. His theoretically predicted switching times were about one-half the measured values. However, his thorough experimental investigation of the switching mechanism in a large-scale model provides a good qualitative description of the physical flow phenomena involved in the transient switching process of a monostable fluid amplifier. Lush's [36] experimental data on the jet deflection angle are the only comprehensive data reported in the open literature for the wall-attachment amplifier; therefore, his data are used in this thesis for comparison with analytically predicted jet deflection angles. Also, his experimental data [36] on the switching time of a bistable fluid amplifier are used in this thesis for the validation of the analytical dynamic model of a monostable fluid amplifier.

Epstein [19] also developed a theoretical model for the "end-wall type switching" process, which is based on Bourque's theory [6]. Employing an unusually large value of the jet spread parameter ($\sigma$ = 31.5), Epstein obtained good agreement with Lush's experimental data [35, 36]. As remarked by Epstein [19], however, the most serious limitation of his theory is the dependence on experiment for a determination of $\sigma$ for each geometrical condition of interest. As mentioned in section 2.1.2, his "hypothetical nozzle" concept with modification and certain geometric relations used in his model are utilized in this thesis in the dynamic modeling of a monostable fluid amplifier, too.

Ozgu and Stenning [46, 47] conducted a theoretical study on the "opposite-wall type switching" process using Simson's jet profile [60]. By including unsteady flow effects at the reattachment point on the flow rate balance in the separation bubble, they obtained good agreement with experimental data. Even though Simson's jet profile fits the measured velocity profile data better than Goertler's jet profile [31, 58], especially in the zone of flow establishment, Ozgu and Stenning obtained quite similar results for the switching time when they used Goertler's profile instead of Simson's profile. Since a monostable fluid amplifier usually has a realtively large opposite wall offset, their model [46] cannot be applicable to the dynamic modeling of the monostable amplifier. However, their study [46, 47] provides justification for using Goertler's profile in the dynamic modeling of a monostable amplifier.

Williams and Colborne [67] analyzed the splitter switching process using Simson's profile. They considered only a sharp splitter in the model.

A common limitation of the four analytical models mentioned above (Lush, Epstein, Ozgu and Stenning, Williams and Colborne) is that the models are applicable only to compute the switching time of the bistable amplifier for a given "step-type" control input signal. Moreover, only one of the three possible switching processes [32, 64] was considered in each model. In an actual device, however, more than one type of switching process could be present, simultaneously. In this thesis, an analytical dynamic model is developed for a monostable fluid amplifier, which includes all three types of switching processes implicitly and considers a time-varying control input signal. Therefore, the four models mentioned above cannot be directly used in this thesis.

Goto and Drzewiecki [23] developed a dynamic model of the bistable amplifier which allowed consideration of time-varying control input signals. They treated each channel (control, output vent, and output channels) as lumped-parameter lines and also included the effect of the momentum "peeling off" from the jet by the splitter in their model, which is based on the Bourque and Newman model [5]. Goto and Drzewiecki's model was not in good agreement with the experimental data, especially for cases where the "inactive control"[3] port was open to ambient pressure. However, Goto and Drzewiecki's treatment of the output channel inertia and splitter effects and certain numerical computation procedures used for their analytical predictions can be used in the present study (see Chapter III for more details).

### 2.2.2 Switching Analysis of the Monostable Amplifier

A difference between the switching time from the NOR to OR output and the switching time from the OR to NOR output[4] in the monostable amplifier was first observed by Steptoe [61].

Foster and Carley [20] conducted an experimental study of the effects of supply pressure, control flow,[5] the rise and decay times of the control flow pulse and output loading on the switching times for a particular monostable and a particular bistable fluid amplifier. However, the data presented by Foster and Carley are of qualitative interest only and cannot be used in the present study for comparison, since no information about the dimensions of the amplifiers were reported.

Ozgu and Stenning [48] conducted a limited experimental study of the effects of geometric variations (opposite-wall offset, splitter offset, and attachment wall shape only), supply pressure, control flow, and output loading on the switching and return times of the monostable amplifier, using a special design large-scale test model. Since the geometry of the test model used in their study is quite different from that of the typical monostable fluid amplifier (i.e., no bias vent and no output vent were provided in the opposite wall, and the attachment wall offset was slightly negative[6]), the data presented by Ozgu and Stenning are of qualitative interest only and not used in the present study for comparison.

## ENDNOTES

[1]Based on the nozzle width: $Re_s = U_s b_s / \nu$.

[2]The separation time is defined as the time elapsed from the moment when control input is applied until the jet is released from the wall.

[3]Control port 2 was called an "inactive control" port by Goto and Drzewiecki [23] when a control input signal is applied to control port 1 (see Figure 2).

[4]The switching time from the NOR to OR output and the switching time from the OR to NOR output were called "switch on delay" and "switch off delay," respectively, by Steptoe [61].

[5]Some investigators, including the author, use control pressure as the independent variable rather than control flow.

[6]The attachment wall offset is defined, in this study, as the distance $d_1$ shown in Figure 11. With this definition, the attachment wall offset of the test model used by Ozgu and Stenning [48] was $d_1 = -0.143b_s$.

## CHAPTER III

## ANALYTICAL MODELS

This chapter presents the development of an analytical model which predicts the steady-state jet reattachment position of a two-dimensional turbulent jet to an offset, inclined wall in the presence of control flow. Bourque's jet reattachment model [6] is used with necessary modifications to include the effects of control flow and the opposite wall.

This chapter also presents the development of an analytical dynamic model which predicts the switching time, the return time, and the transient response of a monostable fluid amplifier to any time-varying input signal. The steady-state jet reattachment model developed in the first part of this chapter is extended to include dynamic flow processes inside the monostable fluid amplifier.

All variables in capital letters are dimensionless. Variables with the dimension of length are normalized with respect to supply nozzle width $b_s$. Variables with the dimensions of area and volume are normalized with respect to $b_s$ and $b_s^2$, respectively, since these variables are defined per unit depth in the present model. Pressures are normalized with respect to supply jet dynamic pressure $\frac{1}{2}\rho U_s^2$, and flow rates are normalized with respect to the supply flow rate per unit depth $q_s$. Times are normalized with respect to the transport time $t_t \equiv b_s/U_s$, i.e., the time required a fluid particle moving at the supply nozzle exit velocity $U_s$ (continuity averaged) to travel a distance of one supply nozzle width.

### 3.1 Steady-State Jet Reattachment Model

#### 3.1.1 Assumptions

The following assumptions are made for the mathematical formulation of the steady-state reattachment model:

1. The jet flow is everywhere two-dimensional and incompressible.

2. Momentum interaction between the control and supply jets takes place in control volume 1 shown in Figure 10; consequently, the supply jet is deflected (angle β with respect to supply nozzle centerline). It is assumed that the deflected jet emerges from a "hypothetical nozzle" of width $b_s$, the exit of which is located at line $\overline{A_1A_2}$ in Figure 10.[1]

3. The velocity profiles at the exits of the control, supply and hypothetical nozzles are uniform.

4. The supply jet velocity profile is describable by Goertler's turbulent-jet profile [31] and is not affected by the presence of the attachment wall. That is,

$$u = \frac{1}{2} \left[\frac{3J\sigma}{(s + s_o)}\right]^{\frac{1}{2}} \quad \text{sech}^2 \left(\frac{\sigma y}{s + s_o}\right) \tag{3.1}$$

where J is the momentum flux per unit depth ($J \equiv \rho b_s U_s^2$), $s_o$ is the distance from the "hypothetical nozzle" exit to the "virtual origin" of the jet, and σ is the jet spread parameter.

5. The static pressure and wall-shear forces acting on control volume 2 in the vicinity of the reattachment point (Figure 10) are

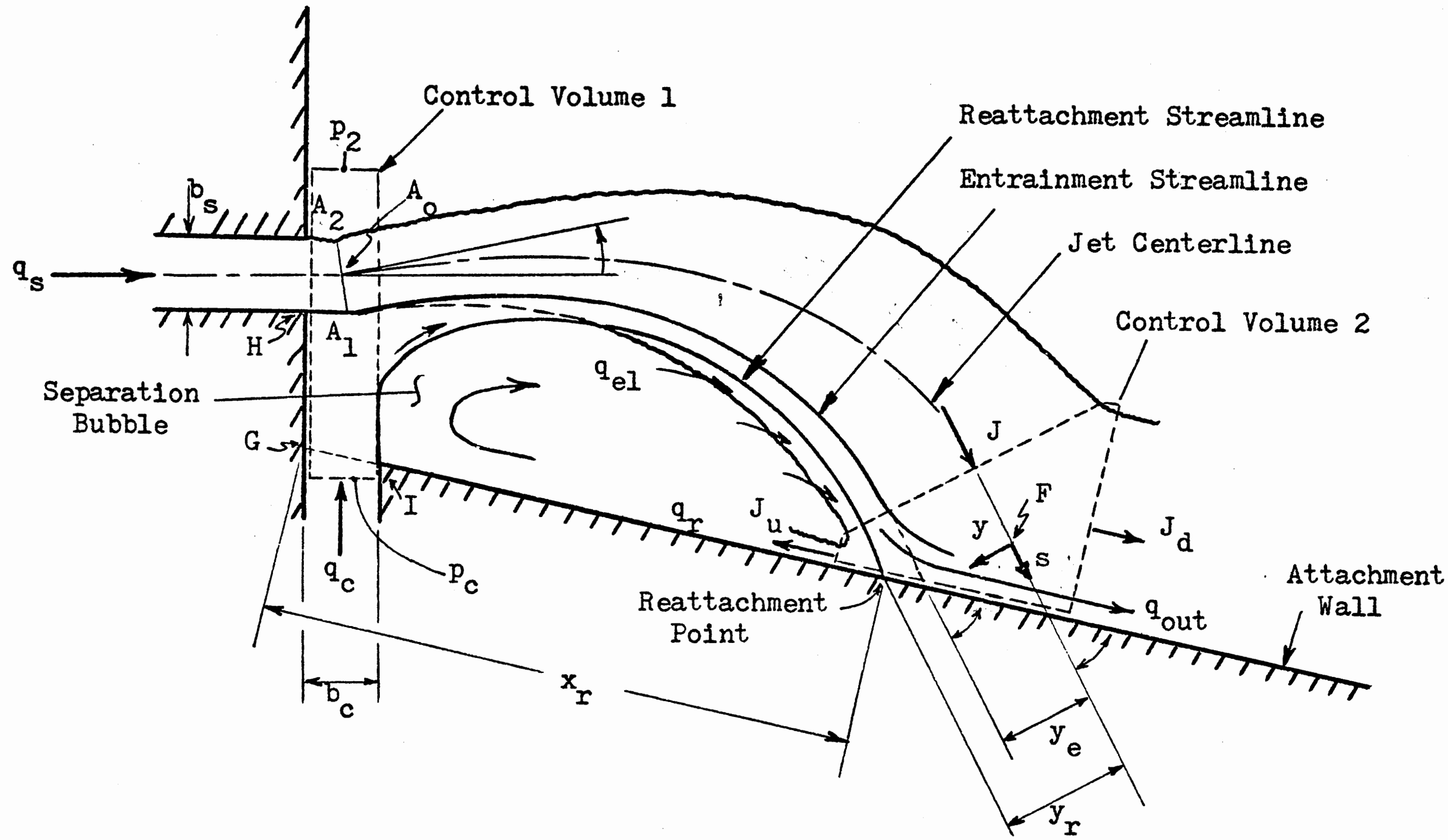


Figure 10. Steady-State Jet Reattachment With Control Flow

negligible compared to the momentum flux of the jet. That is, in the vicinity of the reattachment point, momentum is conserved.

6. The path of the entrainment streamline[2] can be represented by the equation

$$r = k \sin \left(\frac{\theta}{c}\right) \tag{3.2}$$

where k is a scale factor, $\theta$ is defined in Figure 11, and $c \equiv \frac{67}{90}$. (For derivation of this equation, see Reference [6].)

7. Flow entrainment by the concave side of the jet ceases where the extended entrainment streamline intersects the wall (i.e., at point E in Figure 10).

8. The distance measured along the entrainment streamline is approximately equal to the distance measured along the jet centerline. That is, $s_e \cong s_f$ where $s_e \equiv \widehat{A_1E}$ and $s_f \equiv \widehat{A_oF}$ (see Figure 10).[3]

9. The angle included between the extended jet centerline and the wall is approximately the same as the one included between the extended entrainment streamline and the wall ($\gamma$ in Figure 10).

10. The rate of fluid entrainment is the same on both sides of the jet.[4]

11. The supply and control jets retain their identity (i.e., there is no mixing of the jets) within control volume 1 in Figure 10.[5]

12. The net pressure force acting in the longitudinal direction (i.e., parallel to the supply nozzle centerline) on control volume 1 in Figure 10 is negligible compared to the supply jet dynamic pressure.

13. The effect of the bias vent flow momentum flux on the jet deflection is negligible; the bias vent flow is "naturally" induced by the low pressure in the region between the jet edge and the opposite wall.

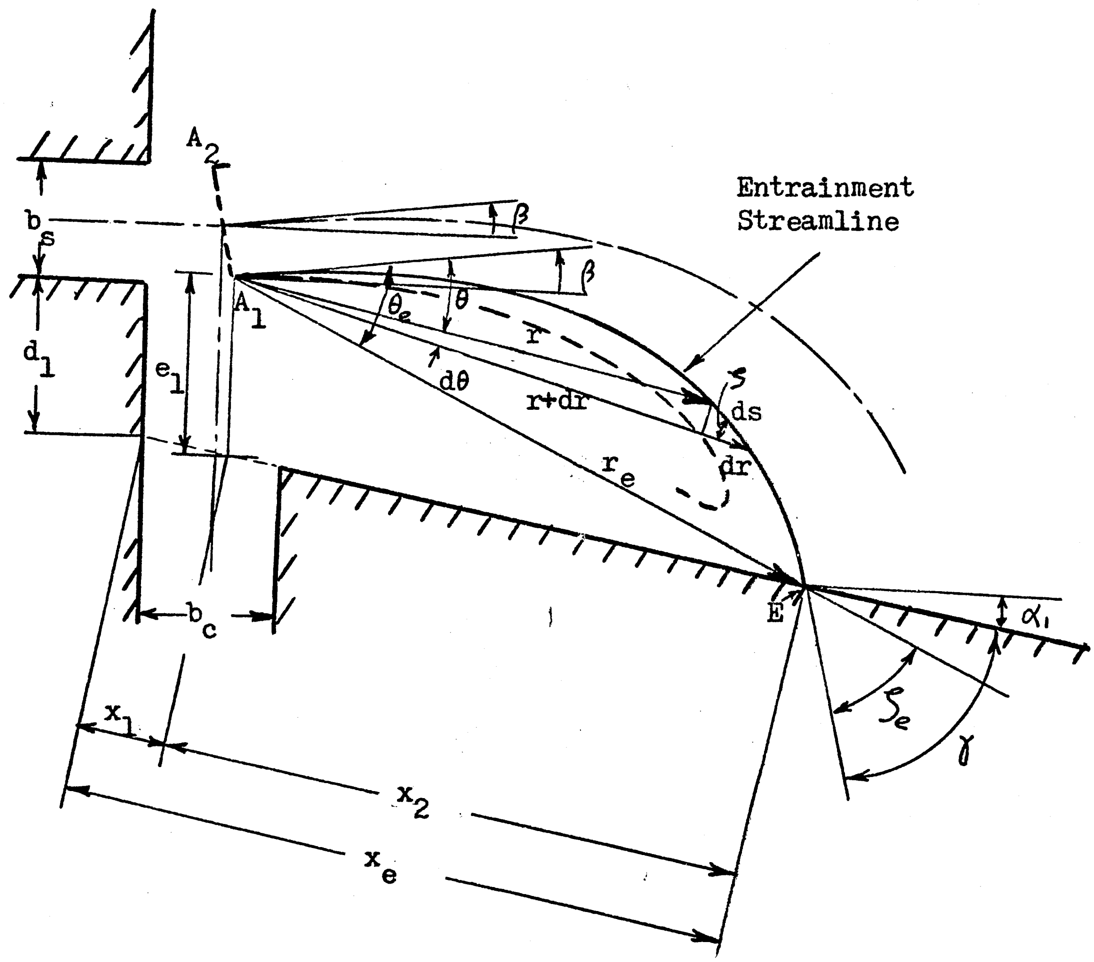


Figure 11. Geometry for the Steady-State Jet Reattachment Model

Assumptions 1, 3-5, 8-10, and 12 are either identical to or consistent with those made by Bourque [6] and Epstein [19].

The major differences between the present model and Epstein's steady-state reattachment model are: (1) in the width of the hypothetical nozzle, (2) in the definition of the separation bubble boundary, and (3) in the calculation of the jet deflection angle.[6]

Based on the assumptions mentioned above, the steady-state jet reattachment model is formulated as follows:

1. Basic equations (continuity, momentum, jet deflection) and geometric relations are written.

2. Each equation is normalized with respect to the associated variables.

3. A numerical computation procedure is established for the solution of the set of normalized equations.

### 3.1.2 Continuity Equation

The separation bubble is defined as the cavity enclosed between the entrainment streamline $\widehat{A_1E}$, attachment wall and lines $\overline{IG}$, $\overline{GH}$, and $\overline{HA_1}$ (see Figure 10). The flow balance in the separation bubble in the steady state is

$$0 = q_c - q_{out} \tag{3.3}$$

and

$$q_{out} = q_{e1} - q_r \tag{3.3a}$$

where $q_{e1}$ is the flow rate entrained by the concave side of the jet. Equations (3.3) and (3.3a), when combined and normalized, yield

$$Q_c = Q_{e1} - Q_r \tag{3.4}$$

where $Q_c \equiv q_c/q_s$; $Q_{e1} \equiv q_{e1}/q_s$; $Q_r \equiv q_r/q_s$.

Referring to Figure 10 and assumptions 4, 7 and 8, the entrained flow rate (per unit depth) can be written as

$$q_{e1} = \int_o^\infty u \, dy \Big|_{s=s_e} - \frac{q_s}{2} \tag{3.5}$$

where $s_e \cong s_f = \widehat{A_oF}$ (Figure 10).

Equations (3.1) and (3.5), when combined and normalized, yield

$$Q_{e1} = \frac{1}{2} \left(\sqrt{1 + \frac{S_e}{S_o}} - 1\right) \tag{3.5a}$$

where $S_e \equiv s_e/b_s$; $S_o \equiv s_o/b_s = \sigma/3$.[7]

Referring to Figure 10 and assumptions 4 and 8, the return flow rate (per unit depth) can be written as

$$q_r = \int_{y_r}^\infty u \, dy \Big|_{s=s_e} \tag{3.6}$$

where $y_r$ is the value of y corresponding to the location of the reattachment point (see Figure 10). Equations (3.1) and (3.6), when combined and normalized, yield

$$Q_r = \frac{1}{2} \sqrt{1 + \frac{S_e}{S_o}} \, (1 - T_r) \tag{3.6a}$$

where

$$T_r \equiv \tanh \left(\frac{\sigma Y_r}{S_e + S_o}\right) \tag{3.6b}$$

$$Y_r \equiv \frac{y_r}{b_s}.$$

Equations (3.4), (3.5a), and (3.6a), when combined, yield the steady-state relation,

$$Q_c = \frac{1}{2} (T_r \sqrt{1 + \frac{S_e}{S_o}} - 1). \tag{3.7}$$

### 3.1.3 Momentum Equation at Reattachment

Referring to Figure 10 and assumptions 4, 5, 8, and 9, the following momentum equation can be written for control volume 2 in the vicinity of the reattachment point [6]:

$$J \cos \gamma = J_d - J_u \tag{3.8}$$

or

$$J \cos \gamma = \left| \rho \int_{-\infty}^{y_r} u^2 dy - \rho \int_{y_r}^{\infty} u^2 dy \right|_{s=s_e} \tag{3.8a}$$

Equations (3.1) and (3.8a), when combined, yield

$$\cos \gamma = \frac{3}{2} T_r - \frac{1}{2} T_r^3 . \tag{3.9}$$

Solving for $T_r$ gives

$$T_r = 2 \cos (\frac{\pi + \gamma}{3}) \tag{3.10}$$

where $0 < \gamma < \frac{\pi}{2}$.

### 3.1.4 Jet Deflection

Referring to Figure 10 and assumptions 2, 3, and 11-13, the momentum equation in the longitudinal direction for control volume 1 is

$$(J + J_c)\cos\beta - \rho \frac{q_s^2}{b_s} = 0 \qquad (3.11)$$

where J and $J_c$ are momentum flux of the supply and control jets, respectively. The momentum equation in the transverse direction (i.e., perpendicular to the supply nozzle centerline) is

$$(p_c - p_2)\, b_c = (J + J_c)\sin\beta - \rho \frac{q_c^2}{b_c} \qquad (3.12)$$

where $p_c$ is the control nozzle exit pressure, and $p_2$ is the unattached-side pressure. Equations (3.11) and (3.12), when combined, yield

$$\beta = \tan^{-1}\left[\frac{(p_c - p_2)\, b_c + \rho q_c^2/b_c}{\rho q_s^2/b_s}\right] \qquad (3.13)$$

and when normalized,

$$\beta = \tan^{-1}\left[\frac{1}{2}(P_c - P_2)B_c + \frac{Q_c^2}{B_c}\right] \qquad (3.13a)$$

where $P_c \equiv p_c/\frac{1}{2}\rho U_s^2$; $P_2 \equiv p_2/\frac{1}{2}\rho U_s^2$; $B_c \equiv b_c/b_s$.

The control nozzle exit pressure $p_c$ can be obtained by writing an energy equation between sections $Z_1$ and $Z_2$ in Figure 12. Losses due to an abrupt change in the direction of the control flow are accounted for through use of a minor loss coefficient $K_L$, i.e.,

$$p_c + \frac{1}{2}\rho\left(\frac{q_c}{b_c}\right)^2 = p_{cb} + \frac{1}{2}\rho\left(\frac{q_c}{a_c}\right)^2 + K_L\left[\frac{1}{2}\rho\left(\frac{q_c}{b_c}\right)^2\right] \qquad (3.14)$$

where $a_c$ is the area (per unit depth) of the control flow passage (section $Z_2$ in Figure 12). Here, $p_{cb} = (p_1 + p_2)/2$ is assumed based on pressure distribution measurements along the attachment wall [63]. This

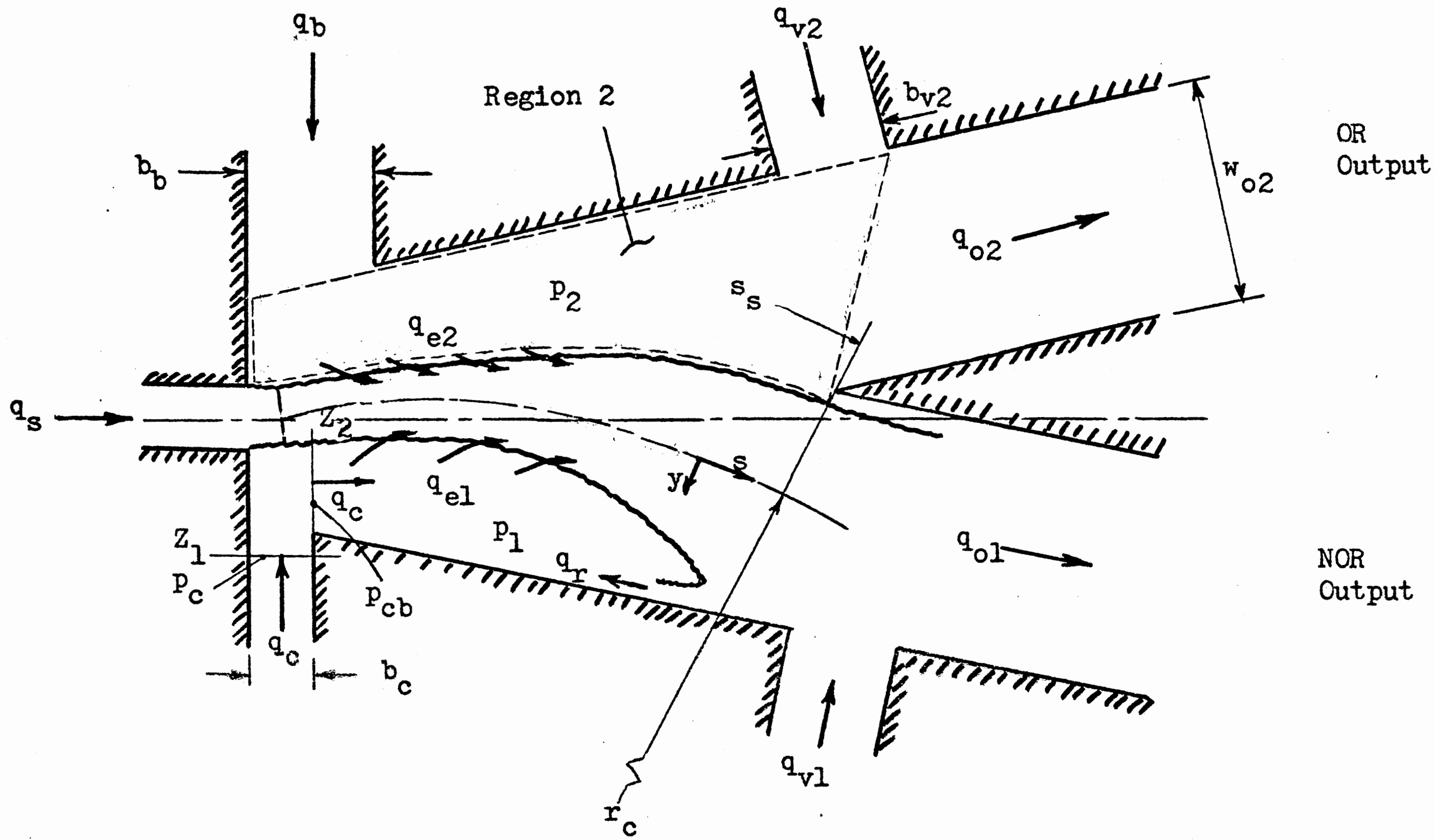


Figure 12. Overall Steady-State Flow Model for a Monostable Fluid Amplifier

assumption was also used by Goto and Drzewiecki [23] without justification. Equation (3.14), when normalized and rearranged, yields

$$P_c = P_{cb} + Q_c^2 \left(\frac{1}{A_c^2} + \frac{K_L - 1}{B_c^2}\right) \tag{3.14a}$$

where $P_{cb} \equiv p_{cb}/\frac{1}{2}\,\rho U_s^2$; $A_c \equiv a_c/b_s$. If $A_c \geq B_c$, then the term $A_c$ in Equation (3.14a) must be replaced by $B_c$, since the control jet retains its width $B_c$ within control volume 1. Then,

$$P_c = P_{cb} + K_L \left(\frac{Q_c}{B_c}\right)^2 . \tag{3.14b}$$

From Figure 13,

$$A_c = \frac{1}{2} B_c \sin\beta + (D_1 + \frac{1}{2} + B_c \tan\alpha_1) \cos\beta - \frac{1}{2} \tag{3.15}$$

where $D_1 \equiv d_1/b_s$.

Various investigators have used Euler's equation written in the direction (y) normal to the jet centerline to calculate the pressure difference $\Delta p$ across the jet [19, 23, 36, 39, 57, 62]. Referring to Figure 12,

$$\frac{\partial p}{\partial y} = \frac{\rho}{r_c} \left(\frac{q_s}{b_s}\right)^2$$

$$\Delta p \cong \frac{\rho\, q_s^2}{r_c\, b_s}$$

or

$$\Delta p \cong p_2 - p_1 \cong \frac{J}{r_c}$$

where $p_1$ is the average pressure in the separation bubble, $p_2$ is the average pressure in region 2 shown in Figure 12 (called the unattached-

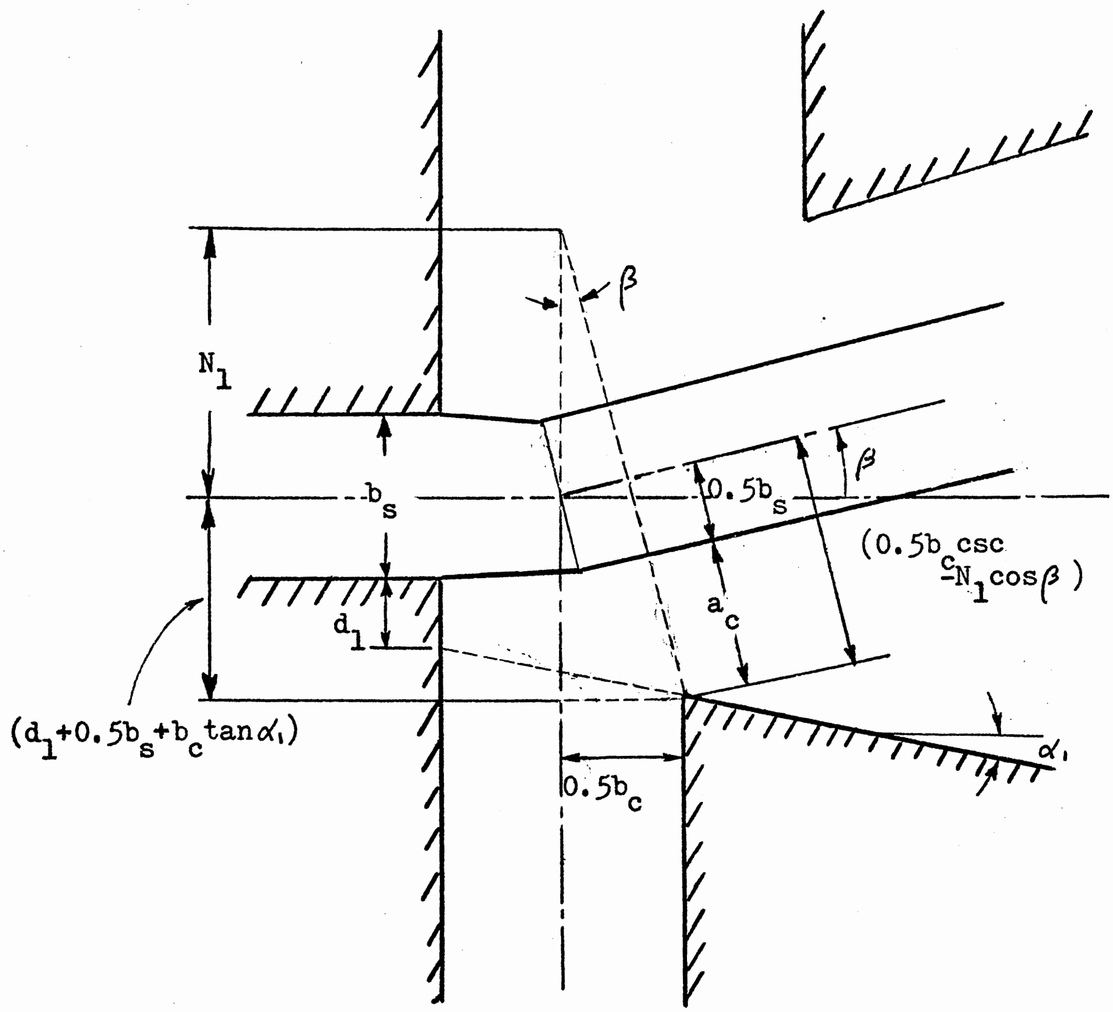


Figure 13. Control Flow Passage Width

side pressure), J is the momentum flux of the supply jet, and $r_c$ is the average radius of curvature of the jet centerline. Equation (3.16), when normalized, yields

$$P_1 \cong P_2 - \frac{2}{R_c} \tag{3.16a}$$

where $P_1 \equiv p_1/\frac{1}{2}\,\rho U_s^2$; $R_c \equiv r_c/b_s$.

The steady-state flow rate balance for the control volume designated as region 2 in Figure 12 is

$$\Sigma q = (q_b + q_{v2} - q_{o2}) - q_{e2} = 0 \tag{3.17}$$

The flow rates into the region ($q_b$, $q_{v2}$, $q_{o2}$) can be evaluated based on the average pressure in the region $p_2$. That is,

$$q_b = b_b\sqrt{\frac{-2p_2}{\rho}} \tag{3.17a}$$

$$q_{v2} = b_{v2}\sqrt{\frac{-2p_2}{\rho}} \tag{3.17b}$$

$$q_{o2} = -w_{o2}\sqrt{\frac{-2p_2}{\rho}} \tag{3.17c}$$

Here, it is assumed that the discharge coefficients for Equations (3.17a) through (3.17c) are all equal to unity and that the ambient pressure is zero and the OR output channel is open to the ambient. The flow rate $q_{e2}$ is entrained by the convex side of the jet. That is,

$$q_{e2} = \int_0^\infty u\,dy\Big|_{s=s_s} - \frac{q_s}{2} \tag{3.17d}$$

Equations (3.1) and (3.17) through (3.17d), when normalized and combined, yield

$$P_2 = - \left[\frac{Q_{e2}}{B_b + B_{v2} + W_{o2}}\right]^2 \tag{3.18}$$

where

$$Q_{e2} \equiv \frac{q_{e2}}{q_s} = \frac{1}{2} \left(\sqrt{1 + \frac{S_s}{S_o}} - 1\right),$$

and $B_b \equiv b_b/b_s$; $B_{v2} \equiv b_{v2}/b_s$; $W_{o2} \equiv w_{o2}/b_s$; $S_s \equiv s_s/b_s$. Equation (3.18) is valid for the case with the splitter. If the splitter is removed, there is less blockage of the flow into the region between the opposite wall and the jet edge. Therefore, it is reasonable to assume that $P_2 \cong 0$.

### 3.1.5 Geometric Relations

Referring to Figure 11, the following geometric relations can be written in normalized form:

$$R_e = K \sin \left(\frac{\theta_e}{c}\right) \tag{3.2a}$$

$$\alpha_1 + \gamma = \zeta_e + \theta_e - \beta \tag{3.19}$$

$$E_1 = D_1 + X_1 \sin\alpha_1 + \frac{1}{2} (1 - \cos\beta) \tag{3.20}$$

or

$$E_1 = R_e \sin (\theta_e - \beta - \alpha_1) \sec\alpha_1 \tag{3.21}$$

$$X_1 = \frac{1}{2} (B_c + \sin\beta) \sec\alpha_1 \tag{3.22}$$

$$X_2 = R_e \cos (\theta_e - \beta) \sec\alpha_1 \tag{3.23}$$

$$X_e = X_1 + X_2 \tag{3.24}$$

where

$E_1 \equiv e_1/b_s$; $R_e \equiv r_e/b_s$;

$K \equiv k/b_s$ (scale factor); $X_1 \equiv x_1/b_s$;

$X_2 \equiv x_2/b_s$; $X_e \equiv x_e/b_s$;

$c \equiv 67/90$.

Also, from Figure 11,

$$ds = [(rd\theta)^2 + (dr)^2]^{\frac{1}{2}} \tag{3.25}$$

Equations (3.2) and (3.25), when combined and integrated, yield

$$S_e = K \int_o^{\theta_e/c} [1 - (1 - c^2) \sin^2 (\frac{\theta}{c})]^{\frac{1}{2}} d(\frac{\theta}{c}) \tag{3.26}$$

where $S_e \equiv s_e/b_s$ and $s_e \equiv \widehat{A_1E}$. Equation (3.26) is an elliptic integral of the second kind which is well tabulated. For computational purposes, Equation (3.26) may be approximated as[8]

$$S_e \cong K [0.62 (\frac{\theta_e}{c}) + 0.38 \sin (\frac{\theta_e}{c})]. \tag{3.26a}$$

From Figure 11,

$$\zeta_e = \tan^{-1} (\frac{rd\theta}{dr} \Big|_{\theta=\theta_e}). \tag{3.27}$$

Equations (3.2) and (3.27), when combined, yield

$$\zeta_e = \tan^{-1} (c \tan \frac{\theta_e}{c}). \tag{3.27a}$$

Referring to Figures 10 and 11 and assumptions 8 and 9, the reattachment distance is

$$X_r = X_e - (Y_r - Y_e) \csc\gamma \tag{3.28}$$

where $X_r \equiv x_r/b_s$, $Y_e \equiv y_e/b_s$, and $y_e$ is the value of y corresponding to the location of point E (Figure 10).

From Equation (3.6b):

$$Y_r = (\frac{S_e + S_o}{\sigma}) \tanh^{-1} T_r. \tag{3.29}$$

By the definition of the entrainment streamline, the flow rate between the jet centerline and the entrainment streamline is equal to one-half the flow rate at the supply nozzle exit. Thus, from assumptions 3 and 4,

$$\int_o^{y_e} u \, dy \bigg|_{s=s_e} = \frac{1}{2} U_s b_s. \tag{3.30}$$

Equations (3.1) and (3.30) yield

$$\tanh (\frac{\sigma y_e}{s_e + s_o}) = \frac{s_o}{s_e + s_o}$$

or

$$Y_e = (\frac{S_e + S_o}{\sigma}) \tanh^{-1} (\sqrt{\frac{S_o}{S_e + S_o}}) \tag{3.30a}$$

Equations (3.28), (3.29), and (3.30a) yield

$$X_r = X_e - \frac{S_e + S_o}{\sigma} [\tanh^{-1} T_r - \tanh^{-1} \sqrt{\frac{S_o}{S_e + S_o}}] \operatorname{scs}\gamma. \tag{3.31}$$

The average radius of curvature of the jet centerline is assumed to be the radius $r_c$ of the circular arc which is tangent to the jet centerline at the hypothetical nozzle exit and which passes at a distance $y_p$ from point P (see Figure 14).[9]

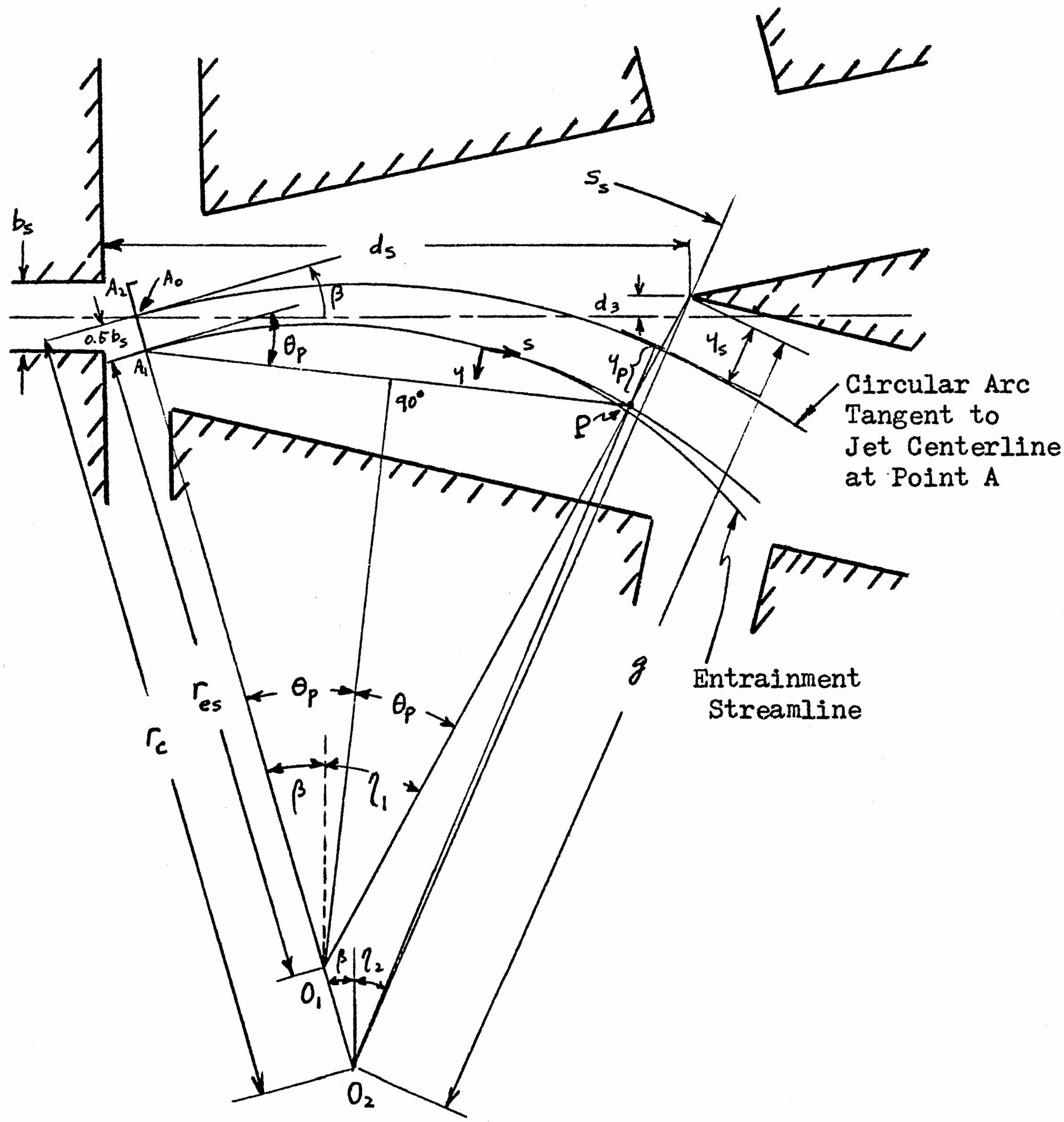


Figure 14. Geometry of Jet Centerline Curvature

That is,

$$R_c = R_{es} + \frac{1}{2}\,[1 + \frac{(\frac{1}{2} - Y_p)(2R_{es} + \frac{1}{2} - Y_p)}{R_{es}\,(\cos 2\theta_p - 1) - \frac{1}{2} + Y_p}] \tag{3.32}$$

where $R_c \equiv r_c/b_s$; $R_{es} \equiv r_{es}/b_s$; $Y_p \equiv y_p/b_s$. The distance $Y_p$ can be obtained by the definition of the entrainment streamline (refer to Equation (3.30a)), i.e.,

$$Y_p = (\frac{S_p + S_o}{\sigma})\,\tanh^{-1}\,(\sqrt{\frac{S_o}{S_p + S_o}}) \tag{3.33}$$

where $S_p \equiv s_p/b_s$; $s_p = \widehat{A_1P}$ (Figure 14). Referring to Figures 11 and 14, the radius $r_{es}$ of the circular arc which is tangent to the entrainment streamline at point $A_1$ can be expressed as

$$r_{es} = [\frac{ds}{d(\theta + \zeta)}]_{\theta=0} = [\frac{ds/d\theta}{1 + d\zeta/d\theta}]_{\theta=0} \tag{3.34}$$

Equations (3.2), (3.25), (3.34), and $\zeta = \tan^{-1}(\frac{rd\theta}{dr})$, when combined and normalized, yield

$$R_{es} = \frac{K}{2c}. \tag{3.34a}$$

From Figure 14, the following relations can also be written:

$$\eta_1 = \tan^{-1}\,[\frac{D_s - \frac{1}{2}B_c - (R_{es} + \frac{1}{2})\sin\beta}{(R_{es} + \frac{1}{2})\cos\beta + D_3}] \tag{3.35}$$

$$\theta_p = \frac{1}{2}\,(\beta + \eta_1) \tag{3.36}$$

$$S_p = 2\,R_{es}\theta_p \tag{3.37}$$

$$\eta_2 = \tan^{-1}\,[\frac{D_s - \frac{1}{2}B_c - R_c\sin\beta}{R_c\cos\beta + D_3}] \tag{3.38}$$

$$S_s = R_c\ (\beta + \eta_2) \tag{3.39}$$

where $D_s \equiv d_s/b_s$; $D_3 \equiv d_3/b_s$.

### 3.1.6 Numerical Computation Procedure

Given the geometry and control flow rate $Q_c$, any steady-state value of a variable (e.g., steady-state jet reattachment distance, jet deflection angle, etc.) can be obtained by numerically solving the basic equations and the geometric relations derived above. The following are the list of the basic equations and the geometric relations to be solved: Equations (3.2a), (3.7), (3.10), (3.13a), (3.14a) or (3.14b), (3.15), (3.16a), (3.18) through (3.24), (3.26a), (3.27a), (3.31) through (3.33), (3.34a), and (3.35) through (3.39). The detailed computation procedure and computer program listing is given in Appendix C.

The analytical predictions of the steady-state jet reattachment distance and the jet deflection angle are compared with experimental data in Chapter V.

## 3.2 Dynamic Model

For convenience, the transient switching process is divided into two phases: the process before the jet reattaches to the opposite wall is called phase I, and the process after the jet reattaches to the opposite wall is called phase II. The criteria for the end of phase I are given in assumption 6 in section 3.2.1.

### 3.2.1 Assumptions

The following assumptions are made for the mathematical formulation of the dynamic model:[10]

1. The transient switching process can be treated as quasi-steady.

2. The variation in the supply flow rate caused by changes in the supply nozzle exit pressure is negligible.

3. When the jet reattaches on the output vent area, a "hypothetical reattachment point" exists between points $K_1$ and $K_2$ (Figure 15), and momentum is still conserved in the vicinity of the "hypothetical reattachment point" (see assumption 5 in section 3.1.1).

4. The edge of the jet is assumed to be the locus of points at which the jet axial velocity component is 0.1 of the local centerline velocity. The calculation of the flow passage width $a_v$ (Figure 17) and the flow passage width $a_w$ (Figure 19) between the jet edge and the opposite wall is based on this assumption.

5. The dynamic pressures at the inlet of the OR and NOR output channels are one-half of the average momentum flux impinging on the inlet area of the OR and NOR output channels, respectively (see Equations (3.58) and (3.59) in section 3.2.3.6) [23].

6. Phase I ends when the following conditions are met: (a) the jet centerline passes the splitter point such that $y_s \geq d_2 - d_1 - d_3$ (see Figure 16), and (b) the flow rate at the exit plane of the OR output channel reaches 95 percent of the steady-state value corresponding to the total pressure at the inlet of the OR output channel at $y_s = d_2 - d_1 - d_3$ (see Equation (3.64) in section 3.2.3.7).[11]

7. The transition between the end of phase I and the beginning of phase II is instantaneous. That is, the jet switches over and reattaches to the opposite wall instantaneously when the conditions given in assumption 6 are met. During the transition, the hypothetical nozzle center shifts from the intersection of centerlines of supply and control nozzles

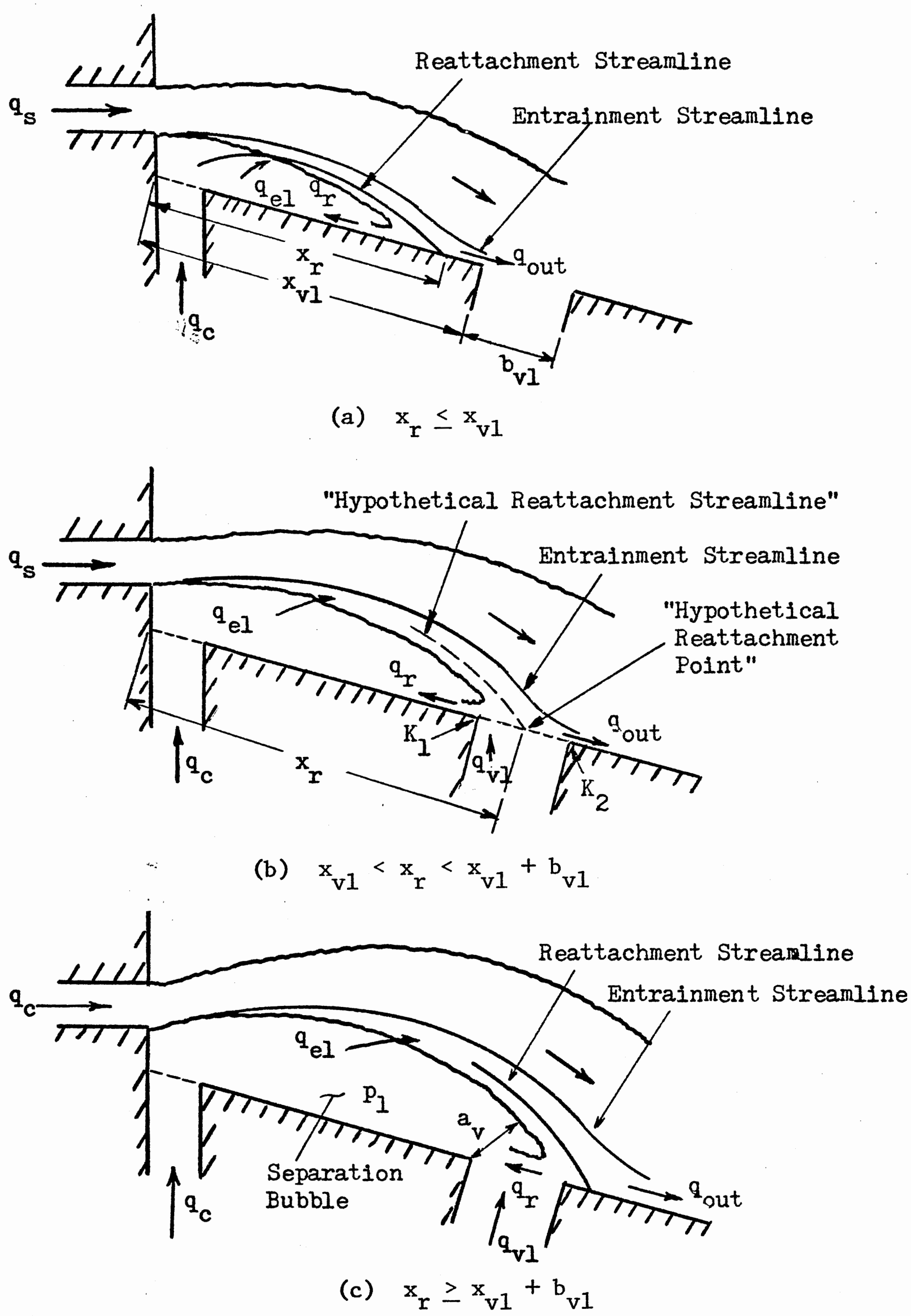


Figure 15. Flow Model for the Separation Bubble

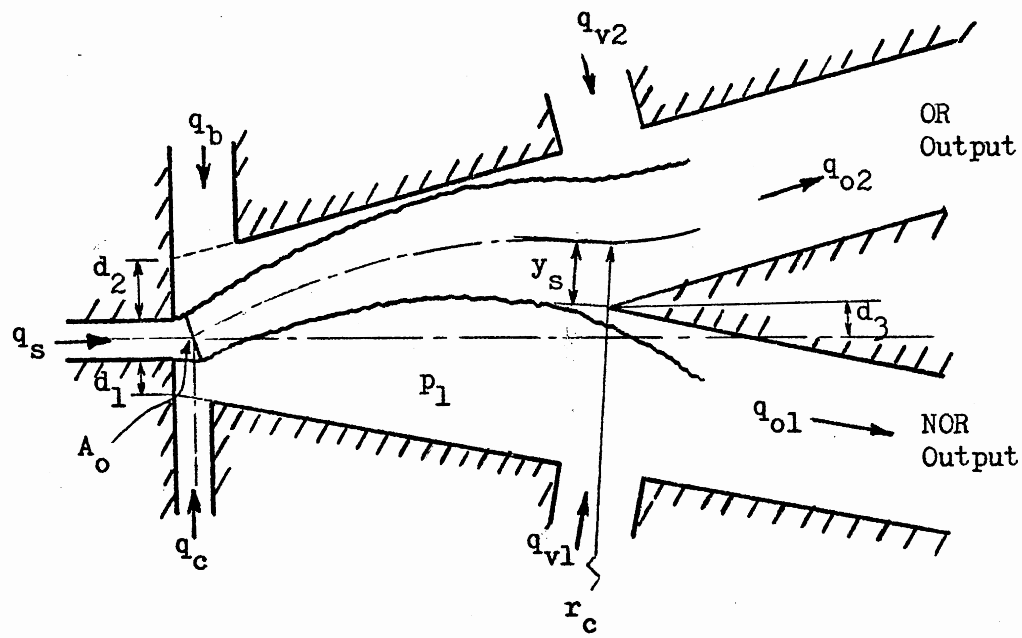


(a) End of Phase I

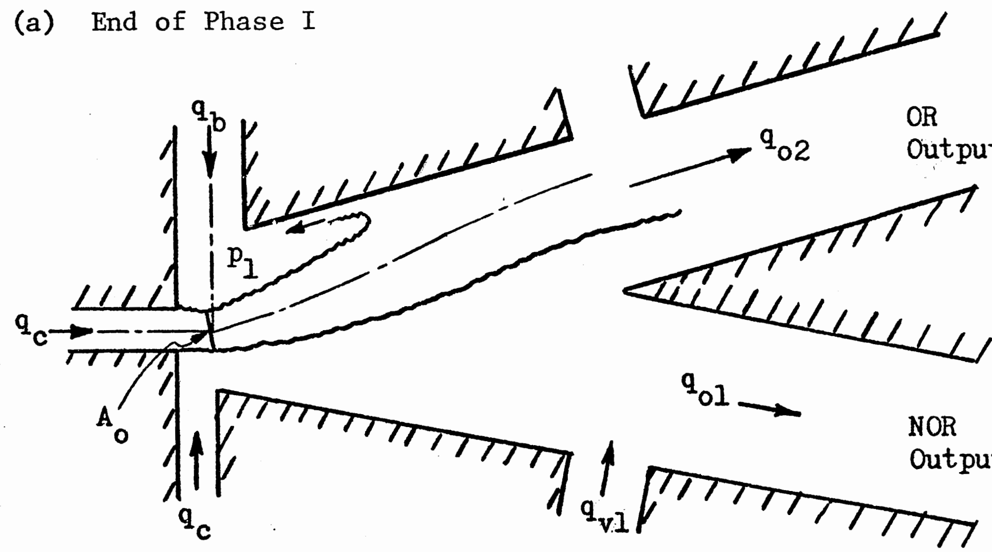


(b) Beginning of Phase II

Figure 16. Transition Between Phase I and Phase II

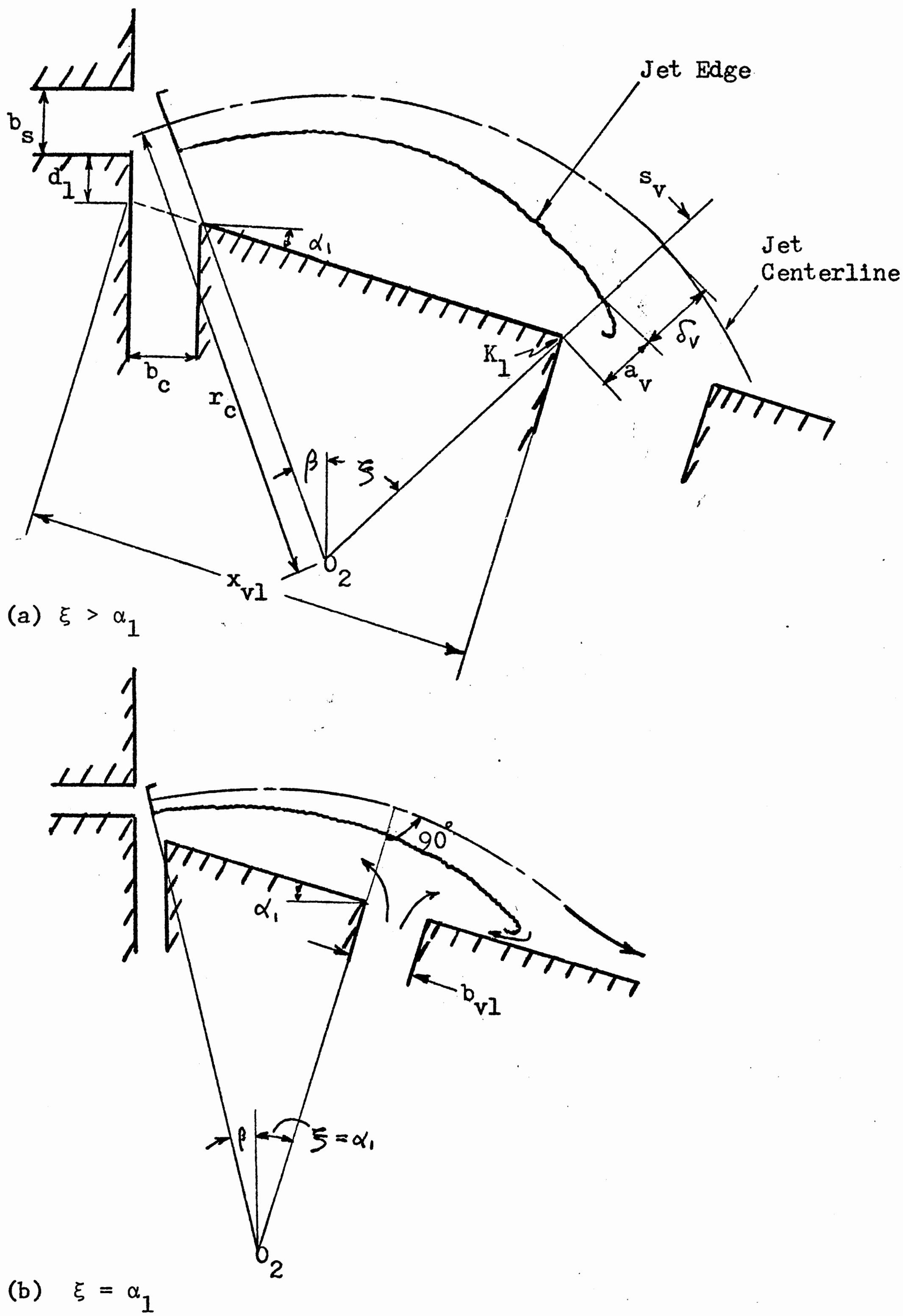


Figure 17. Output Vent Flow Passage Width

to the intersection of centerlines of supply and bias vent nozzles. Initial conditions for phase II are those which are associated with the steady-state reattachment of the jet on the opposite wall for $p_{tc}$ which exists at the end of phase I.

Remark: Assumptions 6 and 7 are made for the switching process from the NOR to OR output. Assumptions similar to those are also made for the switching process from the OR to NOR output (i.e., for the return process).

### 3.2.2 Discussion of Assumptions in Section 3.2.1

This section contains a discussion of the selected assumptions made in the preceding section:

Assumption 1. The following specific assumptions directly result from the quasi-steady assumption:

(1) The time rate of change of momentum within control volume 2 (Figure 10) is assumed to be negligible.

(2) Equation (3.16) in section 3.1.4 is assumed to hold, but it is continuously up-dated at each time step in the dynamic simulation.

(3) Assumptions 1 through 13, which are made for the steady-state jet reattachment model in section 3.1.1, are also valid at each time step in the dynamic simulation.

For the quasi-steady assumption to be valid, the downstream tarvel velocity of the jet reattachment point along the wall should be very slow compared to the jet velocity. In other words, the switching time should be much larger than the fluid particle transport time through the amplifier, i.e.,

$$\frac{d_s}{U_s} << t_s$$

where $d_s$ is the splitter distance downstream of the supply nozzle exit, $U_s$ is the continuity averaged velocity at the supply nozzle exit, and $t_s$ is the switching time [19, 22, 26]. In normalized form, this condition becomes

$$D_s << \tau_s$$

where $D_s \equiv d_s/b_s$; $\tau_s \equiv U_s t_s/b_s$. This quasi-steady assumption can be justified only a posteriori. Analytical predictions and experimental results indicate that the normalized switching time is much larger than $D_s$; for the geometry chosen in this study, $\tau_s$ is at least of the order of 20 times $D_s$ (see Figure 34 in Chapter V).

Assumption 3. Wada et al. [63] showed in their flow visualization study that after the jet reaches the output vent edge (point $K_1$ in Figure 15), the jet does not move downstream of the vent edge until the separation bubble grows large enough to make the jet jump over the vent and reattach to the wall downstream of the vent.

A rigorous analysis of the fluid dynamic process near the vent would be quite complex. For simplicity in this study it is assumed that a "hypothetical reattachment point" exists between points $K_1$ and $K_2$ (Figure 15), as if the vent is a solid wall.

Assumption 4. With jet edges assumed in this way, 95 percent of the total volume flow and 99.6 percent of the total momentum flux pass along the jet. From Goertler's jet profile (Equation (3.1)), the jet half-width becomes $\delta = 1.825 \left(\frac{s + s_o}{\sigma}\right)$.

Assumption 6. Assumption 6(a) is based on the experimental study of the static switching characteristics [63] which showed that the larger the opposite wall offset, the more the jet is required to pass the splitter point before the jet reattaches to the opposite wall. Assumption 6(b) is based on the effect of the fluid inertia in the output channel. It was found during the preliminary stage of this study that for a relatively high control pressure, the analytically predicted output flow rate was still negative (note the sign convention of the output flow given in Figure 12) when $y_s = d_2 - d_1 - d_3$. In other words, because of the fluid inertia in the OR output channel, the flow which was initially induced into the internal region of the amplifier was not completely reversed, even though the jet centerline passed the splitter point such that $y_s = d_2 - d_1 - d_3$. It is assumed that the flow in the OR output channel must be completely reversed and reach the specified level before the jet reattaches to the opposite wall.

Assumption 7. This assumption is not strictly correct. However, it is believed that it takes a small time compared to the switching time for the jet to move from its position at the end of phase I to the position at the beginning of phase II.

Assumptions 3 through 7, like assumption 1, can be justified only *a posteriori*. The analytically predicted switching times are in good agreement with experimental data for various offset $d_1$'s and $d_2$'s. Although the good agreement does not justify these assumptions on an individual basis, it suggests justification on a collective basis.

### 3.2.3 Analysis of Phase I

3.2.3.1 Continuity Equation. Referring to Figure 15, the growth rate of the separation bubble is:

$$\frac{dv}{dt} = \begin{cases} q_c - q_{out} & \text{for } x_r \leq x_{v1} \\ q_c - q_{out} + q_{v1} & \text{for } x_r > x_{v1} \end{cases} \tag{3.40}$$

where

$$q_{out} = q_{e1} - q_r.$$

The flow from the output vent into the separation bubble is restricted by an orifice between the vent edge and the jet edge (i.e., $a_v$ in Figure 15(c)). Assuming the discharge coefficient of the orifice is unity and the ambient pressure is zero,

$$q_{v1} = a_v \sqrt{-\frac{2p_1}{\rho}} \tag{3.41}$$

Equations (3.5a), (3.6a), (3.40), and (3.41), when normalized, yield

$$\frac{dV}{d\tau} = \begin{cases} Q_c + \frac{1}{2}\left(1 - T_r\sqrt{1 + \frac{S_e}{S_o}}\right) & \text{for } X_r \leq X_{v1} \\ Q_c + \frac{1}{2}\left(1 - T_r\sqrt{1 + \frac{S_e}{S_o}}\right) + A_v\sqrt{-P_1} & \text{for } X_r > X_{v1} \end{cases} \tag{3.42}$$

where

$$V \equiv v/b_s^2;\ \tau \equiv U_s t/b_s;\ Q_c \equiv q_c/q_s;$$

$$A_v \equiv a_v/b_s;\ X_r \equiv x_r/b_s;\ X_{v1} \equiv x_{v1}/b_s;$$

$$P_1 \equiv p_1/\tfrac{1}{2}\rho U_s^2.$$

From Figure 16(a),

$$A_v = R_c - \Delta_v - (X_{v1} \cos\alpha_1 - R_c \sin\beta - \frac{1}{2} B_c) \csc\xi \tag{3.43}$$

where

$$\xi \equiv \tan^{-1} [\frac{X_{v1} \cos\alpha_1 - R_c \sin\beta - \frac{1}{2} B_c}{R_c \cos\beta - X_{v1} \sin\alpha_1 - (D_1 + \frac{1}{2})}]$$

$$S_v \equiv \frac{s_v}{b_s} = R_c \ (\beta + \xi)$$

$$\Delta_v \equiv \frac{\delta_v}{b_s} = 1.825 \ (\frac{S_v + S_o}{\sigma})$$

If the reattachment point moves far downstream of the output vent, the separation bubble becomes completely open to the vent and the flow through the vent is restricted only by the vent width $b_{v1}$. In the analytical model, this case is represented as follows: the term $A_v$ in Equation (3.42) is replaced by $B_{v1} \equiv b_{v1}/b_s$ if $\xi \leq \alpha_1$ (see Figure 16b).

3.2.3.2 Momentum Equation at Reattachment. As the control flow is increased, the momentum flux which strikes the attachment wall at angle $\gamma$ is reduced by the amount of the momentum separated by the splitter (see Figure 18). This splitter effect may be included in Equation (3.8) as follows:

$$(J - J_s) \cos\gamma = J_d - J_u \tag{3.44}$$

or

$$[J - \rho \int_{-\infty}^{y_s} u^2 \, dy \Big|_{s=s_s}] \cos\gamma = [\rho \int_{y_s}^{y_r} u^2 \, dy - \rho \int_{y_r}^{\infty} u^2 \, dy]_{s=s_e} \tag{3.44a}$$

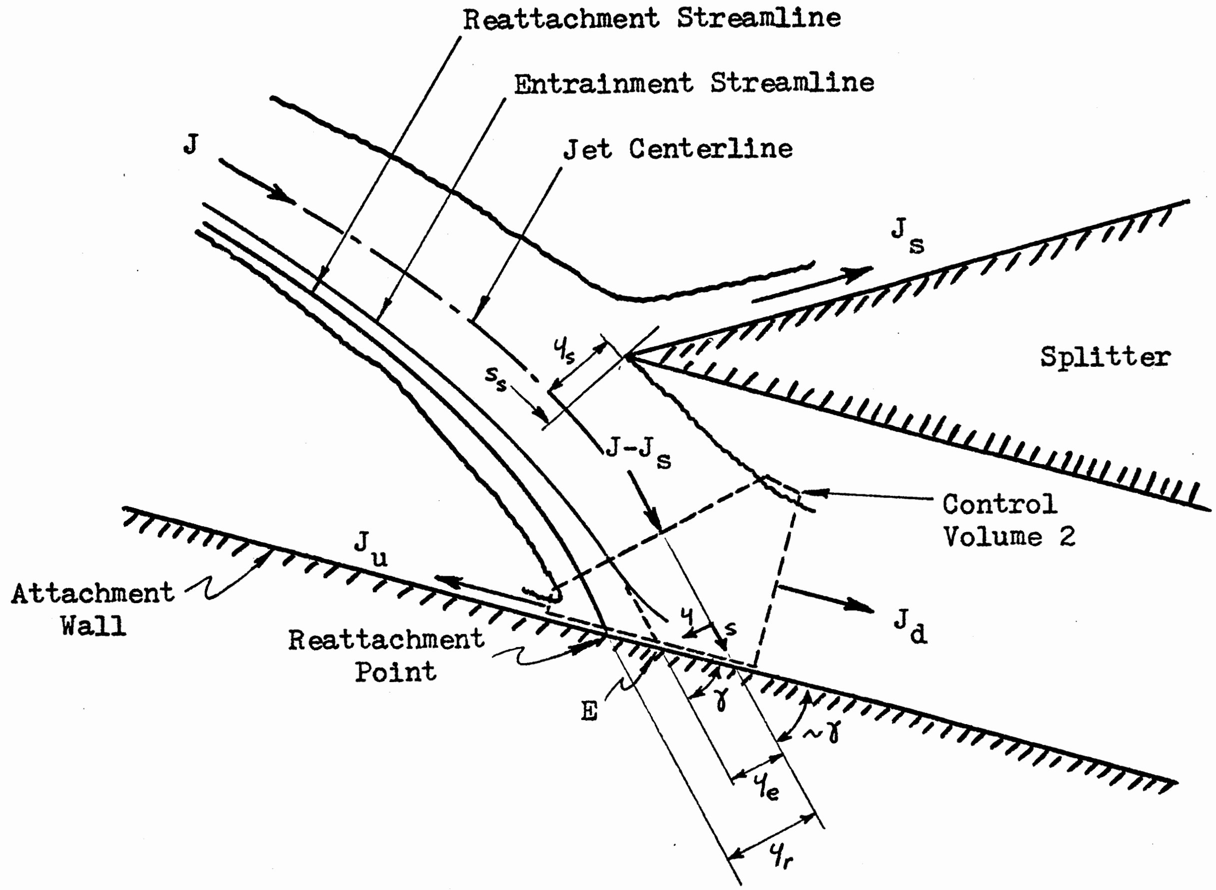


Figure 18. Momentum Balance in the Vicinity of the Reattachment Point

Equations (3.1) and (3.44a), when combined and normalized, yield

$$(1 - \frac{3}{2} T_s + \frac{1}{2} T_s^3) \cos\gamma = -1 + 3T_r - T_r^3 - \frac{3}{2} T_s + \frac{1}{2} T_s^3 \quad (3.45)$$

where

$$T_s \equiv \tanh (\frac{\sigma Y_s}{S_s + S_o}); \quad T_r \equiv \tanh (\frac{\sigma Y_r}{S_e + S_o})$$

$$Y_s \equiv y_s/b_s; \quad Y_r \equiv y_r/b_s; \quad S_s \equiv s_s/b_s.$$

Solving Equation (3.45) for $T_r$, we get

$$T_r = 2\cos [\frac{\pi + \cos^{-1} (\lambda/2)}{3}] \quad (3.46)$$

where

$$\lambda = (1 - \frac{3}{2} T_s + \frac{1}{2} T_s^3) \cos\gamma + 1 + \frac{3}{2} T_s - \frac{1}{2} T_s^3.$$

This treatment of the splitter effect is similar to that employed by Goto and Drzewiecki [23].

3.2.2.3 Unattached-Side and Separation Bubble Pressures. As the jet moves toward the opposite wall, the spacing $a_w$ between the opposite wall and the jet edge restricts the flow from region 2b into region 2a (see Figure 19). Thus, the average pressure in region 2a becomes less than the average pressure in region 2b. This nonuniform pressure distribution in the unattached-side is confirmed by the results of static pressure measurements along the opposite wall [36].

It is assumed that the unattached-side pressure is represented by two pressures: average pressure $p_{2a}$ in region 2a and average pressure $p_{2b}$ in region 2b. At each time step, the normalized pressure $P_{2a}$ is

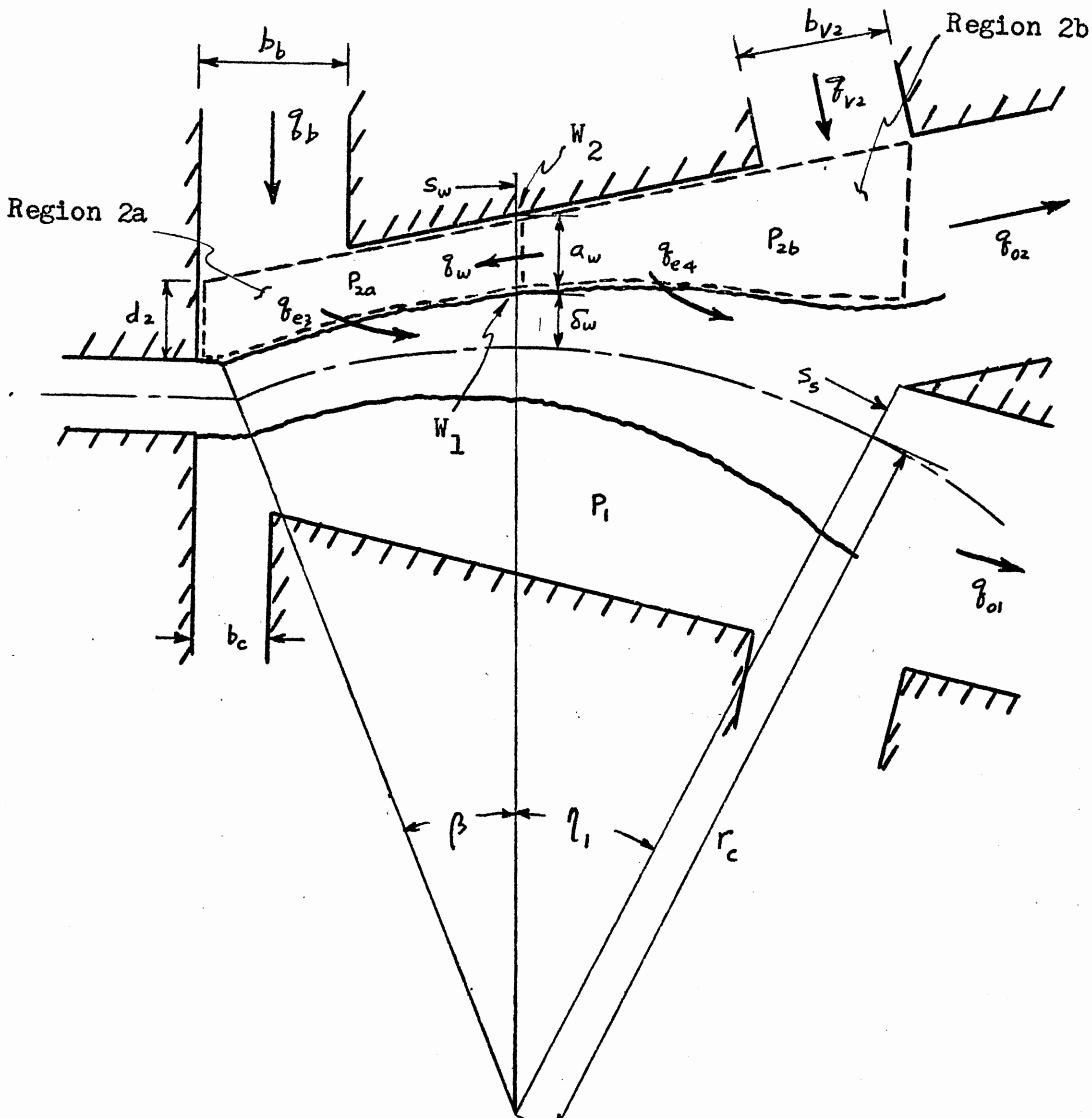


Figure 19. Flow and Geometric Model for Unattached-Side Pressure

approximately obtained by considering a flow rate balance in region 2a in a way similar to that employed for calculating pressure $P_2$ in the steady-state jet reattachment model (see Equations (3.17) through (3.18)). That is,

$$\Sigma Q = (Q_b + Q_w) - Q_{e3} = 0 \tag{3.47}$$

where

$$Q_b \equiv \frac{q_b}{q_s} = B_b \sqrt{-P_{2a}} \tag{3.47a}$$

$$Q_w \equiv \frac{q_w}{q_s} = A_w \sqrt{P_{2b} - P_{2a}} \tag{3.47b}$$

$$Q_{e3} \equiv \frac{q_{e3}}{q_s} = \frac{1}{2} \left(\sqrt{1 + \frac{S_w}{S_o}} - 1\right) \tag{3.47c}$$

$$S_w \equiv \frac{s_w}{b_s} = R_c \ \beta \tag{3.47d}$$

$$A_w \equiv a_w/b_s$$

$$P_{2a} \equiv p_{2a}/\tfrac{1}{2}\rho U_s^2; \ P_{2b} \equiv p_{2b}/\tfrac{1}{2}\rho U_s^2$$

Similarly, the normalized pressure $P_{2b}$ is approximately obtained by considering a flow balance in region 2b (Figure 19) at each time step:

$$\Sigma Q = \begin{cases} Q_{v2} - Q_{o2} - Q_w - Q_{e4} = 0 & \text{for } Q_{o2} < 0 \\ Q_{v2} - Q_w - Q_{e4} = 0 & \text{for } Q_{o2} \geq 0 \end{cases} \tag{3.48}$$

where

$$Q_{v2} \equiv \frac{q_{v2}}{q_s} = B_{v2} \sqrt{-P_{2b}}$$

$$Q_{e4} \equiv \frac{q_{e4}}{q_s} = \frac{1}{2} (\sqrt{1 + \frac{S_s}{S_o}} - 1) - Q_{e3}$$

$$B_{v2} \equiv b_{v2}/b_s$$

and $Q_{o2}$ is given by Equation (3.56a) in section 3.2.3.6. In the second equation of Equation (3.48), it is assumed that all flow into the OR output channel comes from the jet if $Q_{o2} > 0$. Since Equations (3.47) and (3.48) cannot be solved explicitly, a suitable iteration method has to be used to determine $P_{2a}$ and $P_{2b}$ (see Appendix C for detail).

From Figure 19, the normalized flow passage width $A_w$ can be written as[12]

$$A_w = (R_c \sin\beta + \frac{1}{2} B_c) \tan\alpha_2 + D_2 + \frac{1}{2} - R_c (1 - \cos\beta) - \Delta_w \tag{3.49}$$

where

$$\Delta_w \equiv \frac{\delta_w}{b_s} = 1.825 (\frac{S_w + S_o}{\sigma})$$

The separation bubble pressure may be obtained by substituting the average unattached-side pressure $P_2$ into Equation (3.16a), i.e.,

$$P_1 = P_2 - \frac{2}{R_c} \tag{3.50}$$

where

$$P_2 = P_{2a} (\frac{S_w}{S_s}) + P_{2b} (1 - \frac{S_w}{S_s}).$$

<u>3.2.3.4 Jet Deflection</u>. The jet deflection angle can be obtained by substituting the pressure $P_{2a}$ for $P_2$ in Equation (3.13a), i.e.,

$$\beta = \tan^{-1} [\frac{1}{2} (P_c - P_{2a}) B_c + \frac{Q_c^2}{B_c} \tag{3.51}$$

3.2.3.5 Geometric Relations. In addition to the geometric relations derived in section 3.1.5, the following relations can also be written from Figures 11 and 14:

$$R_e = [(X_2 \sin\alpha_1 + E_1)^2 + (X_2 \cos\alpha_1)^2]^{\frac{1}{2}} \tag{3.52}$$

$$Y_s = -(G - R_c) \tag{3.53}$$

where

$$G \equiv \frac{g}{b_s} = [(R_c \cos\beta + D_3)^2 + (D_s - \frac{1}{2} B_c - R_c \sin\beta)^2]^{\frac{1}{2}}$$

$$Y_s \equiv y_s/b_s.$$

From Figure 20 and Equation (3.2a), the normalized separation bubble volume (per unit depth) is

$$V = \frac{1}{b_s^2} (v_1 + v_2 + v_3) \tag{3.54}$$

or

$$V = \frac{cK^2}{4} (\frac{\theta_e}{c} - \frac{1}{2} \sin \frac{2\theta_e}{c}) + \frac{E_1 R_e}{2} \cos (\theta_e - \beta)$$
$$+ \frac{X_1}{2} (D_1 + E_1)\cos\alpha_1 \tag{3.54a}$$

3.2.3.6 Line Equations. The control and output channels are characterized as lumped-parameter line models.[13]

Referring to Figure 21, the control line equation is

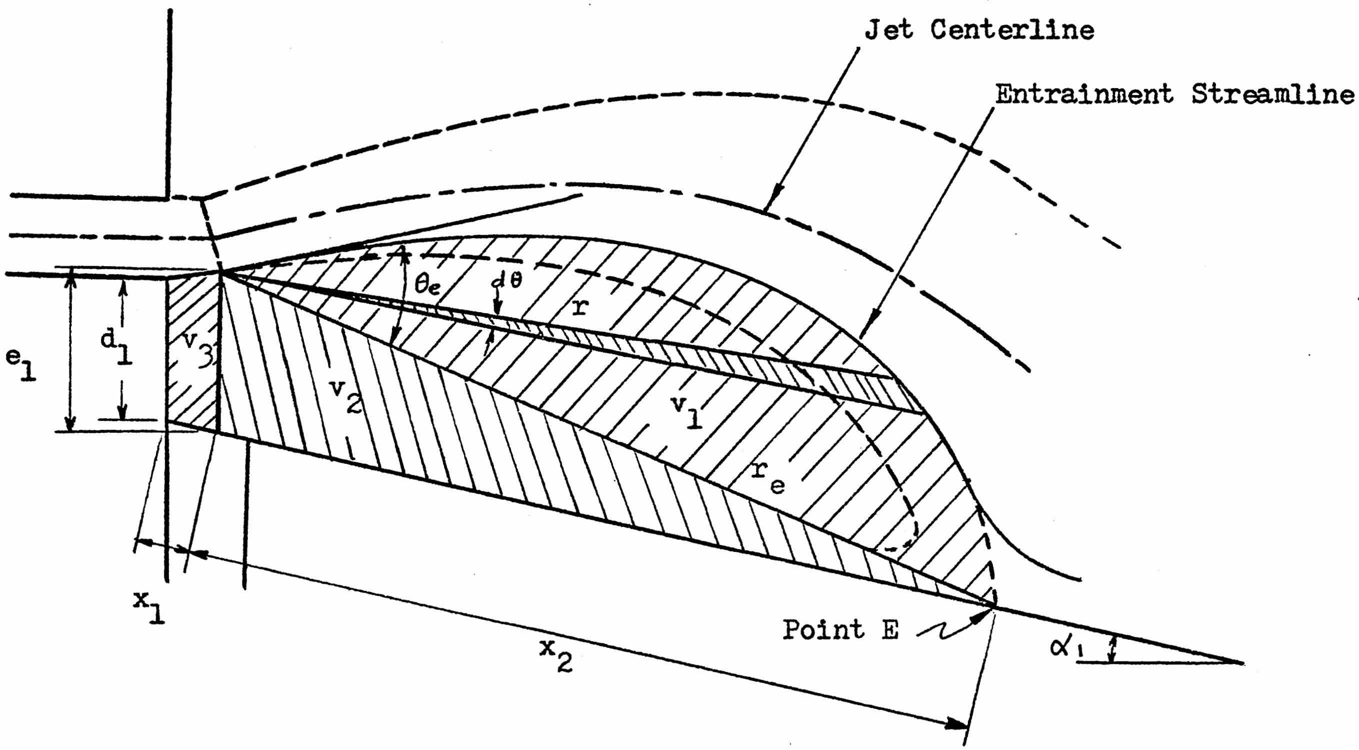


Figure 20. Cross Section of Separation Bubble

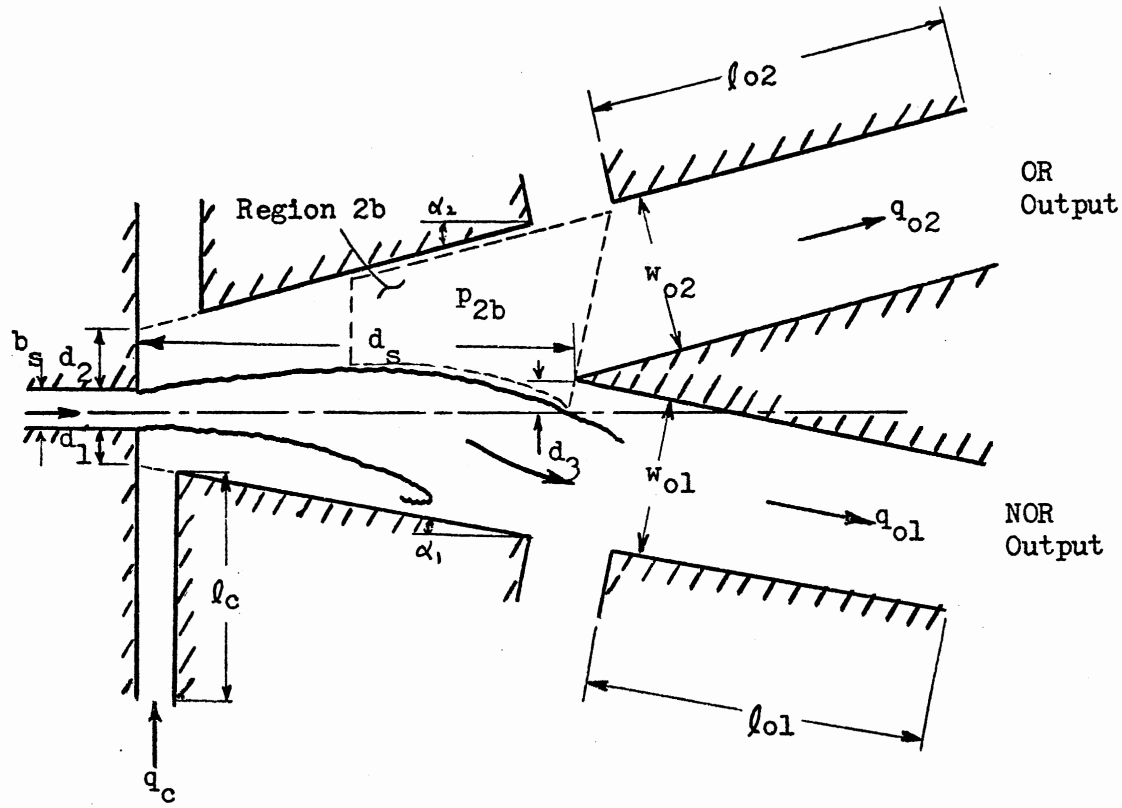


Figure 21. Geometry of Control and Output Channels

$$p_{tc} = p_c + \frac{1}{2}\rho\left(\frac{q_c}{C_{dc}b_c}\right)^2 + \frac{I_c}{C_{dc}}\frac{dq_c}{dt} \tag{3.55}$$

where $I_c \equiv \rho\ell_c/b_c$, and $p_{tc}$ is the total pressure at the inlet of the control channel. Friction losses and contraction effects in the control channel are accounted for through use of the discharge coefficient $C_{dc}$ ($C_{dc} \equiv (q_c)$ actual / $(q_c)$ ideal) [23]. Further discussion of the discharge coefficient is given in Appendix B.

In normalized form, Equation (3.55) becomes

$$P_{tc} = P_c + \left(\frac{Q_c}{C_{dc}B_c}\right)^2 + \frac{I'_c}{C_{dc}}\frac{dQ_c}{d\tau} \tag{3.55a}$$

where

$$P_{tc} \equiv p_{tc}/\frac{1}{2}\rho U_s^2; \quad I'_c \equiv 2L_c/B_c; \quad L_c \equiv \ell_c/b_s;$$

and $P_c$ is given by Equation (3.14a).

Similarly from Figure 21, the following output line equations may be written for the OR and NOR output channels, respectively:

$$p_{2b} + p_{d2} = \frac{1}{2}\rho\,\frac{q_{o2}|q_{o2}|}{w_{o2}^2} + I_{o2}\frac{dq_{o2}}{dt} \tag{3.56}$$

$$p_{2b} + p_{d1} = \frac{1}{2}\rho\,\frac{q_{o1}|q_{o1}|}{w_{o1}^2} + I_{o1}\frac{dq_{o1}}{dt} \tag{3.57}$$

where

$$I_{o2} \equiv \rho\ell_{o2}/w_{o2}, \quad I_{o1} \equiv \rho\ell_{o1}/w_{o1},$$

and $p_{d2}$ and $p_{d1}$ are the dynamic pressures at the inlet of the OR and NOR output channels, respectively.

The total pressures $(p_{2b} + p_{d2})$ and $(p_{2b} + p_{d1})$ are considered as the internal "driving force" to the OR and NOR output channels, respectively.[14] Friction losses in both output channels are assumed negligible. Equations (3.56) and (3.57), when normalized, yield

$$P_{2b} + P_{d2} = \frac{Q_{o2}|Q_{o2}|}{W_{o2}^2} + I'_{o2}\frac{dQ_{o2}}{d\tau} \tag{3.56a}$$

$$P_{2b} + P_{d1} = \frac{Q_{o1}|Q_{o1}|}{W_{o1}^2} + I'_{o1}\frac{dQ_{o1}}{d\tau} \tag{3.57a}$$

where

$$P_{d2} \equiv p_{d2}/\tfrac{1}{2}\rho U_s^2; \quad P_{d1} \equiv p_{d1}/\tfrac{1}{2}\rho U_s^2;$$

$$I'_{o2} \equiv 2L_{o2}/W_{o2}; \quad I'_{o1} \equiv 2L_{o1}/W_{o1};$$

$$L_{o2} \equiv \ell_{o2}/b_s; \quad L_{o1} \equiv \ell_{o1}/b_s;$$

$$W_{o2} \equiv w_{o2}/b_s; \quad W_{o1} \equiv w_{o1}/b_s.$$

Referring to Figures 18 and 21 and assumption, 5, the dynamic pressures at the inlet of the OR and NOR output channels are:

$$p_{d2} = \frac{J_s}{2w_{o2}} = \frac{\rho}{2w_{o2}}\int_{-\infty}^{y_s} u^2\, dy\Big|_{s=s_s} \tag{3.58}$$

$$p_{d1} = \frac{J_d}{2w_{o1}} = \frac{\rho}{2w_{o1}}\int_{y_s}^{y_r} u^2\, dy\Big|_{s=s_e} \tag{3.59}$$

Equations (3.1) and (3.58) and Equations (3.1) and (3.59), when combined and normalized, yield respectively:

$$P_{d2} = \frac{1}{4W_{o2}}(2 + 3T_s - T_s^3) \tag{3.58a}$$

$$P_{d1} = \frac{1}{4W_{o1}}(3T_r - T_r^3 - 3T_s + T_s^3) \tag{3.59a}$$

Output channel widths are provided from the geometry or can be obtained from other geometric parameters, i.e. (from Figure 21),

$$W_{o2} = (D_2 - D_3 + \frac{1}{2}) \cos\alpha_2 + D_s \sin\alpha_2 \qquad (3.60)$$

$$W_{o1} = (D_1 + D_3 + \frac{1}{2}) \cos\alpha_1 + D_s \sin\alpha_1. \qquad (3.61)$$

3.2.3.7 End of Phase I. By assumption 6, phase I ends when the following conditions are met:

$$Y_s \geq Y_I \qquad (3.62)$$

and

$$Q_{o2} = 0.95\, W_{o2} \sqrt{(P_{2b} + P_{d2})_{Y_s = Y_I}} \qquad (3.63)$$

where

$$Y_I = D_2 - D_1 - D_3.$$

### 3.2.4 Analysis of Phase II

The basic equations and geometric relations for phase II are briefly presented without detailed derivations because of their similarity in form to those for phase I.

3.2.4.1 Continuity Equation. Referring to Figure 22 and Equation (3.42), the growth rate of the separation bubble is (in normalized form):

$$\frac{dV}{d\tau} = \begin{cases} Q_b + \frac{1}{2}\,(1 - T_r \sqrt{1 + \frac{S_e}{S_o}}) & \text{for } X_r \leq X_{v2} \\ Q_b + \frac{1}{2}\,(1 - T_r \sqrt{1 + \frac{S_e}{S_o}}) + A_v \sqrt{-P_1} & \text{for } X_r > X_{v2} \end{cases} \qquad (3.64)$$

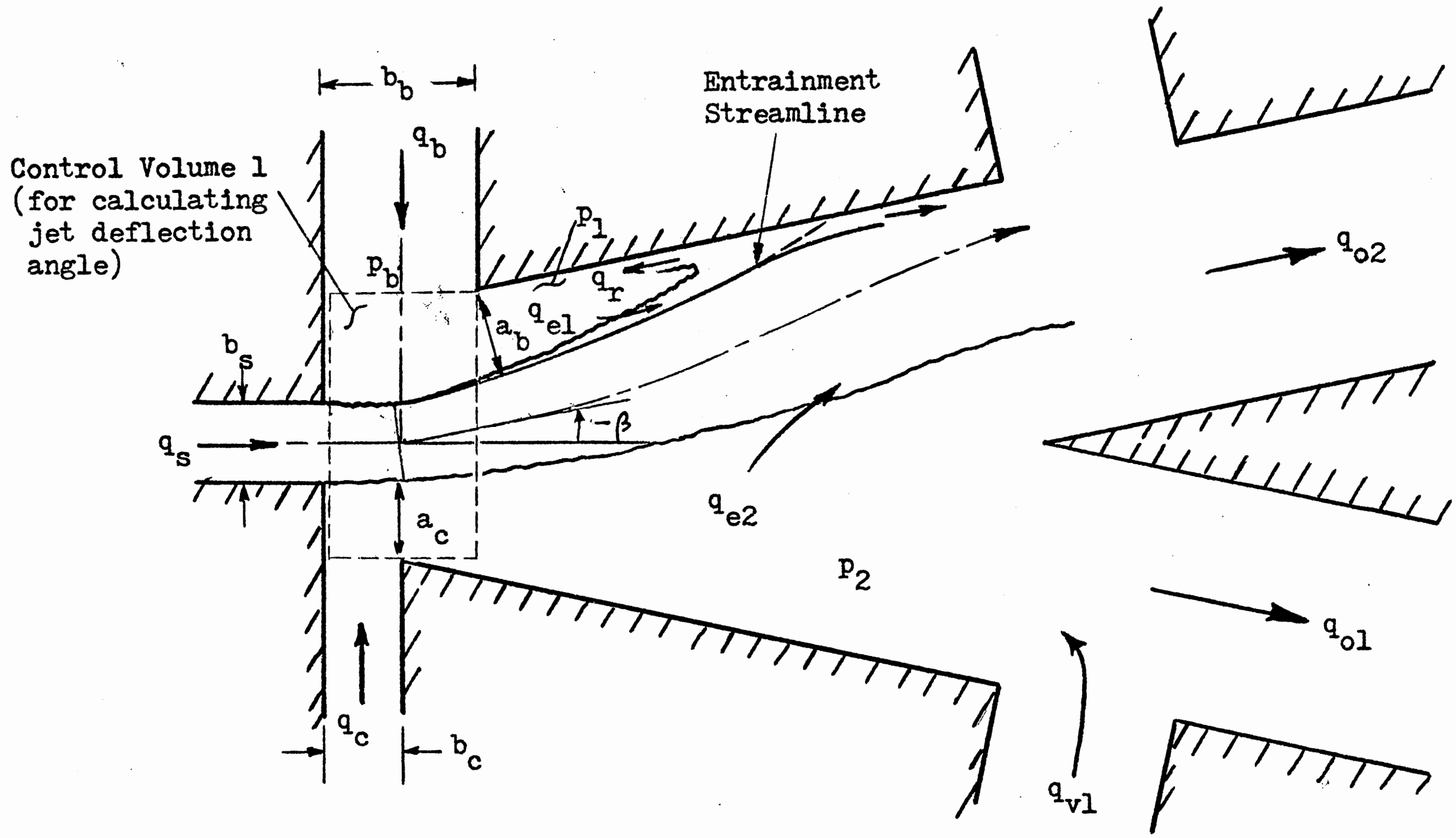


Figure 22. Flow Model for Phase II

The bias vent flow rate $q_b$ into the separation bubble is restricted by an orifice $a_b$ (Figure 22), if $a_b < b_b$, or by the bias vent width $b_b$, if $a_b \geq b_b$. Assuming the discharge coefficient of the orifice is unity and the ambient pressure is zero, the normalized bias vent flow rate is:

$$Q_b = \begin{cases} A_b \sqrt{-P_1} & \text{for } A_b < B_b \\ B_b \sqrt{-P_1} & \text{for } A_b \geq B_b \end{cases} \tag{3.65}$$

where $Q_b \equiv q_b/q_s$; $A_b \equiv a_b/b_s$; $B_b \equiv b_b/b_s$.

From Figure 23,

$$A_b = \frac{1}{2} B_b \sin\beta + (D_2 + \frac{1}{2} + B_b \tan\alpha_2) \cos\beta - \frac{1}{2} \tag{3.66}$$

where $D_2 = d_2/b_s$.

The output vent flow passage for phase II can be written similarly to Equation (3.43):

$$A_v = R_c - \Delta_v - (X_{v2} \cos\alpha_2 - R_c \sin\beta - \frac{1}{2} B_b) \csc\xi \tag{3.67}$$

where

$$\xi \equiv \tan^{-1} \left[\frac{X_{v2} \cos\alpha_2 - R_c \sin\beta - \frac{1}{2} B_b}{R_c \cos\beta - X_{v2} \sin\alpha_2 - (D_2 + \frac{1}{2})}\right]$$

$$\Delta_v = 1.825 \, (S_v + S_o)/\sigma$$

$$S_v = R_c \, (\beta + \xi).$$

If $\xi \leq \alpha_2$, the term $A_v$ in Equation (3.65) is replaced by $B_{v2} \equiv b_{v2}/b_s$. (See the discussion in section 3.2.3.1.)

<u>3.2.4.2 Momentum Equation at Reattachment</u>. The momentum equation written for a control volume in the vicinity of the reattachment point

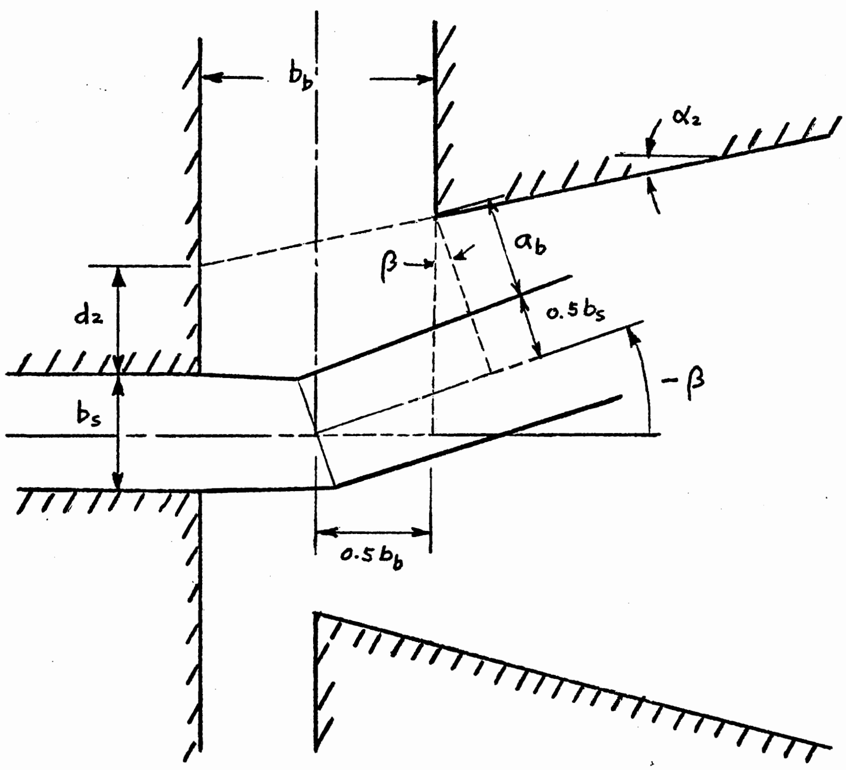


Figure 23. Bias Vent Flow Passage Width

is identical in form to that for phase I (Equation (3.46)). That is,

$$T_r = 2\cos\left[\frac{\pi + \cos^{-1}(\lambda/2)}{3}\right] \tag{3.46}$$

where

$$\lambda = (1 - \frac{3}{2} T_s + \frac{1}{2} T_s^3) \cos\gamma + 1 + \frac{3}{2} T_s - \frac{1}{2} T_s^3$$

$$T_s \equiv \tanh [\sigma Y_s/(S_s + S_o)].$$

3.2.4.3 Unattached-Side and Separation Bubble Pressures. If the jet deflection angle is negative (note that the sign convention of $\beta$ is changed in phase II; see Figure 22), the minimum area between the jet edge and the attachment wall is the flow passage width $a_c$ (see Figure 22). Thus, it is assumed that the unattached-side pressure is represented by the single average pressure $p_2$ in the region downstream of $a_c$. At each time step, the normalized pressure $P_2$ is approximately obtained by considering a flow rate balance in the region downstream of $a_c$ in a way similar to that employed for calculating pressure $P_2$ in the steady-state jet reattachment model (see Equations (3.17) through (3.18)). That is,

$$\Sigma Q = (Q_c + Q_{v1} - Q_{o1}) - Q_{e2} = 0 \tag{3.68}$$

where

$$Q_{v1} = B_{v1} \sqrt{-P_2}$$

$$Q_{e2} \equiv \frac{q_{e2}}{q_s} = \frac{1}{2} \left(\sqrt{1 + \frac{S_s}{S_o}} - 1\right)$$

and $S_s$ is similarly defined as that shown in Figure 19.

If the jet deflection angle becomes positive with decreased control flow, the unattached-side pressure is assumed to be represented by two pressures: average pressure $p_{2a}$ in region 1 and average pressure $p_{2b}$ in region 2, which are similarly defined as those for phase I (see Figure 19). Referring to Equation (3.47), the normalized pressure $P_{2a}$ at each time step is approximately determined by

$$\Sigma Q = (Q_c + Q_w) - Q_{e3} = 0 \tag{3.69}$$

where

$$Q_w = A_w \sqrt{P_{2b} - P_{2a}}$$

$$Q_{e3} = \frac{1}{2} \left(\sqrt{1 + \frac{S_w}{S_o}} - 1\right)$$

$$S_w = R_c \beta$$

$$A_w \equiv a_w / b_s$$

$$P_{2a} \equiv p_{2a} / \frac{1}{2} \rho U_s^2$$

$$P_{2b} \equiv p_{2b} / \frac{1}{2} \rho U_s^2$$

and $a_w$ is similarly defined as that shown in Figure 19.

Referring to Equation (3.48), the normalized pressure $P_{2b}$ at each time step is approximately determined by

$$Q = \begin{cases} (Q_{v1} - Q_{o1}) - (Q_w + Q_{e4}) = 0 & \text{for } Q_{o1} < 0 \\ Q_{v1} - (Q_w + Q_{e4}) = 0 & \text{for } Q_{o1} \geq 0 \end{cases} \tag{3.70}$$

where

$$Q_{v1} = B_{v1} \sqrt{-P_{2b}}$$

$$Q_{e4} = Q_{e2} - Q_{e3}$$

and $Q_{o1}$ is given by Equation (3.58) in section 3.2.3.6. Iteration procedures for solutions to Equations (3.68) through (3.70) are given in Appendix C.

The area $A_w$ can be written similarly to Equation (3.49):

$$A_w = (R_c \sin\beta + \frac{1}{2} B_b) \tan\alpha_1 + D_1 + \frac{1}{2} - R_c (1 - \cos\beta) - \Delta_w \tag{3.71}$$

where

$$\Delta_w = 1.825 \left(\frac{S_w + S_o}{\sigma}\right).$$

Referring to Figure 22 and Equation (3.50), the separation bubble pressure is:

$$P_1 = \begin{cases} P_2 - \dfrac{2}{R_c} & \text{for } \beta \leq 0 \\ P_{2a} \left(\dfrac{S_w}{S_s}\right) + P_{2b} \left(1 - \dfrac{S_w}{S_s}\right) - \dfrac{2}{R_c} & \text{for } \beta > 0. \end{cases} \tag{3.72}$$

<u>3.2.4.4 Jet Deflection</u>. As shown in Figure 22, the supply jet interacts with the control and bias vent flows in control volume 1 during phase II. It is assumed that the bias vent flow has a momentum interaction with the supply jet in the control volume during phase II. The return flow in the separation bubble has a tendency to make the vent flow impinge directly on the supply jet. Referring to Figure 22 and Equation (3.51),

$$\beta = \tan^{-1} \left[\frac{1}{2} \{P_b B_b - P_c B_c - P_{2a} (B_b - B_c)\} + \frac{Q_b^2}{B_b} - \frac{Q_c^2}{B_c}\right] \tag{3.73}$$

where

$$P_c = \begin{cases} P_2 + Q_c^2 \left[\frac{1}{A_c^2} + \frac{K_L - 1}{B_c^2}\right] & \text{for } A_c < B_c \\ P_2 + K_L \left(\frac{Q_c}{B_c}\right)^2 & \text{for } A_c \geq B_c \end{cases}$$

$$A_c = -\frac{1}{2} B_c \sin\beta + (D_1 + \frac{1}{2} + B_c \tan\alpha_1) \cos\dot{\beta} - \frac{1}{2}.$$

If $\beta > 0$, the pressure $P_2$ in Equation (3.73) is replaced by $P_{2a}$ (see section 3.2.4.3 for discussion).

The bias vent exit pressure $p_b$ may be obtained from the Bernouli's equation for the bias vent, i.e.,

$$0 = p_b + \frac{1}{2}\rho\left(\frac{q_b}{b_b}\right)^2 = p_1 + \frac{1}{2}\rho\left(\frac{q_b}{a_b}\right)^2 \tag{3.74}$$

Equation (3.74), when normalized and rearranged, yields

$$P_b = \begin{cases} -\left(\frac{Q_b}{B_b}\right)^2 & \text{for } A_c < B_b \\ P_1 & \text{for } A_c \geq B_b. \end{cases} \tag{3.74a}$$

If the "forced" control flow rate becomes less than the flow rate which is "naturally" induced by the low pressure in the region between the jet edge and the attachment wall, i.e., $Q_c \leq C_{dc} B_c \sqrt{-P_{2a}}$, then the jet deflection angle may be written as

$$\beta = \tan^{-1} \left[\frac{1}{2} (P_b - P_{2a}) B_b + \frac{Q_b^2}{B_v}\right] \tag{3.75}$$

by the assumption that the momentum effect of the induced flow on the jet deflection is negligible.

3.2.4.5 Geometric Relations. Referring to Figure 24, the following geometric relations can be written in normalized form:

$$\alpha_2 + \gamma = \zeta_e + \theta_e - \beta \tag{3.76}$$

$$E_2 = D_2 + X_1 \sin\alpha_2 + \frac{1}{2}(1 - \cos\beta) \tag{3.77}$$

or

$$E_2 = R_e \sin(\theta_e - \beta - \alpha_2) \sec\alpha_2 \tag{3.78}$$

$$X_1 = \frac{1}{2}(B_b + \sin\beta) \sec\alpha_2 \tag{3.79}$$

$$X_2 = R_e \cos(\theta_e - \beta) \sec\alpha_2 \tag{3.80}$$

$$X_e = X_1 + X_2 \tag{3.24}$$

$$R_e = K \sin\left(\frac{\theta_e}{c}\right) \tag{3.2a}$$

or

$$R_e = [(X_2 \sin\alpha_2 + E_2)^2 + (X_2 \cos\alpha_2)^2]^{\frac{1}{2}} \tag{3.81}$$

$$S_e = K \int_0^{\theta_e/c} [1 - (1 - c^2) \sin^2 (\frac{\theta}{c})]^{\frac{1}{2}} d(\frac{\theta}{c}) \tag{3.26}$$

$$\zeta_e = \tan^{-1}\left(c \tan \frac{\theta_e}{c}\right) \tag{3.27a}$$

where

$$E_2 \equiv e_2/b_s; \quad R_e \equiv r_e/b_s;$$

$$X_1 \equiv x_1/b_s; \quad X_2 \equiv x_2/b_s.$$

Additional geometric relations are written below without derivations because of their similarity to those for phase I:

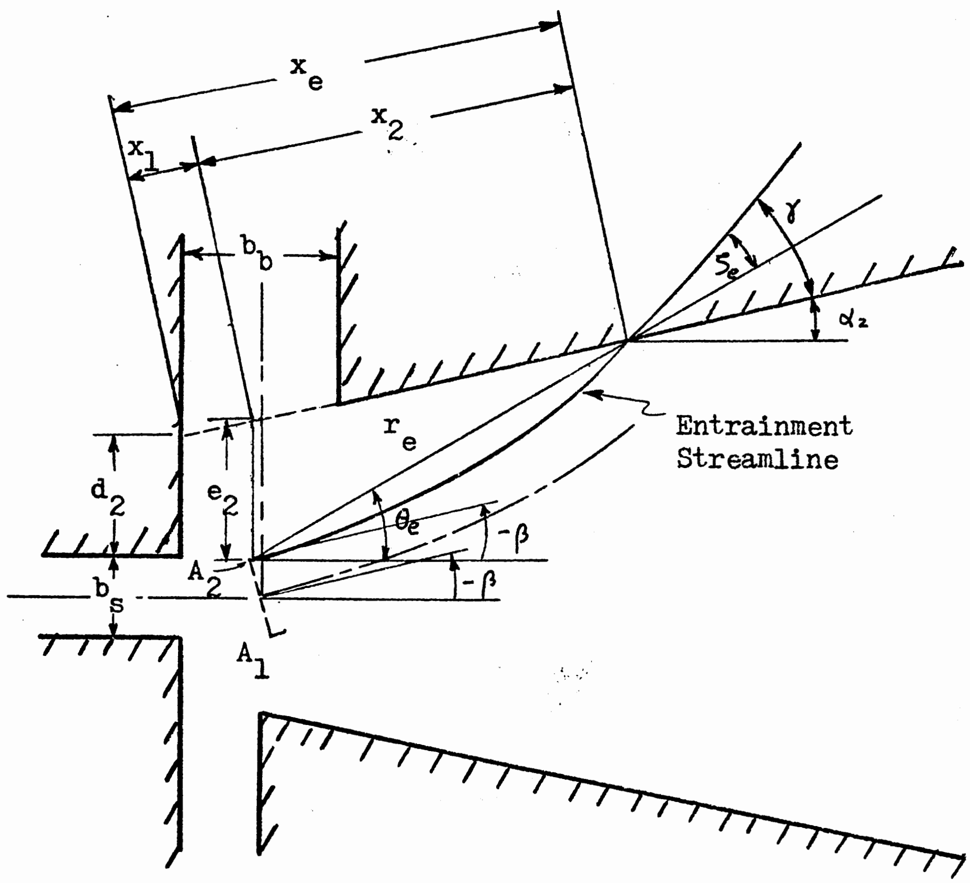


Figure 24. Geometry of the Attached Jet for Phase II

$$X_r = X_e - \left(\frac{S_e + S_o}{\sigma}\right) \left[\tanh^{-1} T_r - \tanh^{-1} \left(\sqrt{\frac{S_o}{S_e + S_o}}\right)\right] \csc\gamma$$

(3.41)

$$R_c = R_{es} + \frac{1}{2} \left[1 + \frac{(\frac{1}{2} - Y_p)(2R_{es} + \frac{1}{2} - Y_p)}{R_{es} \ (\cos 2\theta_p - 1) - \frac{1}{2} + Y_p}\right] \tag{3.82}$$

where

$$R_{es} = K/2c$$

$$Y_p = \left(\frac{S_p + S_o}{\sigma}\right) \tanh^{-1} \left(\sqrt{\frac{S_o}{S_p + S_o}}\right)$$

$$S_p = 2R_{es} \ \theta_p$$

$$\theta_p = \frac{1}{2} (\beta + \eta_1)$$

$$\eta_1 = \tan^{-1} \left[\frac{D_s - \frac{1}{2} B_b - (R_{es} + \frac{1}{2}) \sin\beta}{(R_{es} + \frac{1}{2}) \cos\beta - D_3}\right]$$

and

$$S_s = R_c \ (\beta + \eta_2) \tag{3.83}$$

where

$$\eta_2 = \tan^{-1} \left[\frac{D_s - \frac{1}{2} B_b - R_c \sin\beta}{(\frac{1}{2} + R_c) \cos\beta - D_3}\right]$$

and

$$Y_s = -(G - R_c) \tag{3.84}$$

where

$$G = [(R_c \cos\beta - D_3)^2 + (D_s - \frac{1}{2} B_b - R_c \sin\beta)^2]^{\frac{1}{2}}$$

and

$$V = \frac{cK^2}{4} (\frac{\theta_e}{c} - \frac{1}{2} \sin \frac{2\theta_e}{c}) + \frac{E_2 R_e}{2} \cos (\theta_e - \beta)$$

$$+ \frac{X_1}{2} (D_2 + E_2) \cos\alpha_2 \qquad (3.85)$$

3.2.4.6 Line Equations. The control line equation (Equation (3.55a)) and the output line equations (Equations (3.56a) and (3.57a)) are used both for phase I and for phase II. But, the equations for the dynamic pressures $P_{d1}$ and $P_{d2}$ should be modified as follows because of the jet reattachment to the opposite wall during phase II:

$$P_{d2} = \frac{1}{4W_{o2}} (3T_r - T_r^3 - 3T_s + T_s^3) \qquad (3.86)$$

$$P_{d1} = \frac{1}{4W_{o1}} (2 + 3T_s - T_s^3) \qquad (3.87)$$

3.2.4.7 End of Phase II. It is assumed that the jet switches back and reattaches to the attachment wall when the following conditions are met:

$$Y_s \geq 0 \qquad (3.88)$$

and

$$Q_{o1} = 0.95\, W_{o1} \sqrt{(P_{2b} + P_{d1})\, Y_{sp}} = 0. \qquad (3.89)$$

### 3.2.5 Digital Simulation

The analytical dynamic model formulated above may be simulated on a digital computer (IBM 370/158) using DYSIMP (Dynamic Simulation

Program).[15] The following are the list of the basic equations and the geometric relations to be simulated on the computer: Equations (3.2a), (3.19) through (3.24), (3.26a), (3.27a), (3.31) through (3.33), (3.34a), (3.35) through (3.39), (3.42), (3.43), (3.46) through (3.53), (3.54a), (3.55a), (3.56a), (3.57a), (3.58a), (3.59a), (3.60) through (3.73), (3.74a), and (3.75) through (3.89). A computer flow chart and computer program listings are given in Appendix C.

The analytical predictions of the switching time, the return time, and the transient response are compared with experimental data in Chapter V.

## ENDNOTES

[1] Moynihan and Reilly [40] showed in their experimental study on the jet deflection in a proportional fluid amplifier that the effective "pivot point" of the deflected jet is approximately at the intersection of the centerlines of the supply and control nozzles.

[2] The entrainment streamline is defined as the line which originates at point $A_1$ (Figure 10) and divides the flow originally in the jet from the fluid entrained by the concave side of the jet.

[3] Errors due to this assumption are of the order of 10 percent of $s_f$ for $Q_c = 0$ and 1 percent of $s_f$ for $Q_c = 0.3$ for a typical geometry of a monostable fluid amplifier.

[4] This assumption is not strictly correct. Sawyer [57] indicated that the rate of fluid entrainment is greater on the convex side of the jet than that on the concave side of the jet. However, Epstein [19] showed that the analytically predicted jet reattachment distances obtained from Sawyer's model [57] (Sawyer used the different rate of entrainment on each side of the jet) are almost identical to those obtained from Bourque's model [6] (Bourque used the same rate of entrainment on both sides of the jet). Both Bourque and Sawyer treated only the jet reattachment problem with no control flow.

[5] This assumption is based on the flow visualization and velocity profile measurements of the interacting jets by Douglas and Neve [14].

[6] Epstein [19] assumed (1) that the control and supply jets form a combined jet emerging from a "hypothetical nozzle" after the momentum interaction; (2) the reattachment streamline as the separation bubble boundary, while in the present model the entrainment streamline is assumed as the boundary to be consistent with assumption 2. In the present steady-state model, the reattachment streamline is defined as the line which originates at point I (Figure 10) and divides the flow proceeding downstream along the wall from the flow recirculating within the separation bubble; and (3) the control nozzle exit pressure $p_c$ (Figure 10) is known for the calculation of the jet deflection angle, but in the present model $p_c$ is determined analytically (see section 3.1.4 for detail).

[7]Referring to assumptions 2, 3 and 4, the value of $s_o$ can be determined by matching the flow rate through the hypothetical nozzle to the flow rate determined by integrating Goertler's velocity profile at distance $s_o$ from the "virtual origin" of the jet, i.e.,

$$U_s b_s = \int_{-\infty}^{\infty} u \, dy \Big|_{s=0}$$

Using Equation (3.1), the above equation reduces to $s_o = \frac{\sigma b_s}{3}$.

[8]Epstein [19] demonstrated that the error introduced by this approximation is less than 0.5 percent of the exact value for $0 < \theta_e/c < 4/9\,\pi$ and near 1.5 percent for $4/9\,\pi < \theta_e/c < \pi/2$.

[9]The error incurred by taking $y_p$ from point P instead of from the entrainment streamline is less than 0.3 percent of $R_c$ for $D_1 = 0.5$, $D_s = 11$, $\alpha_1 = 12°$.

[10]These assumptions are discussed in section 3.2.2.

[11]For a bistable fluid amplifier, Goto and Drzewiecki [23] assumed that phase I ends when $y_s = 0$.

[12]$A_w$ is assumed the minimum area between the jet edge and the opposite wall. It is believed that this assumption is adequate for the determination of approximate values of $P_{2a}$ and $P_{2b}$.

[13]This lumped-parameter approximation is valid whenever the time required for a pressure signal to travel the length of the line is short with respect to the period of the highest frequency signal that is to be transmitted. For the test amplifier used in this study, the period of the highest frequency pressure signal in the control line is of the order of 1 millisecond, while the time required for the signal to travel 1 inch long control channel is of the order of 0.1 millisecond

$$\left(\frac{1 \text{ in.}}{1000 \times 12 \text{ in/sec}} = 10^{-4} \text{ sec}\right).$$

[14]This "driving force" concept is attributed to Goto and Drzewiecki [23].

[15]DYSIMP is a packaged program for the digital simulation of dynamic systems, which is written in FORTRAN IV. It has been developed by the School of Mechanical and Aerospace Engineering, Oklahoma State University.

# CHAPTER IV

# EXPERIMENTAL APPARATUS AND PROCEDURE

## 4.1 Apparatus

Experimental work was carried out on a large-scale test model (about ten times actual size) of a typical monostable fluid amplifier. Figure 25 is a plan view and Figure 26 is a photograph of the test amplifier. The major components of the test amplifier were a base plate, a cover plate, and movable internal blocks. By using a large-scale amplifier rather than an actual sized one, it was possible (1) to locate the internal blocks accurately, and (2) to lengthen the switching and return times, thereby enhancing accuracy of measurement of these quantities.

The interior geometry of the amplifier was formed with seven 0.31 inch thick aluminum blocks. Except for the two nozzle blocks, slots were provided for each block to allow a certain range of adjustment (see arrows in Figure 25). Gage blocks (Fonda Gage Company) and a vernier caliper were used to locate these blocks. After these blocks were firmly bolted to a 1/2 inch thick aluminum base plate, a 1/2 inch thick plexiglass cover plate was attached to the top of the device and then the entire assembly was fastened by 24 setscrews. Silicon lubricant was applied between the plates to minimize leakage.

The supply nozzle width ($b_s$) was fixed at 0.1 inch, which resulted in an aspect ratio of 3.1. Wire screens and sponge-type packing material

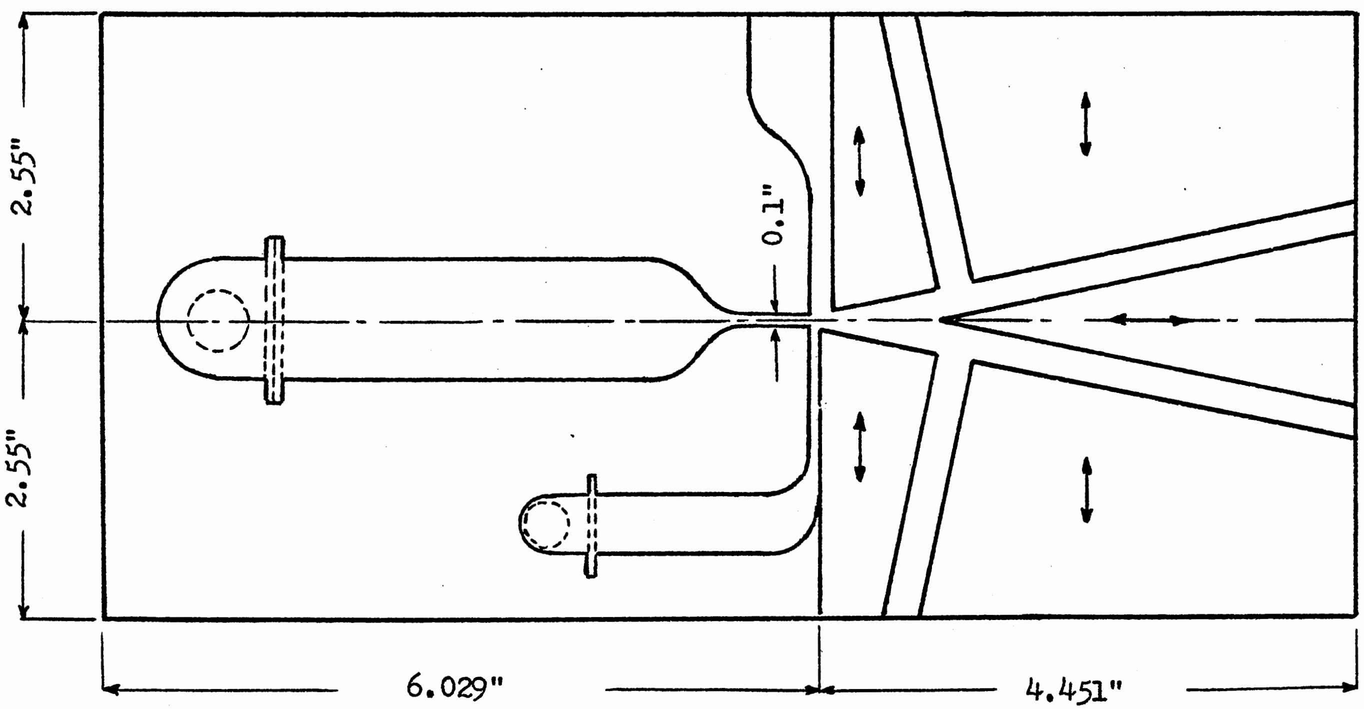


Figure 25. Plan View of Large-Scale Test Amplifier

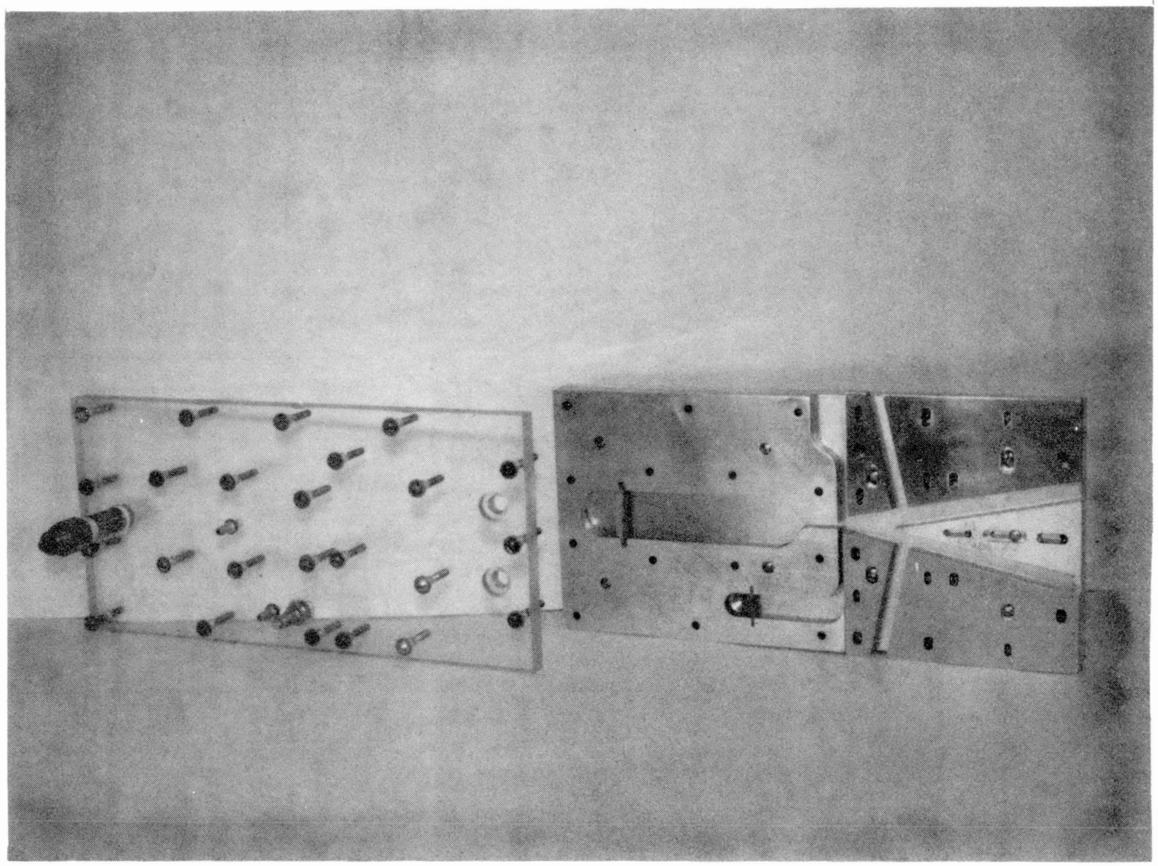

Figure 26. Photograph of the Test Amplifier

were provided in the inlet region of the supply nozzle chamber to reduce swirl and scale of turbulence. Also, the long supply chamber (length of constant area section was $36b_s$) and the bell-mouth nozzle entry served to further reduce swirl in the flow. Similar precautions were taken for the control nozzle chamber.

Pressure taps (0.0635 inch diameter) were drilled in the cover plate at locations $15.7b_s$ and $13.4b_s$ upstream of the entrances to the supply and control nozzles, respectively. A pressure transducer was flush-mounted in the cover plate $7.2b_s$ upstream of the entrance to the control nozzle. Dimensions of the supply and control chambers and the bias vent port and locations of the pressure taps and transducer are listed in Appendix A.

Figure 27 shows internal geometry of the test amplifier. In order to reduce the total number of combinations of geometric variations, a "nominal" configuration was chosen and each geometric parameter (such as attachment wall offset, opposite wall offset and angle, splitter distance and offset, and bias vent width) was varied through a suitable range, while the others were kept constant at a "nominal" value. The configuration given in Table I was based on scaling (approximately ten times) a typical monostable amplifier [3].

A schematic of the experimental apparatus is shown in Figure 28. Air was supplied to the amplifier through precision pressure regulators. Air entered the supply chamber through a 0.38 inch inside diameter tube mounted on the cover plate.

A solenoid valve (Skinner type V52; 3/8 inch orifice diameter) was employed to generate a "step" (with finite rise/decay time) pressure input to the control chamber. A 3/4 inch long flexible plastic tubing

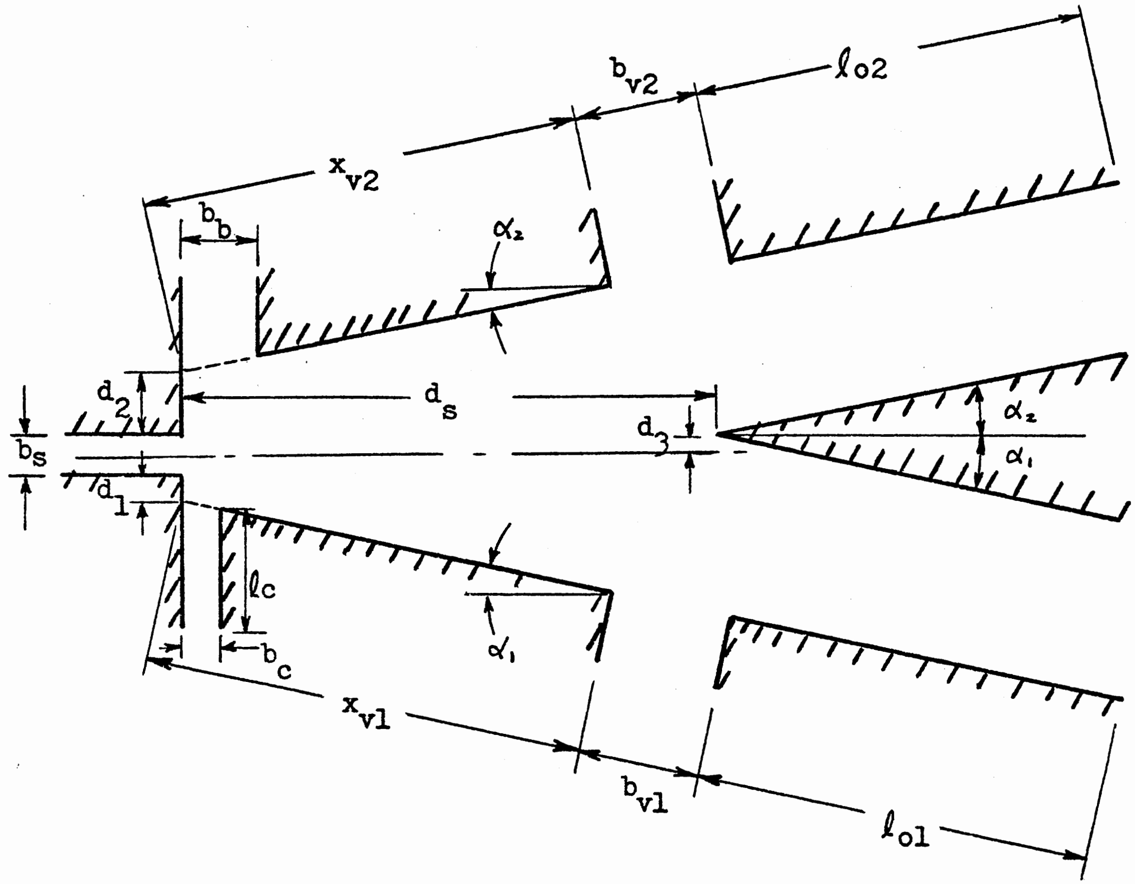


Figure 27. Internal Geometry of the Test Amplifier

TABLE I

NOMINAL CONFIGURATION

| Geometric Parameter | Nominal Geometry |
|---|---|
| Supply nozzle width ($b_s$) | 0.10 inch |
| Control nozzle width ($b_c/b_s$) | 1.00 |
| Bias vent width ($b_b/b_s$) | 2.00 |
| Attachment wall offset ($d_1/b_s$) | 0.50 |
| Opposite wall offset ($d_2/b_s$) | 1.00 |
| Attachment wall angle ($\alpha_1$) | 12° |
| Opposite wall angle ($\alpha_2$) | 12° |
| Attachment wall length ($x_{v1}/b_s$) | 10.94 |
| Opposite wall length ($x_{v2}/b_s$) | 10.94 |
| Splitter distance ($d_s/b_s$) | 11.00 |
| Splitter offset ($d_3/b_s$) | 0.00 |
| NOR output vent width ($b_{v1}/b_s$) | 3.05 |
| OR output vent width ($b_{v2}/b_s$) | 3.05 |
| NOR output channel length ($\ell_{o1}/b_s$) | 32.34 |
| OR output channel length ($\ell_{o2}/b_s$) | 32.34 |
| Control channel length ($\ell_c/b_s$) | 9.69 |
| Aspect ratio (AR) | 3.10 |

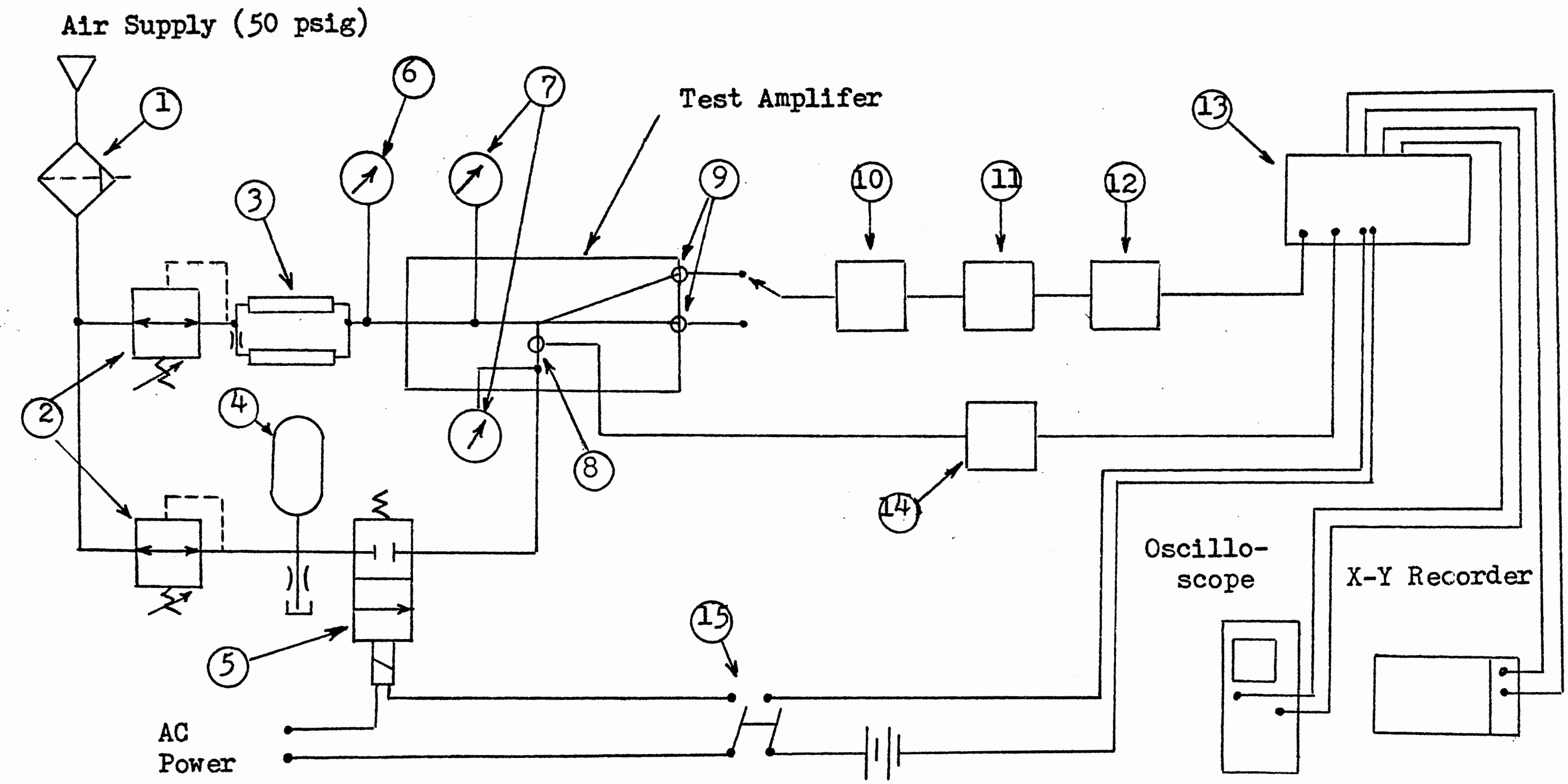


1. Air Filter
2. Pressure Regulator
3. Rotameter-type Flowmeter
4. Accumulator
5. Solenoid Valve
6. Mercury Manometer
7. Merram Manometer
8. Pressure Transducer
9. Hot-wire Probe
10. Low-pass Filter
11. Constant Temperature Anemometer
12. Linearizer
13. Waveform Recorder
14. Perzotron Coupler
15. Trigger Circuit

Figure 28. Schematic of Experimental Apparatus

(3/8 inch inside diameter, 1/2 inch outside diameter) was used to connect the solenoid valve outlet to the control chamber inlet through the base plate. This flexible line minimized the transmission of vibrations from the solenoid valve to the pressure transducer in the control chamber.

### 4.2 Instrumentation and Measurement Procedure

The following quantities were measured:

1. Jet centerline axial velocity distribution in the semi-confined jet (cover plates, but no side walls or splitter).

2. Switching and return times.

3. NOR output total pressure transient response.

All measurements were conducted with a supply total pressure of 10 in. $H_2O$, with one exception. The measurements of the jet centerline axial velocity distribution were also carried out for a supply total pressure of 20 in. $H_2O$ in order to determine any first order effects due to Reynolds number. The Reynolds number associated with the supply total pressures of 10 in. $H_2O$ and 20 in. $H_2O$ are approximately $1.4 \times 10^4$ and $9.8 \times 10^3$, respectively.[1]

The supply total pressure was measured with a Meriam manometer containing unity oil, and the supply volumetric flow rate was measured with two identical Fisher-Porter rotameter-type flowmeters (FP-1/2-G-10/80) connected in parallel. The static pressure just downstream of the flowmeters was measured with a mercury manometer.

Jet centerline axial velocities in the semi-confined jet (no side walls and splitter) were "computed" from the total pressure measurements along the jet axis, assuming the static pressure was constant throughout the jet field. The total pressure was measured midway between the top and bottom plates with a standard total pressure probe (0.065 inch outside diameter) mounted on a traverse mechanism, and a Meriam manometer.

Switching time is defined in this study as the time elapsed from the instant the control total pressure is observed to rise in the control chamber until the velocity at the exit plane of the OR output channel reaches 95 percent of the final value. Similarly, return time is defined as the time elapsed from the instant the control total pressure is observed to decay in the control chamber until the velocity at the exit plane of the NOR output channel reaches 95 percent of its final value.

A Kistler Piezotron pressure transducer (Model 201B5) with a Piezotron coupler (Model 587D) was used to measure the control chamber total pressure. The transducer was calibrated by measuring the control total pressure at the steady-state condition with a Meriam manometer.

The output velocity was measured with a DISA hot-wire (Type 55F31) probe located at the exit plane of the OR (or NOR) output channel. A DISA hot-wire anemometer system (Type 55A01 constant temperature anemometer and Type 55D10 linearizer) was employed for this measurement. An external 7 kc low-pass filter was used to eliminate high frequency jet noise effects in the velocity signal trace.

The control pressure and output flow rate signals were digitized and stored by a Biomation Waveform Recorder (Model 1015). The Biomation Recorder was capable of storing 1024 ten-bit words. The sampling interval for the series of measurements was 0.02 to 0.1 millisecond. Once signals were stored in the Biomation Recorder, they could be retrieved and displayed on an oscilloscope (Tekronix Model 5103N). The switching (or return) time was determined directly from the displayed control pressure and output velocity traces as defined above. Typical traces are shown in Figures 6 and 7.

The output total pressure transient response was measured with a total pressure probe located at the exit plane of the NOR output channel. The total pressure probe was connected to a Kistler Piezoelectric pressure transducer (Model 601L); the transducer was connected to a Kistler charge amplifier (Model 504A). The transient output pressure signal was digitized and stored by a Biomation Recorder. This signal was retrieved and plotted on a Hewlett Packard X-Y recorder (Model 135A). With the plotting speed of the order of 50 seconds, the transient signal could be reproduced quite precisely without adding undesirable dynamics of the plotting instrument.

It was found that as the control total pressure increased, the supply chamber total pressure also increased due to the increased pressure in the supply nozzle exit region. (That is, there is some coupling between the supply and control pressures.) However, the supply flow rate remained almost constant even when the control pressure increased to 10 in. $H_2O$ (the decrease in the supply flow rate was less than 1.5 percent of that with zero control pressure). This effect was also observed by Weikert and Moses [65]. For each set of measurements, the supply total pressure was set to 10 in. $H_2O$ with the control chamber open to ambient pressure, and the supply flow rate was measured. This supply flow rate measurement was used to compute the supply jet dynamic pressure $\frac{1}{2}\rho\left(\frac{q_s}{b_s}\right)^2$.

ENDNOTE

[1]Based on the supply nozzle width: $Re_s \equiv U_s b_s/\nu$.

# CHAPTER V

## RESULTS AND DISCUSSION

Unless otherwise mentioned, the coordinates of the graphs presented in this chapter are normalized with respect to the associated variables defined in Chapter III. The following measured values were used for the normalization:

$$q_s = 230.9 \text{ in}^2/\text{sec}$$

$$U_s = \frac{q_s}{b_s} = 2309 \text{ in/sec}$$

$$\frac{1}{2} U_s^2 = 0.3 \text{ psig } (8.28 \text{ in. } H_2O)$$

$$t_t = \frac{b_s}{U_s} = 4.33 \times 10^{-2} \text{ millisecond.}$$

### 5.1 Jet Spread Parameter

Goertler's jet velocity profile [31] given by Equation (3.1) has an experimentally derived parameter $\sigma$ which is called a jet spread parameter. A value of $\sigma = 7.67$ was found for the two-dimensional jet [58]. However, that value of $\sigma$ does not hold for the semi-confined jet because the top and bottom plates reduce the jet entrainment. A value of $\sigma$ for the semi-confined jet can be determined either by measuring the transverse velocity profile at a given axial distance from the nozzle, or by measuring the jet centerline axial velocity distribution.

Figure 29 shows jet centerline axial velocity distributions in the semi-confined jet (no side walls and splitter; aspect ratio = 3.1). The measured velocities are normalized with respect to continuity averaged velocity $U_s$ at the supply nozzle exit plane. The uncertainty in these measurements is of the order of one percent of full scale ($\frac{u_c}{U_s} = 1.0$). Due to the boundary layer development in the nozzle, $u_c/U_s$ is greater than one in the "zone of flow establishment." Goertler's theory [31] with $\sigma \cong 10.5$ yields best match with the experimental data for $s/b_s \geq 25$ (the length of the entrainment streamline during the switching process is $3 < s_e/b_s < 35$ for the monostable fluid amplifier with the nominal geometry). Since the constant-velocity "potential core" region is not considered in Goertler's theory, the agreement between his theory and the experimental data is generally poor in the "zone of flow establishment." For the range of $4 < s/b_s < 15$, $\sigma = 20$ yields better agreement with the experimental data than $\sigma = 10.5$.

Although it is possible to use Albertson's two-dimensional theory [31; dashed line in Figure 29] in the dynamic modeling of a monostable fluid amplifier, the resulting equations will be unnecessarily complex and difficult to solve. Two previous studies [6, 46][1] provide justification for using Geortler's profile in the present study.

## 5.2 Comparison of Steady-State Jet Reattachment Model Predictions With Experimental Data

One of the contributions of the present work to the literature is the development of the steady-state jet reattachment model which can correctly predict the steady-state jet reattachment distance and jet deflection angle.

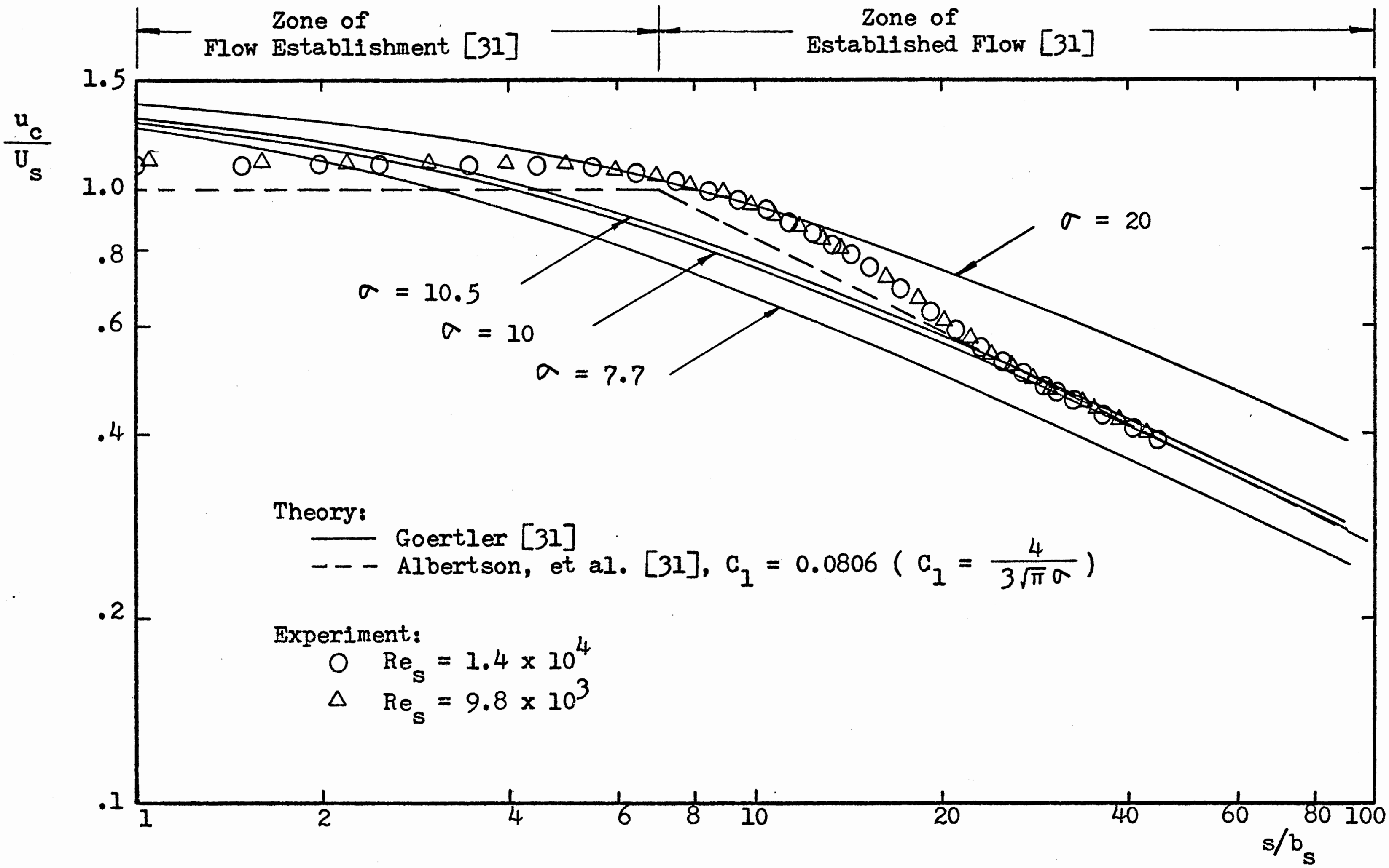


Figure 29. Jet Centerline Axial Velocity Distributions in the Semi-Confined Jet (AR = 3.1)

Figures 30 and 31 show the variations of steady-state reattachment distance with control flow rate for offsets $D_1 = 0.5$ and $D_1 = 1.0$, respectively. Since Goertler's theory with a single value of $\sigma$ does not correctly predict the measured centerline velocity for the entire range of s (Figure 29), steady-state jet reattachment distances were calculated using two values of $\sigma$ (i.e., $\sigma = 10.5$ and $\sigma = 20$).

With $\sigma = 10.5$, analytically predicted reattachment distances are in good agreement with experimental data (Kimura and Mitsuoka [30]) (see solid lines in Figures 30 and 31). Although Goertler's theory with $\sigma = 20$ yields better agreement with the measured centerline velocity in the zone of flow establishment than with $\sigma = 10.5$, analytically predicted reattachment distances (with $\sigma = 20$) are not in good agreement with the experimental data [30]. Therefore, in this thesis a value of $\sigma = 10.5$ was used both for the steady-state jet reattachment model and for the dynamic model.

Analytical predictions of two additional investigators [19, 23] are also compared with the experimental data [30] in Figures 30 and 31. Predictions using the present model ($\sigma = 10.5$) correlate significantly better with the experimental data than do those of other investigators.

Figures 32 and 33 show the variations of jet deflection angle with control flow rate for several different values of the wall offset $D_1$. Some of the early investigators [30, 68, 69] assumed that the jet deflection was only due to the control-to-supply momentum ratio; others [8, 19, 36, 65, 67] assumed that the control nozzle exit pressure $p_c$ was known or to be experimentally determined. Goto and Drzewiecki [23] assumed that the control nozzle exit pressure $p_c$ is equal to the average value of the separation bubble pressure and the unattached-side pressure

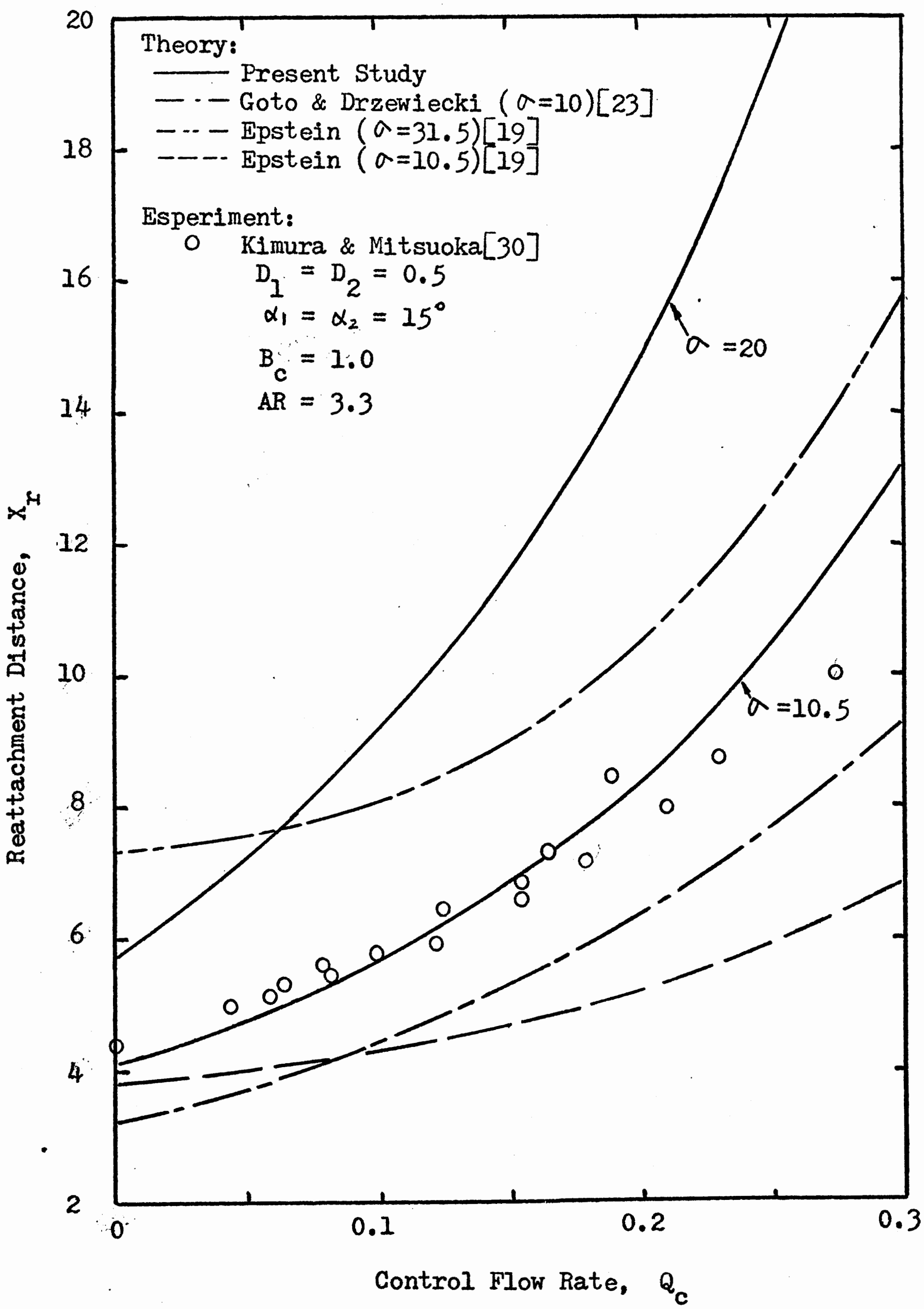


Figure 30. Variation of Steady-State Reattachment Distance With Control Flow Rate for $D_1 = 0.5$ and $\alpha_1 = 15°$

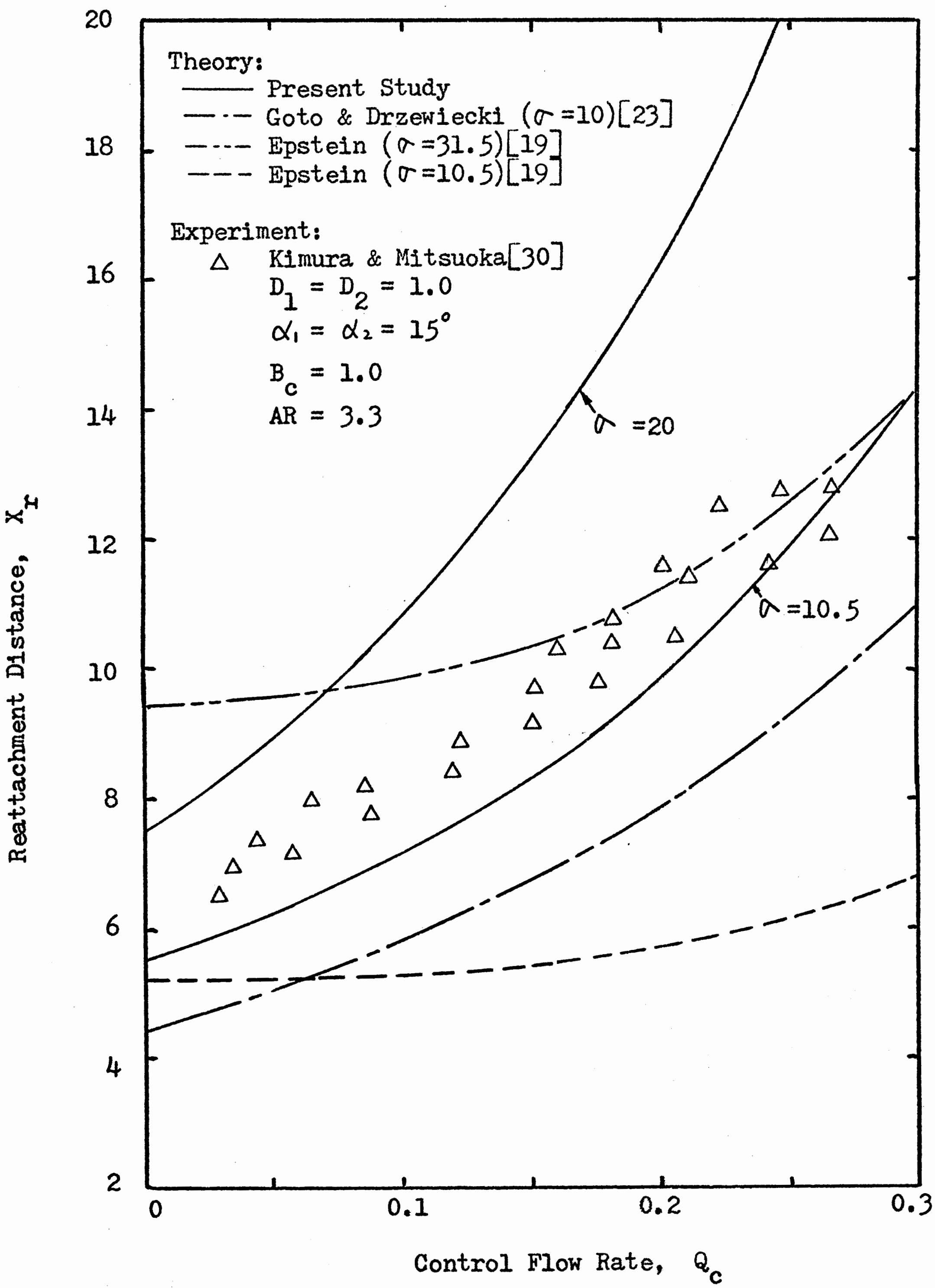


Figure 31. Variation of Steady-State Reattachment Distance With Control Flow Rate for $D_1 = 1.0$ and $\alpha_1 = 15°$

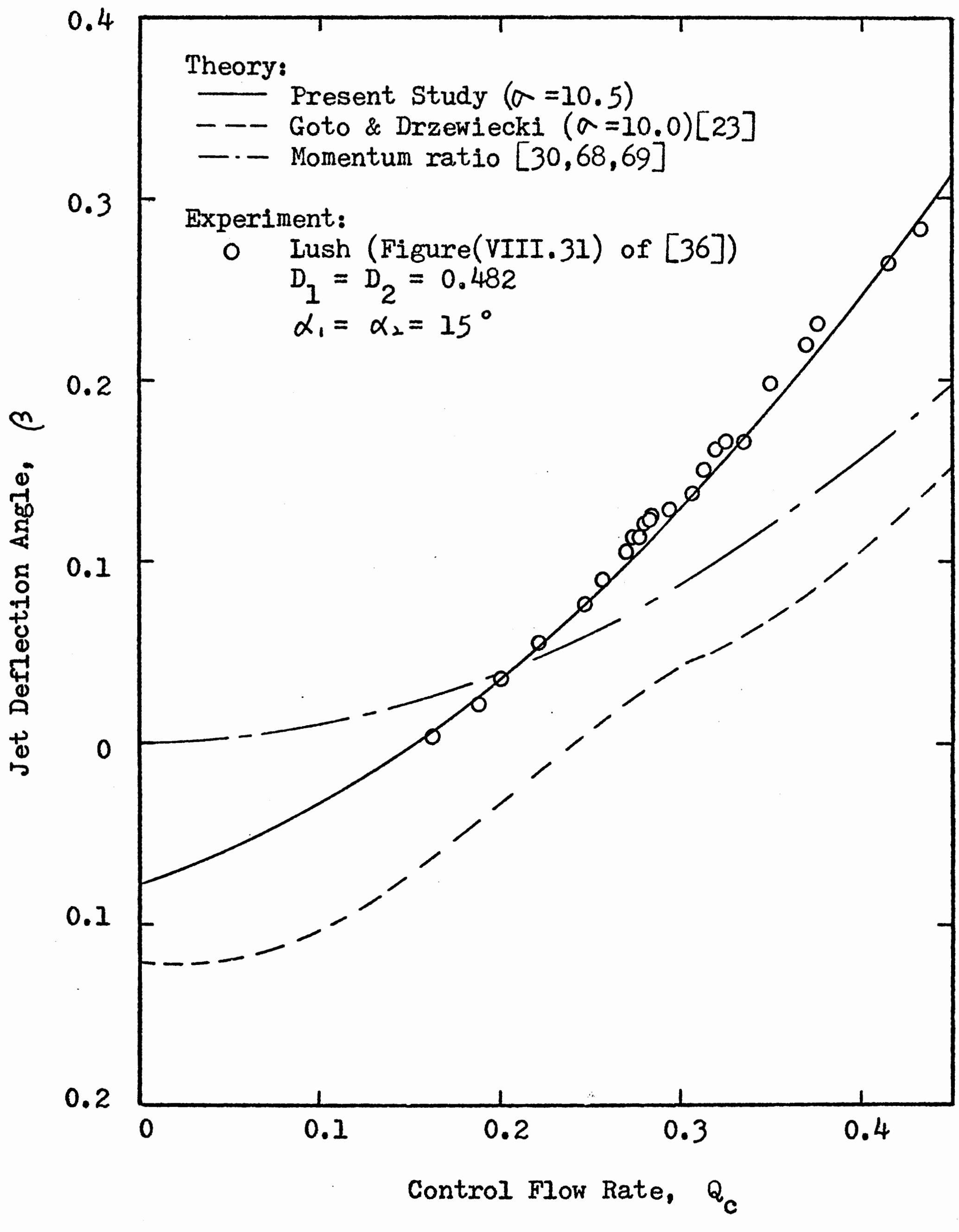


Figure 32. Variation of Jet Deflection Angle With Control Flow Rate for $D_1$ = 0.482 and $\alpha_1$ = 15°

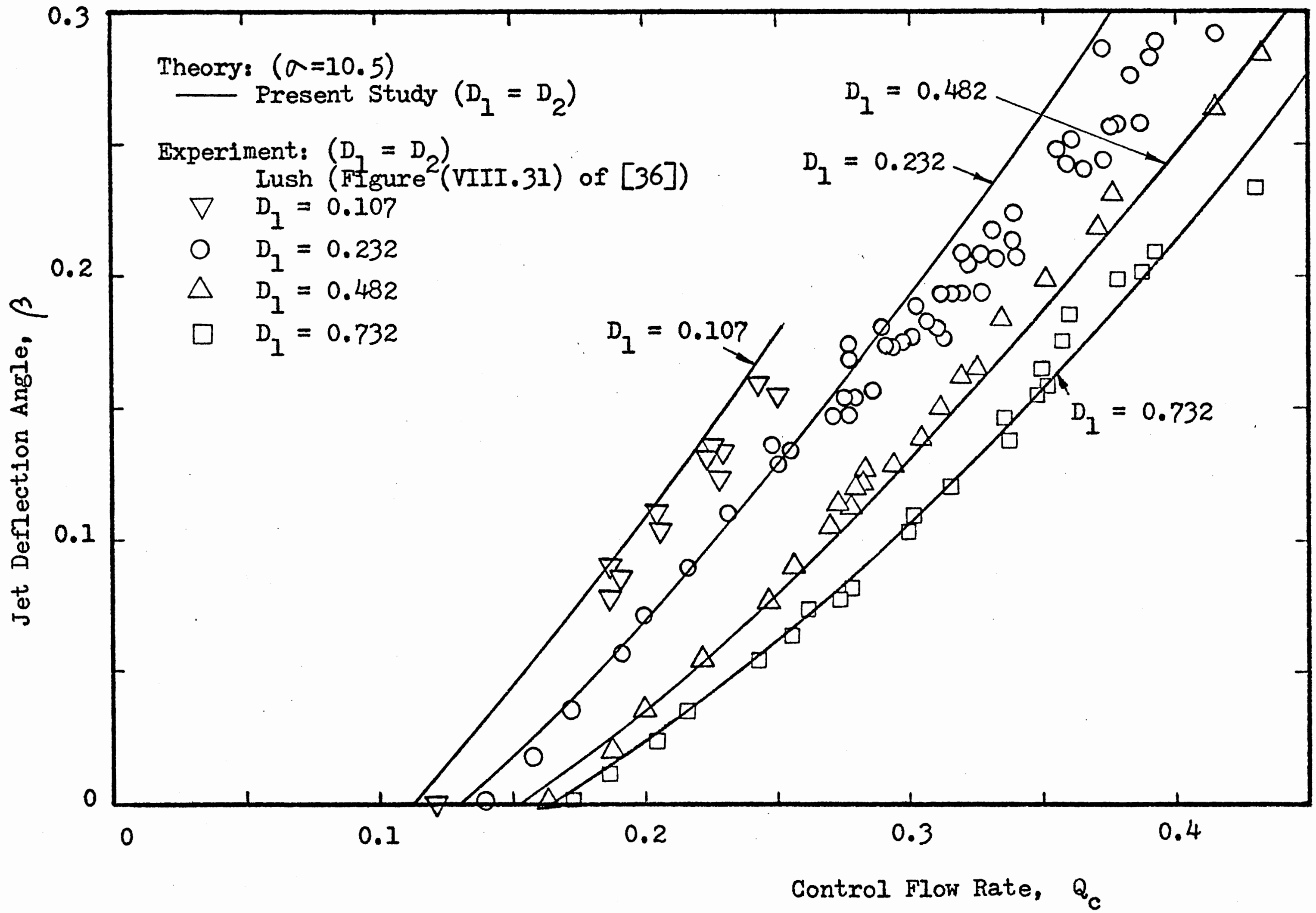


Figure 33. Variation of Jet Deflection Angle With Control Flow Rate

(i.e., $p_c = (p_1 + p_2)/2$); consequently, the value of $p_c$ was always negative for any control flow rate. Lush [36] showed in static pressure measurements at the control nozzle exit plane that the value of $p_c$ is positive for $Q_c > 0.11$ and $D_1 = 0.107$, or for $Q_c > 0.22$ and $D_1 = 0.482$. As shown in Figure 32, analytical predictions of other investigators [23, 30, 68, 69] do not agree well with the experimental data of Lush [36; Figure (VIII.31)].

The value of minor loss coefficient $K_L$ used in the present model was chosen to be unity by matching a predicted jet deflection angle with a particular measured value [36; Figure (VIII.31)] for $Q_c = 0.25$ and $D_1 = 0.482$. However, as shown in Figures 32 and 33, the present model predictions agree well with the experimental data [36] for the entire range of the control flow rate used, and for the wall offset $D_1$ of 0.107 to 0.732.

The computer execution time for an analytical prediction (i.e., for each point on each curve) in Figures 30 through 33 on an IBM 370/158 was of the order of 0.4 second.

### 5.3 Comparison of Dynamic Model Predictions With Experimental Data

Figure 34 shows a comparison between analytically predicted switching times and the author's experimental data for the monostable fluid amplifier with the nominal geometry. For these predictions and measurements the amplifier input (control total pressure, hereafter called control pressure) was a terminated ramp-type signal with a preselected saturation level. The measured control input rise time (from the first discernible change in the initial control pressure to the final value $P_{tc}$) was between 2 and 3 milliseconds. For the analytical prediction, the

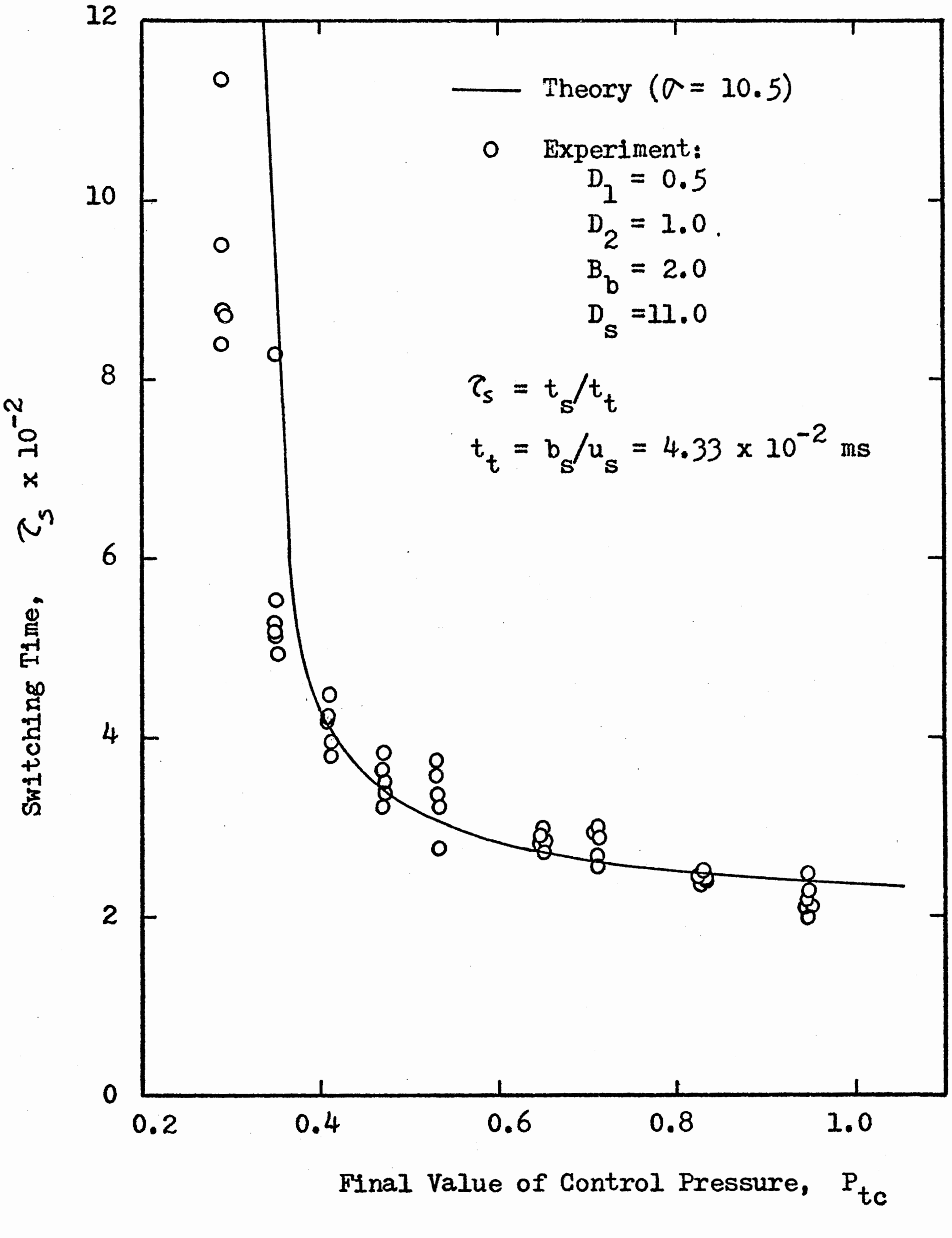


Figure 34. Variation of Switching Time With Control Pressure for the Monostable Fluid Amplifier With the Nominal Geometry

rise time was assumed to be 2.5 milliseconds. The effect of the rise time variations ($\pm$0.5 millisecond) on the analytical prediction was $\pm$0.6 percent of full scale (i.e., in this case, $\tau$ = 1200).

The agreement between theory (with $\sigma$ = 10.5) and experiment in Figure 34 is excellent except for the low control pressure range. For control pressures less than $P_{tc}$ = 0.4, corresponding switching times are large and repeatability[2] of the measurements is poor. Because of this poor repeatability and large switching time, the use of control pressure below $P_{tc}$ = 0.4 is not practical in the application of the monostable amplifier.

Figure 35 shows a comparison between analytically predicted return times and experimental data for the monostable fluid amplifier with the nominal geometry. The control pressure was initially applied to the control chamber and then "suddenly" removed from the chamber by closing the solenoid valve. When the solenoid valve was closed, the inlet to the control chamber was open to the ambient. The measured control input decay time (from the first discernible change in the control pressure $P_{tc}$ to an ambient pressure) was between 1 and 2 milliseconds. In the analytical predictions, the decay time was assumed to be 1.5 milliseconds. The effect of decay time variations ($\pm$ 0.5 millisecond) on the analytical predictions was $\pm$ 1.2 percent of reading.

The experimental results (Figure 35) show that the effect of the initial control pressure level on the return time is negligible. This is expected since return to the attachment wall is governed mainly by the flow through the bias vent port after the control pressure decreases below a "threshold value." However, the analytical prediction of the return time is slightly affected by the initial value of the control pressure.

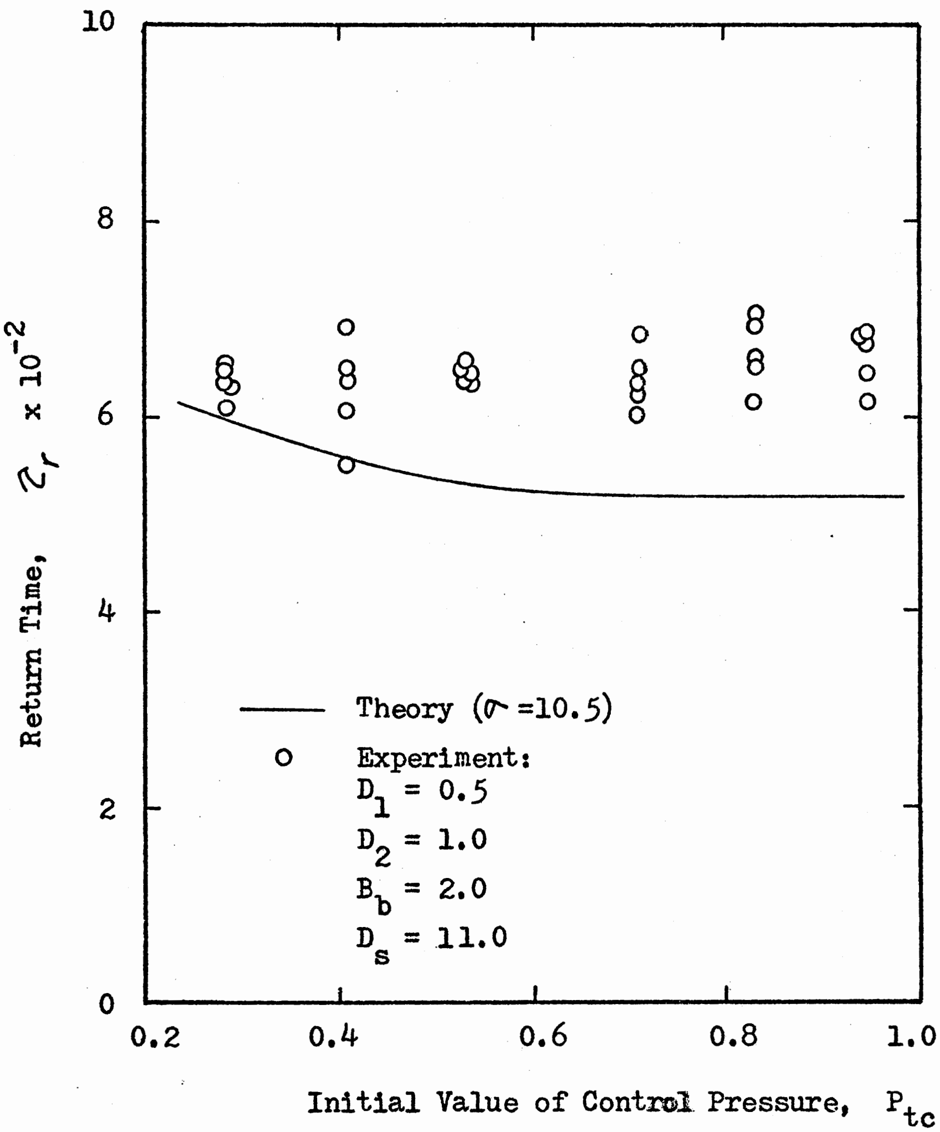


Figure 35. Variation of Return Time With Control Pressure for the Monostable Fluid Amplifier With the Nominal Geometry

The analytical predictions exhibit a maximum error of 20 percent of reading[3] over the range of the control pressure tested.

Figure 36 shows the effect of the jet spread parameter ($\sigma$) variation on the analytical predictions of the switching time for the monostable amplifier. The effect is not significant in the range of $10.5 < \sigma < 20$ for $P_{tc} > 0.4$. A change in $\sigma$ from 10.5 to 7.7 causes a significant increase in the "threshold value" of the control pressure (below which no switching occurs). A value of $\sigma = 20$ gives better correlation with the measured switching times for $P_{tc} < 0.7$, than does $\sigma = 10.5$. However, in the present study a value of $\sigma = 10.5$ was used for the dynamic model because (1) the steady-state jet reattachment model with $\sigma = 20$ cannot correctly predict the jet reattachment distance (see the discussion in section 5.2), and (2) the control pressure range of practical interest is $P_{tc} > 0.4$.

Figure 37 shows a comparison between analytically predicted switching times (using the present model) and the experimental data of Goto and Drzewiecki [23][4] for a bistable fluid amplifier. The dimensions of the Goto and Drzewiecki test model is given in Table II, along with the dimensions of the Lush test model. The rise time in the referenced experiment was between 1 and 2 milliseconds. A rise time of 1.5 milliseconds was assumed for the analytical prediction; Goto and Drzewiecki [23] also used this rise time.

Goto and Drzewiecki defined the switching time as the time elapsed from the first discernible change in the control pressure until the hot-film probe located at the point of the splitter registered the maximum signal. For the analytical prediction it was assumed that the hot-film probe registered the maximum signal just before the jet reattached to the opposite wall (i.e., at the end of phase I). The agreement between the

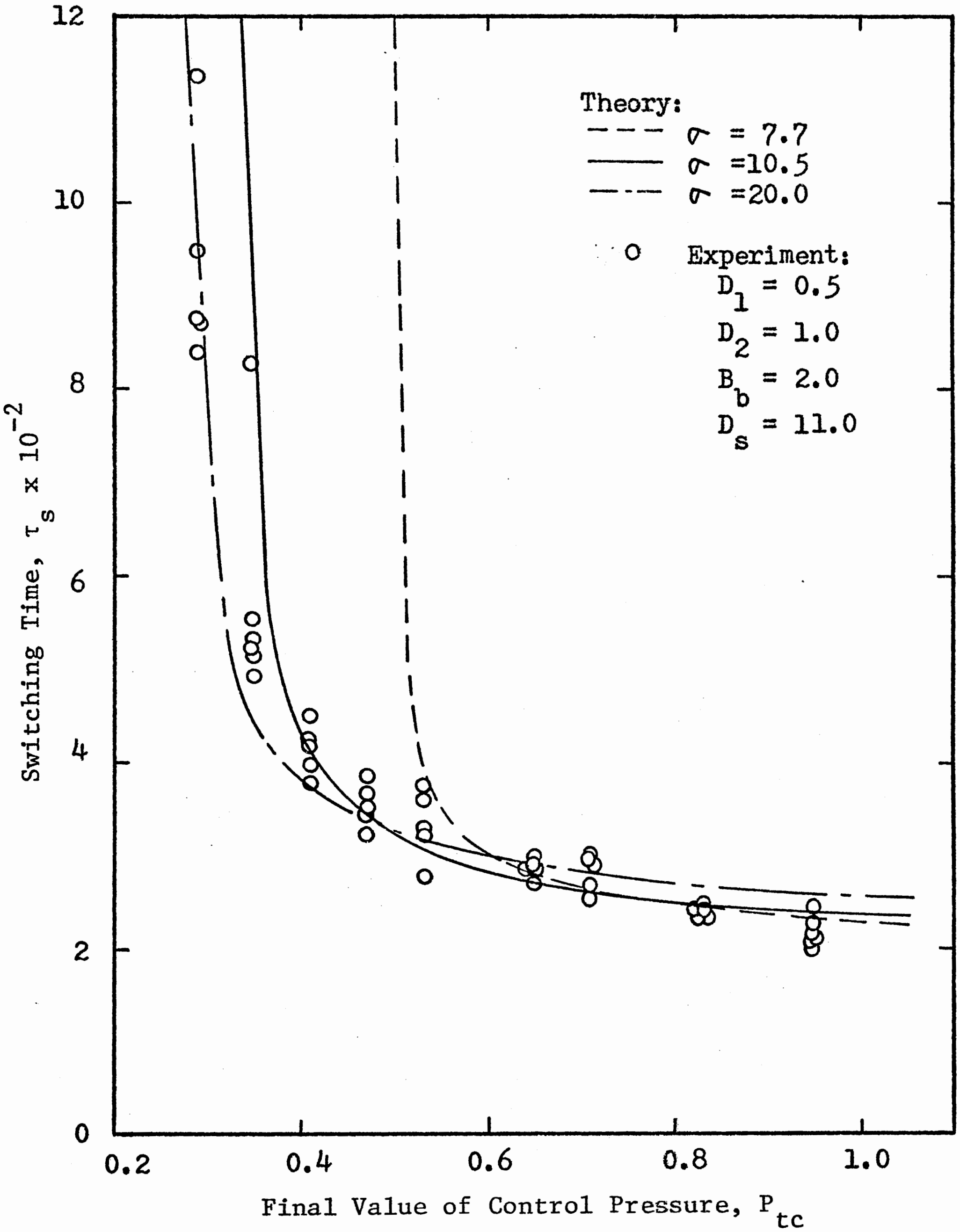


Figure 36. Effect of Jet Spread Parameter (σ) Variation on the Switching Time for the Monostable Fluid Amplifier

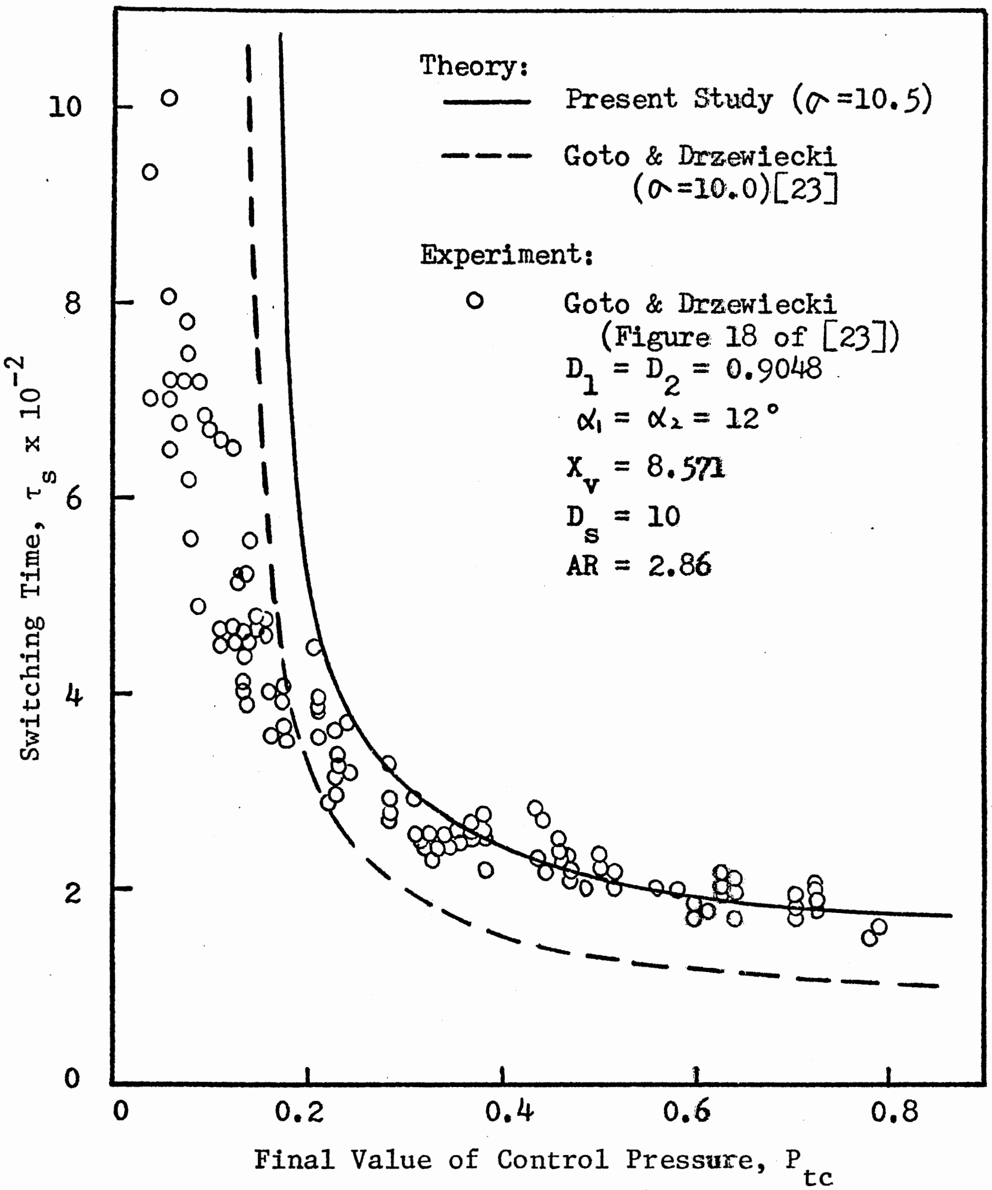


Figure 37. Variation of Switching Time With Control Pressure for a Bistable Fluid Amplifier

TABLE II

GEOMETRIES OF TEST MODELS

| Geometric Parameter | Goto and Drzewiecki [23] (Test Model 1) | Lush [36] |
|---|---|---|
| Supply nozzle width ($b_s$) | 0.983 inch | 1.0 inch |
| Control nozzle width ($b_c/b_s$) | 1.0 | 1.0 |
| Bias vent width ($b_b/b_s$) | 1.0 | 1.0 |
| Attachment wall offset ($d_1/b_s$) | 0.905 | 0.482 |
| Opposite wall offset ($d_2/b_s$) | 0.905 | 0.482 |
| Attachment wall angle ($\alpha_1$) | 12° | 15° |
| Opposite wall angle ($\alpha_2$) | 12° | 15° |
| Attachment wall length ($x_{v1}/b_s$) | 8.57 | 13.035 |
| Opposite wall length ($x_{v2}/b_s$) | 8.57 | 13.035 |
| Splitter distance ($d_s/b_s$) | 10.0 | 14.0 |
| Output vent width ($b_v/b_s$) | 1.905 | 2.2 |
| Control channel length ($\ell_c/b_s$) | 0.476 | 15.0 |
| Output channel length ($\ell_o/b_s$) | 26.67 | 8.8 |
| Aspect ratio (AR) | 2.86 | 1.0 |

See Table I in Chapter IV for the geometry of the monostable.

present model predictions and the experimental data is very good for $P_{tc} > 0.25$ and superior to that due to Goto and Drzewiecki.

Figure 38 shows a comparison between analytically predicted switching times and the experimental data of Lush [36][5] for a bistable fluid amplifier. The dimensions of the Lush test model is given in Table II. Lush reported that the static pressure and flow rate just upstream of the control nozzle exit plane took the order of 20 milliseconds to rise to their steady value. For the analytical prediction in Figure 38, the rise time of the total pressure at the inlet of the control channel was calculated by considering the inertance and resistance of the channel so that the rise time of the flow rate at the control nozzle exit plane was 20 milliseconds.

Lush defined the experimental switching time as the time elapsed from the first discernible change in the control pressure until the total pressure probe located at the end of the opposite wall registered a maximum signal. (The total pressure probe was positioned so that it was near to the jet centerline after switching had finished.) For the analytical prediction it was assumed that the probe registered a maximum signal at the beginning of phase II.

Although Lush obtained data from a test amplifier which had an aspect ratio of unity, the prediction using the present model is still in good agreement with his data except for the low control pressure range.

Figure 39 shows a comparison of an analytically predicted NOR output total pressure transient response with an experimentally measured one. A "negative step" input signal having a decay time of 1.5 milliseconds approximates the experimental input condition. The present model predicts the overall transient response reasonably well, even though the predicted

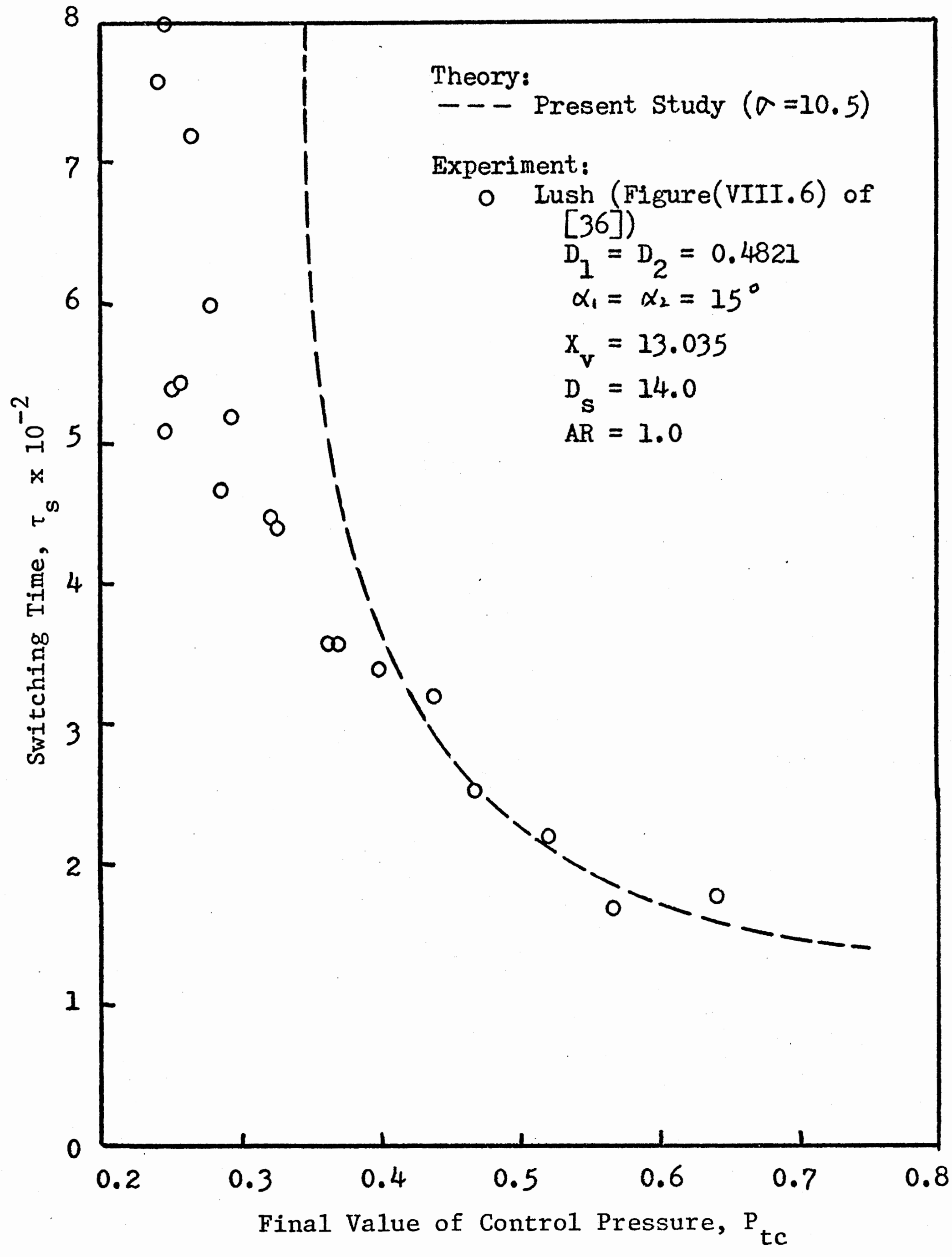


Figure 38. Variation of Switching Time With Control Pressure for a Bistable Fluid Amplifier

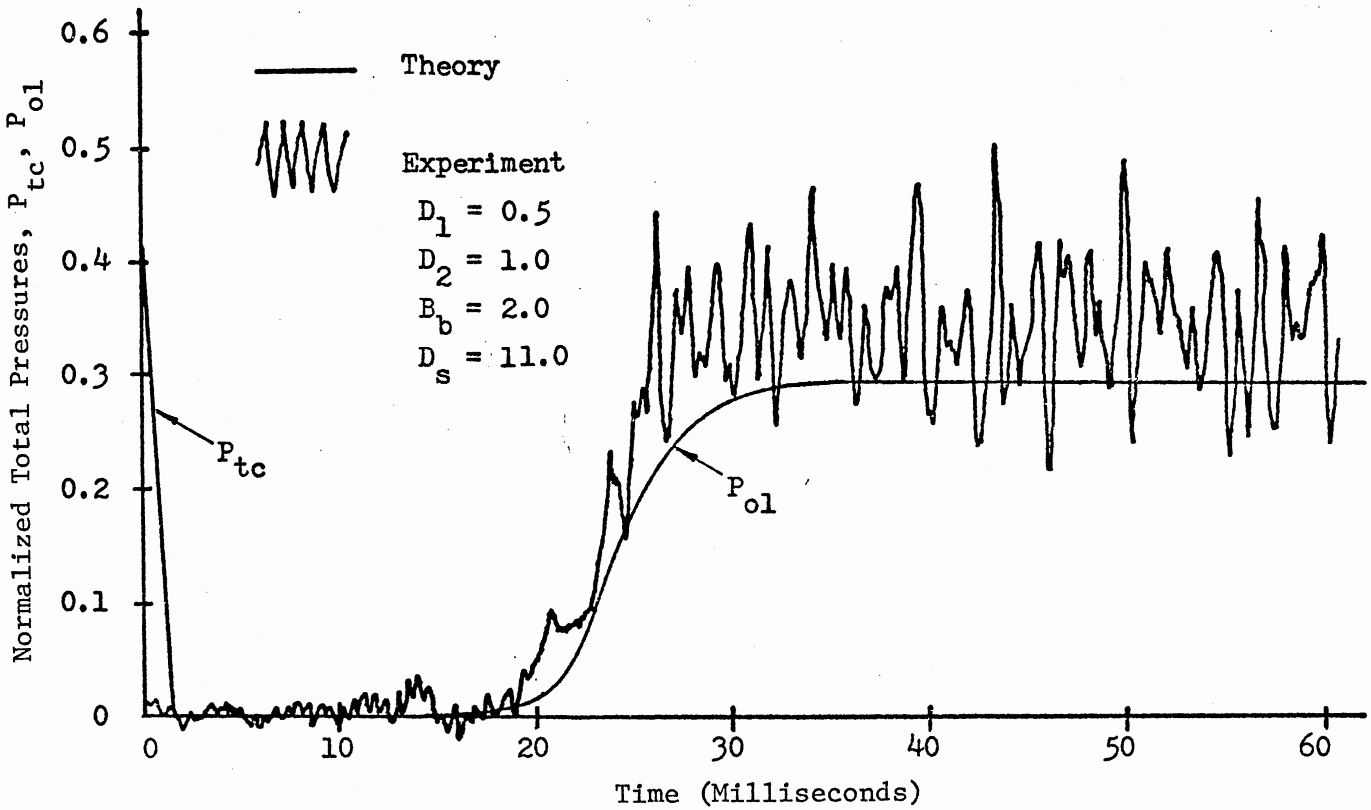


Figure 39. NOR Output Total Pressure Transient Response of the Monostable Fluid Amplifier

final value of the total pressure is 15 percent less than the measured mean value.

The noise in the measured output response in Figure 39 is mostly due to the turbulence of the jet. The value of the turbulence intensity ($\frac{\overline{u'^2}}{U_{o1}^2}$ ; $U_{o1}$ = mean velocity at the output exit plane) measured at the NOR output channel exit plane was of the order of 0.014. In contrast, the maximum value of a semi-confined jet turbulence intensity ($\frac{\overline{u'^2}}{u_c^2}$ ; $u_c$ = jet centerline velocity) reported in References [7, 25, 28] is of the order of 0.083.

Figure 40 shows the predicted effect of the control input pressure "shape" on the OR output total pressure transient response of the monostable fluid amplifier. Two control input pressures of different shapes are used for the analytical predictions: one (dashed line) is a terminated ramp-type input signal having a rise time of 2.5 milliseconds and the other (solid line) is an exponential input signal having a time constant of 10 milliseconds. Both control pressures have the same initial value of -0.154 and final value of 0.41. The output response time (or switching time) for the exponential input signal is almost twice as long as that for the terminated ramp-type input signal. Although the predicted output responses are not validated by experiment, it is expected that they are valid within the range of error which the predicted NOR output response exhibits (see Figure 39).

The computer simulation time for an analytical prediction (e.g., a switching time for a given control pressure) on an IBM 370/158 was of the order of 15 seconds.

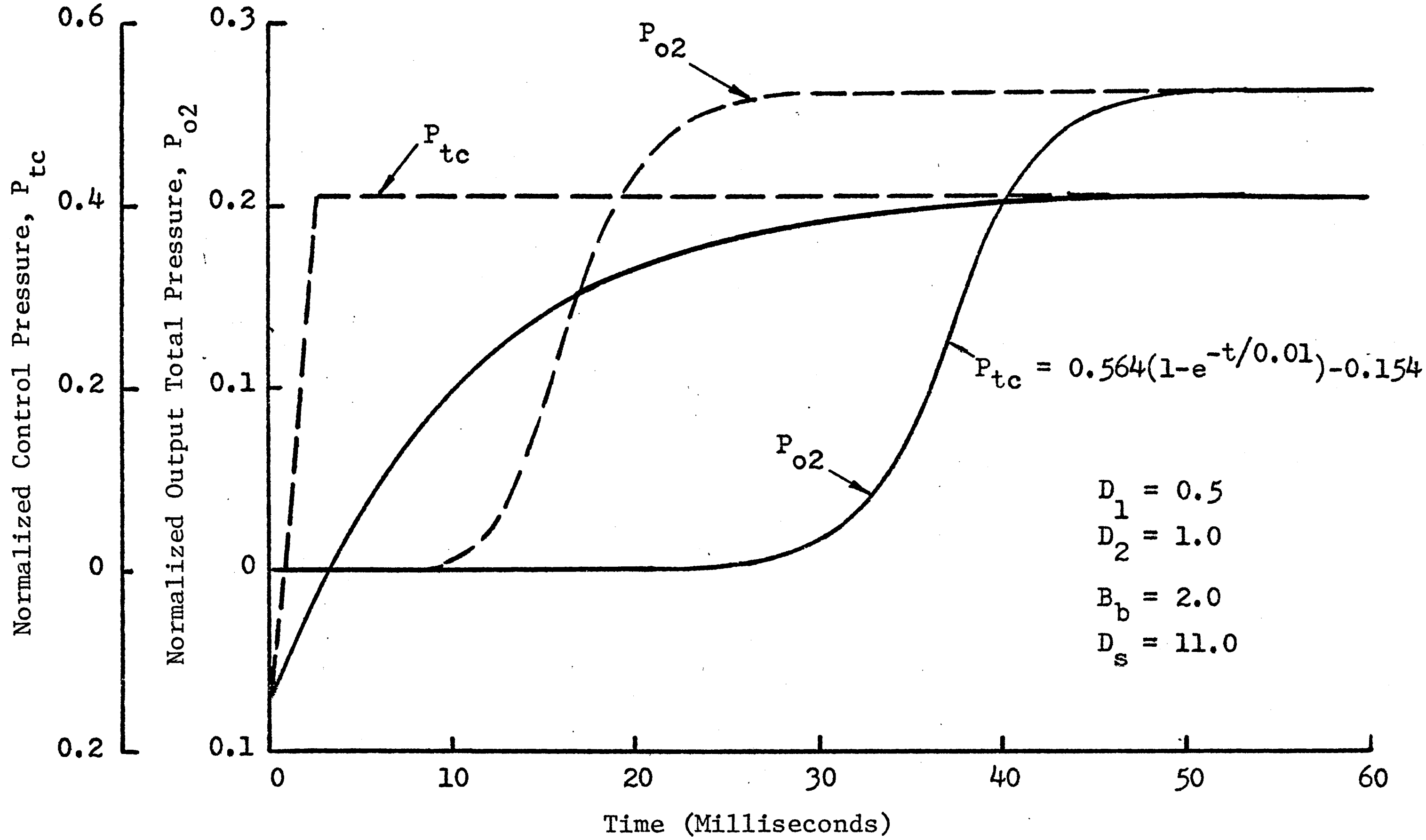


Figure 40. Predicted Effect of Control Input Pressure Shape on the OR Output Total Pressure Transient Response of the Monostable Fluid Amplifier

## 5.4 Experimental Data Repeatability

The scatter of the experimental data shown in Figures 34 through 36 was due to: (1) the variation of the control pressure rise (or decay) time, (2) the difficulty of measuring the mean value from the output velocity trace, and (3) the nature of the fluid dynamic process inside the monostable fluid amplifier. The scatter in the switching and return time data for low control pressures was due mainly to the latter effect as explained below.

Experimental studies [36, 63] have shown that the growth rate of the separation bubble decreases after the reattachment point reaches the output vent edge (point K, in Figure 15b), because of the reduced return flow into the bubble. If the control flow is not large enough to make the jet "jump" over the output vent and attach to the wall downstream of it, then a stable situation develops with the jet remaining at the end of the wall. However, turbulent eddies traveling down the edges of the jet tend to destabilize the flow balance near the end of the wall and the jet may "jump" over the output vent, depending on how close the control flow is to the threshold value (below which no switching occurs). The poor repeatability for low control pressures (see Figure 34) is probably due to this indeterminate "dwell period" before the jet "jump" [36].

## 5.5 Effects of Geometric Variations on Switching and Return Times

This section presents the results of experimental and analytical investigations of the effects of geometric variations on the switching and return times of the monostable fluid amplifier.

### 5.5.1 Effect of Attachment Wall Offset, $D_1$

Figure 41 shows the effects of varying attachment wall offset $D_1$ on the switching and return times of the monostable amplifier. The experimental results show that an increase in the offset $D_1$ reduces the switching time, but increases the return time greatly. Analytical predictions also show the trend very well.

If a fast return and a fast switching time is taken as a criterion for a "best" design of a monostable fluid amplifier, a "best" offset $D_1$ may be obtained by observing the intersection of the two curves shown in Figure 41. That is, with this criterion $D_1 \cong 0.4$ is the "best" geometry in this study.

Poor repeatability of the measurements for an offset in the region of $D_1 = 0.25$ is probably due to the indeterminate "dwell period" before the jet "jump" (see section 5.3 for detailed discussion).

### 5.5.2 Effect of Opposite Wall Offset, $D_2$

Figure 42 shows the variation of switching time with opposite wall offset, $D_2$. An increase in the offset $D_2$ results in a great increase in the measured switching time. Analytical predictions also show the trend very well. Repeatability of the measurements is poor for offsets greater than $D_2 = 1.0$.

Figure 43 shows the variation of return time with offset $D_2$. The experimental results show that the effect of varying $D_2$ on the return time is negligible in the range of $D_2 \geq 1.5$. But in the range of $D_2 < 1.5$ a decrease in the offset results in a great increase in the return time, because the reduced passage between the jet edge and the opposite wall

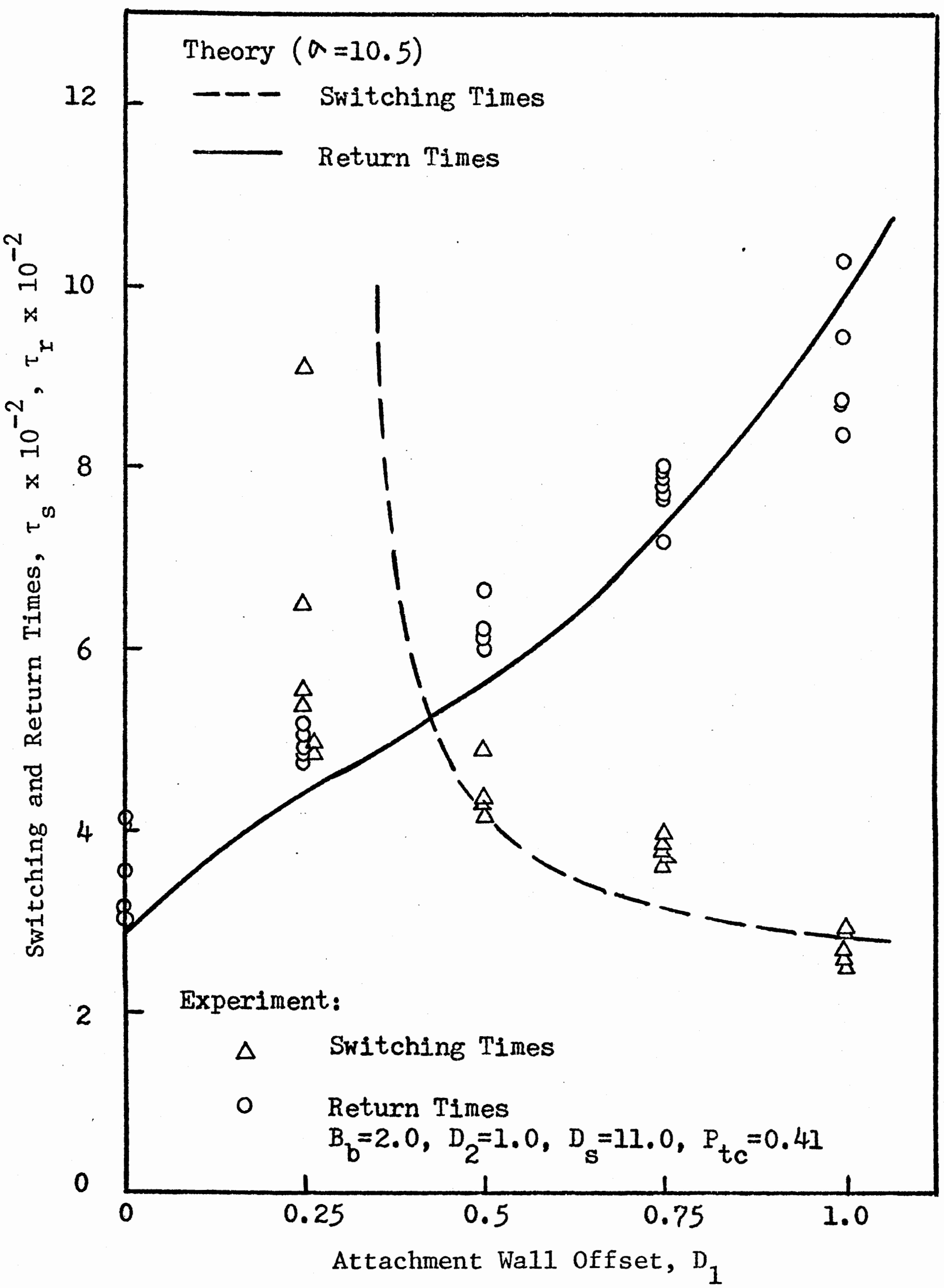


Figure 41. Variation of Switching and Return Times With Attachment Wall Offset

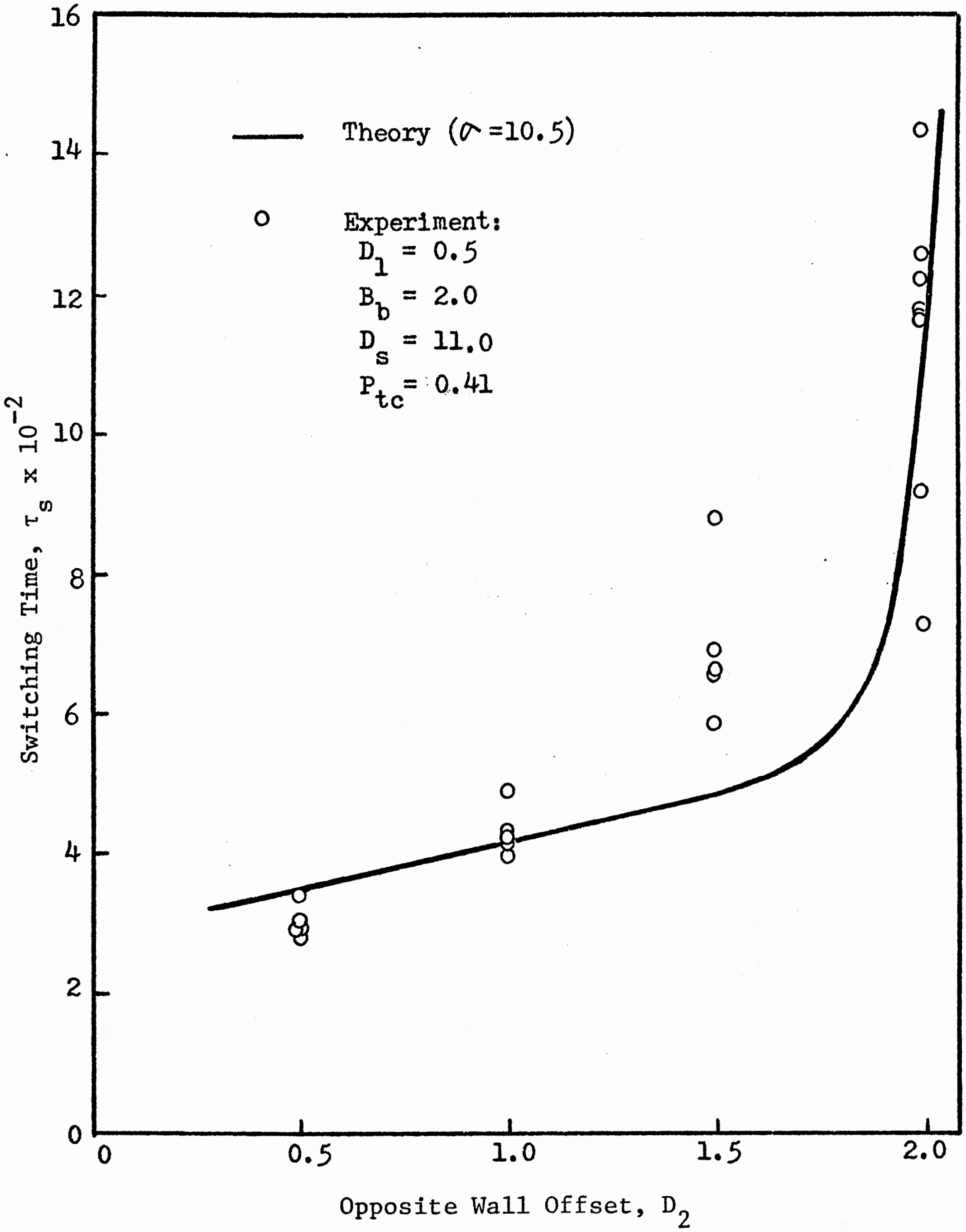


Figure 42. Variation of Switching Time With Opposite Wall Offset

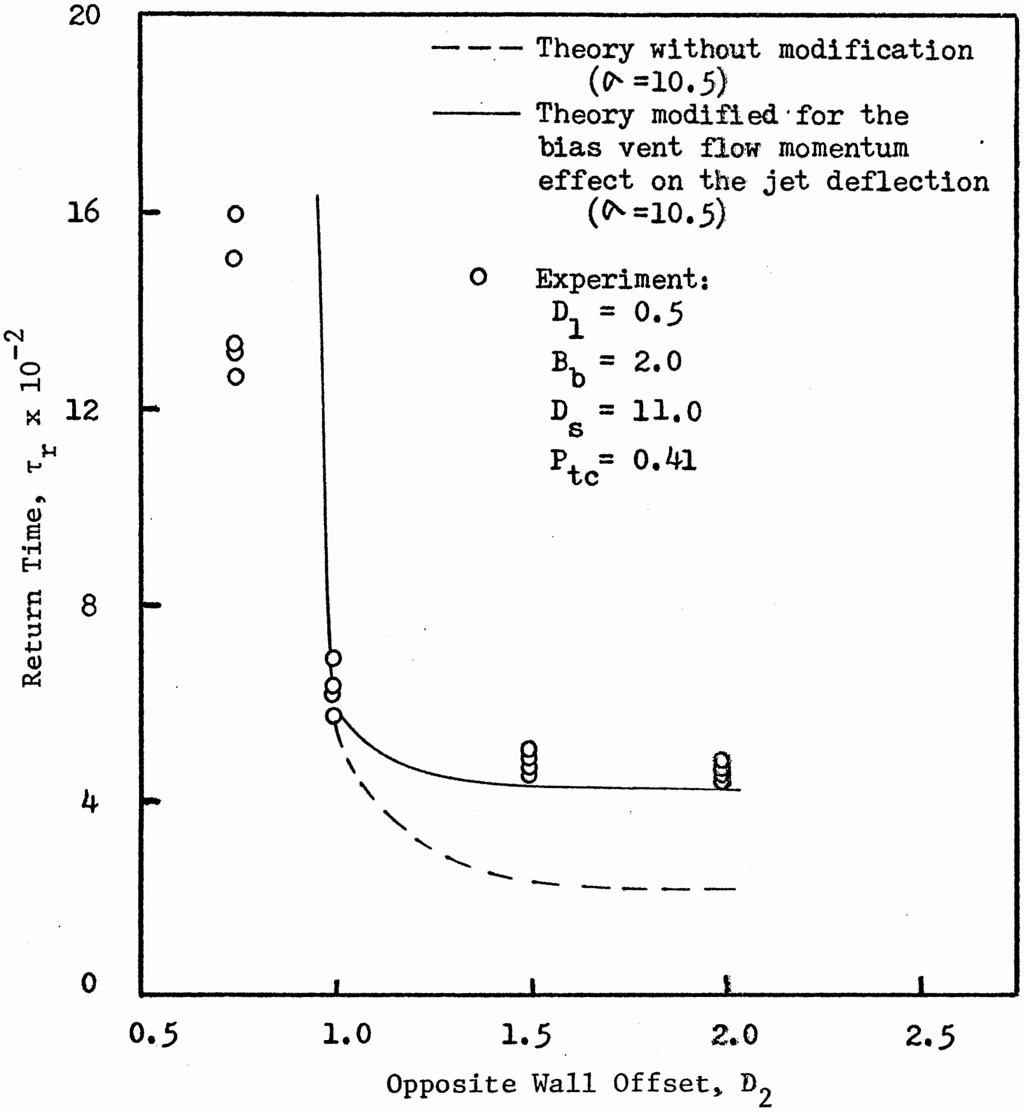


Figure 43. Variation of Return Time With Opposite Wall Offset

($a_b$ in Figure 44) restricts the induced flow from the bias vent port. For $D_2 < 0.75$, there is no return at all; that is, the jet remains attached to the opposite wall.

If the passage $a_b$ is greater than bias vent width $b_b$, the momentum ($J_b$) of the induced flow from the vent is no longer parallel to the jet centerline (see Figure 44). Therefore, Equations (3.73) and (3.75), which are derived from the momentum balance in the control volume (Figure 44), need to be modified. A simple modification has been made empirically. With a 36 percent reduction in the momentum flux of the bias vent flow,[6] the present model (with $\sigma = 10.5$) can predict the return time within 6 percent of the measured value for $D_2 > 1$ (see the solid line in Figure 43).

For $D_2 < 1$ the present model (with $\sigma = 10.5$) can only show the general trend. However, an offset less than unity is not important in the practical design of the monostable amplifier because of the large return time.

If a fast return and a fast switching time is taken as a criterion for a "best" design of a monostable fluid amplifier, a "best" offset $D_2$ can be obtained in a way similar to that discussed in section 5.5.1. That is, with this criterion $D_2 \cong 1.2$ is the "best" geometry in this study.

### 5.5.3 Effect of Splitter Distance, $D_S$

Figure 45 shows the variation of switching time with splitter distance $D_s$. The effect of varying the splitter distance on the measured switching time is negligible in the range of $10.5 < D_s < 13$. An increase in a splitter distance over $D_s = 13$ results in a great increase in the

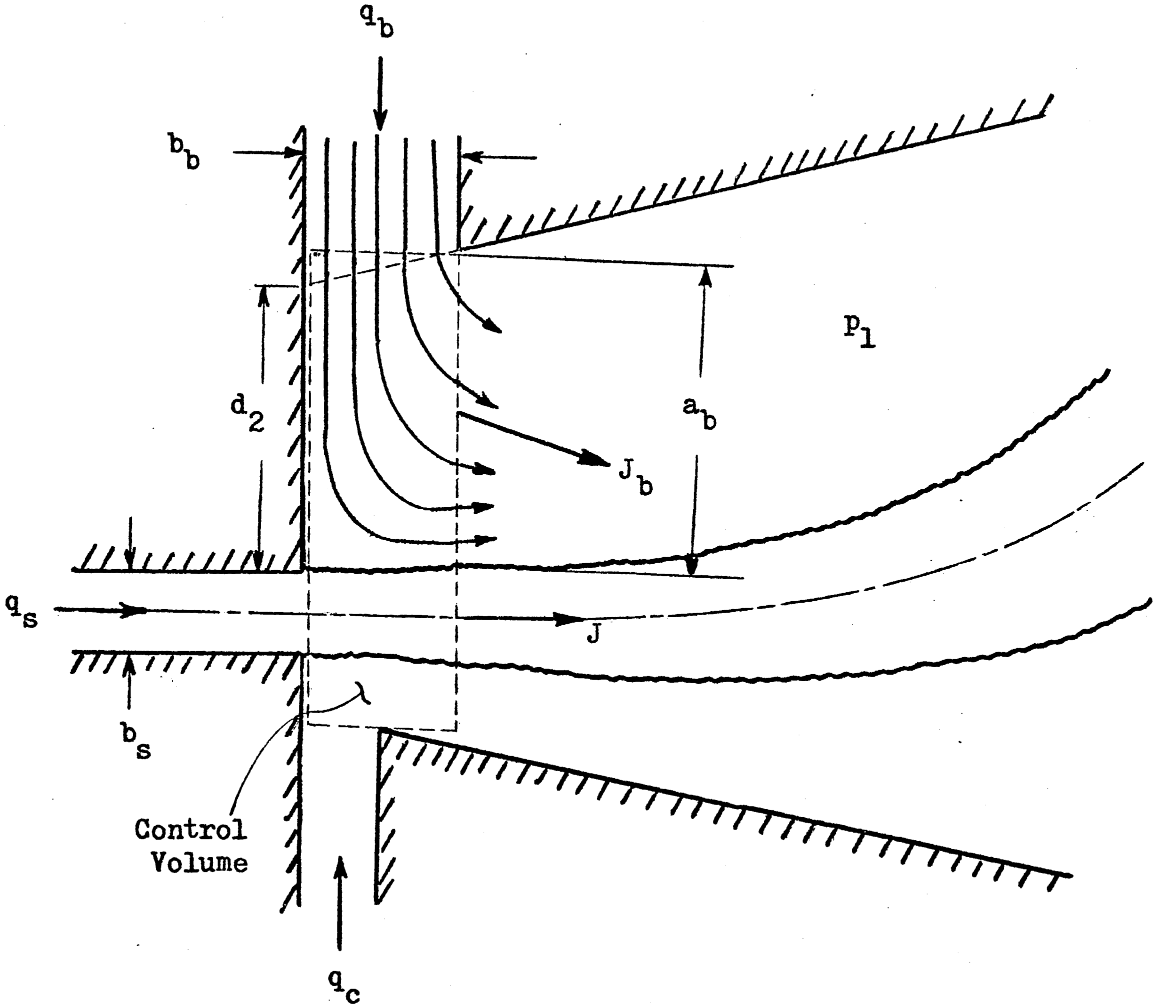


Figure 44. Bias Vent Flow Passage Width

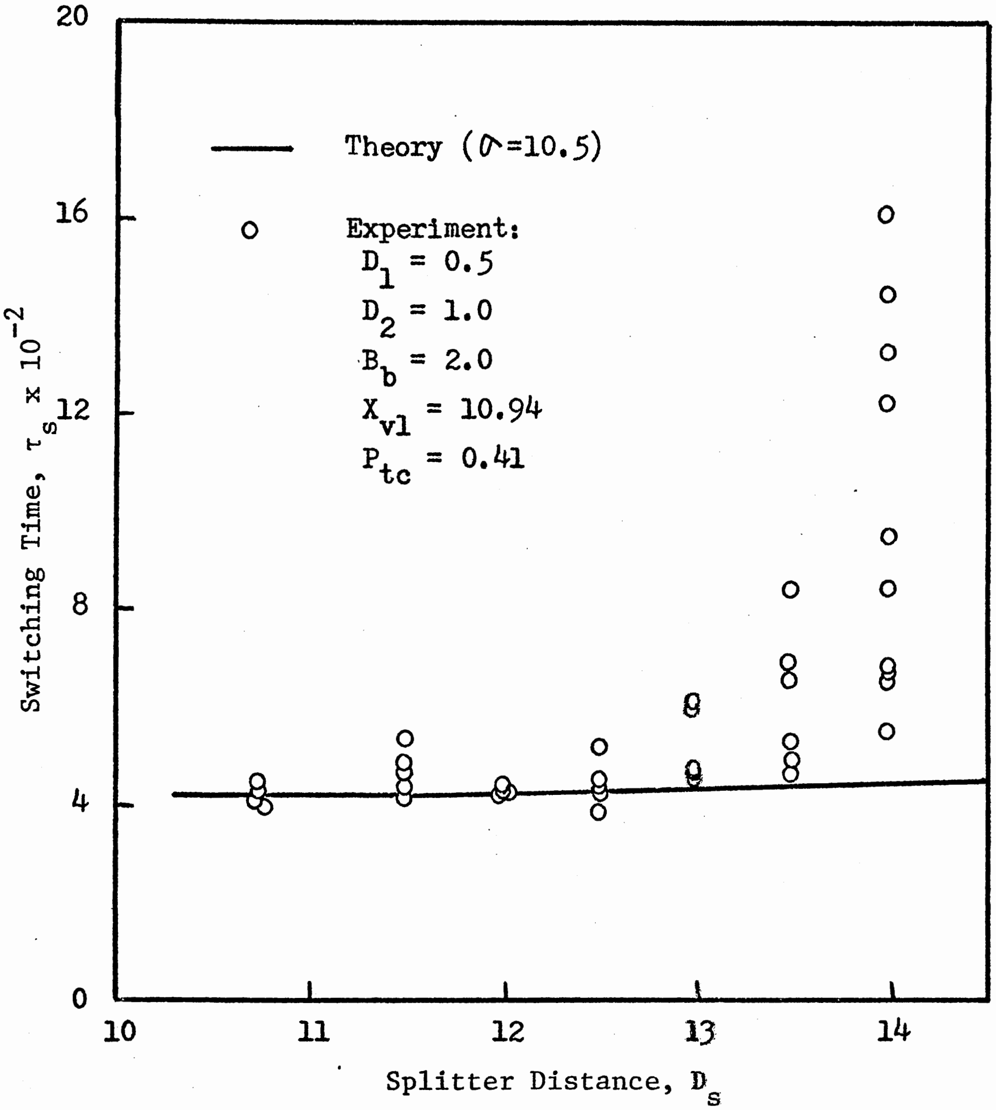


Figure 45. Variation of Switching Time With Splitter Distance

measured switching time; repeatability of the measurements is also poor for large $D_s$, probably because the vortex developed in the separation bubble becomes unstable near the output vent for $D_s > 13$ (the output vent distance is $X_{v1} = 10.94$).

The analytically predicted switching time agrees well with the measurements in the range of $10.5 < D_s < 13$. But the present theory underestimates the switching time for $D_s > 13$, because the vortex effect is not considered in the model.

Figure 46 shows the variations of return time with splitter distance. Although the experimental data are not sufficient to allow a reasonable conclusion, the analytical results show that a minimum return time can be obtained with $D_s$ in the range of 10.9. It is interesting that Savkar et al. [55] also found a minimum switching time as they varied the splitter distance ($D_s$) for the bistable fluid amplifier. However, their results cannot be compared with the result of this study since their test amplifier is quite different from that used in this study.

Wada et al. [63] show in their experimental study that the separation bubble growth is suppressed by the splitter if the splitter distance is smaller than a "critical distance" $d_s^*$ defined in Figure 47. A normalized critical distance is $D_s^* = d_s^*/b_s = 11.4$ for the geometry chosen in this study (i.e., $X_{v1} = 10.94$, $D_1 = 0.5$, and $\alpha_1 = 12°$). As the splitter distance is decreased below 10.9, it seems that the splitter suppresses the separation bubble growth, resulting in increased return times.

### 5.5.4 Effect of Bias Vent Width, $B_b$

Figure 48 shows the effect of varying bias vent width $B_b$ on the switching time of the monostable amplifier.

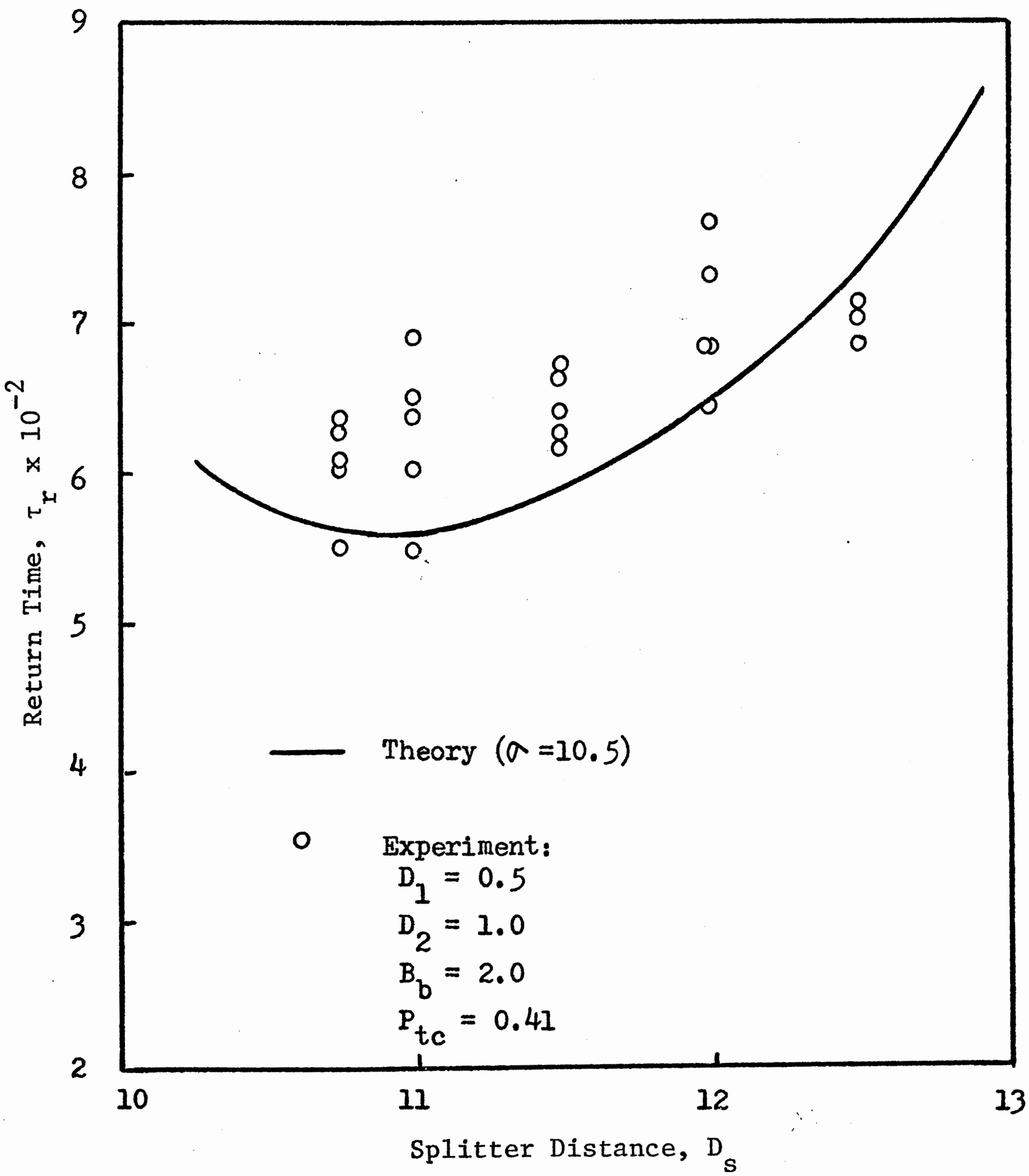


Figure 46. Variation of Return Time With Splitter Distance

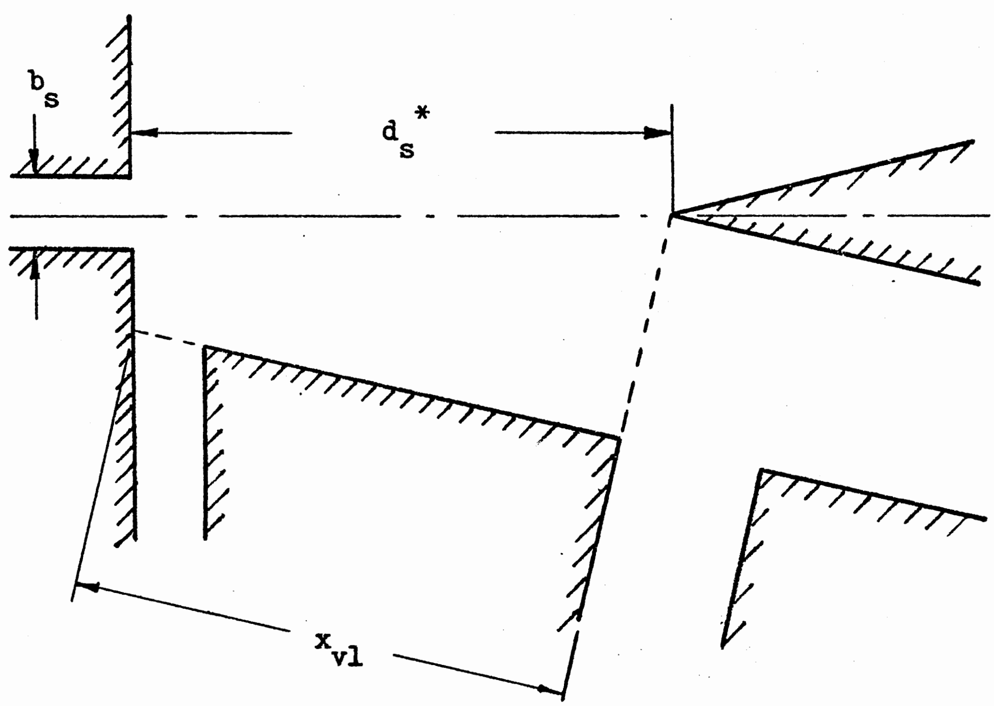


Figure 47. Critical Splitter Distance [63]

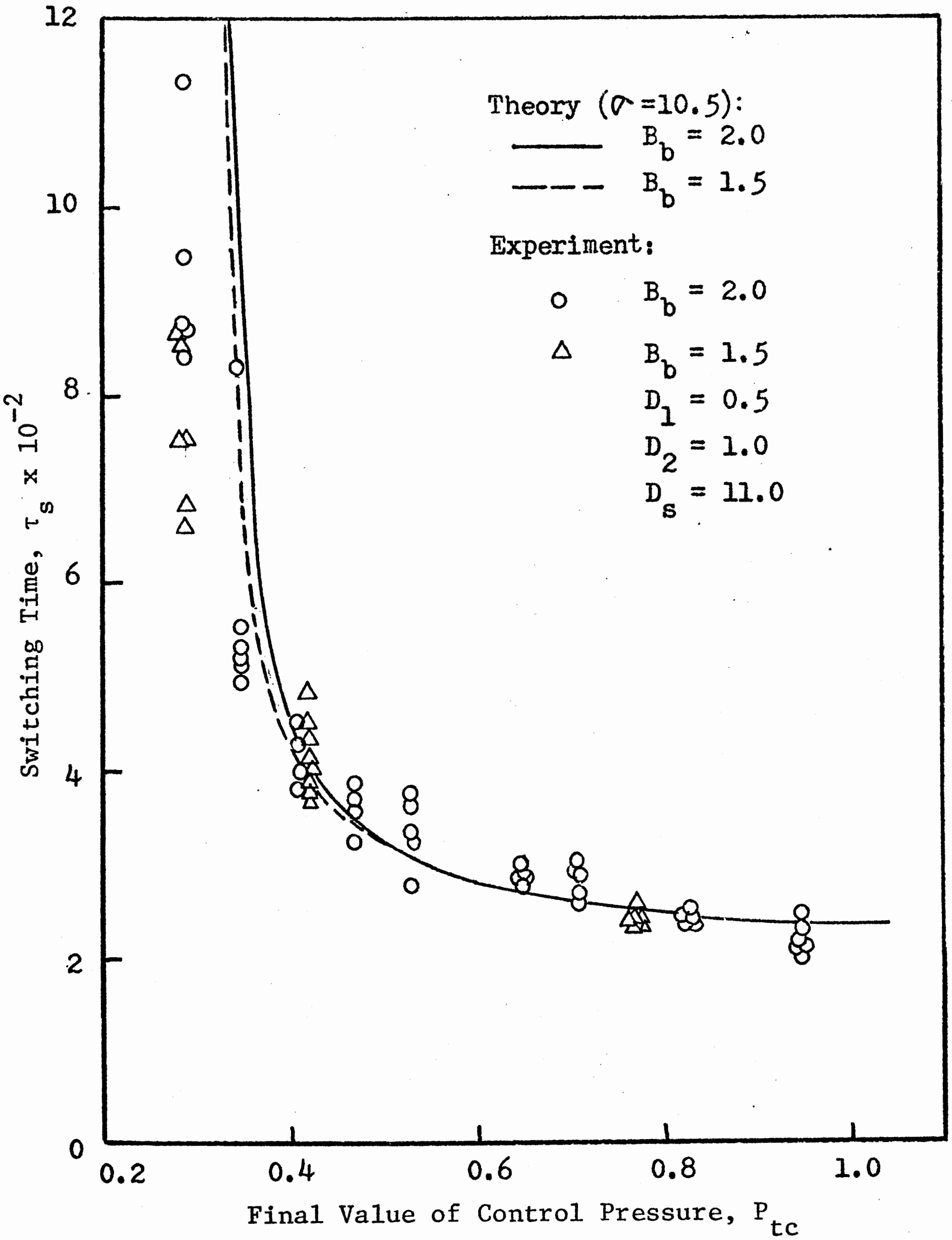


Figure 48. Effect of Bias Vent Width on the Switching Time

For the high control pressure range (say, $P_{tc} > 0.4$), there is no appreciable effect within the accuracy of the measurements. For the low control pressure range (say, $P_{tc} \leq 0.4$), the measured switching time slightly decreases as $B_b$ varies from 2.0 to 1.5 for a given value of $P_{tc}$.

The analytically predicted switching times agree well with the measured values for $B_b = 1.5$ as well as $B_b = 2.0$, except for the low control pressure range.

Figure 49 shows the variation of return time with bias vent width $B_b$. Although the experimental data were taken only for two values of $B_b$, the effect of varying the vent width on the return time is proved significant. A decrease in the vent width from 2.0 to 1.5 results in a great increase in the return time; repeatability of the measurements is poor because the induced flow from the bias vent reduces close to a threshold value (below which no return occurs). The analytical predictions show the general trend well.

Thus, we may conclude that increasing the bias vent width is one of the most effective ways to reduce the return time without affecting the switching time.

### 5.5.5 Effect of Opposite Wall Angle, $\alpha_2$

Figure 50 shows the variations of switching and return times with opposite wall angle $\alpha_2$. In this figure, experimental data are shown only for one value of $\alpha_2$, i.e., $\alpha_2 = 12°$; these data were obtained for the nominal geometry at $P_{tc} = 0.41$ (see Figures 34 and 35). Since overall correlation of the analytical predictions with the experimental data is generally good for the aforementioned geometric variations, it is hoped that analytical predictions without experimental validation can correctly

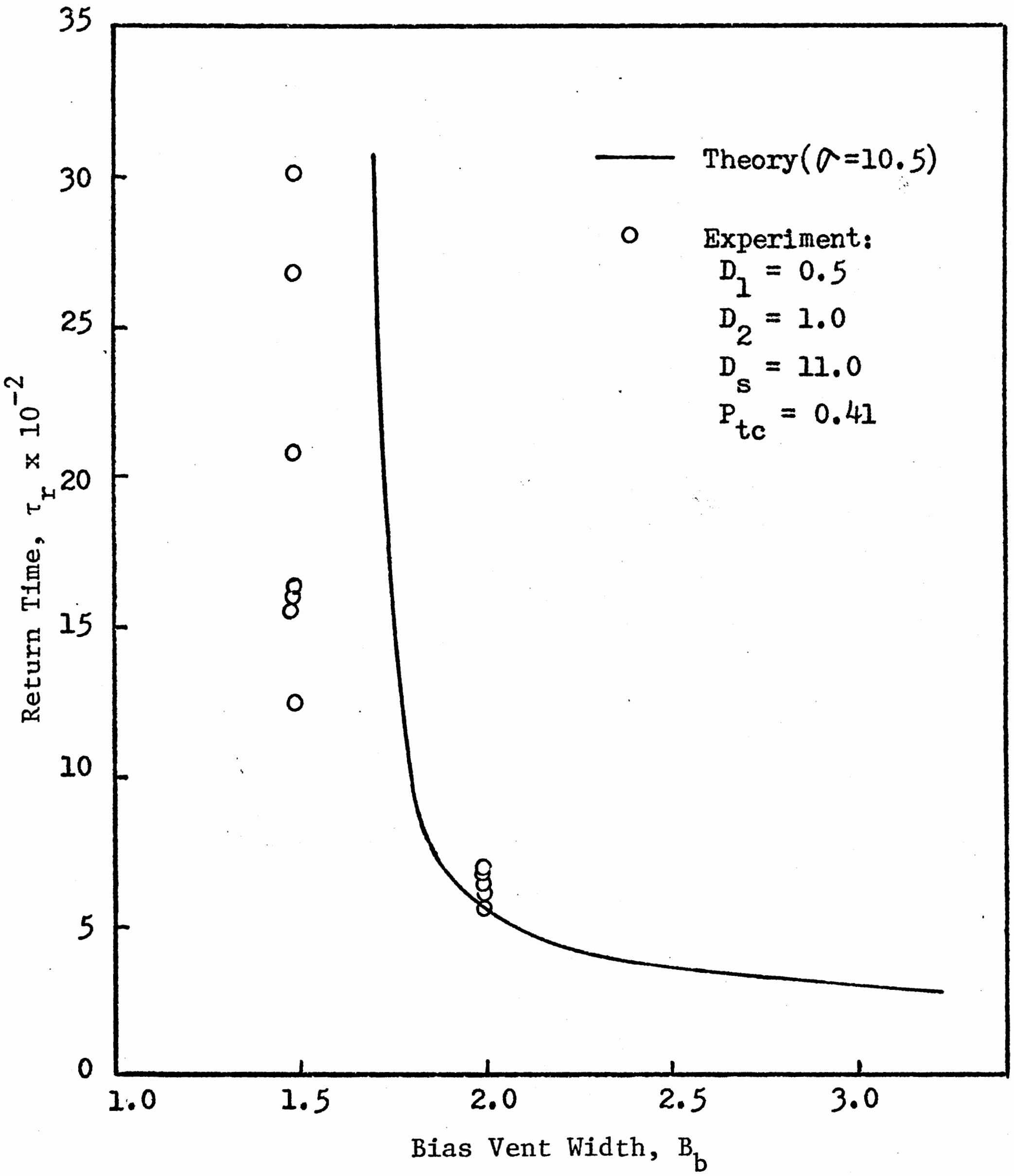


Figure 49. Variation of Return Time With Bias Vent Width

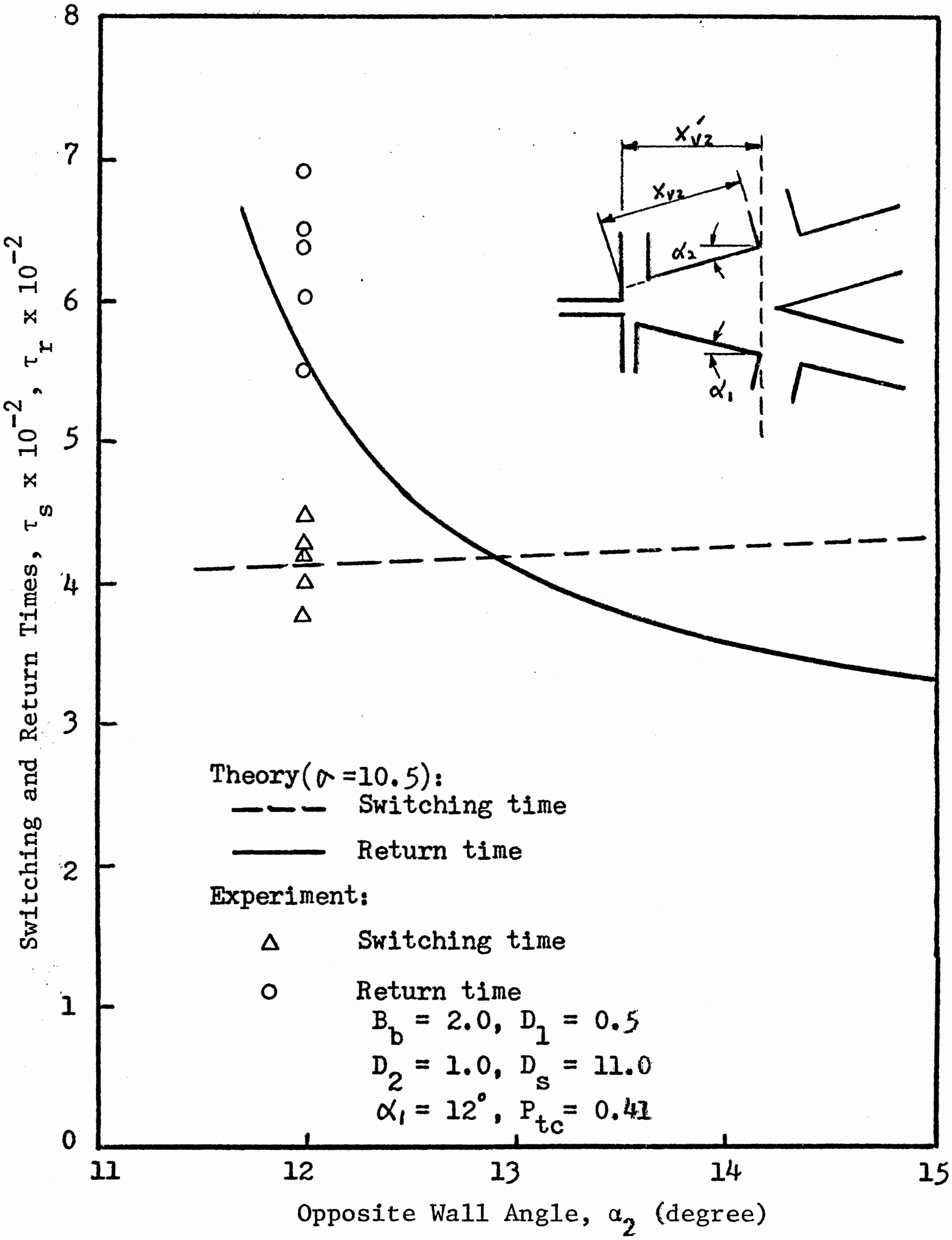


Figure 50. Variation of Switching and Return Times With Opposite Wall Angle

present the principal effects of varying $\alpha_2$ and $D_3$ (see next section) on the switching and return times of the monostable amplifier.

When $\alpha_2$ is varied, the following two ways are available to hold other variables constant at the nominal geometry: (1) opposite wall length $x_{v2}$ is kept constant, or (2) output vent location is kept constant (i.e., $x'_{v2}$ = constant; see the insert in Figure 49). The second way was chosen in this study.

The effect of varying the opposite wall angle on the switching time is negligible; however, an increase in the opposite wall angle results in a substantial decrease in the return time. Thus, we may conclude that this geometric change is another effective way to reduce the return time without sacrificing the switching time.

### 5.5.6 Effect of the Splitter Offset, $D_3$

Figure 51 shows the variations of switching and return times with splitter offset $D_3$. In this figure the experimental data are shown only for one value of $D_3$, i.e., $D_3 = 0$; these data were obtained for the nominal geometry at $P_{tc} = 0.41$ (see Figures 34 and 35).

An increase in the splitter offset toward the opposite wall reduces the switching time slightly. The effect of varying the splitter offset on the return time is negligible for $D_2 < 0.2$, but an increase in the splitter offset over $D_3 = 0.2$ results in the substantial increase in the return time.

## 5.6 Limitation of the Model

Figure 52 shows the effect of output loading (blockage of OR output channel) on the switching time. A 0.118 inch inside diameter orifice was

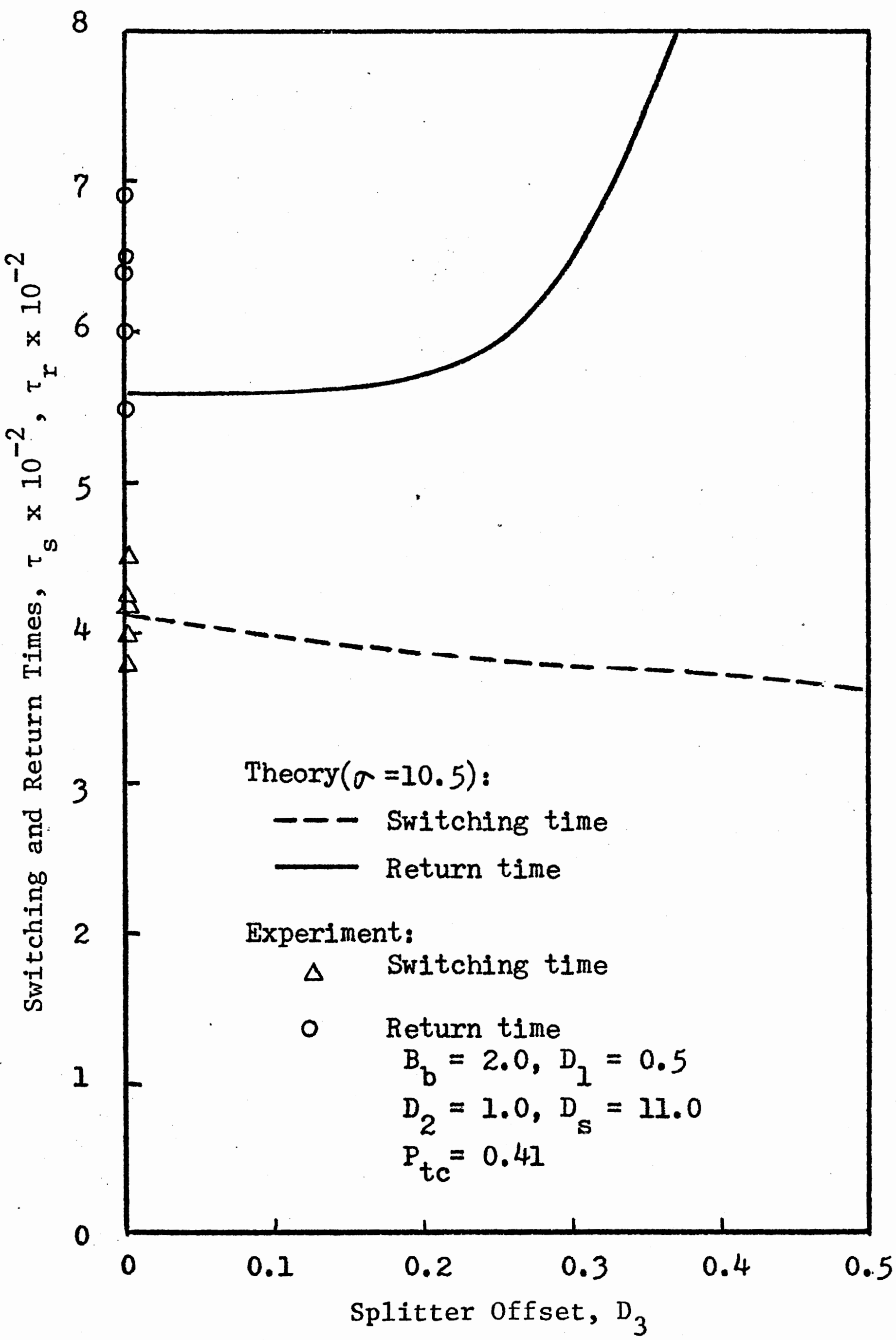


Figure 51. Variation of Switching and Return Times With Splitter Offset

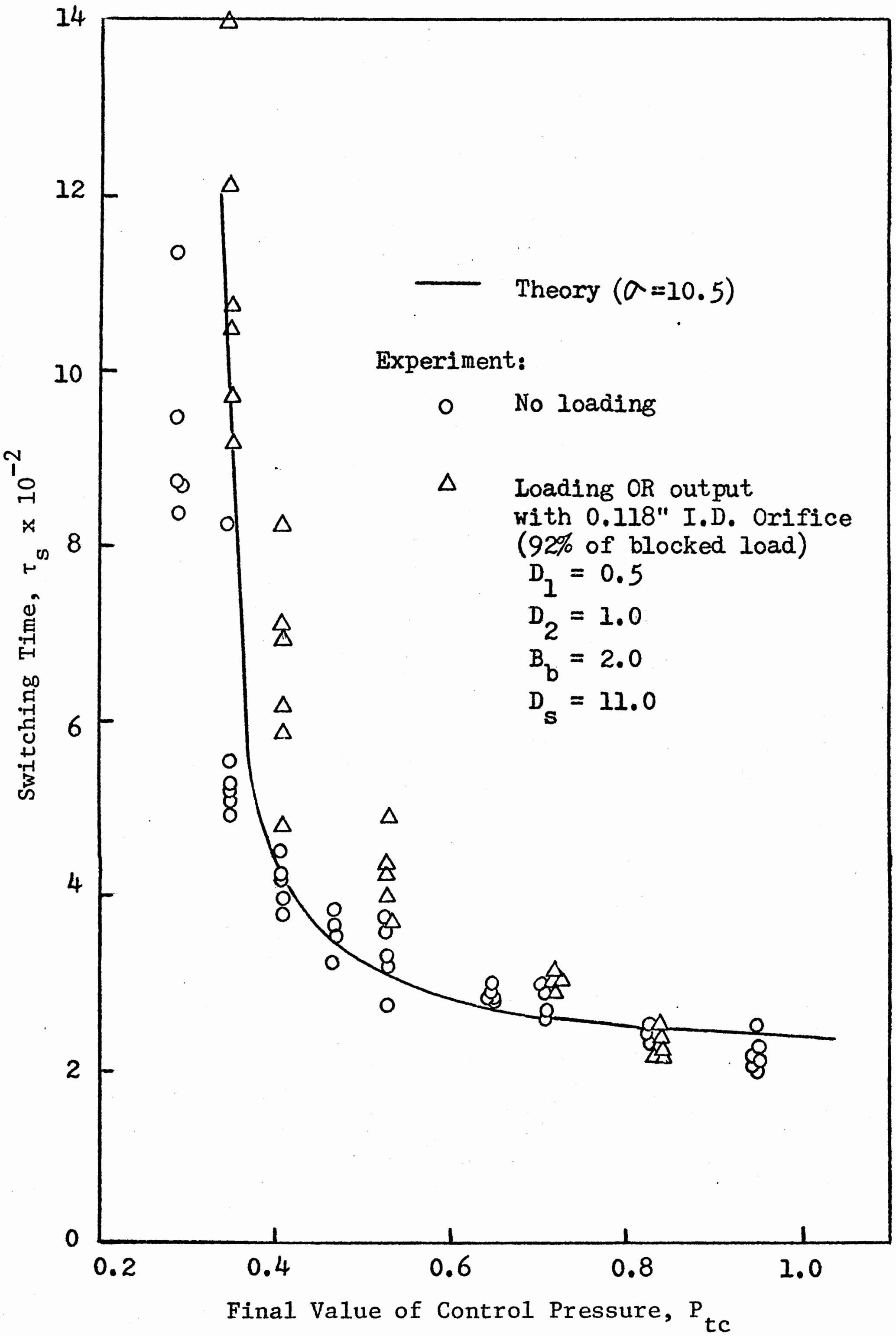


Figure 52. Effect of Output Loading on the Switching Time

mounted at the exit of the OR output channel; this resistance produced a static pressure in the channel which was 92 percent of the blocked load pressure recovery.

The switching time increases with OR output channel blockage. The effect of the blockage is stronger at low control pressures than that at high control pressures. However, in general, the effect of the blockage depends on the geometry of the output vent and splitter. This effect can be minimized or even eliminated by an appropriate design, such as employing an output decoupling vent in the output channel [18].

## ENDNOTES

[1]See Chapter II for details.

[2]Repeatability of the experimental data is discussed in the next section.

[3]The average value of readings repeated five times at a given $P_{tc}$ was used for the error calculation.

[4]Among the several different experimental data sets they obtained, the data for the test model 1 (with splitter and inactive control open; Figure 18 of [23]) are chosen for this comparison. Since their data were normalized in a slightly different way from this study, they were replotted (Figure 37) with the following transformation: the control pressures are divided by $(C_{ds})^2$ and the switching times are multiplied by $C_{ds}$ where $C_{ds}$ is the supply nozzle discharge coefficient ($C_{ds}$ = 0.85 was used by Goto and Drzewiecki [23]).

[5]Lush [36] measured the switching times for two different splitter distances (i.e., $D_s$ = 14 and $D_s$ = 20) of the bistable fluid amplifier. The experimental data for $D_s$ = 14 (Figure (VII.6) of [36]) are chosen for this comparison because that geometry is more similar to the device used in the present study. Since Lush presented the measured switching times as a function of the jet deflection angle, his data were replotted (Figure 38) with the following transformation: $P_{tc} = 2\beta$ (from his expression for $\beta$; [36], p. 52).

[6]The reduction in the momentum flux of the bias vent flow may be obtained by substituting a modified bias vent flow $Q_b$ for $Q_b$ in Equations (3.73) and (3.75). The modified vent flow is given by

$$Q_b' = \begin{cases} 0.8\ (\frac{B_b}{A_b})\ Q_b & \text{for } A_b < B_b \\ 0.8\ Q_b & \text{for } A_b \geq B_b \end{cases}$$

# CHAPTER VI

# SUMMARY, CONCLUSIONS, AND RECOMMENDATIONS

## 6.1 Summary

The jet centerline axial velocity distribution in the semi-confined jet was measured to investigate the effect of the top and bottom plates on the effective jet spread in the test amplifier. A value of the jet spread parameter $\sigma$ in the region of 10.5 yields the best match with the experimental data for $s/b_s \geq 25$. However, for a range of $4 < s/b_s < 15$, $\sigma = 20$ yields a better match with the experimental data.

A steady-state jet reattachment model was developed which is capable of accurately predicting the reattachment position of a two-dimensional, incompressible, turbulent jet to an offset, inclined wall in the presence of control flow. With $\sigma = 10.5$, analytically predicted reattachment distances are in good agreement with experimental data due to Kimura and Mitsuoka [30]. Based on this correlation and the measured jet centerline axial velocity distribution, the value of $\sigma = 10.5$ is established for the present study. The analytically predicted jet deflection angles are also in excellent agreement with Lush's experimental data due to Lush [36] for attachment wall offsets of $0.107 \leq D_1 \leq 0.732$.

Based on the steady-state jet reattachment model, an analytical dynamic model was developed which is capable of predicting the switching time, the return time, and the transient response of a monostable fluid amplifier to any time-varying input signal. The analytically predicted switching times are within 10 percent of measured values except for the low control pressure range. The analytically predicted return times are within 20 percent of measured values over the range of the control pressure tested for the nominal configuration of the monostable amplifier.

Correlation of the analytical predictions with the published experimental data for a bistable fluid amplifier is also very good except for the low control pressure range.

The NOR output total pressure transient response to a "negative step" in control pressure (with finite decay time) was measured and compared with an analytically predicted response. The dynamic model predicts the output response reasonably well, even though the predicted final output total pressure is 15 percent less than the measured mean value. The OR output total pressure transient responses to control input pressures of two different shapes (i.e., a terminated ramp-type and an exponential type) were simulated to demonstrate the versatility of the present model and to show the effect of control input pressure shape on the switching time and the output transient response of the monostable amplifier.

The effect of the jet spread parameter ($\sigma$) variation on the predicted switching time was studied. It was found that the effect is not significant in the range of $10.5 < \sigma < 20$ for $P_{tc} > 0.4$. A change in $\sigma$ from 10.5 to 7.7 causes a significant increase in the predicted "threshold value" of the control pressure.

The effects of geometric variations on the switching and return times were studied experimentally and analytically (see Figure 27 for the geometry). A summary of the results follows:

1. Attachment wall offset, $D_1$: An increase in the offset $D_1$ reduced the switching time, but increased the return time greatly. If a fast

return and a fast switching time is taken as a criterion for a "best" design of a monostable fluid amplifier, a "best" offset $D_1$ can be obtained.

2. Opposite wall offset, $D_2$: An increase in the offset $D_2$ reduced the return time, but increased the switching time greatly. For $D_2 > 1.5$, the offset $D_2$ variation had a negligible effect on the return time. There was no return for $D_2 < 0.75$. If a fast return and fast switching time are taken as criteria for a "best" design of a monostable fluid amplifier, a "best" offset $D_2$ can be obtained.

3. Splitter distance, $D_s$: With the splitter located near the output vent (i.e., $D_s = 10.9$; $X_{v1} = 10.94$), a minimum return time was predicted and "stable" switching was observed experimentally. But the splitter distance variation had a negligible effect on the measured switching time for $10.5 < D_s < 13$.

4. Bias vent width, $B_b$: An increase in the vent width $B_b$ reduced the return time greatly. But the vent width variation had a negligible effect on the switching time. Thus, increasing the bias vent width is one of the most effective ways to reduce the return time without sacrificing the switching time.

5. Opposite wall angle, $\alpha_2$: An increase in the angle $\alpha_2$ reduced the return time greatly, but the angle $\alpha_2$ had a negligible effect on the switching time. Thus, increasing the opposite wall angle is another effective way to reduce the return time without affecting the switching time.

6. Splitter offset, $D_3$: An increase in the offset $D_3$ reduced the switching time slightly. The offset variation had a negligible effect

on the return time for $D_3 < 0.2$, but increasing $D_3$ over 0.2 resulted in an increase in the return time.

A limited experimental study was conducted to investigate the effect of the output (OR) loading (blockage) on the switching time of the monostable amplifier. It was found that the effect of loading is stronger at low control pressures than that at high control pressures. However, in general, the effect of output loading depends on the geometry of the output vent and the splitter, and can be minimized or even eliminated by an appropriate design of the amplifier (e.g., by employing an output decoupling vent shown in Reference [18]).

## 6.2 Conclusions

The analytical dynamic model has been shown to be capable of predicting not only the switching and return times but also the transient response of a monostable fluid amplifier to any time-varying control input signal. This model can be utilized as an analytical design tool for a monostable fluid amplifier. This model can also be used in the simulation of digital fluidic circuits.

The steady-state jet reattachment model has also been shown to be capable of predicting the reattachment position of a two-dimensional, incompressible, turbulent jet to an offset, inclined wall in the presence of control flow. This steady-state model can be used to determine the attachment and opposite wall lengths[1] (defined in Figure 27 and Table I) for the design of a monostable fluid amplifier.

The results obtained from the study of effects of geometrical variations on the switching and return times for the test monostable amplifier should be usable as a general guide in the design of monostable fluid amplifiers.

The steady-state jet reattachment model and the dynamic model are also applicable to a bistable fluid amplifier. The dynamic model should also be useful in identifying the digital data handling speed of wall-attachment fluid amplifiers and in detecting hazards in digital fluidic systems employing such amplifiers.

## 6.3 Recommendations for Future Study

The following areas are recommended for future study:

1. An input vent port (see Figure 5) is usually provided for control input signal isolation in a wall-attachment fluid amplifier. The static and dynamic characteristics of the control flow in the input vent should be studied to broaden the range of application of the present dynamic model.

2. The effect of the aspect ratio (AR) on the semi-confined jet spread (i.e., $\sigma$) should be studied for AR < 6.

3. The effect of perpendicularly impinging control flow on the supply jet spreading (i.e., $\sigma$) should be studied experimentally.

4. The assumption on the dynamic pressure at the inlet of the OR and NOR output channels should be validated by experiment.

5. The criterion for the end of phase I should be further investigated.

6. Error in the final value of the output total pressure should be investigated.

7. Further experimental study should be done to investigate the effects of varying the opposite wall angle and the splitter offset on the switching and return times of a monostable fluid amplifier.

ENDNOTE

[1] The walls must be long enough so that when the control port is open to ambient pressure, the steady-state jet reattachment position is on the upstream side of the output vent. The following relation was suggested by Drzewiecki [18]:

$$\text{Wall length} = \text{Steady-state jet reattachment distance} + 2b_s.$$

## BIBLIOGRAPHY


1. Abramovich, G. N. The Theory of Turbulent Jets. Cambridge: The M.I.T. Press, 1963.

2. Bain, D. C. and P. J. Baker. Technical and Market Survey of Fluidics in the United Kingdom. Cranfield: The British Hydromechanics Research Association, 1969.

3. Bermel, T. W. and W. R. Brown. "Development of a Pure Fluid NOR-GATE and a NORLOGIC Binary to Decimal Converter." Fluid Amplification Symp. Proc., 3 (1965), pp. 37-61.

4. Boucher, R. F. "Incompressible Jet Reattachment Using a Good Free Jet Model." Third Cranfield Fluidics Conf. Proc., Paper F1, 1968.

5. Bourque, C. and B. G. Newman. "Reattachment of a Two Dimensional Incompressible Jet to an Adjacent Flat Plat." Aeronautical Quart., 11, 3 (August, 1960), pp. 201-232.

6. Bourque, C. "Reattachment of a Two Dimensional Jet to an Adjacent Flat Plate." Advances in Fluidics. Ed. F. T. Brown. New York: ASME, 1967, pp. 192-204.

7. Bradbury, L. J. S. "The Structure of a Self-Preserving Turbulent Plane Jet." J. Fluid Mech., 23 (1967), pp. 31-64.

8. Brown, E. F. and F. C. Belen, Jr. "Jet Interaction in a Simplified Model of a Bistable Fluid Amplifier." ASME Paper 72-WA/Flcs-6, 1972.

9. Brown, F. T. "Pneumatic Pulse Transmission with Bistable Jet Relay Reception and Amplification." (Unpub. Sc.D. dissertation, Massachusetts Institute of Technology, 1962.)

10. Comparin, R. A., H. H. Glaettli, A. E. Mitchell, and H. R. Mueller. "On the Limitations and Special Effects in Fluid Jet Amplifiers." ASME Symp. on Fluid Jet Control Devices, 1962, pp. 65-73.

11. Conway, A., ed. A Guide to Fluidics. London: McDonald, 1971.

12. Doble, P. A. C. and J. Watton. "Multiple Regression Analysis of Fluidics OR-NOR Elements." Fourth Cranfield Fluidics Conf. Proc., Paper X4, 1970.

13. Dodds, J. I. "The Use of Suction or Blowing to Prevent Separation of a Turbulent Boundary Layer." (Unpub. Ph.D. dissertation, University of Cambridge, 1961.)

14. Douglas, J. F. and R. S. Neve. "Investigation into the Behavior of a Jet Interaction Proportional Amplifier." Second Cranfield Fluidics Conf. Proc., Paper C3, 1967.

15. Drzewiecki, T. M. "The Prediction of the Dynamic and Quasi-Static Performance Characteristics of Flueric Wall Attachment Amplifiers." Fluidics Quart., 5, 2 (1973), pp. 96-126.

16. Drzewiecki, T. M. Fluerics 34. Planar-Nozzle Discharge Coefficients. Washington, D.C.: HDL, TM-72-33, 1973.

17. Drzewiecki, T. M. Fluerics 37. A General Planar Nozzle Discharge Coefficient Representation. Washington, D.C.: HDL, TM-74-5, 1974.

18. Drzewiecki, T. M. "The Design of Flueric, Turbulent, Wall Attachment Flip-flop." HDL Fluidic State-of-the-Art Symp., 1 (1974), pp. 433-498.

19. Epstein, M. Theoretical Investigation of the Switching Mechanism in a Bistable Wall Attachment Fluid Amplifier. Ohio: Air Force Avionics Laboratory, TR-70-198, 1970.

20. Foster, K. and J. B. Carley. "The Dynamic Switching of Fluidic Digital Elements and the Effect of Back Pressure." Paper presented at a meeting on Development of Fluidic Drives and Controls. Hanover, Germany: VDMA, 1971, pp. 139-160.

21. Foster, K. and N. S. Jones. "An Examination of the Effect of Geometry on the Characteristics of a Turbulent Reattachment Device." First International Conf. on Fluid Logic and Amplification Proc., Paper B1, 1965.

22. Foster, K. and G. A. Parker. Fluidics Components and Circuits. London: Wiley-Interscience, 1970.

23. Goto, J. M. and T. M. Drzewiecki. Fluerics 32. An Analytical Model for the Response of Flueric Wall Attachment Amplifiers. Washington, D.C.: HDL, TR-1598, 1972.

24. Hamid, S. "Static and Dynamic Analysis of Vortex Resistors." (Unpub. Ph.D. dissertation, Oklahoma State University, 1976.)

25. Heskestad, G. "Hot-Wire Measurements in a Plane Turbulent Jet." Trans. ASME, 87, E (1965), pp. 721-734.

26. Hrubecky, H. F. and L. N. Pearce. "Flow Field Characteristics in a Model Bi-Stable Fluid Amplifier." Fluid Amplification Symp. Proc., 1 (1964), pp. 351-373.

27. Jacoby, M. "Digital Applications of Fluid Amplifiers." Fluidics. Ed. E. F. Humphrey. Ann Arbor: Fluid Amplifier Associates, 1968, pp. 240-249.

28. Johnston, R. P. "Dynamic Studies of Turbulent Reattachment Fluid Amplifiers." (Unpub. M.S. thesis, University of Pittsburgh, 1963).

29. Keto, J. R. "Transient Behavior of Bistable Fluid Elements." Fluid Amplification Symp. Proc., 3 (1964), pp. 5-26.

30. Kimura, M. and T. Mitsuoka. "Analysis and Design of Wall Attachment Devices by a Jet Model of Unsymmetrical Velocity Profile." First IFAC Symp. on Fluidics Proc., Paper A2, 1968.

31. Kirshner, J. M. "Jet Flows." Fluidics Quart., 1, 3 (1968), pp. 33-46.

32. Kirshner, J. M., ed. Fluid Amplifiers. New York: McGraw-Hill Book Company, 1966.

33. Kirshner, J. M. and S. Katz. Design Theory on Fluidic Components. New York: Academic Press, 1975.

34. Levin, S. G. and F. M. Manion. Fluid Amplification 5. Jet Attachment Distance as a Function of Adjacent Wall Offset and Angles. Washington, D.C.: HDL, TR-1987, 1962.

35. Lush, P. A. "A Theoretical and Experimental Investigation of the Switching Mechanism in a Wall Attachment Fluid Amplifier." IFAC Symp. on Fluidics Proc., 1968.

36. Lush, P. A. "The Development of a Theoretical Model for the Switching Mechanism of a Wall Attachment Fluid Amplifier." (Unpub. Ph.D. dissertation, University of Bristol, U.K., 1968.)

37. McRee, D. I. and H. L. Moses. "The Effect of Aspect Ratio and Offset on Nozzle Flow and Jet Reattachment." Advances in Fluidics. Ed. F. T. Brown. New York: ASME, 1967, pp. 142-161.

38. Miller, D. R. and E. W. Comings. "Static Pressure Distribution in the Free Turbulent Jet." J. Fluid Mech., 9 (1957), pp. 1-16.

39. Moses, H. L. and R. A. Comparin. "The Effect of Geometric and Fluid Parameters on Static Performance of Wall-Attachment Type Fluid Amplifiers." HDL Fluidic State-of-the-Art Symp., 1 (1974), pp. 403-431.

40. Moynian. F. A. and R. J. Reilly. "Deflection & Relative Flow of Three Interacting Jets." Fluid Amplification Symp. Proc., 1 (1964), pp. 123-146.

41. Muller, H. R. "Wall Reattachment Device with Pulsed Control Flow." Fluid Amplification Symp. Proc., 1 (1964), pp. 179-216.

42. Muller, H. R. "A Study of the Dynamic Features of a Wall-Reattachment Fluid Amplifier." ASME Paper 64-FE-10, 1964.

43. Olson, R. E. and Y. T. Chin. Studies of Reattaching Jet Flows in Fluid-State Wall-Attachment Devices. Washington, D.C.: HDL, AD62391, 1965.

44. Olson, R. E. and R. C. Stoeffler. "A Study of Factors Affecting the Time Response of Bistable Fluid Amplifiers." ASME Symp. on Fully Separated Flow, 1964, pp. 73-80.

45. Olson, R. E. and R. C. Stoeffler. "A Study of Factors Affecting the Time Response of Bistable Fluid Amplifiers." ASME Symp. on Fully Separated Flow, 1964, pp. 73-80.

46. Ozgu, M. R. and A. H. Stenning. "Theoretical Study of the Switching Dynamics of Bistable Fluidic Amplifiers with Low Setbacks." ASME Paper 71-WA/Flcs-6, 1971.

47. Ozgu, M. R. and A. H. Stenning. "Switching Dynamics of Bistable Fluidic Amplifiers with Low Setbacks." Trans. ASME J. Dynam. Syst. Measurement Contr., 94, 1 (1972).

48. Ozgu, M. R. and A. H. Stenning. "Transient Switching of Monostable Fluid Amplifiers." Fifth Cranfield Fluidics Conf. Proc., Paper X6, 1972.

49. Parker, G. A. and B. Jones. "Protection Against Hazards in Fluidic Adder and Subtractor Circuits." First IFAC Fluidics Symp. Proc., Paper B2, 1968.

50. Pedersen, J. R. C. "The Flow of Turbulent Incompressible Two-Dimensional Jets over Ventilated Cavities." Fluid Amplification Symp. Proc., 1 (1965), pp. 93-109.

51. Perry, C. C. "Two-Dimensional Jet Attachment." Advances in Fluidics. Ed. F. T. Brown. New York: ASME, 1967.

52. Reid, K. N. "Static Characteristics of Fluid Amplifiers." Fluid Power Research Conf. Proc., Oklahoma State University, 1967.

53. Ries, J. P. "Dynamic Modeling and Simulation for Transient Wall Attachment." Fluidics Quart. 4, 4 (1972), pp. 93-112.

54. Sarpkaya, T. "Steady and Transient Behavior of a Bistable Amplifier with a Latching Vortex." Fluid Amplification Symp. Proc., 2 (1965), pp. 185-205.

55. Savkar, S. D., A. G. Hansen, and R. B. Keller. "Experimental Study of Switching in a Bistable Fluid Amplifier." ASME Paper 67-WA/FE-37, 1967.

56. Sawyer, R. A. "The Flow Due to a Two Dimensional Jet Issuing Parallel to a Flat Plate." J. Fluid Mech., 9 (1960), pp. 543-560.

57. Sawyer, R. A. "Two-Dimensional Reattaching Jet Flows Including the Effects of Curvature on Entrainment." J. Fluid Mech., 17 (1963), pp. 481-497.

58. Schlichting, H. Boundary-Layer Theory. New York: McGraw-Hill Book Company, 1968.

59. Sher, N. C. "Jet Attachment and Switching in Bistable Fluid Amplifiers." ASME Paper 64-FE-19, 1964.

60. Simson, A. K. "Gain Characteristics of Subsonic Pressure-Controlled, Proportional, Fluid-Jet Amplifiers." Trans. ASME J. Basic Eng., June, 1966, pp. 295-305.

61. Steptoe, B. J. "Steady State and Dynamic Characteristic Variations in Digital Wall-Attachment Devices." Second Cranfield Fluidics Conf. Proc., Paper B3, 1967.

62. Wada, T. and A. Shimizu. "Experimental Study of Attaching Jet Flow on Inclines Flat Plate with Small Offset." Fluidics Quart., 4, 1 (1972), pp. 13-28.

63. Wada. T., M. Takagi, and T. Shimizu. "Effects of a Splitter and Vents on a Reattaching Jet and Its Switching in Wall-Reattachment Fluidic Devices." HDL Fluidic State-of-the-Art Symp., 1 (1974), pp. 499-554.

64. Warren, R. W. "Some Parameters Affecting the Design of Bistable Fluid Amplifier." ASME Symp. on Fluid Jet Control Devices, 1962, pp. 75-82.

65. Weikert, W. F. and H. L. Moses. "Effects of Dimensional Variations on the Performance of a Fluidic Or/Nor Gate." ASME Paper 75-WA/Flcs-8, 1975.

66. White, F. M. Viscous Fluid Flow. New York: McGraw-Hill Book Company, 1974.

67. William, C. J. and W. G. Colborne. "Splitter Switching in Bistable Fluidic Amplifiers." HDL Fluidics State-of-the-Art Symp., 1 (1974), pp. 555-605.

68. Wilson, J. N. A Fluid Analog to Digital Conversion System. Cleveland: Case Institute of Technology, Engineering Design Center Report EDC 7-64-4, 1964.

69. Wilson, M. P. "The Switching Process in Bistable Fluid Amplifiers." ASME Paper 69-Flcs-28, 1969.

# APPENDIX A

## DRAWING OF TEST AMPLIFIER NOZZLE SECTION

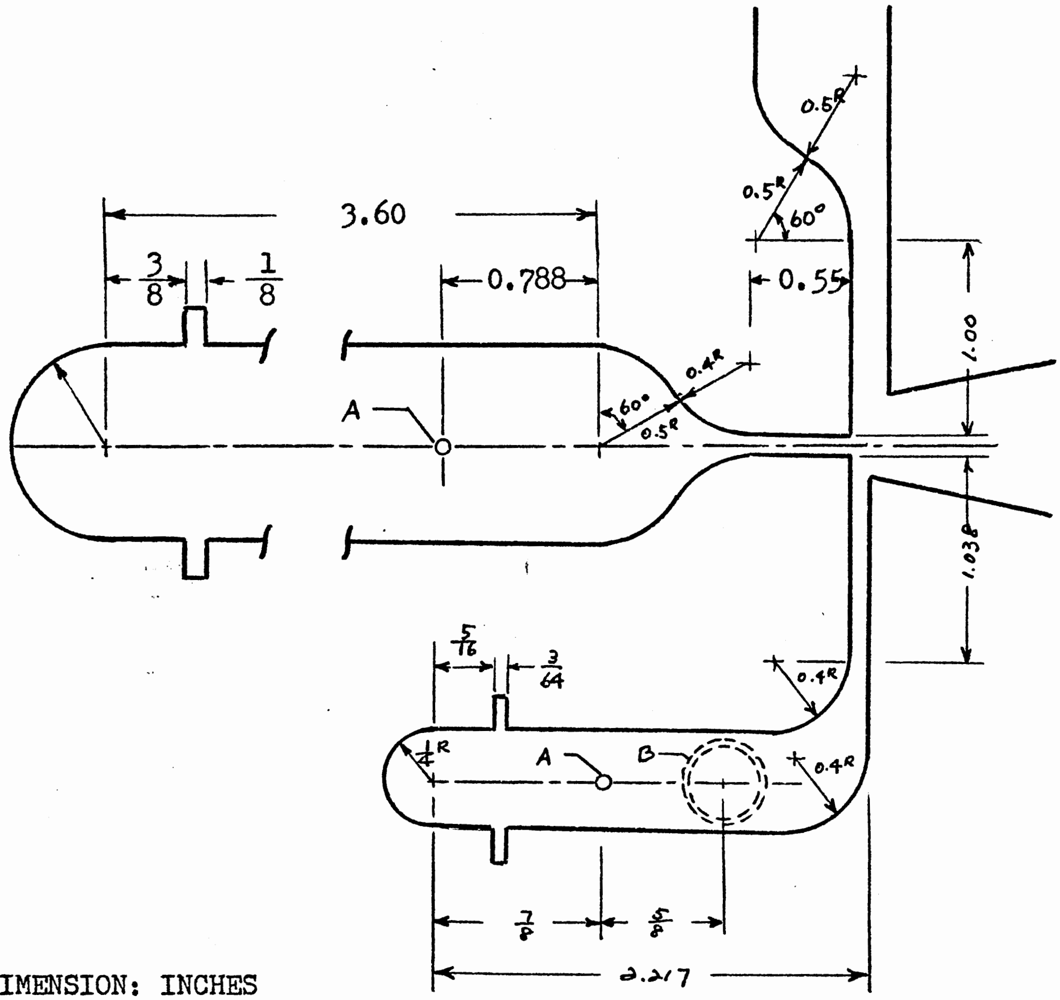


DIMENSION: INCHES
SCALE: FULL SIZE

A: DRILL AND TAP for #10-32 THREAD
1/4 DEEP - #52 (.0635) DRILL (on the cover plate)

B: DRILL AND TAP for 1/8 DRYSEAL NPT
(on the cover plate)

Figure 53. Drawing of Test Amplifier Nozzle Section

# APPENDIX B

# CONTROL NOZZLE DISCHARGE COEFFICIENT

Friction losses and contraction effects in the control channel were accounted for through use of a discharge coefficient $C_{dc}$ in Chapter III. The discharge coefficient was defined as the ratio of actual flow to ideal one-dimensional inviscid flow through the channel, i.e.,

$$C_{dc} \equiv \frac{(q_c)\text{ actual}}{(q_c)\text{ ideal}} = \frac{(q_c)\text{ actual}}{b_c\sqrt{\frac{2p_{tc}}{\rho}}} \tag{B.1}$$

where $p_{tc}$ is the total pressure at the inlet of the control channel. This appendix summarizes the development of empirical relations for the discharge coefficient.

The value of discharge coefficient for a planar nozzle depends on three parameters: the aspect ratio, the effective nozzle length and the Reynolds number based on nozzle width. By introducing a "modified Reynolds number," Drzewiecki [17] demonstrated that the discharge coefficient can be represented as a function of only one parameter. He defined the modified Reynolds number as:

$$Re_c' = \frac{Re_c}{(\frac{\ell_c}{b_c} + 1)(1 + \frac{1}{AR})^2} \tag{B.2}$$

where $Re_c$ is the control jet Reynolds number based on the control nozzle width (i.e., $Re_c = (\frac{q_c}{b_c})\,\frac{b_c}{\nu})$, $\ell_c$ is the control nozzle length, and AR is the aspect ratio.

Figure 54 shows experimentally measured discharge coefficients as a function of the modified Reynolds number reported in Reference [17]. These data were obtained from ten different nozzles (different shapes and aspect ratios). The following empirical relation was developed to conveniently use the experimental data:

$$C_{dc} = \sum_{i=1}^{7} C_i \; (\log_{10} Re_c')^{i-1} \tag{B.3}$$

where

$C_1 = \phantom{-}7.282239 \quad E{-}2$

$C_2 = \phantom{-}1.952439 \quad E{-}1$

$C_3 = \phantom{-}1.876469 \quad E{-}1$

$C_4 = -1.405765 \quad E{-}2$

$C_5 = -5.647645 \quad E{-}2$

$C_6 = \phantom{-}2.207002 \quad E{-}2$

$C_7 = -2.518008 \quad E{-}3.$

Figure 54 also shows experimentally measured discharge coefficients for the test amplifier control nozzle used in the present study. Although Equation (B.3) may be adequate to approximately determine the value of the control nozzle discharge coefficient, the following empirical relation based on the present experimental data has been used in this study:

$$C_{dc} = \sum_{i=1}^{7} C_i \; (\log_{10} Re_c')^{i-1} \tag{B.4}$$

where

$C_1 = \phantom{-}6.905645 \quad E{-}2$

$C_2 = \phantom{-}2.067500 \quad E{-}1$

$C_3 = \phantom{-}2.064129 \quad E{-}1$

$C_4 = -5.814309 \quad E{-}2$

$C_5 = -7.139390 \quad E{-}2$

$C_6 = \phantom{-}4.834454 \quad E{-}2$

$C_7 = -8.477535 \quad E{-}3.$

The calculated values of the discharge coefficient using Equations (B.3) and (B.4) are shown in Figure 53.

For the comparison between the analytically predicted switching times and Goto and Drzewiecki's [23] experimental data (see Figure 37 in Chapter V), experimentally measured discharge coefficients of the control nozzle (Figure 14 of Reference [23]) was used for the analytical predictions.

Lush [36] employed resistors in both control lines of the bistable fluid amplifier. The control line resistances were made equal and adjusted such that the loss of total pressure in each control line was equivalent to the control flow dynamic pressure $\frac{1}{2}\rho\left(\frac{q_c}{b_c}\right)^2$. For the comparison between the analytically predicted switching times and Lush's [36] experimental data (see Figure 38 in Chapter V), the loss in the control line was simulated to be equal to the control flow dynamic pressure for the analytical predictions.

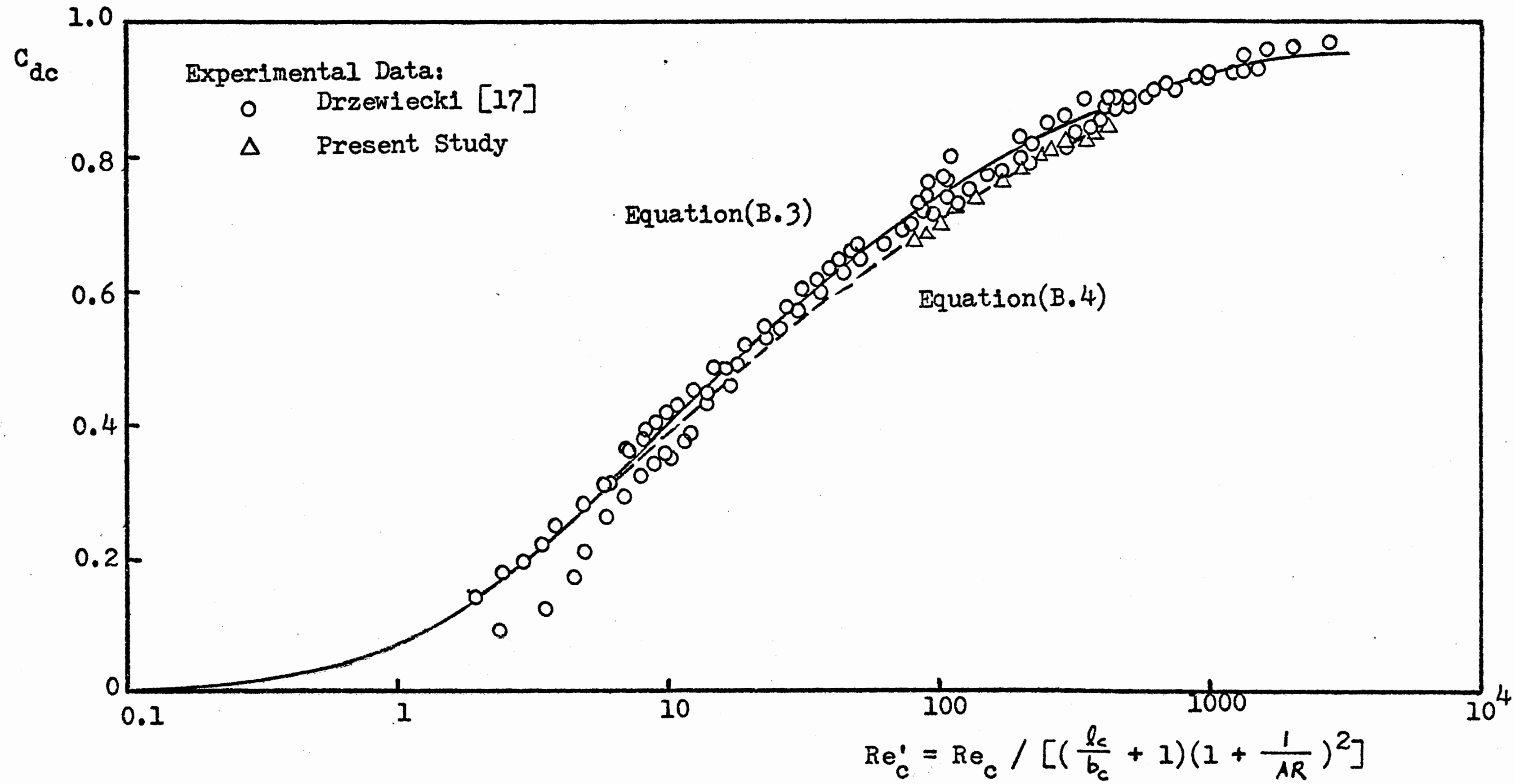


Figure 54. Control Nozzle Discharge Coefficient

# APPENDIX C

## COMPUTATION PROCEDURES AND SELECTED COMPUTER PROGRAM LISTINGS

## C.1 Computation Procedures

Given the geometry and control flow rate $Q_c$, the steady-state jet reattachment distance (or jet deflection angle) may be computed as follows:

Step 1. Compute an initial value of $\beta$ from $\beta = \tan^{-1}(\frac{Q_c^2}{B_c})$.

2. Compute $S_1$ from Equation (3.22).

3. Compute $E_1$ from Equation (3.20).

4. Try a value of $\theta_e$.

5. Compute $\zeta_e$ from Equation (3.27a).

6. Compute $\gamma$ from Equation (3.19).

7. Compute $T_r$ from Equation (3.10).

8. Solve Equation (3.7) for $S_e$.

9. Solve Equation (3.26a) for K.

10. Compute $R_e$ from Equation (3.2a).

11. Compute $E_1$ from Equation (3.21).

12. If $|E_1$ (Step 3) $- E_1$ (Step 11)$| < \varepsilon$, go to Step 13. Otherwise, try another value of $\theta_e$ and repeat Steps 5 through 11.

13. Compute $X_2$ from Equation (3.23).

14. Compute $X_e$ from Equation (3.24).

15. Compute $X_r$ from Equation (3.31).

16. Compute $R_{es}$ from Equation (3.34a).

17. Compute $\eta_1$ from Equation (3.35).

18. Compute $\theta_p$ from Equation (3.36).

19. Compute $S_p$ from Equation (3.37).

20. Compute $Y_p$ from Equation (3.33).

21. Compute $R_c$ from Equation (3.32).

22. Compute $\eta_2$ from Equation (3.38).

23. Compute $S_s$ from Equation (3.39).

24. Compute $P_2$ from Equation (3.18).

25. Compute $P_1$ from Equation (3.16a).

26. Compute $A_c$ from Equation (3.15).

27. Compute $P_c$ from Equation (3.14a).

28. Compute $\beta$ from Equation (3.13a).

29. If $|\beta_i - \beta_{i-1}| < \varepsilon$, go to Step 30. Otherwise, repeat Steps 2 through 28.

30. Print $X_r$ and $\beta$.

A computer program for the above procedure is listed at the end of this appendix. A flow chart for computations of the switching time and the OR output total pressure transient response is shown in Figure 55. A flow chart for computations of the return time and the NOR output total pressure transient response is not included in this thesis because of its similarity to Figure 55. However, a computer program for the computation of the return time is listed at the end of this appendix. In Figure 55, an implicit iteration to solve Equation (3.54a) is based on Wegstein's method.[1]

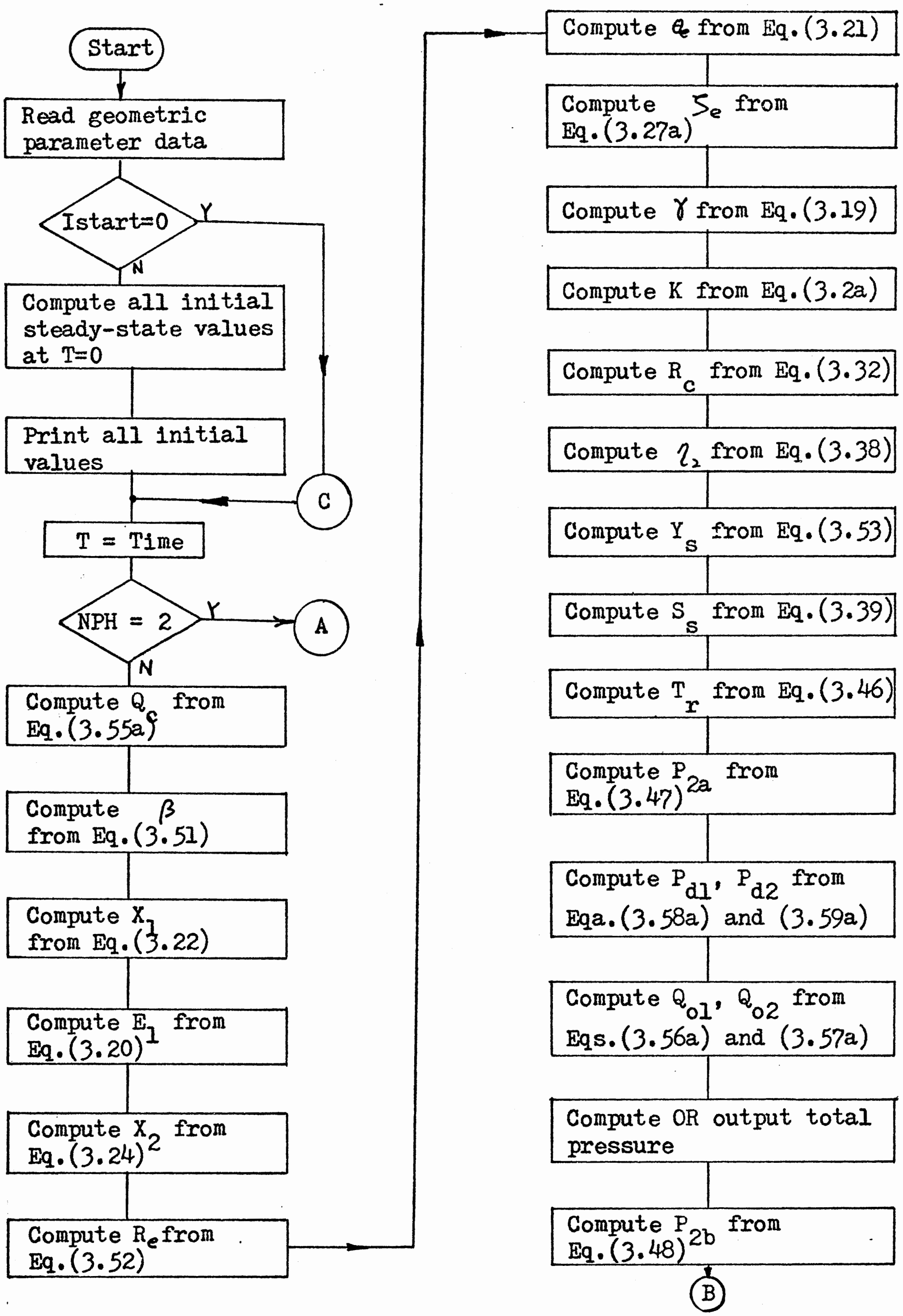


Figure 55. Flow Diagram for OR Output Pressure Transient Response Prediction

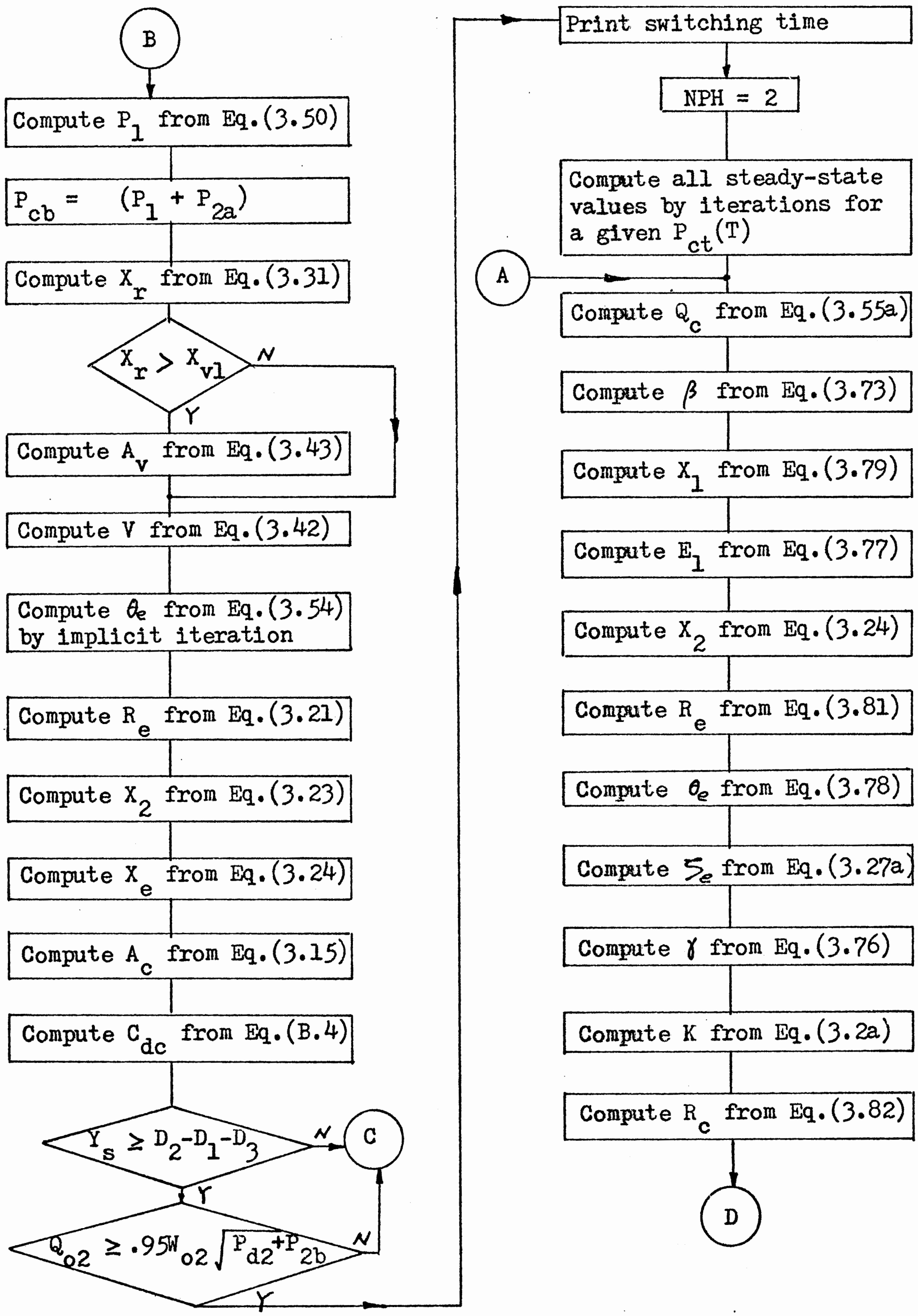


Figure 55. (Continued)

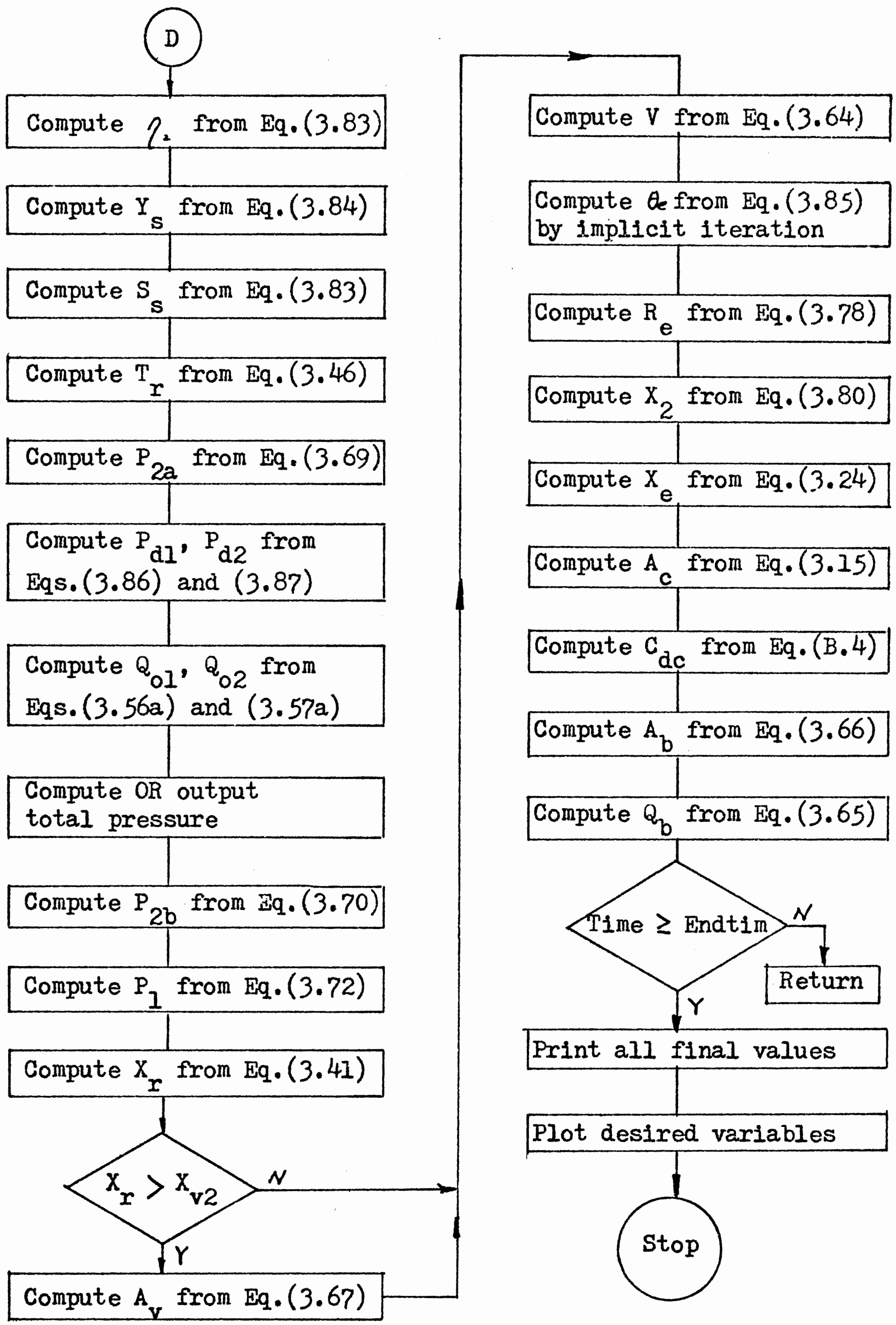


Figure 55. (Continued)

Values of the unattached-side pressures ($P_{2a}$ and $P_{2b}$) may be determined by iterations at each time step. Since these iterations at every time step require excessive computer time, the following alternative method was chosen. For example, the pressure $P_{2a}$ may be computed as follows:

Step 1. Compute $Q_b$ from Equation (3.47a) based on the value of $P_{2a}(t - \Delta t)$.

2. Compute $Q_w$ from Equation (3.47b) based on the values of $P_{2a}(t - \Delta t)$ and $P_{2b}(t - \Delta t)$.

3. Compute $S_w$ from Equation (3.47d).

4. Compute $Q_{e3}$ from Equation (3.47c).

5. Compute the net flow rate into region 2a from $\Sigma Q = Q_b + Q_w - Q_{e3}$.

6. Compute a differential pressure $\Sigma P_{2a}$ from

$$\Delta P_{2a} = \frac{\Sigma Q|\Sigma Q|}{(B_b + A_w)^2} .$$

7. Compute a new $P_{2a}$ from $P_{2a}(t) = P_{2a}(t - \Delta t) + \Delta P_{2a}$.

## C.2 Selected Computer Program Listings

The following computer programs are listed in this section:

1. Computer program 2 which was used for the computation of the steady-state jet reattachment distance;

2. Computer program 2 which was used for computations of the switching time and the OR output total pressure transient response; and

3. Computer program 3 which was used for the computation of the return time.

Since these computer programs were primarily written to calculate predicted values to be compared with experimental data, they are only cursorily documented. User-oriented programs could be evolved from these programs. The definitions of variables and parameters used in the programs are presented in Table III.

TABLE III

DEFINITIONS OF VARIABLES AND PARAMETERS

| | | | |
|---|---|---|---|
| P (1) = $\alpha_1$ | P(51) = $\pi$ | X(27) = $P_{cb}$ | X(62) = $\eta_2$ |
| P (2) = $\alpha_2$ | P(52) = $180/\pi$ | X(28) = $P_c$ | X(65) = $W_{o1}$ |
| P (3) = $D_1$ | P(53) = c | X(29) = $P_{tc}$ | X(66) = $W_{o2}$ |
| P (4) = $D_2$ | = 67/90 | X(33) = $\eta_1$ | X(67) = $C_{dc}$ |
| P (5) = $D_3$ | P(58) = $\cos\alpha_1$ | X(34) = $P_{2a}$ (phase II) | X(69) = $Re_c$ |
| P (6) = $B_c$ | P(59) = $\sin\alpha_1$ | X(35) = $\theta_p$ | X(70) = $Re'_c$ |
| P (7) = $B_b$ | P(60) = $\cos\alpha_2$ | X(36) = $P_{2a}$ (phase I) | X(74) = $\cos\beta$ |
| P (8) = $B_{v1}$ | P(61) = $\sin\alpha_2$ | = $P_b$ (phase II) | X(75) = $\sin\beta$ |
| P (9) = $D_s$ | P(62) = $S_o$ | X(37) = $R_{es}$ | X(76) = $\theta_e/c$ |
| P(10) = $X_{v1}$ | X (1) = $X_e$ | X(38) = $Z_w$ | X(77) = $\lambda$ |
| P(11) = $L_c$ | X (2) = $X_r$ | X(39) = $\xi$ | Y (1) = $Q_c$ |
| P(13) = $L_{o1}$ | X (3) = $S_e$ | X(40) = $S_p$ | Y (2) = V |
| P(14) = $L_{o2}$ | X (4) = $R_e$ | X(41) = $T_p$ | Y (3) = $Q_{o1}$ |
| P(15) = $L_{th}$ | X (5) = $R_c$ | X(42) = $Y_p$ | Y (4) = $Q_{o2}$ |
| P(16) = $b_s$ | X (6) = $Y_s$ | X(43) = $Q_{e3}$ | |
| P(17) = AR | X (8) = $\theta_e$ | X(44) = $Q_w$ | |
| P(18) = $\sigma$ | X (9) = $\gamma$ | X(45) = $Q_{e4}$ | |
| P(19) = $\nu$ | X(10) = $\beta$ | X(46) = $S_w$ | |
| P(20) = $\rho$ | X(11) = $T_r$ | X(47) = $\Delta_w$ | |
| P(22) = $q_s$ | X(12) = $T_s$ | X(50) = $X_1$ | |
| P(23) = $U_s$ | X(13) = $A_c$ | X(51) = $X_2$ | |
| P(24) = $Re_s$ | X(14) = $A_v$ | X(52) = K | |
| P(26) = $t_t$ | X(15) = $A_b$ | X(53) = $E_1$ | |
| P(31) = $I'_c$ | X(16) = $Q_{e2}$ | X(54) = $E_2$ | |
| P(33) = $I'_{o1}$ | X(18) = $Q_b$ | X(55) = $Y_r$ | |
| P(34) = $I'_{o2}$ | X(20) = $P_{o2}$ | X(57) = $S_s$ | |
| P(36) = $X_{v2}$ | X(21) = $P_1$ | X(58) = $S_v$ | |
| P(41) = Final value of $P_{tc}$ | X(22) = $P_{2b}$ | X(59) = $\Delta_v$ | |
| | X(23) = $P_{d1}$ | X(60) = G | |
| P(42) = $\tau_{ri}$ | X(24) = $P_{d2}$ | X(61) = $\zeta$ | |

```
C
C  COMPUTER PROGRAM 1 - COMPUTATION OF THE
C  STEADY-STATE JET REATTACHMENT DISTANCE
C
      DIMENSION              CI(7),P(100),X(100),Y(5)
      DO 100 II=1,100
      P(II)=0.0
 100  X(II)=0.0
      DO 200 II=1,5
 200  Y(II)=0.0
      P(1)=15.
      P(2)=15.
      P(3)=0.5
      P(4)=P(3)
      P(5)=0.0
      P(6)=1.0
      P(7)=1.0
      P(8)=2.2
      P(9)=20.0
      P(10)=13.035
      P(11)=4.0
      P(12)=4.0
      P(13)=30.0
      P(14)=30.
      P(15)=3.2
      P(16)=1.0
      P(17)=1.0
      P(18)=10.5
      P(19)=2.2517E-2
      P(20)=1.123E-7
      P(50)=1.E-5
      P(51)=3.141592654
      P(52)=180./P(51)
      P(53)=67./90.
      P(54)=67./P(52)
      P(56)=P(1)/P(52)
      P(57)=P(2)/P(52)
      P(58)=COS(P(56))
      P(59)=SIN(P(56))
      P(60)=COS(P(57))
      P(61)=SIN(P(57))
      P(62)=P(18)/3.
      P(63)=1./P(52)
      P(65)=(1.+1./P(17))**2
      X(65)=(P(3)+P(5)+0.5)*P(58)+P(9)*P(59)
      X(66)=(P(4)-P(5)+0.5)*P(60)+P(9)*P(61)
C
      WRITE(6,1200)
 1200 FORMAT('1')
      WRITE(6,1300) P(3)
 1300 FORMAT(3X,'D1=',F7.4)
      Y(1)=0.0
      DO 300 JJ=1,7
      X(10)=ATAN(Y(1)*Y(1)/P(6))
10    X(43)=X(10)
      X(74)=COS(X(10))
      X(75)=SIN(X(10))
      X(50)=0.5*(P(6)+X(75)) /P(58)
      X(53)=P(3)+X(50)*P(59)+0.5*(1.0-X(74))
C
C     ITERATIONS FOR X(8)
C
      KOUNT=0
```

```
      P(55)=0.05
      X(8) =(P(56)+P(54))/3.0
      X(76)=X(8)/P(53)
      X(82)=P(53)*TAN(X(76))
      X(61)=ATAN(X(82))
      X(9)=X(61)+X(8)-X(10)-P(56)
      X(11)=2.0*COS((P(51)+X(9))/3.)
      X(81)=((2.*Y(1)+1.)/X(11))**2
      X(3)=P(62)*(X(81)-1.)
      X(52)=X(3)/(0.62*X(76)+0.38*SIN(X(76)))
      X(4)=X(52)*SIN(X(76))
      X(84)=X(4)*SIN(X(8)-X(10)-P(56))/P(58)
      P(66)=X(84)-X(53)
      IF(ABS(P(66)).LT.1.E-4*X(53)) GO TO 26
 20   KOUNT=KOUNT+1
      IF(KOUNT.GT.100) GO TO 46
      X(8)=X(8)+P(55)
      X(76)=X(8)/P(53)
      X(82)=P(53)*TAN(X(76))
      X(61)=ATAN(X(82))
      X(9)=X(61)+X(8)-X(10)-P(56)
      X(11)=2.0*COS((P(51)+X(9))/3.)
      X(81)=((2.*Y(1)+1.)/X(11))**2
      X(3)=P(62)*(X(81)-1.)
      X(52)=X(3)/(0.62*X(76)+0.38*SIN(X(76)))
      X(4)=X(52)*SIN(X(76))
      X(84)=X(4)*SIN(X(8)-X(10)-P(56))/P(58)
      P(67)=X(84)-X(53)
      IF(ABS(P(67)).LT.1.E-4*X(53)) GO TO 26
      IF((P(66)*P(67).GT.0.0).AND.(ABS(P(67)).LT.ABS(P(66)))) GO TO 22
      IF((P(66)*P(67).GT.0.0).AND.(ABS(P(67)).GT.ABS(P(66)))) GO TO 24
      IF (P(66)*P(67).LT.0.0)  GO TO 25
 22   P(66)=P(67)
      GO TO 20
 24   P(66)=P(67)
      P(55)=-P(55)
      GO TO 20
 25   P(66)=P(67)
      P(55)=-0.1*P(55)
      GO TO 20
C
C     END OF ITERATIONS FOR X(8)
C
 26   X(51)=X(4)*COS(X(8)-X(10))/P(58)
      X(1)=X(50)+X(51)
C
C     XR
C
      X(80)=X(3)+P(62)
      X(63)=SQRT(P(62)/X(80))
      X(81)=0.5*X(80)/P(18)
      X(82)=((1.+X(11))/(1.-X(11)))*((1.-X(63))/(1.+X(63)))
      X(2)=X(1) -X(81)*ALOG(X(82))/SIN(X(9))
C
C     RCL
C
      X(37)=0.5*X(52)/P(53)
      X(80)=X(37)+0.5
      X(81)=P(9)-0.5*P(6)-X(80)*X(75)
      X(82)=X(80)*X(74)+P(5)
      X(33)=ATAN(X(81)/X(82))
      X(35)=0.5*(X(10)+X(33))
      X(40)=2.*X(37)*X(35)
      X(81)=X(40)+P(62)
      X(41)=SQRT(P(62)/X(81))
      X(42)=(.5*X(81)/P(18))*ALOG((1.+X(41))/(1.-X(41)))
```

```
      X(82)=0.5-X(42)
      X(83)=COS(2.*X(35))-1.0
      X(5)=X(37)+.5*(1.+X(82)*(2.*X(37)+X(82))/(X(37)*X(83)-X(82)))
C
C     ETA2 , SS
C
      X(81)=P(9)-0.5*P(6)-X(5)*X(75)
      X(82)=X(5)*X(74)+P(5)
      X(62)=ATAN(X(81)/X(82))
      X(57)=X(5)*(X(10)+X(62))
C
C     P2 , P1
C
      X(16)=0.0
      X(22)=0.0
      X(21)=X(22)-2.0/X(5)
C
C     PCB
C
      X(27)=(X(21)+X(22))/2.
C
C     AC
C
      X(13)=0.5*P(6)*X(75)+(P(3)+0.5*P(6)*TAN(P(56)))*X(74)-0.5
      IF(X(13)-P(6)) 36,35,35
 35   X(13)=P(6)
 36   CONTINUE
      X(18)=0.0
C
C     BT
C
      X(28)=X(27)+ (Y(1)/X(13))**2
      X(81)=Y(1)*Y(1)/P(6)
      X(83)=0.5*(X(28)-X(22))*P(6)
      X(10)=ATAN(X(83)+X(81))
      X(80)=X(48)-X(10)
      IF (ABS(X(80)).LT.1.E-4) GO TO 50
      GO TO 10
 46   WRITE(6,1002)
 1002 FORMAT('0',3X,'WARNING 3 = ITERATIONS FOR X(8) DO NOT CONVERSE')
 50   WRITE(6,2200) Y(1),X(2),X(10),KOUNT
 2200 FORMAT('0', 3X,2F12.6,E16.6,3X,I3)
 70   Y(1)=Y(1)+0.05
 300  CONTINUE
      STOP
      END
```

```
C
C  COMPUTER PROGRAM 2 - COMPUTATIONS OF THE SWITCHING TIME
C  AND THE OR OUTPUT TOTAL PRESSURE TRANSIENT RESPONSE
C
      DIMENSION  F(101),Z(101),CI(7)
      IF (ISTART.EQ.0) GO TO 50
      NPH=1
      ID2=0
      ID3=0
      DO 500 II=1,100
500   X(II)=0.0
      P(51)=3.141592654
      P(52)=180./P(51)
      P(53)=67./90.
      P(54)=67./P(52)
      P(56)=P(1)/P(52)
      P(57)=P(2)/P(52)
      P(58)=COS(P(56))
      P(59)=SIN(P(56))
      P(60)=COS(P(57))
      P(61)=SIN(P(57))
      P(62)=P(18)/3.
      P(63)=1./P(52)
      P(65)=(1.+1./P(17))**2
      X(65)=(P(3)+P(5)+0.5)*P(58)+P(9)*P(59)
      X(66)=(P(4)-P(5)+0.5)*P(60)+P(9)*P(61)
C
C     COEFF FOR CD
      CI(1)= 6.905645E-2
      CI(2)= 2.067500E-1
      CI(3)= 2.064129E-1
      CI(4)=-5.814309E-2
      CI(5)=-7.139390E-2
      CI(6)= 4.834454E-2
      CI(7)=-8.477535E-3
C
      P(26)=P(16)/P(23)
      P(42)=2.5E-3/P(26)
C
C
      Y(1)=0.0
      X(10)=0.
      DO 410 I=1,10
      X(74)=COS(X(10))
      X(75)=SIN(X(10))
      X(50)=0.5*(P(6)+X(75)) /P(58)
      X(53)=P(3)+X(50)*P(59)+0.5*(1.0-X(74))
C
C     ITERATIONS FOR X(8)
C
      KOUNT=0
      P(55)=0.05
      X(8) =(P(56)+P(54))/3.0
      X(76)=X(8)/P(53)
      X(82)=P(53)*TAN(X(76))
      X(61)=ATAN(X(82))
      X(9)=X(61)+X(2)-X(10)-P(56)
      X(11)=2.0*COS((P(51)+X(9))/3.)
      X(81)=((2.*Y(1)+1.)/X(11))**2
      X(3)=P(62)*(X(81)-1.)
      X(52)=X(3)/(0.62*X(76)+0.38*SIN(X(76)))
      X(4)=X(52)*SIN(X(76))
      X(84)=X(4)*SIN(X(8)-X(10)-P(56))/P(58)
```

```
      P(66)=X(84)-X(53)
      IF(ABS(P(66)).LT.1.E-4*X(53)) GO TO 426
420   KOUNT=KOUNT+1
      IF(KOUNT.GT.100) GO TO 446
      X(8)=X(8)+P(55)
      X(76)=X(8)/P(53)
      X(82)=P(53)*TAN(X(76))
      X(61)=ATAN(X(82))
      X(9)=X(61)+X(8)-X(10)-P(56)
      X(11)=2.0*COS((P(51)+X(9))/3.)
      X(81)=((2.*Y(1)+1.)/X(11))**2
      X(3)=P(62)*(X(81)-1.)
      X(52)=X(3)/(0.62*X(76)+0.38*SIN(X(76)))
      X(4)=X(52)*SIN(X(76))
      X(84)=X(4)*SIN(X(8)-X(10)-P(56))/P(58)
      P(67)=X(84)-X(53)
      IF(ABS(P(67)).LT.1.E-4*X(53)) GO TO 426
      IF((P(66)*P(67).GT.0.0).AND.(ABS(P(67)).LT.ABS(P(66)))) GO TO 422
      IF((P(66)*P(67).GT.0.0).AND.(ABS(P(67)).GT.ABS(P(66)))) GO TO 424
      IF (P(66)*P(67).LT.0.0)  GO TO 425
422   P(66)=P(67)
      GO TO 420
424   P(66)=P(67)
      P(55)=-P(55)
      GO TO 420
425   P(66)=P(67)
      P(55)=-0.1*P(55)
      GO TO 420
C
C     END OF ITERATIONS FOR X(8)
C
426   X(51)=X(4)*COS(X(8)-X(10))/P(58)
      X(1)=X(50)+X(51)
C
C     XR
C
      X(80)=X(3)+P(62)
      X(63)=SQRT(P(62)/X(80))
      X(81)=0.5*X(80)/P(18)
      X(82)=((1.+X(11))/(1.-X(11)))*((1.-X(63))/(1.+X(63)))
      X(2)=X(1) -X(81)*ALOG(X(82))/SIN(X(9))
C
C     RCL
C
      X(37)=0.5*X(52)/P(53)
      X(80)=X(37)+0.5
      X(81)=P(9)-0.5*P(6)-X(80)*X(75)
      X(82)=X(80)*X(74)+P(5)
      X(33)=ATAN(X(81)/X(82))
      X(35)=0.5*(X(10)+X(33))
      X(40)=2.*X(37)*X(35)
      X(81)=X(40)+P(62)
      X(41)=SQRT(P(62)/X(81))
      X(42)=(.5*X(81)/P(18))*ALOG((1.+X(41))/(1.-X(41)))
      X(82)=0.5-X(42)
      X(83)=COS(2.*X(35))-1.0
      X(5)=X(37)+.5*(1.+X(82)*(2.*X(37)+X(82))/(X(37)*X(83)-X(82)))
C
C     ETA2 , SS
C
      X(81)=P(9)-0.5*P(6)-X(5)*X(75)
      X(82)=X(5)*X(74)+P(5)
      X(62)=ATAN(X(81)/X(82))
      X(57)=X(5)*(X(10)+X(62))
C
C     QE2
```

```
C
      X(16)=0.5*(SQRT(1.+X(57)/P(62))-1.)
C
C     P1
C
      X(82)=      P(7)+P(8)+X(66)
      X(22)= -(X(16)/X(82))**2
      X(21)=X(22)-2.0/X(5)
C
C     PCB
C
      X(27)=(X(21)+X(22))/2.
C
C     AC
C
      X(13)=0.5*P(6)*X(75)+(P(3)+0.5*P(6)*TAN(P(56)))*X(74)-0.5
      IF(X(13)-P(6))436,435,435
435   X(13)=P(6)
436   CONTINUE
C
C     QB
C
      X(18)=      P(7)*SQRT(-X(22))
C
C     BT
C
      X(28)=X(27)
      X(83)=0.5*(X(28)-X(22))*P(6)
      X(10)=ATAN(X(83))
 410   CONTINUE
C
C     QC2(T0)
C
445   Y(4)=-X(66)*SQRT(-X(22))
      X(12)=-1.0
      X(23)=.25*(3.*X(11)-X(11)**3-3.*X(12)+X(12)**3)/X(65)
      X(31)=X(23)
      Y(3)=X(65)*SQRT(X(31))
C
C     V(T0)
C
      X(86)=0.25*P(53)*X(52)*X(52)*(X(76) - 0.5*SIN(2.*X(76)))
      X(87)=.5*X(53)*X(4)*COS(X(8)-X(10))
      X(88)=C.5*X(50)*(P(3)+X(53))*P(58)
      Y(2)=X(86)+X(87)+X(88)
      X(36)=X(22)
      X(67)=0.01
      P(46)=X(28)
      Y(1)=0.0
      GO TO 50
446   WRITE(6,1002)
 1002 FORMAT('0',3X,'WARNING 3 = ITERATIONS FOR X(8) DO NOT CONVERGE')
50    GO TO (51,200), NPH
 51   X(29)=(P(41)-P(46))*(1.-EXP(-TIME/P(42)))+P(46)
 101  DY(1)=X(67)*(X(29)-X(28)-Y(1)*ABS(Y(1))/(X(67)*P(6))**2)/P(31)
      IF(Y(1).LT.0.0) Y(1)=0.0
C     BT
      X(28)=X(27)+ (Y(1)/X(13))**2
      X(81)=Y(1)*Y(1)/P(6)
      X(83)=0.5*(X(28)-X(36))*P(6)
      X(10)=ATAN(X(83)+X(81))
      X(74)=COS(X(10))
      X(75)=SIN(X(10))
      X(50)=0.5*(P(6)+X(75)) /P(58)
      X(53)=P(3)+X(50)*P(59)+0.5*(1.0-X(74))
      X(51)=X(1)-X(50)
```

```
      X(81)=(X(51)*P(59)+X(53))**2+(X(51)*P(58))**2
      X(4)=SQRT(X(81))
      X(81)=X(53)*P(58)/X(4)
      X(8)=ARSIN(X(81))+X(10)+P(56)
      X(76)=X(8)/P(53)
      X(82)=P(53)*TAN(X(76))
      X(61)=ATAN(X(82))
      X(9)=X(61)+X(8)-X(10)-P(56)
C     RCL
      X(52)=X(4)/SIN(X(76))
      X(37)=0.5*X(52)/P(53)
      X(80)=X(37)+0.5
      X(81)=P(9)-0.5*P(6)-X(80)*X(75)
      X(82)=X(80)*X(74)+P(5)
      X(33)=ATAN(X(81)/X(82))
      X(35)=0.5*(X(10)+X(33))
C     SP
      X(40)=2.*X(37)*X(35)
C     YP
      X(81)=X(40)+P(62)
      X(41)=SQRT(P(62)/X(81))
      X(42)=(.5*X(81)/P(18))*ALOG((1.+X(41))/(1.-X(41)))
      X(82)=0.5-X(42)
      X(83)=COS(2.*X(35))-1.0
      X(5)=X(37)+.5*(1.+X(82)*(2.*X(37)+X(82))/(X(37)*X(83)-X(82)))
C     ETA2
      X(81)=P(9)-0.5*P(6)-X(5)*X(75)
      X(82)=X(5)*X(74)+P(5)
      X(62)=ATAN(X(81)/X(82))
C     YS
      X(83)=X(81)**2+X(82)**2
      X(60)=SQRT(X(83))
      X(6)=X(5)-X(60)
C     SS
      X(57)=X(5)*(X(10)+X(62))
C     TS
      X(80)=P(18)*X(6)/(X(57)+P(62))
      X(81)=EXP(X(80))
      X(82)=EXP(-X(80))
      X(12)=(X(81)-X(82))/(X(81)+X(82))
C     SPLITTER EFFECT
      X(77)=(1.-1.5*X(12)+.5*X(12)**3)*COS(X(9))+1.+1.5*X(12)-
     1 0.5*X(12)**3
      X(78)=ARCOS(X(77)/2.)
      X(11)=2.0*COS((P(51)+X(78))/3.)
C     PBE
      X(18)= P(7)*SQRT(-X(36))
      IF(X(10)) 164,164,102
  102 X(82)=X(5)*X(75)+.5*P(6)
      X(83)=P(36)*P(60)
      IF(X(82)-X(83)) 172,172,173
  172 X(46)=X(5)*X(10)
      X(47)=1.825*(X(46)+P(62))/P(18)
      X(38)=X(82)*TAN(P(57))+P(4)+.5-X(5)*(1.-X(74))-X(47)
      GO TO 174
  173 X(47)=1.825*(X(46)+P(62))/P(18)
      X(38)=P(36)*P(61)+P(4)+.5-(X(6)+P(5))-X(47)
  174 IF(X(38)) 103,103,104
  103 X(38)=0.0
      X(44)=0.0
      GO TO 163
  104 X(80)=X(22)-X(36)
      IF(X(80)) 162,161,161
  161 X(44)=X(38)*SQRT(X(80))
      GO TO 163
  162 X(44)=-X(38)*SQRT(-X(80))
```

```
  163 X(43)=0.5*(SQRT(1.+X(46)/P(62))-1.)
      X(83)=X(18)+X(44)-X(43)
      X(84)= P(7)+X(38)
      X(36)=X(36)+X(83)*ABS(X(83))/X(84)**2
      IF(X(36).GE.0.0) X(36)=0.0
      GO TO 165
  164 X(46)=0.0
      X(47)=0.5
      X(36)=X(22)
      X(44)=-X(18)
      X(43)=0.0
      X(38)=P(7)
C
C     PD2
C     QD2
  165 X(23)=.25*(3.*X(11)-X(11)**3-3.*X(12)+X(12)**3)/X(65)
      X(31)=X(23)
      DY(3)=(X(31)-X(26)-Y(3)*ABS(Y(3))/X(65)**2)/P(33)
      X(24)=.25*(2.+3.*X(12)-X(12)**3)/X(66)
      X(32)=X(22)+X(24)
      IF(X(57)-X(46)) 175,176,176
  175 X(82)=X(46)
      GO TO 177
  176 X(82)=X(57)
  177 X(45)=0.5*(SQRT(1.+X(82)/P(62))-1.)-X(43)
      DY(4)=(X(32)-X(26)-Y(4)*ABS(Y(4))/X(66)**2)/P(34)
      IF(Y(4)) 107,108,108
  107 X(82)=P(8)*SQRT(-X(22))-Y(4)-X(44)-X(45)
      IF(X(44)) 166,167,167
  166 X(83)=P(8)+X(66)+X(38)
      GO TO 168
  167 X(83)=P(8)+X(66)
  168 X(17)=X(82)*ABS(X(82))/X(83)**2
      GO TO 109
  108 X(82)=P(8)*SQRT(-X(22))-X(44)-X(45)
      IF(X(44)) 169,170,170
  169 X(83)=P(8)+X(38)
      GO TO 171
  170 X(83)=P(8)
  171 X(17)=X(82)*ABS(X(82))/X(83)**2
C     POUT
      X(20)=(Y(4)/X(66))**2
  109 X(22)=X(22)+X(17)
      IF(X(22).GE.0.0) X(22)=0.0
C     P1
      X(81)=X(46)/X(57)
      X(21)=X(81)*X(36)+(1.-X(81))*X(22)-2./X(5)
C     PCB
      X(27)=(X(21)+X(36))/2.
C     XR
      X(3)=X(52)*(0.62*X(76)+0.38*SIN(X(76)))
      X(80)=X(3)+P(62)
      X(63)=SQRT(P(62)/X(80))
      X(81)=0.5*X(80)/P(18)
      X(82)=((1.+X(11))/(1.-X(11)))*((1.-X(63))/(1.+X(63)))
      X(2)=X(1) -X(81)*ALOG(X(82))/SIN(X(9))
C     DY/DT
      IF(X(2)-P(10)) 110,110,111
  110 DY(2)=Y(1)+0.5*(1.0-X(11)/X(63))
      X(14)=0.0
      X(19)=0.0
      GO TO 120
  111 IF(ID2.EQ.1) GO TO 116
      X(81)=P(10)*P(58)-X(5)*X(75)-0.5*P(6)
      X(82)=X(5)*X(74)-P(10)*P(59)-(P(3)+0.5)
      X(39)=ATAN(X(81)/X(82))
```

```
      IF(X(39)-P(56)) 112,112,113
 112  ID2=1
      GO TO 115
 113  X(58)=X(5)*(X(10)+X(39))
      X(59)=1.825*(X(58)+P(62))/P(18)
      X(14)=X(5)-X(59)-X(81)/SIN(X(39))
      IF(X(14)) 110,110,114
 114  IF(X(14)-P(8)) 116,115,115
 115  X(14)=P(8)
 116  X(19)=X(14)*SQRT(-X(21))
      DY(2)=Y(1)+0.5*(1.-X(11)/X(63))+X(19)
C
C     IMPLICIT FN FOR THE
C
 120  F(1)=X(8)
      Z(2)=X(8)
      X(85)=X(1)
      X(88)=0.5*X(50)*(P(3)+X(53))*P(58)
      DO 130 N=2,30
      I=0
 121  X(8)=ABS(Z(N))
      IF(X(8).GE.P(54)) X(8)=P(54)-P(63)
      IF(X(8).LE.0.0)  X(8)=P(63)
      X(76)=X(8)/P(53)
      X(4)=X(53)*P(58)/SIN(ABS(X(8)-X(10)-P(56)))
      X(52)=X(4)/SIN(X(76))
      X(87)=.5*X(53)*X(4)*COS(ABS(X(8)-X(10)))
      X(81)=4.*(Y(2)-X(87)-X(88))/(X(52)*X(52))+.5*P(53)*SIN(2.*X(76))
      F(N+1)=ABS(X(81))
      IF(N.GT.2) GO TO 123
      IF(I) 123,122,123
 122  Z(N-1)=F(N-1)
      Z(N)=F(N+1)
      F(N)=F(N+1)
      I=I+1
      IF(I.GT.20) GO TO 132
      GO TO 121
 123  IF(Z(N)-Z(N-1)) 125,124,125
 124  Z(N+1)=Z(N)
      GO TO 135
 125  P(68)=(F(N+1)-F(N))/(Z(N)-Z(N-1))
      IF(P(68).EQ.1.) GO TO 122
      P(69)=P(68)/(P(68)-1.)
      Z(N+1)=P(69)*Z(N)+(1.-P(69))*F(N+1)
      P(70)=ABS(Z(N+1)-Z(N))
      IF(P(70).LE.1.E-6) GO TO 135
 130  CONTINUE
 132  WRITE(6,1100)
 1100 FORMAT('0',3X,'WARNING 4= IMPLICIT FN FOR X(8) DOES NOT CONVERSE')
 135  X(8)=Z(N+1)
C
C     END OF IMPLICIT FN FOR THE
C
      IF((X(8).LE.(X(10)+P(56))).OR.(X(8).GE.P(54))) GO TO 139
      X(4)=X(53)*P(58)/SIN(ABS(X(8)-X(10)-P(56)))
      X(51)=X(4)*COS(X(8)-X(10))/P(58)
      X(1)=X(50)+X(51)
      GO TO 140
 139  X(1)=X(85)
 140  CONTINUE
C     AC
      X(13)=0.5*P(6)*X(75)+(P(3)+0.5*P(6)*TAN(P(56)))*X(74)-0.5
      IF(X(13)-P(6)) 137,136,136
 136  X(13)=P(6)
 137  CONTINUE
C     CDC
```

```
      IF(Y(1).EQ.0.0) GO TO 147
      X(69)=Y(1)*P(24)
      X(70)=X(69)/((P(11)+1.)*P(65))
      X(80)=ALOG10(X(70))
      X(67)=CI(1)
      DO 146 J=1,6
 146  X(67)=X(67)+CI(J+1)*X(80)**J
      IF(X(67).LE.0.0) X(67)=0.01
C     CB
 147  CONTINUE
C
C     SWITCHING
      IF(ID3.EQ.1) GO TO 155
      IF(X(6).LE.(P(4)-P(3)))     GO TO 295
      X(7)=0.95*X(66)*SQRT(X(79))
      ID3=1
 155  IF(Y(4).LT.X(7)) GO TO 300
      NPH=2
      ENDTIM=TIME+700.0
      WRITE(6,160)P(41),TIME,Y(1),Y(4),X(7),X(6),X(20)
 160  FORMAT('0',3X,F16.5,F16.3,1P5E16.6)
C
C
      SAVE1=P(1)
      P(1)=P(2)
      P(2)=SAVE1
      SAVE2=P(3)
      P(3)=P(4)
      P(4)=SAVE2
      SAVE3=P(6)
      P(6)=P(7)
      P(7)=SAVE3
      SAVE4=P(10)
      P(10)=P(36)
      P(36)=SAVE4
      P(5)=-P(5)
      SAVE5=P(11)
      P(11)=P(12)
      P(12)=SAVE5
      X(68)=X(67)
      X(67)=0.0
      P(50)=1.E-3
C     ITERARATIONS FOR QB(TO)
      NCR=0
      ITER=0
      ID5=0
      X(18)=0.2
      X(65)=X(18)
      X(81)=Y(1)*Y(1)/P(7)
      X(82)=X(18)*X(18)/P(6)
      X(10)= ATAN(X(82)-X(81))
 10   ITER=ITER+1
      IF(ITER.GT.20) NCR=2
      X(74)=COS(X(10))
      X(75)=SIN(X(10))
      X(50)=0.5*(P(6)+X(75)) /P(58)
      X(53)=P(3)+X(50)*P(59)+0.5*(1.0-X(74))
C
C     ITERATIONS FOR X(8)
C
      IF(X(10).GT.-0.35) GO TO 11
      ID5=1
      X(8)=0.06
      GO TO 12
 11   KOUNT=0
      P(55)=0.02
```

```
      X(8) =0.1
 12   X(76)=X(8)/P(53)
      X(82)=P(53)*TAN(X(76))
      X(61)=ATAN(X(82))
      X(9)=X(61)+X(8)-X(10)-P(56)
      X(11)=2.0*COS((P(51)+X(9))/3.)
      X(81)=((2.*X(18)+1.)/X(11))**2
      X(3)=P(62)*(X(81)-1.)
      X(52)=X(3)/(0.62*X(76)+0.38*SIN(X(76)))
      X(4)=X(52)*SIN(X(76))
      X(84)=X(4)*SIN(X(8)-X(10)-P(56))/P(58)
      IF(ID5.EQ.1) GO TO 26
      P(66)=X(84)-X(53)
      IF(ABS(P(66)).LT.1.E-4*X(53)) GO TO 26
 20   KOUNT=KOUNT+1
      IF(KOUNT.GT.100) GO TO 46
      X(8)=X(8)+P(55)
      VM=P(63)/3.0
      IF(X(8).LE.0.0)  X(8)=VM
      X(76)=X(8)/P(53)
      X(82)=P(53)*TAN(X(76))
      X(61)=ATAN(X(82))
      X(9)=X(61)+X(8)-X(10)-P(56)
      X(11)=2.0*COS((P(51)+X(9))/3.)
      X(81)=((2.*X(18)+1.)/X(11))**2
      X(3)=P(62)*(X(81)-1.)
      X(52)=X(3)/(0.62*X(76)+0.38*SIN(X(76)))
      X(4)=X(52)*SIN(X(76))
      X(84)=X(4)*SIN(X(8)-X(10)-P(56))/P(58)
      P(67)=X(84)-X(53)
      IF(ABS(P(67)).LT.1.E-4*X(53)) GO TO 26
      IF((P(66)*P(67).GT.0.0).AND.(ABS(P(67)).LT.ABS(P(66)))) GO TO 22
      IF((P(66)*P(67).GT.0.0).AND.(ABS(P(67)).GT.ABS(P(66)))) GO TO 24
      IF (P(66)*P(67).LT.0.0)  GO TO 25
 22   P(66)=P(67)
      GO TO 20
 24   P(66)=P(67)
      P(55)=-P(55)
      GO TO 20
 25   P(66)=P(67)
      P(55)=-0.1*P(55)
      GO TO 20
C
C     END OF ITERATIONS FOR X(8)
 46   WRITE(6,1002)
 1002 FORMAT('0',3X,'WARNING 3 = ITERATIO5S FOR X(8) DO NOT CONVERSE')
C
 26   X(51)=X(4)*COS(X(8)-X(10))/P(58)
      X(1)=X(50)+X(51)
C
C     XR
C
      X(80)=X(3)+P(62)
      X(63)=SQRT(P(62)/X(80))
      X(81)=0.5*X(80)/P(18)
      X(82)=((1.+X(11))/(1.-X(11)))*((1.-X(63))/(1.+X(63)))
      X(2)=X(1) -X(81)*ALOG(X(82))/SIN(X(9))
C
C     RCL
C
      X(37)=0.5*X(52)/P(53)
      X(80)=X(37)+0.5
      X(81)=P(9)-0.5*P(6)-X(80)*X(75)
      X(82)=X(80)*X(74)-P(5)
      X(33)=ATAN(X(81)/X(82))
      X(35)=0.5*(X(10)+X(33))
```

```
      X(40)=2.*X(37)*X(35)
      X(81)=X(40)+P(62)
      X(41)=SQRT(P(62)/X(81))
      X(42)=(.5*X(81)/P(18))*ALOG((1.+X(41))/(1.-X(41)))
      X(82)=0.5-X(42)
      X(83)=COS(2.*X(35))-1.0
      X(5)=X(37)+.5*(1.+X(82)*(2.*X(37)+X(82))/(X(37)*X(83)-X(82)))
      IF((X(5)-X(37))-20.0) 17,15,15
 15   X(5)=X(80)
C
C     ETA2 , SS
C
 17   X(81)=P(9)-0.5*P(6)-X(5)*X(75)
      X(82)=P(8)+X(65)
      X(62)=ATAN(X(81)/X(82))
      X(57)=X(5)*(X(10)+X(62))
C
C     QE2
C
      X(16)=0.5*(SQRT(1.+X(57)/P(62))-1.)
C
C     PI
C
      X(83)=X(16)-Y(1)
      IF(X(83).LE.0.0) X(83)=0.0
      X(82)=P(8)+P(29)*X(66)
      X(22)= -(X(83)/X(82))**2
      X(21)=X(22)-2.0/X(5)
      IF(X(21).GE.0.0) X(21)=-0.02
C
C     AB
C     QB
C
      ID4=0
      X(15)=      0.5*P(6)*X(75)+(P(3)+.5+P(6)*TAN(P(56)))*X(74)-.5
      IF(X(15)-P(6)) 31,30,30
 30   X(15)=P(6)
      X(18)= P(6)*SQRT(-X(21))
      X(36)=X(21)
      ID4=1
      GO TO 32
 31   X(18)=X(15)*SQRT(-X(21))
      X(36)=-(X(18)/P(6))**2
      IF(X(15).GE.0.80 *P(6))   ID4=1
 32   CONTINUE
      IF(ABS(X(18)-X(85)).LE.P(50)) NCR=1
C     BT
      X(81)=Y(1)*Y(1)/P(7)
      X(28)=X(22)+(Y(1)/X(13))**2
      IF(ID4.EQ.1) GO TO 33
      X(82)=X(18)*X(18)/P(6)
      GO TO 34
 33   X(80)=(0.80 )*(P(6)/X(15))*X(18)
      X(82)=X(80)*X(80)/P(6)
 34   X(84)=P(7)/P(6)
      X(71)=X(28)*X(84)+X(22)*(1.-X(84))
      X(83)=0.5*(X(36)-X(71))*P(6)
      X(10)= ATAN(X(83)+X(82)-X(81))
      IF(NCR.EQ.1) GO TO 45
      IF(NCR.EQ.2) GO TO 43
      X(85)=X(18)
      GO TO 10
 43   WRITE(6,1004)
 1004 FORMAT('0',3X,'WARNING 2 = ITERATIONS FOR QB(TO) DO NOT CONVERGE')
C
C     AC
```

```
 45   X(80)=-X(75)
      X(13)=0.5*P(7)*X(80)+(P(4)+0.5+P(7)*TAN(P(57)))*X(74)-0.5
      IF(X(13)-P(7)) 36,35,35
 35   X(13)=P(7)
 36   CONTINUE
C
C     V(T0)
C
      X(86)=0.25*P(53)*X(52)*X(52)*(X(76) - 0.5*SIN(2.*X(76)))
      X(87)=.5*X(53)*X(4)*COS(X(8)-X(10))
      X(88)=0.5*X(50)*(P(3)+X(53))*P(58)
      X(48)=X(86)+X(87)+X(88)
      IK=0
      ID2=0
      ID3=0
      ID4=0
      X(34)=X(22)
C
C     END OF ITERATIONS FOR QB(T0)
C
C
200   IF(ID3.EQ.1) GO TO 201
      Y(2)=X(48)
      DY(2)=0.0
      IK=IK+1
      IF(IK.EQ.4)    ID3=1
201   X(29)=(P(41)-P(46))*(1.-EXP(-TIME/P(42)))+P(46)
      DY(1)=X(68)*(X(29)-X(28)-Y(1)*ABS(Y(1))/(X(66)*P(7))**2)/P(31)
C     BT
      X(28)=X(34)+ (Y(1)/X(13))**2
      X(81)=Y(1)*Y(1)/P(7)
      IF(ID4.EQ.1) GO TO 286
      X(82)=X(18)*X(18)/P(6)
      GO TO 287
286   X(80)=(0.80 )*(P(6)/X(15))*X(18)
      X(82)=X(80)*X(80)/P(6)
287   X(84)=P(7)/P(6)
      X(71)=X(28)*X(84)+X(34)*(1.-X(84))
      X(83)=0.5*(X(36)-X(71))*P(6)
      X(10)= ATAN(X(83)+X(82)-X(81))
      X(74)=COS(X(10))
      X(75)=SIN(X(10))
      X(50)=0.5*(P(6)+X(75)) /P(58)
      X(53)=P(3)+X(50)*P(59)+0.5*(1.0-X(74))
      X(51)=X(1)-X(50)
      X(81)=(X(51)*P(59)+X(53))**2+(X(51)*P(58))**2
      X(4)=SQRT(X(81))
      IF(X(10).GT.-0.35) GO TO 290
      X(8)=0.06
      GO TO 291
290   X(81)=X(53)*P(58)/X(4)
      X(8)=ARSIN(X(81))+X(10)+P(56)
291   X(76)=X(8)/P(53)
      X(82)=P(53)*TAN(X(76))
      X(61)=ATAN(X(82))
      X(9)=X(61)+X(8)-X(10)-P(56)
C     RCL
      X(52)=X(4)/SIN(X(76))
      X(37)=0.5*X(52)/P(53)
      X(80)=X(37)+0.5
      X(81)=P(9)-0.5*P(6)-X(80)*X(75)
      X(82)=X(80)*X(74)-P(5)
      X(33)=ATAN(X(81)/X(82))
      X(35)=0.5*(X(10)+X(33))
C     SP
      X(40)=2.*X(37)*X(35)
```

```
C      YP
       X(81)=X(40)+P(62)
       X(41)=SQRT(P(62)/X(81))
       X(42)=(.5*X(81)/P(18))*ALOG((1.+X(41))/(1.-X(41)))
       X(82)=0.5-X(42)
       X(83)=COS(2.*X(35))-1.0
       X(5)=X(37)+.5*(1.+X(82)*(2.*X(37)+X(82))/(X(37)*X(83)-X(82)))
       IF((X(5)-X(37))-20.0) 189,188,188
 188   X(5)=X(80)
C      ETA2
 189   X(81)=P(5)-0.5*P(6)-X(5)*X(75)
       X(82)=X(5)*X(74)-P(5)
       X(62)=ATAN(X(81)/X(82))
C      YS
       X(83)=X(81)**2+X(82)**2
       X(60)=SQRT(X(83))
       X(6)=X(5)-X(60)
C      SS
       X(57)=X(5)*(X(10)+X(62))
C      TS
       X(20)=P(18)*X(6)/(X(57)+P(62))
       X(81)=EXP(X(80))
       X(82)=EXP(-X(60))
       X(12)=(X(81)-X(82))/(X(81)+X(82))
C      SPLITTER EFFECT
       X(77)=(1.-1.5*X(12)+.5*X(12)**3)*COS(X(9))+1.+1.5*X(12)-
      1 0.5*X(12)**3
       X(78)=ARCOS(X(77)/2.)
       X(11)=2.0*COS((P(51)+X(78))/3.)
C      PBE
       X(31)=X(68)*P(7)
       IF(X(10)) 264,264,202
 202   X(82)=X(5)*X(75)+.5*P(6)
       X(83)=P(36)*P(60)
       IF(X(82)-X(83)) 272,272,273
 272   X(46)=X(5)*X(10)
       X(47)=1.825*(X(46)+P(62))/P(18)
       X(38)=X(82)*TAN(P(57))+P(4)+.5-X(5)*(1.-X(74))-X(47)
       GO TO 274
 273   X(47)=1.825*(X(46)+P(62))/P(18)
       X(38)=P(36)*P(61)+P(4)+.5-(X(6)-P(5))-X(47)
 274   IF(X(38)) 203,203,204
 203   X(38)=0.0
       X(44)=0.0
       GO TO 263
 204   X(80)=X(22)-X(34)
       IF(X(80)) 262,261,261
 261   X(44)=X(38)*SQRT(X(80))
       GO TO 263
 262   X(44)=-X(38)*SQRT(-X(80))
 263   X(43)=0.5*(SQRT(1.+X(46)/P(62))-1.)
       X(23)=Y(1) +X(44)-X(43)
       X(84)=X(81)+X(38)
       X(34)=X(34)+X(83)*ABS(X(83))/X(84)**2
       IF(X(34).GE.0.0) X(34)=0.0
       GO TO 265
 264   X(46)=0.0
       X(47)=0.5
       X(34)=X(22)
       X(44)=-Y(1)
       X(43)=0.0
       X(38)=X(81)
C
C      PD2
C      CD2
 265   X(23)=.25*(2.+3.*X(12)-X(12)**3)/X(65)
```

```
      X(31)=X(22)+X(23)
      X(24)=.25*(3.*X(11)-X(11)**3-3.*X(12)+X(12)**3)/X(66)
      X(32)=X(24)
      IF(X(57)-X(46)) 275,276,276
 275  X(82)=X(46)
      GO TO 277
 276  X(82)=X(57)
 277  X(45)=0.5*(SQRT(1.+X(82)/P(62))-1.)-X(43)
      DY(4)=(X(32)-X(26)-Y(4)*ABS(Y(4))/X(66)**2)/P(34)
      DY(3)=(X(31)-X(26)-Y(3)*ABS(Y(3))/X(65)**2)/P(33)
      IF(Y(3)) 207,208,208
 207  X(82)=P(8)*SQRT(-X(22))-Y(3)-X(44)-X(45)
      IF(X(44)) 266,267,267
 266  X(83)=P(8)+X(65)+X(38)
      GO TO 268
 267  X(83)=P(8)+X(65)
 268  X(17)=X(82)*ABS(X(82))/X(83)**2
      GO TO 209
 208  X(82)=P(8)*SQRT(-X(22))-X(44)-X(45)
      IF(X(44)) 269,270,270
 269  X(83)=P(8)+X(38)
      GO TO 271
 270  X(83)=P(8)
 271  X(17)=X(82)*ABS(X(82))/X(83)**2
C     POUT
      X(20)=(Y(4)/X(66))**2
C
 209  X(22)=X(22)+X(17)
      IF(X(22).GE.0.0) X(22)=0.0
C     PI
      X(81)=X(46)/X(57)
      X(21)=X(81)*X(34)+(1.-X(81))*X(22)-2./X(5)
C     XR
      X(3)=X(52)*(0.62*X(76)+0.38*SIN(X(76)))
      X(80)=X(3)+P(62)
      X(63)=SQRT(P(62)/X(80))
      X(81)=0.5*X(80)/P(18)
      X(82)=((1.+X(11))/(1.-X(11)))*((1.-X(63))/(1.+X(63)))
      X(2)=X(1) -X(81)*ALOG(X(82))/SIN(X(9))
C     DV/DT
      IF(X(2)-P(10)) 210,210,211
 210  DY(2)=X(18)+0.5*(1.0-X(11)/X(63))
      X(14)=0.0
      X(19)=0.0
      GO TO 217
 211  IF(ID2.EQ.1) GO TO 216
      X(81)=P(10)*P(58)-X(5)*X(75)-0.5*P(6)
      X(82)=X(5)*X(74)-P(10)*P(59)-(P(3)+0.5)
      X(39)=ATAN(X(81)/X(82))
      IF(X(39)-P(56)) 212,212,213
 212  ID2=1
      GO TO 215
 213  X(58)=X(5)*(X(10)+X(39))
      X(59)=1.825*(X(58)+P(62))/P(18)
      X(14)=X(5)-X(59)-X(81)/SIN(X(39))
      IF(X(14)) 210,210,214
 214  IF(X(14)-P(8)) 216,215,215
 215  X(14)=P(8)
 216  X(19)=X(14)*SQRT(-X(21))
      DY(2)=X(18)+0.5*(1.-X(11)/X(63))+X(19)
C
C     IMPLICIT FN FOR THE
C
 217  IF(X(10).GT.-0.35) GO TO 220
      X(8)=0.06
      GO TO 238
```

```
  220  F(1)=X(8)
       Z(2)=X(8)
       X(85)=X(1)
       X(88)=0.5*X(50)*(P(3)+X(53))*P(58)
       DO 230 N=2,30
       I=0
  221  X(8)=ABS(Z(N))
       IF(X(8).GE.P(54)) X(8)=P(54)-P(63)
       IF(X(8).LE.0.0)  X(8)=P(63)
       X(76)=X(8)/P(53)
       X(4)=X(53)*P(58)/SIN(ABS(X(8)-X(10)-P(56)))
       X(52)=X(4)/SIN(X(76))
       X(87)=.5*X(53)*X(4)*COS(ABS(X(8)-X(10)))
       X(81)=4.*(Y(2)-X(87)-X(88))/(X(52)*X(52))+.5*P(53)*SIN(2.*X(76))
       F(N+1)=ABS(X(81))
       IF(N.GT.2) GO TO 223
       IF(I) 223,222,223
  222  Z(N-1)=F(N-1)
       Z(N)=F(N+1)
       F(N)=F(N+1)
       I=I+1
       IF(I.GT.20) GO TO 232
       GO TO 221
  223  IF(Z(N)-Z(N-1)) 225,224,225
  224  Z(N+1)=Z(N)
       GO TO 235
  225  P(68)=(F(N+1)-F(N))/(Z(N)-Z(N-1))
       IF(P(68).EQ.1.) GO TO 222
       P(69)=P(68)/(P(68)-1.)
       Z(N+1)=P(69)*Z(N)+(1.-P(69))*F(N+1)
       P(70)=ABS(Z(N+1)-Z(N))
       IF(P(70).LE.1.E-6) GO TO 235
  230  CONTINUE
  232  WRITE(6,2100)
  2100 FORMAT('0',3X,'WARNING 4= IMPLICIT FN FOR X(8) DOES NOT CONVERSE')
       GO TO 239
  235  X(8)=Z(N+1)
       IF(X(8).LT.0.06) X(8)=0.06
C
C      END OF IMPLICIT FN FOR THE
C
       IF((X(8).LE.(X(10)+P(56))).OR.(X(8).GE.P(54))) GO TO 239
  238  X(4)=X(53)*P(58)/SIN(ABS(X(8)-X(10)-P(56)))
       X(51)=X(4)*COS(X(8)-X(10))/P(58)
       X(1)=X(50)+X(51)
       GO TO 240
  239  X(1)=X(85)
C      AC
  240  X(80)=-X(75)
       X(13)=0.5*P(7)*X(80)+(P(4)+0.5*P(7)*TAN(P(57)))*X(74)-0.5
       IF(X(13)-P(6)) 237,236,236
  236  X(13)=P(6)
  237  CONTINUE
C      COC
       IF(Y(1).EQ.0.0) GO TO 247
       X(69)=Y(1)*P(24)
       X(70)=X(69)/((P(12)+1.)*P(65))
       X(80)=ALOG10(X(70))
       X(68)=CI(1)
       DO 246 J=1,6
  246  X(68)=X(68)+CI(J+1)*X(80)**J
       IF(X(68).LE.0.0) X(68)=0.01
C      OB
C      AB
  247  X(15)=      0.5*P(6)*X(75)+(P(3)+.5+P(6)*TAN(P(56)))*X(74)-.5
       IF(X(15)-P(6)) 249,248,248
```

```
 248  X(15)=P(6)
      X(18)= P(6)*SQRT(-X(21))
      X(36)=X(21)
      ID4=1
      GO TO 250
 249  X(18)=X(15)*SQRT(-X(21))
      X(36)=-(X(18)/P(6))**2
      IF(X(15).GE.0.80*P(6))    ID4=1
 250  CONTINUE
      GO TO 300
 295  X(79)=X(32)
300   CONTINUE
C .... DUMMY
TMDATA : PTC=0.41
 $DAMAIN NY=4, NP=72, NX=88,
 DELT=1.5, PRDEL=3.0,
 ENDTIM=1000.,
 IRK=4,
 YI(1)=0.0,2.0,2.0,-1.5E-1,
 P(41)=0.41,
 P(4)=1.0,
 P(34)=17.2285,
 P(3)=0.5,
 P(11)=9.687,
 P(31)=19.374,
 P(9)=11.0,
 P(1)=12.0,
 P(2)=12.0,
 P(5)=0.0,
 P(6)=1.0,
 P(7)=2.0,
 P(8)=3.05,
 P(10)=10.942,
 P(36)=10.942,
 P(12)=10.0,
 P(13)=32.34,
 P(14)=32.34,
 P(15)=5.5,
 P(16)=0.1,
 P(17)=3.075,
 P(18)=10.5,
 P(19)=2.360E-2,
 P(20)=1.123E-7,
 P(22)=230.8872,
 P(23)=2308.8715,
 P(24)=9783.0,
 P(33)=19.8090,
 TABLE1=-29,-20,1,-2,3,-31,-6,-32,4,
 PLOT1=-29,1,-20,
 $END
```

```
C
C  COMPUTER PROGRAM 3 - COMPUTATIONS OF THE RETURN TIME
C
      DIMENSION F(101),Z(101),CI(7)
      IF (ISTART.EQ.0) GO TO 50
      IFIND=0
      ID1=0
      ID2=0
      ID3=0
      DO 500 II=1,100
500   X(II)=0.0
      P(50)=1.E-3
      P(51)=3.141592654
      P(52)=180./P(51)
      P(53)=67./90.
      P(54)=67./P(52)
      P(56)=P(1)/P(52)
      P(57)=P(2)/P(52)
      P(58)=COS(P(56))
      P(59)=SIN(P(56))
      P(60)=COS(P(57))
      P(61)=SIN(P(57))
      P(62)=P(19)/3.
      P(63)=1./P(52)
      P(65)=(1.+1./P(17))**2
      X(65)=(P(3)-P(5)+0.5)*P(58)+P(9)*P(59)
      X(66)=(P(4)+P(5)+0.5)*P(60)+P(9)*P(61)
C
C     COEFF FOR CD
      CI(1)= 6.905645E-2
      CI(2)= 2.067500E-1
      CI(3)= 2.064129E-1
      CI(4)=-5.814309E-2
      CI(5)=-7.139390E-2
      CI(6)= 4.834454E-2
      CI(7)=-8.477535E-3
C
      P(26)=P(16)/P(23)
      P(42)=1.5E-3/P(26)
C
C     ITERAPATIONS FOR QC(TO)
      X(10)=-2.688563E-1
      X(13)=8.018093E-1
      X(28)=1.897294E-1
      X(68)=7.934437E-1
      Y(1)=4.035499E-1
      IT=0
      ID5=0
      X(86)=Y(1)
      X(18)=0.2
      X(85)=X(18)
 80   IT=IT+1
      IF(IT.GT.5)  GO TO 85
C
C     ITERAPATIONS FOR QB(TO)
      NCR=0
      ITER=0
 10   ITER=ITER+1
      IF(ITER.GT.20) NCR=2
      X(74)=COS(X(10))
      X(75)=SIN(X(10))
      X(50)=0.5*(P(6)+X(75)) /P(58)
      X(53)=P(3)+X(50)*P(59)+0.5*(1.0-X(74))
```

```
C
C     ITERATIONS FOR X(8)
C
      IF(X(10).GT.-0.35) GO TO 11
      ID5=1
      X(8)=0.06
      GO TO 12
 11   KOUNT=0
      P(55)=0.02
      X(8) =0.1
 12   X(76)=X(8)/P(53)
      X(82)=P(53)*TAN(X(76))
      X(61)=ATAN(X(82))
      X(9)=X(61)+X(8)-X(10)-P(56)
      X(11)=2.0*COS((P(51)+X(9))/3.)
      X(81)=((2.*X(18)+1.)/X(11))**2
      X(3)=P(62)*(X(81)-1.)
      X(52)=X(3)/(0.62*X(76)+0.38*SIN(X(76)))
      X(4)=X(52)*SIN(X(76))
      X(84)=X(4)*SIN(X(8)-X(10)-P(56))/P(58)
      IF(ID5.EQ.1) GO TO 26
      P(66)=X(84)-X(53)
      IF(ABS(P(66)).LT.1.E-4*X(53)) GO TO 26
 20   KOUNT=KOUNT+1
      IF(KOUNT.GT.100) GO TO 46
      X(8)=X(8)+P(55)
      VM=P(63)/3.0
      IF(X(8).LE.0.0)  X(8)=VM
      X(76)=X(8)/P(53)
      X(82)=P(53)*TAN(X(76))
      X(61)=ATAN(X(82))
      X(9)=X(61)+X(8)-X(10)-P(56)
      X(11)=2.0*COS((P(51)+X(9))/3.)
      X(81)=((2.*X(18)+1.)/X(11))**2
      X(3)=P(62)*(X(81)-1.)
      X(52)=X(3)/(0.62*X(76)+0.38*SIN(X(76)))
      X(4)=X(52)*SIN(X(76))
      X(84)=X(4)*SIN(X(8)-X(10)-P(56))/P(58)
      P(67)=X(84)-X(53)
      IF(ABS(P(67)).LT.1.E-4*X(53)) GO TO 26
      IF((P(66)*P(67).GT.0.0).AND.(ABS(P(67)).LT.ABS(P(66)))) GO TO 22
      IF((P(66)*P(67).GT.0.0).AND.(ABS(P(67)).GT.ABS(P(66)))) GO TO 24
      IF (P(66)*P(67).LT.0.0)  GO TO 25
 22   P(66)=P(67)
      GO TO 20
 24   P(66)=P(67)
      P(55)=-P(55)
      GO TO 20
 25   P(66)=P(67)
      P(55)=-0.1*P(55)
      GO TO 20
C
C     END OF ITERATIONS FOR X(8)
 46   WRITE(6,1002)
 1002 FORMAT('0',3X,'WARNING 3 = ITERATIO5S FOR X(8) DO NOT CONVERSE')
C
 26   X(51)=X(4)*COS(X(8)-X(10))/P(58)
      X(1)=X(50)+X(51)
C
C     XR
C
      X(80)=X(3)+P(62)
      X(63)=SQRT(P(62)/X(80))
      X(81)=0.5*X(80)/P(18)
      X(82)=((1.+X(11))/(1.-X(11)))*((1.-X(63))/(1.+X(63)))
      X(2)=X(1) -X(81)*ALOG(X(82))/SIN(X(9))
```

```
C
C     RCL
C
      X(37)=0.5*X(52)/P(53)
      X(80)=X(37)+0.5
      X(81)=P(9)-0.5*P(6)-X(80)*X(75)
      X(82)=X(80)*X(74)-P(5)
      X(33)=ATAN(X(81)/X(82))
      X(35)=0.5*(X(10)+X(33))
      X(40)=2.*X(37)*X(35)
      X(81)=X(40)+P(62)
      X(41)=SQRT(P(62)/X(81))
      X(42)=(.5*X(81)/P(18))*ALOG((1.+X(41))/(1.-X(41)))
      X(82)=0.5-X(42)
      X(83)=COS(2.*X(35))-1.0
      X(5)=X(37)+.5*(1.+X(82)*(2.*X(37)+X(82))/(X(37)*X(83)-X(82)))
      IF((X(5)-X(37))-20.0) 17,15,15
 15   X(5)=X(80)
C
C     ETA2 , SS
C
 17   X(81)=P(9)-0.5*P(6)-X(5)*X(75)
      X(82)=X(5)*X(74)-P(5)
      X(62)=ATAN(X(81)/X(82))
      X(57)=X(5)*(X(10)+X(62))
C
C     QE2
C
      X(16)=0.5*(SQRT(1.+X(57)/P(62))-1.)
C
C     PI
C
      X(83)=X(16)-Y(1)
      IF(X(83).LE.0.0) X(83)=0.0
      X(82)=P(8)+X(66)
      X(22)= -(X(83)/X(82))**2
      X(21)=X(22)-2.0/X(5)
      IF(X(21).GE.0.0) X(21)=-0.02
C
C     AB
C     QB
C
      ID4=0
      X(15)=      0.5*P(6)*X(75)+(P(3)+.5+P(6)*TAN(P(56)))*X(74)-.5
      IF(X(15)-P(6)) 31,30,30
 30   X(15)=P(6)
      X(18)= P(6)*SQRT(-X(21))
      X(36)=X(21)
      ID4=1
      GO TO 32
 31   X(18)=X(15)*SQRT(-X(21))
      X(36)=-(X(18)/P(6))**2
      IF(X(15).GE.0.80 *P(6))   ID4=1
 32   CONTINUE
      IF(ABS(X(18)-X(85)).LE.P(50)) GO TO 82
      GO TO 27
 82   NCK=3
C     AC
      X(80)=-X(75)
      X(13)=0.5*P(7)*X(80)+(P(4)+0.5+P(7)*TAN(P(57)))*X(74)-0.5
      IF(X(13)-P(7)) 36,35,35
 35   X(13)=P(7)
 36   CONTINUE
C     QC
      X(81)=1./X(13)**2+(P(35)-1.)/P(7)**2+1./(X(68)*P(7))**2
      Y(1)=SQRT((P(41)-X(22))/X(81))
```

```
      IF(NCR.EQ.4) GO TO 29
      IF(ABS(Y(1)-X(86)).LE.1.E-4) NCR=1
C     CDC
 29   IF(Y(1).EQ.0.0) GO TO 44
      X(69)=Y(1)*P(24)
      X(70)=X(69)/((P(12)+1.)*P(65))
      X(80)=ALOG10(X(70))
      X(68)=CI(1)
      DO 146 J=1,6
 146  X(68)=X(68)+CI(J+1)*X(80)**J
      IF(X(68).LE.0.0) X(68)=0.01
 44   X(80)=1./X(13)**2+(P(35)-1.)/P(7)**2
      X(28)=X(22)+(Y(1)**2)*X(80)
C     BT
 27   X(81)=Y(1)*Y(1)/P(7)
      IF(ID4.EQ.1) GO TO 33
      X(82)=X(18)*X(18)/P(6)
      GO TO 34
 33   X(80)=(0.80 )*(P(6)/X(15))*X(18)
      X(82)=X(80)*X(80)/P(6)
 34   X(84)=P(7)/P(6)
      X(71)=X(28)*X(84)+X(22)*(1.-X(84))
      X(83)=0.5*(X(36)-X(71))*P(6)
      X(10)= ATAN(X(83)+X(82)-X(81))
      GO TO (45,43,28,28), NCR
      X(85)=X(18)
      ID5=0
      GO TO 10
 43   NCR=4
      GO TO 82
C     END OF ITERATIONS FOR QB(TO)
 28   X(86)=Y(1)
      GO TO 80
 85   WRITE(6,1004)
 1004 FORMAT('0',3X,'WARNING 2 = ITERATIONS FOR QC(TO) DO NOT CONVERGE')
C     END OF ITERATIONS FOR QC(TO)
C
C     QO2(TO)
C
 45   Y(4)=-X(66)*SQRT(-X(22))
      X(12)=-1.0
      X(23)=.25*(3.*X(11)-X(11)**3-3.*X(12)+X(12)**3)/X(65)
      X(31)=X(22)+X(23)
      Y(3)=X(65)*SQRT(X(31))
C
C     V(TO)
C
      X(86)=0.25*P(53)*X(52)*X(52)*(X(76) - 0.5*SIN(2.*X(76)))
      X(87)=.5*X(53)*X(4)*COS(X(8)-X(10))
      X(88)=0.5*X(50)*(P(3)+X(53))*P(58)
      Y(2)=X(86)+X(87)+X(88)
 50   IF(IFIND.EQ.1) GO TO 200
      IF(TIME.GE.P(42)) GO TO 100
      X(29)=P(41)-(P(41)-P(46))*TIME/P(42)
      GO TO 101
 100  X(29)=P(46)
      IF(ID1.EQ.1) GO TO 180
      X(73)=X(68)*P(7)*SQRT(-X(34))
      IF(Y(1)-X(73)) 182,182,101
 182  Y(1)=X(73)
      DY(1)=0.0
      ID1=1
      GO TO 183
 101  DY(1)=X(68)*(X(29)-X(28)-Y(1)*ABS(Y(1))/(X(68)*P(7))**2)/P(31)
C     BT
      X(28)=X(34)+ (Y(1)/X(13))**2
```

```
      X(81)=Y(1)*Y(1)/P(7)
      IF(ID4.EQ.1) GO TO 186
      X(82)=X(18)*X(18)/P(6)
      GO TO 187
186   X(80)=(0.80 )*(P(6)/X(15))*X(18)
      X(82)=X(80)*X(80)/P(6)
187   X(84)=P(7)/P(6)
      X(71)=X(28)*X(84)+X(34)*(1.-X(84))
      X(83)=0.5*(X(36)-X(71))*P(6)
      X(10)= ATAN(X(83)+X(82)-X(81))
      GO TO 181
180   Y(1)=X(68)*P(7)*SQRT(-X(34))
183   IF(ID4.EQ.1) GO TO 184
      X(82)=X(18)*X(18)/P(6)
      GO TO 185
184   X(80)=(0.80 )*(P(6)/X(15))*X(18)
      X(82)=X(80)*X(80)/P(6)
185   X(83)=0.5*(X(36)-X(34))*P(6)
      X(10)= ATAN(X(83)+X(82))
181   X(74)=COS(X(10))
      X(75)=SIN(X(10))
      X(50)=0.5*(P(6)+X(75)) /P(58)
      X(53)=P(3)+X(50)*P(59)+0.5*(1.0-X(74))
      X(51)=X(1)-X(50)
      X(81)=(X(51)*P(59)+X(53))**2+(X(51)*P(58))**2
      X(4)=SQRT(X(81))
      IF(X(10).GT.-0.35) GO TO 190
      X(8)=0.06
      GO TO 191
190   X(81)=X(53)*P(58)/X(4)
      X(8)=ARSIN(X(81))+X(10)+P(56)
191   X(76)=X(8)/P(53)
      X(82)=P(53)*TAN(X(76))
      X(61)=ATAN(X(82))
      X(9)=X(61)+X(8)-X(10)-P(56)
C     RCL
      X(52)=X(4)/SIN(X(76))
      X(37)=0.5*X(52)/P(53)
      X(80)=X(37)+0.5
      X(81)=P(9)-0.5*P(6)-X(80)*X(75)
      X(82)=X(80)*X(74)-P(5)
      X(33)=ATAN(X(81)/X(82))
      X(35)=0.5*(X(10)+X(33))
C     SP
      X(40)=2.*X(37)*X(35)
C     YP
      X(81)=X(40)+P(62)
      X(41)=SQRT(P(62)/X(81))
      X(42)=(.5*X(81)/P(18))*ALOG((1.+X(41))/(1.-X(41)))
      X(82)=0.5-X(42)
      X(83)=COS(2.*X(35))-1.0
      X(5)=X(37)+.5*(1.+X(82)*(2.*X(37)+X(82))/(X(37)*X(83)-X(82)))
      IF((X(5)-X(37))-20.0) 189,188,188
188   X(5)=X(80)
C     ETA2
189   X(81)=P(9)-0.5*P(6)-X(5)*X(75)
      X(82)=X(5)*X(74)-P(5)
      X(62)=ATAN(X(81)/X(82))
C     YSP
      X(83)=X(81)**2+X(82)**2
      X(60)=SQRT(X(83))
      X(6)=X(5)-X(60)
C     SSP
      X(57)=X(5)*(X(10)+X(62))
C     TS
      X(80)=P(18)*X(6)/(X(57)+P(62))
```

```
      X(81)=EXP(X(80))
      X(82)=EXP(-X(80))
      X(12)=(X(81)-X(82))/(X(81)+X(82))
C     SPLITTER EFFECT
      X(77)=(1.-1.5*X(12)+.5*X(12)**3)*COS(X(9))+1.+1.5*X(12)-
     1 0.5*X(12)**3
      X(78)=ARCOS(X(77)/2.)
      X(11)=2.0*COS((P(51)+X(78))/3.)
C     PBE
      X(81)=X(68)*P(7)
      IF(X(10)) 164,164,102
  102 X(82)=X(5)*X(75)+.5*P(6)
      X(83)=P(36)*P(60)
      IF(X(82)-X(83)) 172,172,173
  172 X(46)=X(5)*X(10)
      X(47)=1.825*(X(46)+P(62))/P(18)
      X(38)=X(82)*TAN(P(57))+P(4)+.5-X(5)*(1.-X(74))-X(47)
      GO TO 174
  173 X(47)=1.825*(X(46)+P(62))/P(18)
      X(38)=P(36)*P(61)+P(4)+.5-(X(6)-P(5))-X(47)
  174 IF(X(38)) 103,103,104
  103 X(38)=0.0
      X(44)=0.0
      GO TO 163
  104 X(80)=X(22)-X(34)
      IF(X(80)) 162,161,161
  161 X(44)=X(38)*SQRT(X(80))
      GO TO 163
  162 X(44)=-X(38)*SQRT(-X(80))
  163 X(43)=0.5*(SQRT(1.+X(46)/P(62))-1.)
      X(83)=Y(1) +X(44)-X(43)
      X(84)=X(81)+X(38)
      X(34)=X(34)+X(83)*ABS(X(83))/X(84)**2
      IF(X(34).GE.0.0) X(34)=0.0
      GO TO 165
  164 X(46)=0.0
      X(47)=0.5
      X(34)=X(22)
      X(44)=-Y(1)
      X(43)=0.0
      X(38)=X(81)
C
C     PD2
C     QD2
  165 X(23)=.25*(3.*X(11)-X(11)**3-3.*X(12)+X(12)**3)/X(65)
      X(31)=X(22)+X(23)
      X(24)=.25*(2.+3.*X(12)-X(12)**3)/X(66)
      X(32)=X(22)+X(24)
      IF(X(57)-X(46)) 175,176,176
  175 X(82)=X(46)
      GO TO 177
  176 X(82)=X(57)
  177 X(45)=0.5*(SQRT(1.+X(82)/P(62))-1.)-X(43)
      DY(4)=(X(32)-X(26)-Y(4)*ABS(Y(4))/X(66)**2)/P(34)
      IF(Y(4)) 107,108,108
  107 X(82)=P(8)*SQRT(-X(22))-Y(4)-X(44)-X(45)
      IF(X(44)) 166,167,167
  166 X(83)=P(8)+X(66)+X(38)
      GO TO 168
  167 X(83)=P(8)+X(66)
  168 X(17)=X(82)*ABS(X(82))/X(83)**2
      GO TO 109
  108 X(82)=P(8)*SQRT(-X(22))-X(44)-X(45)
      IF(X(44)) 169,170,170
  169 X(83)=P(8)+X(38)
      GO TO 171
```

```
 170  X(83)=P(8)
 171  X(17)=X(82)*ABS(X(82))/X(83)**2
C     POUT
      X(20)=(Y(4)/X(66))**2
C
 109  X(22)=X(22)+X(17)
      IF(X(22).GE.0.0) X(22)=0.0
C     P1
      X(81)=X(46)/X(57)
      X(21)=X(81)*X(34)+(1.-X(81))*X(22)-2./X(5).
C     XR
      X(3)=X(52)*(0.62*X(76)+0.38*SIN(X(76)))
      X(80)=X(3)+P(62)
      X(63)=SQRT(P(62)/X(80))
      X(81)=0.5*X(80)/P(18)
      X(82)=((1.+X(11))/(1.-X(11)))*((1.-X(63))/(1.+X(63)))
      X(2)=X(1) -X(81)*ALOG(X(82))/SIN(X(9))
C     DY/DT
      IF(X(2)-P(10)) 110,110,111
 110  DY(2)=X(18)+0.5*(1.-X(11)/X(63))
      X(14)=0.0
      X(19)=0.0
      GO TO 117
 111  IF(ID2.EQ.1) GO TO 116
      X(81)=P(10)*P(58)-X(5)*X(75)-0.5*P(6)
      X(82)=X(5)*X(74)-P(10)*P(59)-(P(3)+0.5)
      X(39)=ATAN(X(81)/X(82))
      IF(X(39)-P(56)) 112,112,113
 112  ID2=1
      GO TO 115
 113  X(58)=X(5)*(X(10)+X(39))
      X(59)=1.825*(X(58)+P(62))/P(18)
      X(14)=X(5)-X(59)-X(81)/SIN(X(39))
      IF(X(14)) 110,110,114
 114  IF(X(14)-P(8)) 116,115,115
 115  X(14)=P(8)
 116  X(19)=X(14)*SQRT(-X(21))
      DY(2)=X(18)+0.5*(1.-X(11)/X(63))+X(19)
C
C     IMPLICIT FN FOR THE
C
 117  IF(X(10).GT.-0.35) GO TO 120
      X(8)=0.06
      GO TO 138
 120  F(1)=X(8)
      Z(2)=X(8)
      X(85)=X(1)
      X(88)=0.5*X(50)*(P(3)+X(53))*P(58)
      DO 130 N=2,30
      I=0
 121  X(8)=ABS(Z(N))
      IF(X(8).GE.P(54)) X(8)=P(54)-P(63)
      IF(X(8).LE.0.0)  X(8)=P(63)
      X(76)=X(8)/P(53)
      X(4)=X(53)*P(58)/SIN(ABS(X(8)-X(10)-P(56)))
      X(52)=X(4)/SIN(X(76))
      X(87)=.5*X(53)*X(4)*COS(ABS(X(8)-X(10)))
      X(81)=4.*(Y(2)-X(87)-X(88))/(X(52)*X(52))+.5*P(53)*SIN(2.*X(76))
      F(N+1)=ABS(X(81))
      IF(N.GT.2) GO TO 123
      IF(I) 123,122,123
 122  Z(N-1)=F(N-1)
      Z(N)=F(N+1)
      F(N)=F(N+1)
      I=I+1
      IF(I.GT.20) GO TO 132
```

```
      GO TO 121
 123  IF(Z(N)-Z(N-1)) 125,124,125
 124  Z(N+1)=Z(N)
      GO TO 135
 125  P(68)=(F(N+1)-F(N))/(Z(N)-Z(N-1))
      IF(P(68).EQ.1.) GO TO 122
      P(69)=P(68)/(P(68)-1.)
      Z(N+1)=P(69)*Z(N)+(1.-P(69))*F(N+1)
      P(70)=ABS(Z(N+1)-Z(N))
      IF(P(70).LE.1.E-6) GO TO 135
 130  CONTINUE
 132  WRITE(6,1100)
 1100 FORMAT('0',3X,'WARNING 4= IMPLICIT FN FOR X(8) DOES NOT CONVERSE')
      GO TO 139
 135  X(8)=Z(N+1)
      IF(X(8).LT.0.06) X(8)=0.06
C
C     END OF IMPLICIT FN FOR THE
C
      IF((X(8).LE.(X(10)+P(56))).OR.(X(8).GE.P(54))) GO TO 139
 138  X(4)=X(53)*P(58)/SIN(ABS(X(8)-X(10)-P(56)))
      X(51)=X(4)*COS(X(8)-X(10))/P(58)
      X(1)=X(50)+X(51)
      GO TO 140
 139  X(1)=X(85)
C     AC
 140  X(80)=-X(75)
      X(13)=0.5*P(7)*X(80)+(P(4)+0.5*P(7)*TAN(P(57)))*X(74)-0.5
      IF(X(13)-P(7)) 137,136,136
 136  X(13)=P(7)
 137  CONTINUE
C     CDC
      IF(Y(1).EQ.0.0) GO TO 147
      X(69)=Y(1)*P(24)
      X(70)=X(69)/((P(12)+1.)*P(65))
      X(80)=ALOG10(X(70))
      X(68)=CI(1)
      DO 146 J=1,6
 146  X(68)=X(68)+CI(J+1)*X(80)**J
      IF(X(68).LE.0.0) X(68)=0.01
C     QB
C     AB
 147  X(15)=      0.5*P(6)*X(75)+(P(3)+.5+P(6)*TAN(P(56)))*X(74)-.5
      IF(X(15)-P(6)) 149,148,148
 148  X(15)=P(6)
      X(18)= P(6)*SQRT(-X(21))
      X(36)=X(21)
      ID4=1
      GO TO 150
 149  X(18)=X(15)*SQRT(-X(21))
 149  X(18)=X(15)*SQRT(-X(21))
      X(36)=-(X(18)/P(6))**2
      IF(X(15).GE.0.80*P(6))    ID4=1
 150  CONTINUE
C
C     SWITCHING
      IF(ID3.EQ.1) GO TO 155
      IF(X(6).LE.0.0) GO TO 195
      X(7)=0.95*X(66)*SQRT(X(79))
      ID3=1
 155  IF(Y(4).LT.X(7)) GO TO 200
      IFIND=1
      ENDTIM=TIME
      WRITE(6,160)P(41),TIME,X(18),Y(4),X(7),X(6),X(20)
 160  FORMAT('0',3X,F16.5,F16.3,1P5E16.6)
      GO TO 200
```

```
 195  X(79)=X(32)
 200  CONTINUE
C .... DUMMY
TM DATA : PTC=0.45   IN , D2=1.0
 $DATAIN NY=4, NP=72, NX=88,
 DELT=1.0, PRDEL=4.0,
 ENDTIM=800.0,
 IRK=2,
 YI(1)=3.751458E-1,6.676356,0.0,-3.631318E-2,
 P(41)=0.45,
 P(4)=0.5,
 P(12)=9.687,
 P(31)=19.374,
 P(34)=19.8090,
 P(3)=1.0,
 P(32)=14.0116,
 P(9)=11.0,
 P(1)=12.0,
 P(5)=0.0,
 P(6)=2.0,
 P(7)=1.0,
 P(8)=3.05,
 P(10)=10.942,
 P(36)=10.942,
 P(11)=10.0,
 P(13)=32.34,
 P(14)=32.34,
 P(15)=5.5,
 P(16)=0.1,
 P(17)=3.075,
 P(18)=10.5,
 P(19)=2.360E-2,
 P(20)=1.123E-7,
 P(22)=230.8872,
 P(23)=2308.8715,
 P(24)=9783.0,
 P(46)=0.0,
  GMAX1(3)=1.0,
  GMAX1(4)=1.0,
  GMIN1(3)=1.0,
  GMIN1(4)=1.0,
  TABLE1= 1,101,-2,-18,-10,-14,-19,-6,-32,4,
  PLOT1=1,2,-31,-32,-20,
 $END
```

## ENDNOTE

[1] J. H. Wegstein, "Accelerating Convergence of Iterative Processes," Communications of the Association for Computing Machinery, 1, 6 (June, 1958), pp. 9-13.

VITA

Hyo Whan Chang

Candidate for the Degree of

Doctor of Philosophy

Thesis: DYNAMIC ANALYSIS OF A MONOSTABLE FLUID AMPLIFIER

Major Field: Mechanical Engineering

Biographical:

Personal Data: Born in Chulwon, Korea, March 22, 1945, the son of Mr. and Mrs. Sung Ryong Chang.

Education: Graduated from Seoul High School, Seoul, Korea, in 1963; received the Bachelor of Science in Engineering degree in Mechanical Engineering from Seoul National University, Seoul, Korea, in 1968; received the Master of Science degree in Mechanical Engineering from the State University of New York at Buffalo, New York, in 1972; enrolled in the Systems Engineering doctoral program at Case Western Reserve University, 1972-73; completed requirements for the Doctor of Philosophy degree at Oklahoma State University in July, 1978.

Professional Experience: Ordnance Maintenance Officer, Korean Army, 1968-70; graduate research assistant, State University of New York at Buffalo, 1970-72; Laboratory Instructor, Systems Engineering Division, Case Western Reserve University, 1972-73; graduate research assistant, Oklahoma State University, 1974 to date.

Professional Affiliations: American Society of Mechanical Engineers; Korean Scientists and Engineers Association in America.